Unequal Error Protection Adaptive Modulation in Multicarrier Systems

BY KHALED SHAWKY HASSAN
k.hassan@jacobs-university.de

Ph.D. Dissertation
in Electrical Engineering

Dissertation Committee:
Prof. Dr.-Ing. Werner Henkel, Jacobs University Bremen
Prof. Dr.-Ing. Sören Peik, Jacobs University Bremen
Prof. Dr. Götz Pfander, Jacobs University Bremen
Prof. Dr.-Ing. Robert Fischer, University of Erlangen-Nuremberg
Prof. Dr.-Ing. Jürgen Lindner, University of Ulm

Bremen: September, 2010
School of Engineering and Science
Jacobs University Bremen

Abstract

Unequal Error Protection (UEP) is the key to future prioritized data communication, multilevel quality of services (QoSs), and scalable multimedia transmission. This means that these applications provide data of different importance and require different error protection. Under these conditions, multicarrier modulation is highly recommended due to its suitability for adapting individual sub-carriers, which are subject to different channel conditions, with different bit rates, code rates, and powers according to any given performance constraints.

So far, many channel adaptive bit-loading algorithms in multicarrier systems have been developed and new coding schemes have dramatically enhanced the system performance. However, these algorithms treat all sub-carriers equally (non-UEP), i.e., the average error rate will roughly be the same for all subcarriers. Based on some of these readily available bit-loading algorithms, we propose a set of new UEP bit-loading schemes that allow for allocating an arbitrary number of bits with arbitrary noise margins or symbol error-ratios (SERs), thereby realizing UEP at the modulation level. In these schemes, the subcarriers are subdivided into smaller sets, where each set is dedicated to a certain priority class. Moreover, we propose different partitioning schemes that require minimum complexity and overhead.

In general, adaptive transmission techniques require closed-loop communications by using feedback links or exploiting the channel reciprocity. In this thesis, closed-loop adaptive schemes have been realized for two different physical single-input single-output (SISO) channels, the wired and the wireless. In wired systems, the channel transfer function is considered to be deterministic and, therefore, requires very limited monitoring. However, it suffers from non-stationary impulse noise. In this case, a robust signal-to-noise ratio (SNR) sorting scheme has been proposed to better protect the high-priority data. In contrast to the wired channels, the wireless ones are more susceptible to varying conditions due to mobility. This implicates a study of the feedback link quality and reliability.

We introduce two different subcarrier allocation methods. The first method is a sub-carrier partitioning mechanism, where a given set of (sorted) subcarriers are divided amongst different priority classes in order to preserve certain QoSs. This can be realized, or approximated, using a set of complex nested iterations. As an alternative to the first method, a multilevel (hierarchical and non-hierarchical) modulation technique has been introduced to avoid lengthy searching and sorting.

As an extension to our work, we modify these prioritized adaptation schemes to realize UEP in multiple-input multiple-output (MIMO) channels as well. Hereto, the spatial and the spectral information, provided by the channel state information (CSI), will be exploited to realize UEP. This new prioritized adaptation, combined with the SNR robust sorting, results in a trade-off between spatial multiplexing and diversity gains in case of CSI uncertainties and different antenna correlations.

Moreover, we consider bit-loading and channel adaptation techniques for multiuser systems with different QoS requirements. This has been performed by extending our conventional UEP approaches to achieve prioritized transmission across a given number of users using orthogonal

frequency division multiple access (OFDMA), block-diagonalized (BD) space division multiple access (SDMA), and non-orthogonal SDMA. Using MIMO-OFDMA, we succeed in maximizing the capacity by utilizing the different users' eigenchannels and exploiting the multiuser diversity. One user in a BD-SDMA enjoys the orthogonal projection to the other users' null-space. Thus, multiuser interference (MUI) is completely eliminated unless the CSI at the transmitter is incorrect. Even then, our UEP adaptive scheme succeeds in protecting the important classes. Finally, we consider the non-diagonal SDMA, which is the most challenging approach in this thesis. However, in this case, our prioritized transmission outperforms the multiuser multiple access technique using MMSE with QoS constraints.

After all, our proposed algorithms succeed in realizing the proposed UEP in wireline and wireless environments under diverse channel conditions and different link-qualities. Furthermore, we show that our prioritized transmission schemes exploit limited feedback regimes efficiently, where they consistently outperform either non-adaptive or adaptive methods with equal error protection (EEP).

Acknowledgements

This work is the outcome of my research in the transmission systems group at the School of Engineering and Science at Jacobs University Bremen, Germany.
First of all, I would like to thank Prof. Dr.-Ing. Werner Henkel for his uncompromising principles and many examples of scholarly work. I have benefited from his insistence on carefully organized writing and clear logic. I am also grateful for the freedom he gave me and the convenient work environment.
Likewise, I want to thank Prof. Dr.-Ing. Jürgen Lindner, Prof. Dr. Götz Pfander, Prof. Dr.-Ing. Sören Peik, and Prof. Dr.-Ing. Robert F.H. Fischer for accepting to join the dissertation committee.
I would also like to thank all my previous and current colleagues at the transmission systems group who have contributed to make this time such a great one. This includes: Neele von Deetzen, Fangning Hu, Apirath Limmanee, Humberto Beltrão Neto, Behrouz Touri, Oana Graur, Khodr Saaifan, Abdul Wakeel, and Jalal Etesami for the interesting, multicultural work environment, for valuable discussions, and the real support with my thesis.
I want to express my sincere love and thanks to my wife, Hala, for her consistent prayers, encouragement, and support during this entire work. I cannot forget my little kids, Mariam and Yusuf. They gave me a continuous smile for the last 5 years.
Finally, I want to thank my family, especially my father Shawky, my mother Manal, my two sweet sisters, Nahla and Nashwa, and my elder brother Amr. Without their encouragement and their moral support, I couldn't have been able to reach this point now.
Special thanks to all my friends here in Bremen who had made my life much easier and more enjoyable: El-Shazly, Iyad, Nour, Dyab, Mousa, and Hamdy.
For funding my work, I would like to thank Jacobs University for the continuous support during my Master's and my Ph.D. I would like express my gratitude towards DFG as well.

Thank you all!

I confirm that this dissertation represents my own work. The contribution of any supervisors and others to the research and to the dissertation was consistent with normal supervisory practice.

Khaled Shawky Hassan
Bremen, September 2010

Dedication

To my mother, my father, and my wife Hala

Contents

List of Algorithms

Chapter 1

Introduction

1.1 Prioritized Adaptive Digital Communication

Modern digital communication has to cope with the drastically growing demands for audio, video, and reliable data communication. There are many schemes which have been traditionally utilized to enhance the communication speed. Time, frequency, and space diversity are examples of these contributions together with enhancing the SNR at the receiver by means of maximum ratio combining [15]. In these schemes, replicas of the transmitted data are received through uncorrelated channels and combined at the receiver in order to have constructive data addition and destructive noise addition. Thereby, the SNR is maximized and higher data rates can be achieved. Transmit diversity has also been used since the early days of digital mobile systems in order to increase the SNR at the receiver and enhance the reliability [16].

However, transmitting fast data symbols over band limited channels will result in a residual inter-symbol interference (ISI), due to the dispersive channel impulse response [16]. In this case, the energy of the transmitted symbols smears into neighboring symbols[1]. Equalizers, which can be represented as tapped delay line filters, have been introduced in literature as an approach to eliminate the remaining ISI due to channel dispersion [15, 16, 17]. The taps of the equalizer are adapted using symbol-by-symbol or sequence estimation algorithms. Those techniques require a huge computational complexity, which increases linearly with the data rate [17]. Vast efforts have been exerted to investigate an equalizer-less communication; this effort brought up multicarrier technique in the mid 60^{th} [18, 19]. In this scheme, the total bandwidth is divided into multiple subcarriers, each of which carries a lower data rate in order to mitigate ISI. When these subcarriers are overlapped orthogonally (not interfering), it is called orthogonal frequency division multiplexing (OFDM) [20] in wireless bandpass multicarrier communication. In baseband communication, such as wireline and cable systems, this is known as discrete multi-tone (DMT). There is no reason for such separation, since wireless multicarrier system is, of course, a discrete multi-tone and the wireline DMT is also an orthogonal frequency division

[1]Morse first noticed it on the transatlantic telegraph cables transmitting messages using dash/dots [17], i.e., causing interference. He solved this problem by slowing down the transmission, which was not efficient from the rate point of view.

multiplexing.

After the OFDM success in combating the residual ISI, the major research efforts have been dedicated to approach the capacity limits of fading channels. Claude Shannon [21] established the theoretical limit of the *channel capacity*, which defines the amount of error free data that can be transmitted over a given channel. In case of fading channels, the capacity limit can be achieved only if the channel varying fading levels are tracked on every subcarrier using the channel side information at both the transmitter and the receiver [22]. A water-filling approach suggests to allocate variable power on each subcarrier with variable data-rates [23] according to the channel state information (CSI) at the transmitter, i.e., closed-loop communication. If the channel reciprocity can be exploited, e.g., when time division duplexing (TDD) is used, the transmitter can easily know the channel from the previous received symbols, where the receiver estimates the channel using either symbol aided or pilot aided schemes [24]. In frequency division duplexing (FDD), the CSI has to be fed back to the transmitter through another feedback channel. This makes the fed back information susceptible to feedback channel errors and rate limitations. Figure 1.1 depicts the suggested closed-loop communication approach with readily available channel state information (CSI).

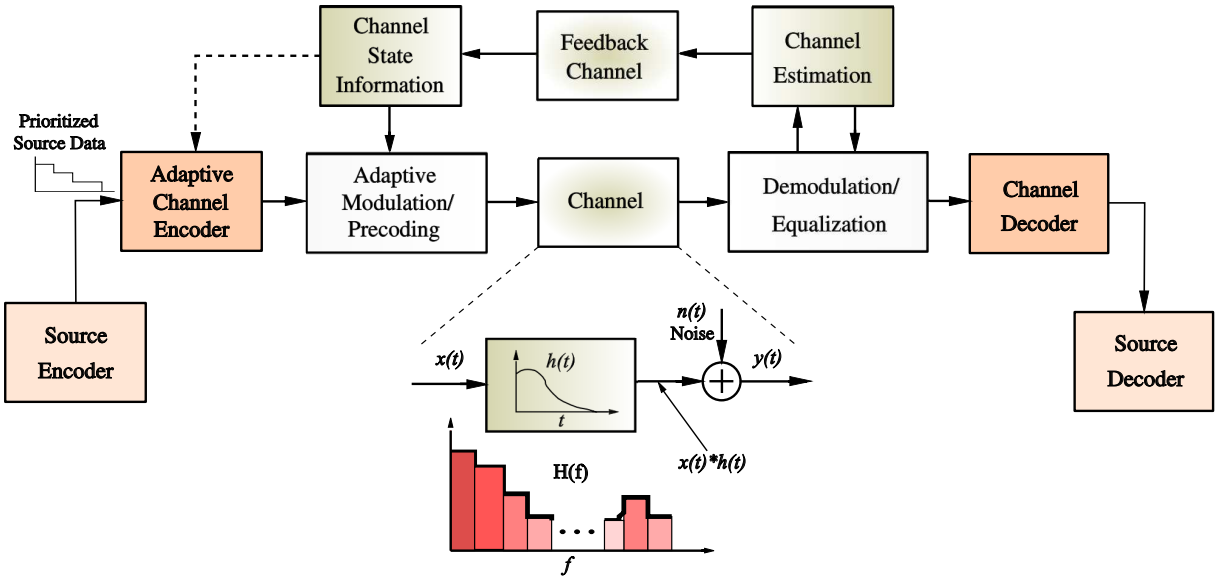

Figure 1.1: Block diagram of an adaptive digital communication system

1.2 Motivation for Prioritized Adaptive Modulation

To attain adaptive communication in a closed-loop link, the different channel gains have to be orthogonalized, i.e., convert the conventional channel into a set of non-interfering parallel transmission links. In case of single-input single-output (SISO) channel that uses OFDM, the linear convolution with the channel is converted into a circular one. This is done by introducing a cyclic prefix (CP), which is longer than the channel dispersion. In addition, an inverse discrete Fourier transform pre-processor (at the transmitter) and a discrete Fourier transform post-

processor (at the receiver) are introduced to diagonalize the channel matrix in order to maintain non-interfering subcarriers [25].

In multiple-input multiple-output (MIMO) systems, the channel spatial coefficients between each receive-transmit antenna pair (i_r,j_t), h_{i_r,j_t}, forms a non-diagonal channel matrix $\mathbf{H}$, which introduces interference at the receiver. Therefore, pre-and post-processing operations are performed to diagonalize $\mathbf{H}$ and convert it to a set of parallel (non-interfering) beams. Hence, the resultant diagonal gains can be utilized to maintain the link adaptation. Therefore, if a MIMO system is combined with an OFDM system (MIMO-OFDM), the adaptation will take place simultaneously in space and frequency. This converts the adaptation process into a two dimensional problem.

Spectrum and time sharing systems have been traditionally exploited in multiuser communications using the two well-known techniques, frequency division multiple access (FDMA) and time division multiple access (TDMA). However, from multiuser information theory, simultaneous reception from different users achieves the multiple-access channel (MAC) capacity region of the MAC channel [26]. Costa in his paper [27] introduced the dirty-paper code (DPC) which achieves multiuser capacity by pre-subtracting the known multiuser interference (MUI) at the transmitter. However, combined with a MIMO system, spatial division multiple access (SDMA) can also be exploited to achieve the capacity region using a full diagonalization technique, e.g., block-diagonalization technique [28]. In such a scheme, MUI is totally suppressed by transmitting to each user a beam that is orthogonal to other users' beams [29]. However, non-orthogonal transmission or quasi-orthogonal transmission can still approach the capacity region with minimal side constrains [30]. Nevertheless, combining these previous approaches with OFDM guarantees a reliable frequency sharing among the users if SDMA is not feasible [31] or the required quality of service (QoS) is not maintained. Accordingly, spatial-frequency adaptive schemes can allocate resources among users according to the required rate, quality of service (QoS), etc..

In the majority of the existing adaptive techniques, the symbol-error rate on every part of the transmitted data is assumed to be constant. However, due to the presence of modern source encoders, e.g., used for scalable video which already delivers data of different importance, prioritized transmission needs to be investigated more. This makes unequal error protection (UEP) a topic of great importance. Throughout this thesis, we consider UEP channel adaptation for OFDM, MIMO, and multiuser systems. This has been achieved by diagonalizing the different fading channels and utilizing the different channel gains and spatial layers (across different antennas or different users) to achieve a certain UEP or QoS profile.

1.3 Channel Models

This section gives an introduction to the dispersive guided (wireless) and unguided (wireline) channel models. In wireline cables, the channel is given by the transfer function of the used cable. It is directly related to the cable characteristics and its length, which are almost deterministic values. Due to this fact, most of the well-known bit and power allocation schemes, e.g., [32, 33], have been designed for wireline communications. In the following, we discuss one of the most convenient DSL cable transfer function which is known as MAR model followed by the frequently used Clark and Gans wireless channel model [34].

1.3.1 Guided Channel: Wireline Model

In wireline communications, the signal propagates in a guided medium, i.e., not allowed to diverse in the space. However, it rather propagates through an isolated copper cable. ADSL and VDSL are known to be data-over-voice systems, where data is transmitted over existing old telephone cables. In this case, data is allocated to the higher frequencies leaving the lower frequencies to the existing voice calls as in Fig. 1.2.a [35]. However, reusing the old infrastructure means transmitting under adverse disturbances like near- and far-end crosstalks, linear (amplitude, phase, and delay) distortion, and impulse noise that comes from relays, hooks, switches, lightning, railways, etc.. The following subsections are devoted to an overview of the wireline channel and its disturbances. Throughout this thesis, we assume ADSL2*plus*-like parameters with -40 dBm average transmitted power [36].

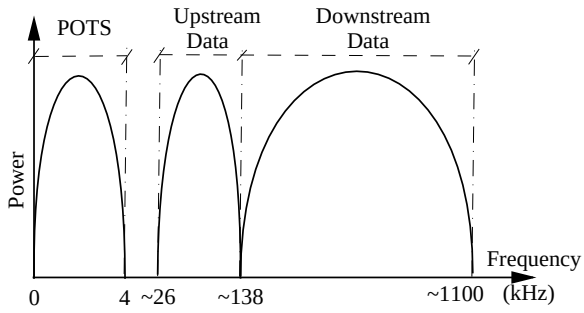

(a) The ADSL spectrum (FDD version)

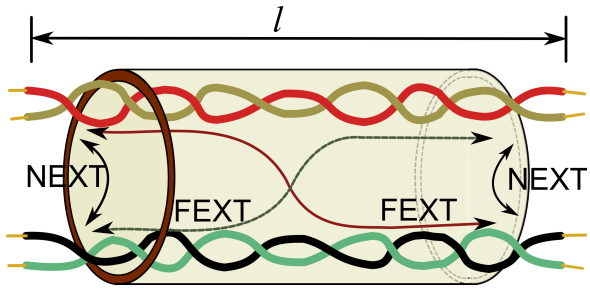

(b) NEXT and FEXT generation in UTP cables

Figure 1.2: ADSl cable spectrum and cross-talks

The old telephone cables used are commonly unshielded twisted pair (UTP) cables. These cables are usually found to be buried in bundled groups or layers. Therefore, some of these pairs may couple their signals into others either at the near ends, which is called near-end crosstalk (NEXT), or at the far ends, which is far-end crosstalk (FEXT), [25]. These are the stationary disturbances in the wireline environment. However, there are non-stationary impulses which are, sometimes, more critical than the previous impairments due to their high amplitudes [37]. In the following we introduce both, stationary and non-stationary noise.

1.3.1.1 Stationary crosstalk noise and AWGN

Figure 1.2.b depicts a model for NEXT and FEXT generation inside cables. Here, the transmitted signal from the upper pair is causing a crosstalk at the near end (NEXT) and the far end (FEXT) to the lower pair, and vice versa. However, in DSL environments, NEXT is a strong impairment, while FEXT is less harmful[2]. This is because FEXT has to propagate through the cable, which additionally attenuates the coupled signal before it reaches the other end [25]. Therefore, we consider only the NEXT disturbance; especially, the most disturbing NEXT signals for ADSL which are coming from T1 and HDSL[3] sources.

1.3.1.2 Non-stationary impulse noise

Non-stationary impulse noise can be generated by a variety of man-made equipment and natural effects, which are divided into external and internal (switching) events. The external events may be electronic discharges, fluorescent tubes, lightning, etc. Internal switching impulses are caused by switching processes, which have been diminished due to the new digital and software defined switches [37]. Sudden voltage changes occurring on the cable pairs were coupled to the next neighboring loops by means of NEXT and FEXT coupling paths. In this thesis, we study real measured impulses. However, to compute a pseudo PSD, the frequency domain of the impulse noise signal was calculated using an FFT assuming it to be a stationary event. This, of course, splits the analysis into two distinct events:

1. Without impulse noise: during non-impulsive reception.
2. With impulse noise: considering only the instant where the impulse noise is applied to the medium. Thus, the sampled data plus impulse FFT values are used to find a pseudo-periodogram (as in [37]).

1.3.1.3 Cable transfer function

For numerical results, an ADSL2 plus with 512 subcarriers [36] is considered using an Austrian 0.4-mm cable of length 2 km. Wireline channels are mainly characterized by propagation losses and linear distortions. The so-acled MAR 1 model, was first introduced by Mossun in [38], was selected due to its causal time domain impulse response. The series-impedance Z_s and shunt-admittance Y_p for the MAR 1 model is given by [39]:

$$Z_s = j2\pi f L_\infty + R_0 \left(\frac{1}{4} + \frac{3}{4} \sqrt{1 + \frac{as(f)(s(f)+b)}{(s(f)+c)}} \right) , \tag{1.1}$$

$$Y_p = 2\pi f C_f \cdot (j + \tan(\delta)) \quad \text{and} \quad s(f) = \frac{\mu_0 j f}{0.75^2 R_0} \approx \frac{jf}{447.6 R_0} , \tag{1.2}$$

for $\mu_0 = 4\pi 10^{-4}$[H/km]. The approximated seven MAR 1 model parameters for an Austrian 0.4-mm cable are given by Table 1.1.

[2] still very relevant in ADSL and VDSL where FEXT is avoided

[3] HDSL is not a strong disturbance

Table 1.1: MAR model parameters for 0.4 mm Austrian cable

Parameter	Definition	Value	Unit
R_0	DC resistance	291.973	[Ω/km]
L_∞	high frequency inductance	$6.3715{\cdot}10^{-4}$	[H/km]
a	Proximity factor a	1.37005	constant
b	Proximity factor b	$1.12015{\cdot}10^{-14}$	constant
c	Proximity factor c	0.161583	constant
δ	shunt-capacity loss angle	0.0058163	constant
$C_{1\text{MHz}}$	capacitance	$3.42986 \cdot 10^{-8}$	[F/km]

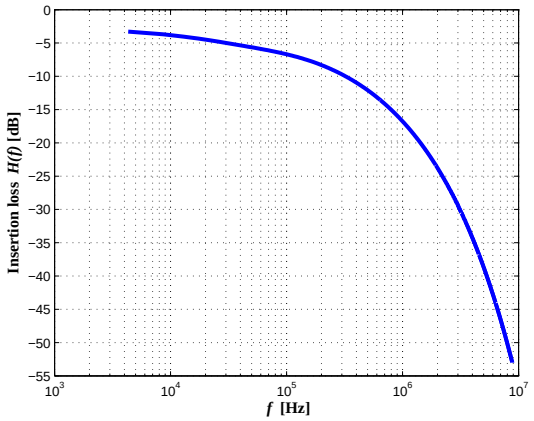

(a) MAR model frequency response

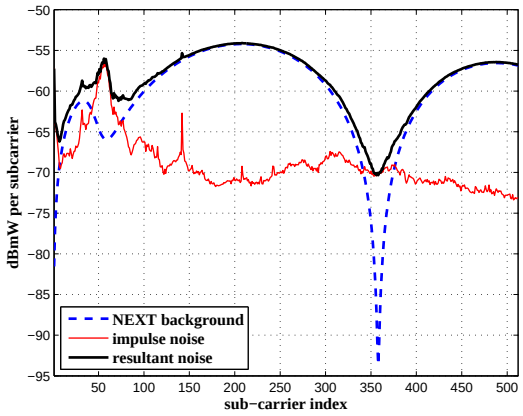

(b) Noise pseudo PSD during an impulse reception

Figure 1.3: Cable impulse response and Next + impulse disturbances

1.3.2 Unguided Channel: Wireless Dispersive Model

Unguided channels, e.g., wireless channel, differ in many respects from the wireline ones, first, the received signal is subject to the propagation path loss [34] which is inversely proportional to the distance between the base station (BS) and the mobile set (MS) and affected by obstacles and shadowing bodies, i.e., large scale fading (path-loss) model. Secondly, in wireless channels, we do not receive only a single dominant line-of-sight component, however, we receive replicas of the transmitted symbol. Each of these received signals is delayed by a certain delay τ_l, making the total impulse response spreads over a time τ_s. Thereby, the total channel impulse response is the superposition of all these received rays at the receive antenna.

Furthermore, when the receiver moves, the channel impulse response varies according to the movement speed and direction. This complicates the analysis and tracking of such fast varying environment. Figure 1.4 depicts the typical wireless channel situations.

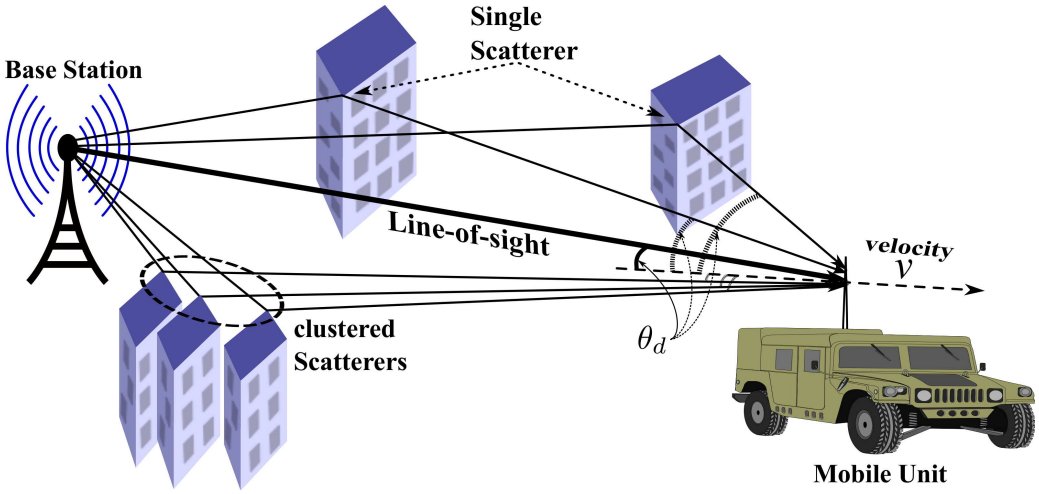

Figure 1.4: Practical wireless channel model

1.3.2.1 Single-path fast-fading wireless channel

As shown in Fig. 1.4, the received signal arrives at the receiver as a delayed-scattered version of the transmitted signal, each version has different gain and different phase [34]. If the differences between delays are much smaller than the symbol duration, these paths are said to be non-resolvable paths. This generally happens in narrow-band channels, if the scatterers are close to each other forming a cluster of condense scatterers [24]. The resulting path is assumed to be the summation of a all scattered/reflected rays that arrive at the receiver with different angle-of-arrival (AoA) and different amplitudes. Finally, these incident rays can be constructively or destructively summed resulting in a gain or a fade, respectively.

If the differences between the delays of these scattered paths are bigger than (or equal) the symbol duration, these paths can be resolved at the receiver antenna forming a tapped delay channel model [15]; this is discussed later in detail. However, for instance, we assume a single path channel or non-resolvable scatters for a moving receiver. As in Clarke [40] and Jakes [41], if a mobile unit moves with a velocity v, a frequency response will have a Doppler spreading

$$f_d = \frac{v}{\lambda} \cos \theta_d \ , \tag{1.3}$$

where λ is the radio wave length and θ_d is the angle-of-arrival (AoA) of the incident wave on a vertically polarized receive antenna. Corresponds to this frequency dispersion, the received phase is distorted with a Doppler phase shift, which is calculated as $\phi_d = 2\pi f_d t$, i.e., assuming a constant Doppler frequency. Therefore, the resultant impulse response can be written as a summation of S in-phase and quadrature-phase sinusoids as

$$E_z(t) = \sum_{s=1}^{S} c_{d_s} e^{j(\phi_{d_s} + \theta_{d_s})} \ , \tag{1.4}$$

where c_d is a real random variable with Gaussian distribution and θ_d is a random phase which has a uniform distribution in $[0, 2\pi)$. If the number of scatterers in the medium is sufficiently high, the summation of the scattered rays results in a complex Gaussian random variable with

a Rayleigh envelope [42][4]. Furthermore, if the reciprocal of this Doppler frequency (coherence time of the channel) is less than the symbol duration, the mobile unit will encounter a fast fading situation, i.e., time-selective characteristic. Jakes also showed in his book [41] that the

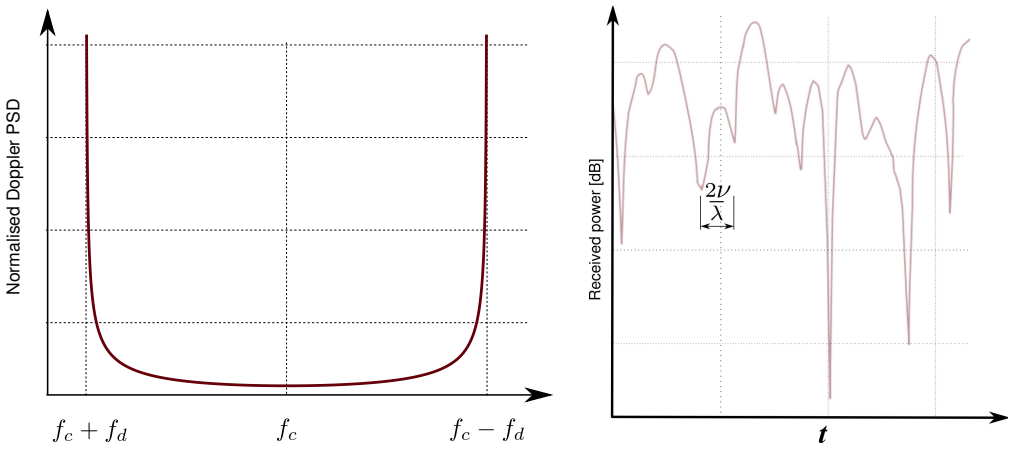

(a) Doppler power spectrum density (b) Fading every $\lambda/2$

Figure 1.5: Rayleigh fading due to Doppler effect

autocorrelation of the in-phase and the quadrature-phase parts of the channel are equal and has the distinct U-shape Doppler power spectrum density (PSD) (also called Jakes' PSD) as in Fig. 1.5.

This can be seen as a periodic fading which occurs every $\lambda/2$ displacement (as in Fig. 1.5.b) for a constant velocity ν. The normalized autocorrelation function in this case is approximated by a zero-order Bessel function of the first kind [15], such that

$$\rho_c(\tau_d) = J_0(2\pi f_d \tau_d) \ , \tag{1.5}$$

where τ_d is the sample spacing in seconds and ρ_c is the channel correlation coefficient. After any given time delay τ_d, the uncertainty indicator (channel uncertainty variance) σ_Ξ^2 is given by

$$\sigma_\Xi^2(\tau_d) = (1 - |\rho_c(\tau_d)|^2)\sigma_h^2 \ , \tag{1.6}$$

where σ_h^2 is the channel variance and σ_Ξ^2 is error variance. For a relatively slow Rayleigh fading channel, the upcoming channel values can be predicted using the previous instantaneous channel samples only. This can be utilized in the adaptive communication using limited feedback regimes, where we can feedback sub-samples of the channel, i.e., every T_s, and predict in between them. According to (1.6), the erroneous channel coefficient $\hat{h}(\tau, \tau_d)$ for a given path l is given by

$$\hat{h}(\tau, \tau_d) = h(\tau) - h_\Xi(\tau_d) \ , \tag{1.7}$$

where the channel errors $h_\Xi \in \mathcal{CN}(0, \sigma_\Xi^2)$. If there are other kinds of errors, e.g., quantization error and channel estimation errors besides the given delay τ_d, the channel errors $h_\Xi(\tau_d)$ can still be assumed to be white Gaussian [44] with the variance in (1.6).

[4]According to central limit theory, the mean of a sufficiently large number of i.i.d. variables will be approximately Gaussian distributed [43].

If a LoS or a significantly strong reflected component is received at the receive antenna, the channel mean will not be zero mean any more. This is known in literature as the Rician channel model, where a dominant path is received plus a number of highly scattered Rayleigh components. The ratio between the signal power of this strong component to the total power in the weak (reflected) ones is K. If K tends to zero, the channel tends to be a pure Rayleigh fading.

1.3.3 Multi-path Fast-fading Channel Impulse Response

Let us assume a dispersive channel $h(t)$ that has L_p resolvable channel paths (echoes). Some of these paths are assumed to be coming from a single scatterer passing through a single rout; the other paths may be subject to a non-resolvable dense scattering clusters, as discussed before. However, each of these echoes will hit the receive antenna at a different delay τ_l, amplitude β_l, and phases θ_l. For those paths coming through the non-resolvable dense scatterers (as in Fig. 1.4), their amplitudes and phases are generated from the superposition of these scattered rays in each cluster, as in Eqn. (1.4). Accordingly, the resulting time-variant channel impulse response of these L_p echoes, at an observation time t, can be defined as [45, 46]

$$h_{\text{scattered}}(t) \quad = \quad \sum_{l=0}^{L_p-1} \beta_l(t) p_l(t) e^{j\theta_l(t)} \delta(t-\tau_l(t)) \; , \tag{1.8}$$

where t is the observation time, β_l is an i.i.d. zero mean random complex Gaussian variable, θ_l is uniformly distributed in $[0, 2\pi)$, and p_l are the factors of a power delay profile which represents the power profile on each path [34]. If the reciprocal of the total delay spread, i.e., $1/\tau_s$, is much smaller than the coherence bandwidth of the channel, the frequency response will be very selective, i.e., different parts of the symbol band undergo different gains [15].

The gain for each path β_l is assumed to have a zero mean, i.e., the ensemble average of each path over time will vanish. This characterizes the Rayleigh fading channels to be zero mean fading models. However, if there exists a dominant path or a line of sight (LoS) component, the channel has a Rician distribution and with a mean K [42]. Now, consider a channel with Rician LoS component and a few other scattered Rayleigh paths; the overall impulse response can be written as

$$\begin{aligned} h(t) &= h_{\text{LoS}}(t) + h_{\text{scattered}}(t) \\ &= \underbrace{\sqrt{\frac{K}{K+1}}\, e^{j\theta_r(t)}}_{\text{Rician mean}} + \underbrace{\sqrt{\frac{1}{K+1}} \sum_{l=0}^{L_p-1} \beta_l(t) p_l(t) e^{j\theta_l(t)} \delta(t-\tau)}_{\text{Rayleigh component}} \; , \end{aligned} \tag{1.9}$$

where θ_r is the random phase of the LoS path, which has a uniform distribution $\in [0, 2\pi)$. Assuming a mobile unit that moves with 40 km/h and 9 different scattered paths. Each of these paths comes from multiple non-resolvable echoes with different Doppler frequencies that span the Doppler PSD in Fig. 1.5.a. The frequency-selective fast-fading channel response in time and frequency is shown in Fig. 1.6.

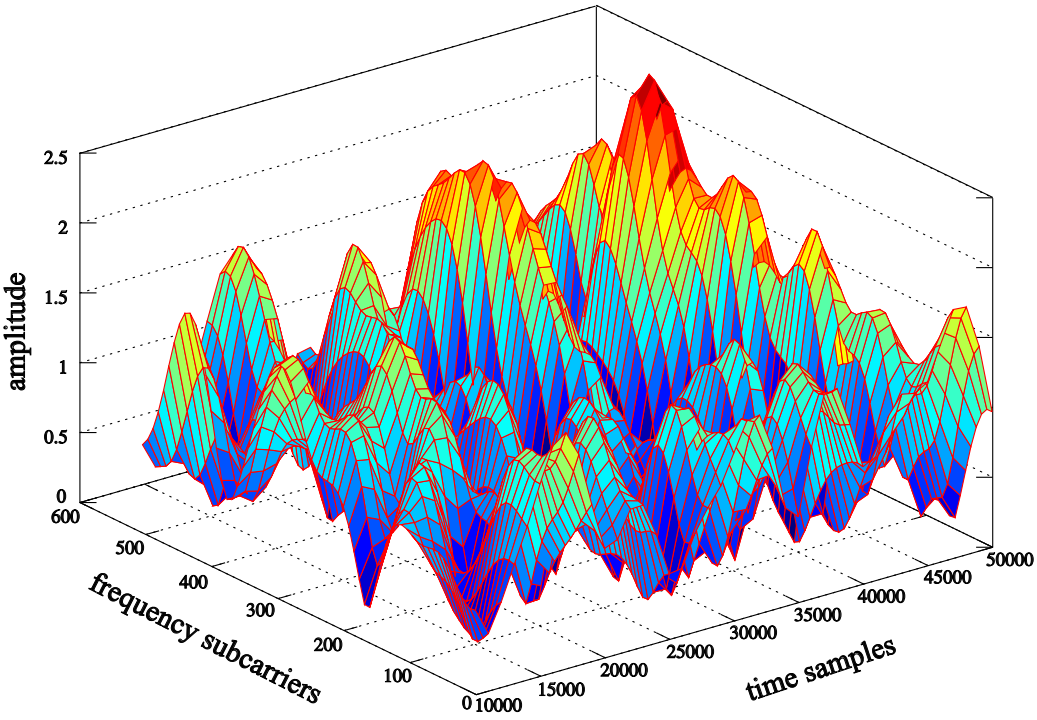

Figure 1.6: Frequency-selective fast-fading wireless channel using multicarrier transmission

In the following section, more details about the research methodology and the thesis contribution are outlined.

Outline of the Thesis

This thesis is basically divided into 6 chapters.

Chapter 2: Diagonalized Transmission Systems

This Chapter introduces some of the diagonalized digital transmission approaches. For single user with SISO channel, OFDM (or DMT in wireline) is used, which succeeds in diagonalizing the channel convolution matrix in frequency domain using discrete Fourier transform (DFT) and inverse DFT (IDFT). We show also how Fourier meets Shannon by adapting power and rates over these diagonal subcarriers using water-filling in order to maximize the channel capacity. In multiple-output multiple-input (MIMO) channels, the diagonalization is done across the spatial dimensions using a simple pre- and post-processing matrices. For multiuser transmission, we discuss both diagonal and non-diagonal multiuser transmission

Chapter 3: Novel UEP Adaptive Algorithms

In this chapter, we introduce some of the readily available bit-loading algorithms in multicarrier modulation. Thereafter, our modifications to these algorithms are discussed in order to realize UEP using adaptive margin separation. Thus, we started with a straightforward subcarrier partitioning method that uses a complex binary search. Later, we introduce another two partitioning schemes, which are less complex. Additionally, we introduce two sorting mechanism. The first one is an intuitive method, and the second is more robust against non-stationary noises.

Chapter 4: Adaptive UEP Multilevel Modulation

In this chapter, we introduce a new technique that utilizes, especially, the greedy bit-loading algorithms, e.g., Hughes-Hartogs, to realize UEP using hierarchical and non-hierarchical modulation. This we call multilevel modulation, where our UEP bit-loading is free to allocate unused subcarriers or embed more constellation resolutions using hierarchical modulation.

Chapter 5: MIMO Channel with Prioritized Transmission

We extend our modified UEP bit-loading to adapt a MIMO-OFDM system. Hereto, we utilize both frequency subcarriers and eigenchannels. This is carried out by exploiting the suitability to sort and adapt the given spatial and spectral resources using our proposed sorting and partitioning schemes. Furthermore, we examine our developed approaches under different limited feedback schemes. Finally, we propose an adaptive successive interference cancellation algorithm that preserves our UEP profile.

Chapter 6: Prioritized Multiuser Transmission

Our developed bit-loading algorithms in Chapter 5 are used for realizing multiuser transmission with different QoS. Using different multiple access schemes, i.e., frequency division multiple access and space division multiple access, we succeed to preserve the users' resources orthogonal or, at least, with minimum interference. Our proposed algorithms succeed in preserving the selected UEP profile with a performance gain compared to the non-adaptive non-prioritized schemes.

Chapter 7: Conclusion and Future Work

Finally, this chapter contains the conclusions and our possible future working directions.

Chapter 2

Diagonalizing Transmission Systems

In order to achieve simultaneous (non-interfering) communication, the channel has to be diagonalized using pre- and post-processing at the transmitter and receiver sides, respectively. This requires building a closed-loop communication with a readily available channel state information (CSI) at both sides. Thereby, in orthogonal frequency division multiplexing (OFDM), multiple-input multiple-output (MIMO), and MIMO-OFDM combination, the channel is converted into a set of parallel sub-channels in frequency and space. For the single-user case, these parallel channels are utilized for simultaneous data transmission. However, these resources can also be used for scheduling multiple users according to their requirements and sub-channel qualities. In the following, we introduce the diagonalization process in OFDM, MIMO, and across multiuser transmission using MIMO-OFDM.

2.1 Orthogonal Multi-Carrier Transmission

Conventional multicarrier modulation succeeds in avoiding the ISI by slowing down the data transmission rate. This has been done by extending the symbol interval through parallel transmission using N narrow frequency subcarriers (non-overlapping), each of which carries a lower symbol rate. However, in total, the required data rate is still maintained. In orthogonal frequency division multiplexing (OFDM), the subcarriers are allowed to overlap, however, with orthogonality maintained by guaranteeing no inter-carrier interference (ICI) at the center frequency of the other subcarriers. In other words, the frequency response of any subcarrier is zeros at multiples of the subcarrier spacing $\Delta f = \frac{1}{T_s}$, where T_s is the OFDM total symbol duration (see Fig. 2.1).

The subcarriers in the DFT domain are modulated in frequency using an inverse discrete Fourier transform (IDFT), as follows (see Fig. 2.2 for more details)

$$x[n] = \frac{1}{\sqrt{N}} \sum_{k=0}^{N-1} s[k] e^{-j\frac{2\pi}{N}kn} \qquad n = 0, ..., N-1 \,, \tag{2.1}$$

Assuming an ideal channel response ($h(t) = \delta(t)$), the received time-domain symbol is orthog-

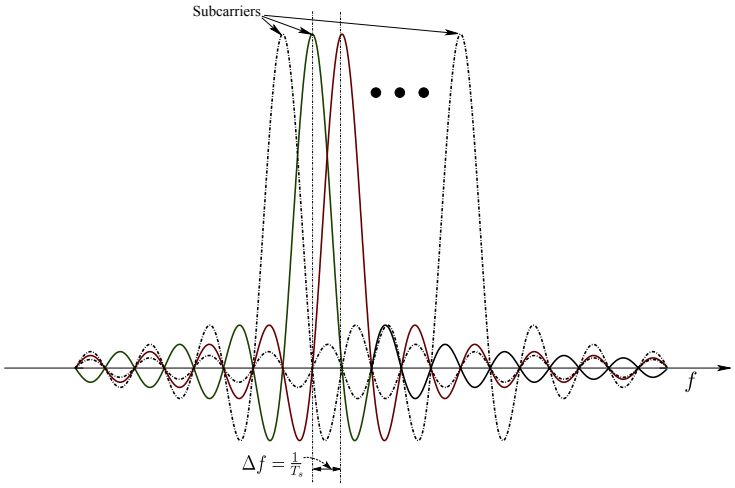

Figure 2.1: OFDM overlapping subcarriers with Δf spacing

onalized at the receiver, using the DFT operator, producing the overlapped sinc(s) depicted in Fig. 2.1.

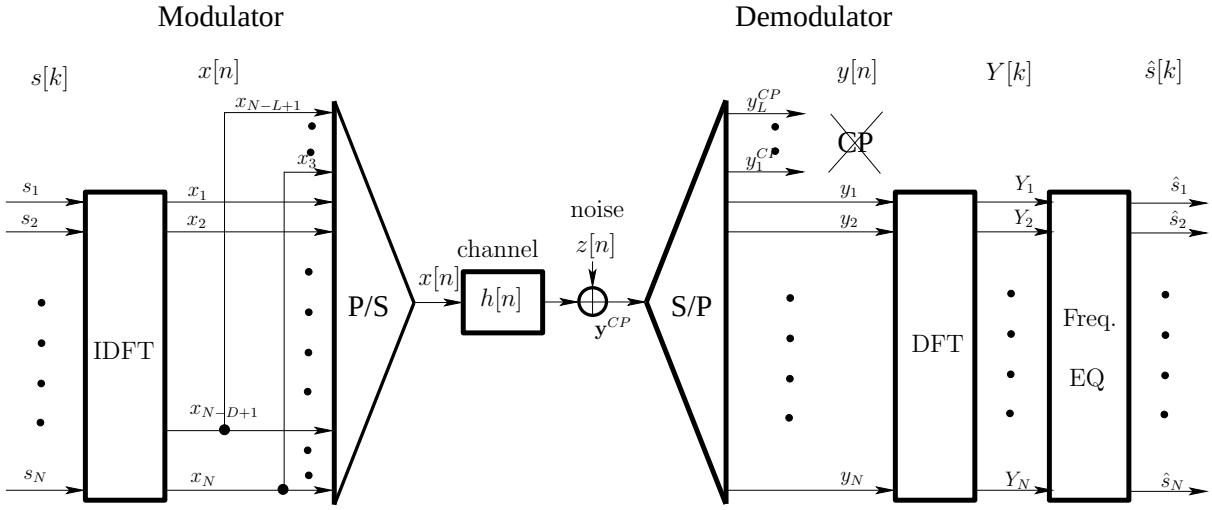

Figure 2.2: OFDM transmitter and receiver block diagram

However, in the presence of a dispersive channel (any non-ideal channel response) with an impulse response length of L_p taps and N transmitted time-domain samples, the linear convolution between them results in $N+L_p-1$ time samples at the receiver input. To maintain orthogonality, the convolution with the channel has to be circular convolution (with only N samples at the receiver output). In order to make the linear convolution pretend to be a circular one, the rear samples (in each OFDM time symbol) have to be copied in front of the time symbol as a cyclic prefix (CP) in time (as shown in Fig. 2.3).

Additionally, dividing the wide frequency band into N narrower subcarriers helps to maintain a flat fading on each subcarrier [47], however, with a single channel gain that varies from subcarrier to another [48], [49], and [25].

As shown in Fig. 2.2 and discussed before, the CP is removed from the sampled input $y[n]$.

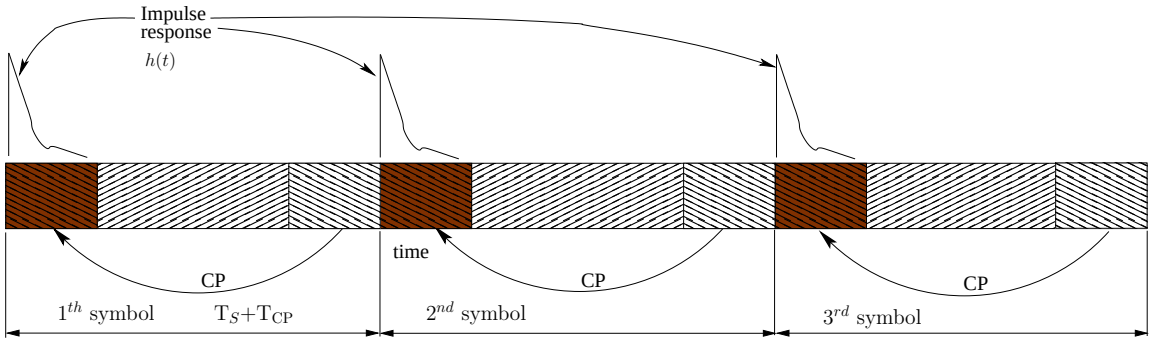

Figure 2.3: Cyclic prefix insertion in OFDM

Thereafter, the remaining time symbol is demodulated at the receiver using a DFT as follows

$$\mathbf{Y}[k] = \frac{1}{\sqrt{N}} \sum_{n=0}^{N-1} y[n] e^{j2\pi \frac{n}{N} k} \qquad k = 0, ..., N-1 \ , \tag{2.2}$$

where $Y[k]$ are the DFT domain samples and $y[n]$ is the sampled received signal, which results from convolving the sampled transmitted signal $x[n]$ (with the CP incorporated into it) and the channel sampled impulse response $h[n]$ as follows

$$y[n] = \sum_{l=0}^{N-1} h[l] x[n-l] + n_0[n] \tag{2.3}$$

As depicted in Fig. 2.2, the CP is removed from each received OFDM time-domain symbol. In wireless systems, the CP is selected to be longer than the channel impulse response (CIR) in order to maintain orthogonality (no ICI) and to overcome ISI between OFDM symbols [47]. Additionally, this converts the channel in the DFT domain to a pure complex multiplication. After the DFT orthogonalization process, a frequency domain equalizer (EQ) is simply a scaling by the inverse of the variable complex channel coefficients. This is sufficient to combat the channel multi-path effect [25, 50].

2.1.1 OFDM Matrix Diagonalization

To have a deeper understanding of the orthogonalization in OFDM, it is worth to study the diagonalization of the channel discrete convolutional (Toeplitz) matrix using a DFT and a CP at the receiver. Assuming no CP to be added for instance, the matrix representation of (2.3) can be written as

$$\mathbf{y} = \mathbf{C}\mathbf{x} + \mathbf{n} \ , \tag{2.4}$$

where $\mathbf{C}$ is the convolutional matrix of Toeplitz form, $\mathbf{n}$ is the added noise vector, and $\mathbf{x}$ is the inverse DFT modulated transmitted vectors, which is defined as

$$\mathbf{x} = \mathbf{W}^{-1}\mathbf{s} \ , \tag{2.5}$$

where $\mathbf{s}$ is the quadrature amplitude modulated (QAM) vector [50] and $\mathbf{W}$ is the DFT (Vandermonde) normalized matrix, defined as

$$\mathbf{W} = \frac{1}{\sqrt{N}} \begin{bmatrix} 1 & 1 & 1 & \cdots & 1 \\ 1 & w_N & w_N^2 & \cdots & w^{(N-1)} \\ 1 & w_N^2 & w_N^4 & \cdots & w^{2(N-1)} \\ \vdots & \vdots & \vdots & & \vdots \\ 1 & w_N^{N-1} & w_N^{2(N-1)} & \cdots & w_N^{(N-1)(N-1)} \end{bmatrix}, \tag{2.6}$$

where $w = e^{\frac{j2\pi}{N}}$ is the N^{th} root of unity, i.e., $x^N = 1$ for a cyclotomic $x^n = 1$ [51] and the factor $1/\sqrt{N}$ is to make $\mathbf{W}$ a unitary matrix such that it satisfies the following condition

$$\mathbf{W} \cdot \mathbf{W}^* = \mathbf{I}\,. \tag{2.7}$$

Exploiting the fact in (2.7), the inverse DFT (IDFT) matrix $\mathbf{W}^{-1}$ can simply be expressed using the Hermitian operator, i.e., $\mathbf{W}^*$. After adding a cyclic prefix of length C_p to $\mathbf{x}$ and neglecting the noise vector $\mathbf{n}$ (for mathematical clarity only), the received vector $\mathbf{y}$, i.e., the full matrix representation of the orthogonal multicarrier system multiplied by the transmitted vector $\mathbf{x}$, is given as

$$\mathbf{y} = \begin{bmatrix} \overbrace{\begin{matrix} h_{C_p} & \cdots & h_1 \\ 0 & \ddots & \vdots \\ \vdots & \ddots & h_{C_p} \\ \vdots & & 0 \\ \vdots & & \vdots \\ \vdots & & \vdots \\ \vdots & & \vdots \\ \vdots & & \vdots \\ 0 & \cdots & 0 \end{matrix}}^{\text{CP extension } (N\times C_p)} & \overbrace{\begin{matrix} h_0 & 0 & \cdots & \cdots & \cdots & \cdots & \cdots & 0 \\ h_1 & h_0 & \ddots & & & & & \vdots \\ \vdots & \ddots & \ddots & \ddots & & & & \vdots \\ h_{C_p} & & \ddots & \ddots & \ddots & & & \vdots \\ & \ddots & \ddots & \ddots & \ddots & \ddots & & \vdots \\ h_{L_p-1} & & \ddots & \ddots & \ddots & \ddots & \ddots & \vdots \\ 0 & h_{L_p-1} & & \ddots & \ddots & \ddots & \ddots & \vdots \\ \vdots & \ddots & \ddots & & \ddots & & \ddots & 0 \\ 0 & \cdots & 0 & h_{L_p-1} & \cdots & h_{C_p} & \cdots & h_1 \quad h_0 \end{matrix}}^{\text{Toeplitz original channel } (N\times N)} \end{bmatrix} \overbrace{\begin{bmatrix} x_{N-C_p} \\ x_{N-C_p+1} \\ \vdots \\ x_{N-1} \\ \cdots\cdots \\ x_0 \\ x_1 \\ \vdots \\ x_{N-1} \end{bmatrix}}^{(N+C_p)\times 1}, \tag{2.8}$$

which is only circulant when $C_p \geq L_p - 1$, i.e., greater than the CIR tail $L_p - 1$. After applying CP, $x_k(-i) = x_k(N-i)\ \forall\ i = 1, 2, ..., C_p$ [52]. Thus, the matrix in (2.8) can be folded producing a new circulant matrix $\tilde{\mathbf{C}}$ which has an effective $N \times N$ entries as follows

$$\begin{bmatrix} y_0 \\ y_1 \\ \vdots \\ \vdots \\ \vdots \\ y_{N-1} \end{bmatrix} = \overbrace{\begin{bmatrix} h_0 & 0 & \cdots & 0 & h_{C_p} & \cdots & h_1 \\ h_1 & h_0 & \ddots & & \ddots & \ddots & \vdots \\ \vdots & \ddots & \ddots & \ddots & & \ddots & h_{C_p} \\ h_{L_p-1} & & \ddots & \ddots & \ddots & & 0 \\ 0 & h_{L_p-1} & & \ddots & \ddots & \ddots & \vdots \\ \vdots & \ddots & \ddots & & \ddots & \ddots & 0 \\ 0 & \cdots & 0 & h_{L_p-1} & \cdots & h_1 & h_0 \end{bmatrix}}^{\text{circulant channel matrix } \tilde{\text{C}}\ (N\times N)} \begin{bmatrix} x_0 \\ x_1 \\ x_2 \\ \vdots \\ x_{N-1} \end{bmatrix}_{N\times 1}. \tag{2.9}$$

Exploiting the fact that the DFT and the IDFT matrices diagonalize any given circulant matrix [53], one can rewrite the circulant matrix $\tilde{\mathbf{C}}$ as

$$\tilde{\mathbf{C}} = \mathbf{W}^* \mathbf{G} \mathbf{W} \,, \tag{2.10}$$

where $\mathbf{G}$ is an $N \times N$ diagonal matrix which contains the complex channel coefficients on every subcarrier, i.e., $\mathbf{G} = \mathrm{diag}\,(h_0, h_1, \cdots, h_{N-1})$. Hence, the circulant channel matrix in (2.9), using the same process of applying the DFT matrix on (2.4), one can rewrite as

$$\begin{aligned} \mathbf{Y} &= \mathbf{W}\mathbf{y} = \overbrace{\mathbf{W}}^{\mathrm{DFT}} \left(\overbrace{\tilde{\mathbf{C}}\mathbf{W}^*\mathbf{s}}^{\mathbf{y}} + \mathbf{n} \right) \,, \\ &= \mathbf{W}\mathbf{W}^*\mathbf{G}\mathbf{W}\mathbf{W}^*\mathbf{s} + \mathbf{W}\mathbf{n} \,. \end{aligned} \tag{2.11}$$

Using the fact that $\mathbf{G}$ is a diagonal matrix and $\mathbf{W}\mathbf{W}^* = \mathbf{I}$, i.e., (2.7), one can rewrite (2.11) as

$$\mathbf{Y} = \begin{bmatrix} h_0 & 0 & \cdots & 0 \\ 0 & h_1 & \ddots & \vdots \\ \vdots & \ddots & \ddots & 0 \\ 0 & \cdots & 0 & h_{N-1} \end{bmatrix} \begin{bmatrix} s_0 \\ s_1 \\ \vdots \\ s_{N-1} \end{bmatrix} + \mathbf{W}\mathbf{n} \,, \tag{2.12}$$

where $|h_k|$ are the channel coefficients in DFT domain.

Diagonalizing the matrix in this way looks very efficient, however, the fact that primitive factor w is symmetric and periodic has not been utilized [54]. This results in an $O(N^2)$ multiply-accumulate (MAc) operations [55] (using DFT) applying either the previous matrix computations or the direct summation in (2.1) and (2.2). The fast Fourier transform (FFT) and the inverse fast Fourier transform (IFFT) exploit these two properties of the primitive w. Therefore, efficient computations of only $O(N \log_2 N)$ MAc can be performed.

Now, it is clear that every element in $\mathrm{diag}(\mathbf{G})$ represents parallel channels with individual gains. Therefore, adapting to the channel conditions achieves a higher capacity. Water-filling is a method used to maximize the capacity in parallel channels; this is described in the next section.

2.1.2 Water-filling: Does Multi-carrier Achieve the Channel Capacity?

As known from Shannon's findings, the channel capacity in case of an AWGN channel with an average channel gain-to-noise ratio $\overline{\nu}$ is given by

$$C|_{\mathrm{AWGN}} = \mathrm{E}\left(\log_2(1+\nu)\right) = \log_2(1+\mathrm{E}(\nu)) = \log_2(1+\overline{\nu}) \,, \tag{2.13}$$

where C is average capacity in bits/Hz and $\nu = \lambda/\sigma_n^2$, as λ is the channel coefficient squared ($|h|^2$) and σ_n^2 is the noise variance. For varying fading channel conditions with a CSI at the receiver only and a constant power (unity) at the transmitter, the average capacity is given by

$$C|_{\mathrm{fading}} = \int_0^\infty \log_2(1+\nu) P(\nu) d\nu \,, \tag{2.14}$$

where $P(\nu)$ is the portion of time where the channel has a gain g, this defines the temporal information at the receiver. Applying Jensen's inequality [24],

$$\mathrm{E}\left(\log_2(1+\nu)\right) = \int_0^\infty \log_2(1+\nu)P(\nu)d\nu \leq \overbrace{\log_2(1+\mathrm{E}(\nu)) = \log_2(1+\overline{\nu})}^{\text{AWGN case}} \ . \tag{2.15}$$

This means that fading channels have a lower average capacity than AWGN channels, if the channel temporal information is only known at the receiver. In order to maximize the capacity for a given channel, a priori CSI is mandatory at the transmitter.

If we assume a slowly fading OFDM channel, the total channel capacity can be maximized by only allocating a proper amount of power on each subcarrier. Assuming N communication channels are given with a variable channel-to-noise value on each sub-channel, the power can be allocated following the following optimization problem

$$\begin{aligned} &\text{maximize} && \sum_{k=0}^{N-1} \log_2\left(1+\nu_k p_k\right) \\ &\text{subject to} && \mathbf{p} \succeq 0 \text{ and }, \ \mathbf{1}^{\mathrm{T}}\mathbf{p} = P_T \ , \end{aligned} \tag{2.16}$$

where p_i represents the power on the i^{th} subcarrier and P_T denotes the maximum allowed power. The "log" operator is a non-decreasing non-convex function [56], however, the "$-\log$" is not. Therefore, one may rewrite this problem as the equivalent minimization problem.

$$\begin{aligned} &\text{minimize} && -\sum_{k=0}^{N-1} \log_2\left(\frac{1}{\nu_k}+p_k\right) \\ &\text{subject to} && \mathbf{p} \succeq 0 \text{ and }, \ \mathbf{1}^{\mathrm{T}}\mathbf{p} = P_T \ . \end{aligned} \tag{2.17}$$

We introduce a Lagrangian multiplier $1/\mu$ considering only the second side conditions in (2.17), i.e., $\mathbf{1}^{\mathrm{T}}\mathbf{p} = P_T$. This is valid since $\mathbf{p} \succeq 0$ will always lead to a slack[1] Lagrange variable [56]. Thus, no need to include it in the Lagrangian process, however, we consider its effect. Therefore, the obtained Karush-Kuhn-Tucker (KKT) conditions [57] are

$$\mathbf{1}^{\mathrm{T}}\mathbf{p} = P_T, \quad \left(1/\mu - 1/\left(1/\nu_k + p_k\right)\right) = 0, \quad \forall\ k = 1, ..., N \ . \tag{2.18}$$

The last condition is only valid if $p_k = 0$ or $\mu = (1/\nu_k + p_k)$, where $p_k \geq 0$ and $1/\nu_k > 0\ \forall\ k$, the power can simply be written as

$$p_k = \max\left\{0, \mu - 1/\nu_k\right\} \ , \tag{2.19}$$

such that $\sum_{k=0}^{N-1} \max\left\{0, \mu - 1/\nu\right\} = P_T$, i.e., as depicted in Fig. 2.4.

2.1.3 Multi-level Water-filling: QoS vs Rate Maximization

Since the previous power allocation uses the error-free Shannon capacity formula, (2.19) might be of less practical importance. We assume a non-error-free system that allows for an arbitrary BER according to the required QoS. This is considered as a shift from the original SNR operating

[1] Is used to represent the difference between the optimal and upper limit (unused or excess value).

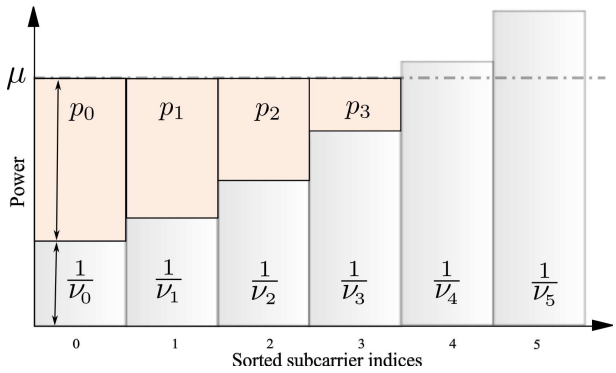

Figure 2.4: Water-filling power allocation for a multicarrier system

point, i.e., the SNR shift is known as noise margin or the so-called noise "gap" γ [32]. Thereby, the modified Shannon capacity now reads

$$C = \log_2(1 + \nu/\gamma) \quad \text{bits/sec/Hz} \; . \tag{2.20}$$

Following the same steps from (2.17) to (2.19), using the previous equation, the modified version of the power allocation in (2.19) is given by

$$p_k = \max\{0, \mu - \gamma/\nu_k\} \; . \tag{2.21}$$

Figure 2.5 depicts the power allocation in OFDM according to (2.21) with different γ(s). Using high noise margin values is equivalent to a low SNR, where the water-filling algorithm utilizes the strong subcarriers only. As γ decreases, the power spreads more over the weaker subcarriers until it achieves a constant power allocation at the lowest noise margin. This also means that it is more suitable to consider constant power allocation at very low SNR.

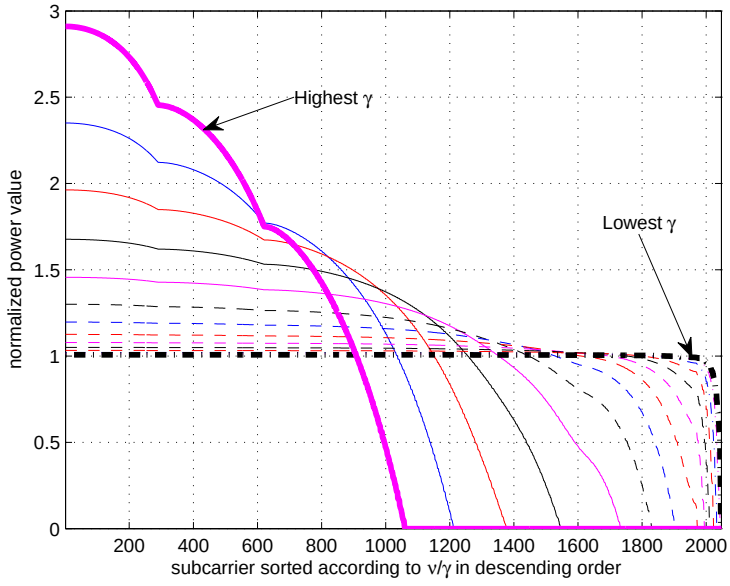

Figure 2.5: Water-filling using multilevel QoS in OFDM system with 2048 sorted subcarriers

2.1.4 Adaptive OFDM with Prioritized Transmission

We know from the multicarrier literature that there exist quite some bit-loading algorithms, which devote different number of bits to different subcarriers based on their carrier gain-to-noise ratio (CGNR), i.e., assuming a constant symbol-error ratio (SER). All these algorithms are mainly utilizing the diagonalization discussed in the previous section. In chapters 3 and 4, we will discuss the possibilities of utilizing such diagonalization in order to realize prioritized data transmission by only considering modifying the preexisting bit-loading algorithms.

2.2 Single-user Adaptive MIMO System

Unlike single-antenna communications, multiple-antenna regimes are capable of enhancing the transmission through utilizing different spatial signatures by applying space-time processing which achieves spatial diversity. [58, 59]. This requires at least one end of the communication links to have multiple antennas. Typically, the base-station of a mobile system can easily deploy an antenna array. This is clear since the required antenna spacing and the extra cost can be easily handled at the base-station rather than the basic mobile unit. During the down-link, when the base-station transmits to the mobile station, the channel is defined as multiple-input single-output (MISO) channel. However, during the up-link, when the mobile-station transmits to the base-station, this is known as single-input multiple-output (SIMO) channel.

If the receiver and the transmitter deploy multiple antenna elements or smart antenna arrays on their front ends, the channel between them is defined as multiple-input multiple-output (MIMO) channel. This leads to a higher diversity gain, however, it also increases the capacity when multiple symbols are multiplexed on different antennas. Nevertheless, the multiplexing gain cannot be utilized if the diversity is fully utilized. This is known as the MIMO paradigm [59]. Many efforts are dedicated to a trade-off between spatial diversity and spatial multiplexing. Adaptive spatial modulation has been proposed in [60]. This technique succeeds in selecting adaptively diversity and spatial multiplexing or a hybrid combination of them that utilizes the CSI. In Chapter 4, we present an adaptive scheme that automatically switches between diversity and multiplexing based on the channel conditions and CSI.

In literature, spatial multiplexed symbols are detected using layered successive interference techniques (BLAST[2] techniques). In this scheme, the CSI is not required at the transmitter (CSIT), however, it is mandatory at the receiver; CSI is a crucial adaptation requirement to perform precoding at the transmitter.

However, dealing with CSI in multiple-antenna requires a better understanding of the different MIMO channels and the channel estimation accuracy. Thereafter, we will study the optimum pre- and post-processing in order to minimize inter-stream interference. In the following, we describe the various MIMO channel models.

[2]BLAST stands for Bell labs LAyered Space-Time architecture; V-BLAST [61] and D-BLAST [62] stands for Vertical and Diagonal BLAST, respectively.

2.2.1 MIMO Channel Models

In this discussion, we restrict our selves to a flat fading channel that is constant during a complete symbol duration. Hence, we exclude subcarrier k and the time t subscripts from our system equations. Now, assume that the mobile station and the base station are equipped with N_R and N_T antennas, respectively. This forms a MIMO channel matrix $\mathbf{H}$. If the scatterers, the antenna spacing d_Δ, and the transmitter-receiver spacing D_Δ are relatively high, the channel matrix has a zero-mean circularly symmetric complex Gaussian (ZMCSCG) distribution, where $\mathbf{H}_w \in \mathbb{C}^{\mathrm{N_R} \times \mathrm{N_T}} \mathcal{N}(0, \mathbf{I})$ [63].

If the transmit and receive antennas are exposed to a limited scattering environment that results in a non-identity correlation matrix, this can be modeled in different ways. We selected the simplest separable correlation model, namely, the Kronecker model [64]. This model facilitates the separation of the transmitter correlation matrix $\mathbf{R}_\mathrm{t}$ and the receiver correlation matrix $\mathbf{R}_\mathrm{r}$, i.e., the receiver directions are uncorrelated with the transmitter directions. This model is not valid if the channel does not support this separation [65]. However, it is still valid for a relatively small number of antennas or large antenna spacing ($d_\Delta >> \lambda/2$), which we assumes in here. There are other models that deal with more practical antenna configurations and relax this separability by allowing any arbitrary coupling between the correlation properties at the transmitter and receiver, e.g., the Weichselberger model [66]. However, it is out of the scope of our research and we will only consider the Kronecker correlation model.

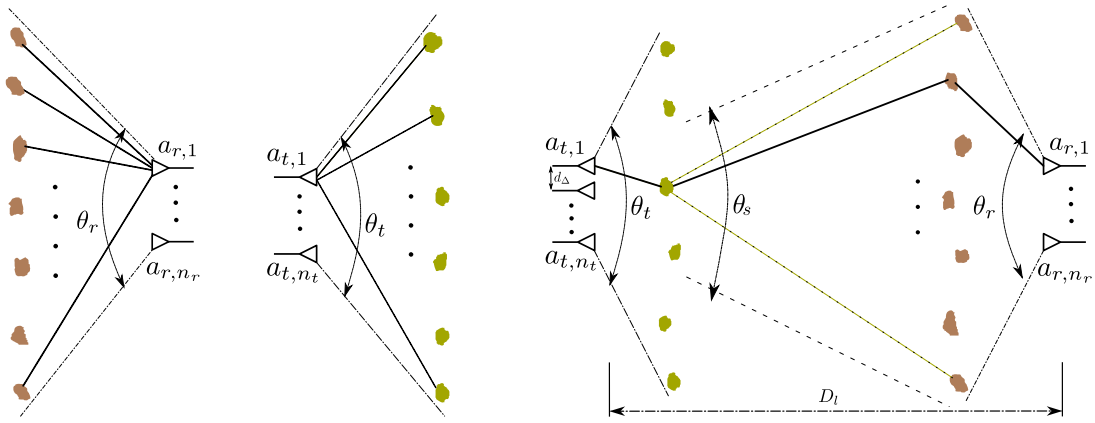

(a) SIMO RX (b) MISO TX (c) MIMO transceiver

Figure 2.6: SIMO (a) and MISO (b) channel model and double bounce MIMO channel model in (c)

To understand MIMO channel models, let us assume a SIMO channel that exploits receiver diversity using N_R receive antennas as in Fig. 2.6.a. The incident plane-wave angles of arrival (AoAs) span an angular spread of θ_r radians assuming a uniform distribution $\in [0, 2\pi)$ [63]. The resulting fading correlation is governed by θ_r and the antenna spacing d_Δ [63]. Assume S -sufficiently high- uncorrelated scatterers around N_R receive antennas, the channel $\mathbf{H}_{N_R,S}$ between the scatterers antenna is given by

$$\mathbf{H}_{N_R,S_R} = \mathbf{\Phi}_\mathrm{r} \mathbf{H}_{w_{S_R}} \qquad \text{with} \qquad \mathbf{H}_{w_{S_R}} \sim \mathbb{C}\mathcal{N}\left(\mathbf{0}, \mathbf{I}_{S_R}\right) , \tag{2.22}$$

where $\mathbf{\Phi}_{\mathrm{r}}^{N_R \times S}$ is a matrix defining the electrical path lengths between the N_R antenna elements and the S_R scatterers for uniformly distributed AoAs $\theta_{r,s}$. Assuming an odd number of scatterers S_R, where $\mathbf{\Phi}_{\mathrm{r}}(n,s)$ with the corresponding AoA, $\theta_{r,s}$, is given by [63]

$$[\mathbf{\Phi}_{\mathrm{r}}(\, n,s)] = \frac{1}{S} \sum_{i=-\frac{S-1}{2}}^{\frac{S-1}{2}} e^{-j2\pi(n-s)d_{\Delta}\sin(\theta_{r,i})} \; . \tag{2.23}$$

Since $\mathbf{\Phi}_{\mathrm{r}}$ is related to the correlation matrix between the receive antenna elements, the receiver correlation matrix is given by

$$\mathbf{R}_{\mathrm{r}} = \mathrm{E}\left\{\mathbf{H}_{N_R,S}\mathbf{H}_{N_R,S}^{*}\right\} = \mathbf{\Phi}_{\mathrm{r}}\mathrm{E}\left\{\mathbf{H}_{w_{S_R}}\mathbf{H}_{w_{S_R}}^{*}\right\}\mathbf{\Phi}_{\mathrm{r}}^{*} = \mathbf{\Phi}_{\mathrm{r}}\mathbf{I}\mathbf{\Phi}_{\mathrm{r}}^{*} = \mathbf{\Phi}_{\mathrm{r}}\mathbf{\Phi}_{\mathrm{r}}^{*} \; . \tag{2.24}$$

For large values of the angle spread and/or d_{Δ}, $\mathbf{R}_{\mathrm{r}}$ will converges to an identity matrix, which means that the receive antenna elements are uncorrelated. Using the analogy between the SIMO and the MISO channels, as in Fig. 2.6.b, one can similarly obtain the transmitter correlation matrix to be

$$\mathbf{R}_{\mathrm{t}} = \mathrm{E}\left\{\mathbf{H}_{S_T,N_T}^{*}\mathbf{H}_{S_T,N_T}\right\} = \mathbf{\Phi}_{\mathrm{t}}^{*}\mathbf{\Phi}_{\mathrm{t}} \; , \tag{2.25}$$

where $\mathbf{\Phi}_{\mathrm{t}}^{S_T \times N_T}$ is a matrix defining the electrical path lengths between the S_T scatterers and the N_T antenna elements. Similar to (2.22), the channel matrix between the transmit antenna elements and the scatterers is given by

$$\mathbf{H}_{S_T,N_T} = \mathbf{H}_{w_{S_t}}\mathbf{\Phi}_{\mathrm{r}} \qquad \text{with} \qquad \mathbf{H}_{w_{S_t}} \sim \mathbb{CN}\left(\mathbf{0},\mathbf{I}_{S_T}\right) \; . \tag{2.26}$$

Accordingly, a MIMO channel with double-bounce scatterers, as in Fig 2.6.c, can be analysed using the SIMO and the MISO correlation models in (2.22) and (2.26). Therefore, one can divide the total MIMO channel (in Fig. 2.6.c) into three clusters: scatterers-to-receiver (N_R-S_R), scatterer-to-scatterer (S_R-S_t), and transmitter-scatterer (S_R-N_T). The total MIMO channel according to (2.22) and (2.26) is given by

$$\mathbf{H}^{N_T \times N_T} = \mathbf{\Phi}_{\mathrm{r}}\mathbf{H}_{w_{S_R}}\mathbf{X}^{S}\mathbf{H}_{w_{S_t}}\mathbf{\Phi}_{\mathrm{t}} \; , \tag{2.27}$$

where $\mathbf{X}^{S}$ is the matrix which connects the two scatterer layers. If the number of scatterers at the transmitter and the receiver is equal and sufficiently high, one can assume $\mathbf{X}^{S}$ to be an identity matrix. This is always valid for uncorrelated antenna elements, which means that the spatial scatterers are uncorrelated. However, if $\mathbf{X}^{N_R \times N_T}$ becomes a rank-deficient matrix, the overall MIMO channel is also a rank-deficient matrix. An extreme case happens when $\mathbf{X}^{S}$ is an all-ones matrix, i.e., rank-1 matrix. This is known in literature as a *key-hole* MIMO channel [63]. Again, using the central-limit theory, the product $\mathbf{H}_{w_{S_R}}\mathbf{H}_{w_{S_t}}$ is found to follow a Rayleigh distribution, where the elements of the product matrix are zero-mean circularly symmetric complex Gaussian (ZMCSCG) variables [67].

If the separable Kronecker channel validity conditions (in [65]) are fulfilled, (2.27) can be rewritten according to (2.24) and (2.25) as follows [63]

$$\mathbf{H} = \mathbf{R}_{\mathrm{r}}^{1/2}\mathbf{H}_{w}\mathbf{R}_{\mathrm{t}}^{1/2} \; , \tag{2.28}$$

where $\mathbf{H} \in \mathbb{C}^{N_R \times N_T}$ is the overall MIMO channel matrix and $\mathbf{H}_w \in \mathbb{C}^{N_R \times N_T}$ is a matrix with i.i.d ZMCSCG entries.

The correlation matrix at the receiver $\mathbf{R}_{\mathrm{r}}$ can be interpreted as a noise-coloring process. A perfect whitening post-processing at the receiver can significantly reduce its effect. Additionally, we assume that the receiver is surrounded with a dense scatter environment, which makes it spatially uncorrelated, i.e., $\mathbf{R}_{\mathrm{r}} = \mathbf{I}$. However, throughout this thesis, we assume that the transmitter is surrounded by either insufficient or very far scatterers that make it spatially correlated with a non-identity correlation matrix $\mathbf{R}_{\mathrm{t}}$. We assume that the receiver can estimate $\mathbf{R}_{\mathrm{t}}$ accurately, due to its slow variations. Henceforth, the receiver can easily estimate $\mathbf{H}_w$ using one of the different channel estimation techniques, e.g., minimum mean-square error (MMSE) estimation. Then, $\mathbf{H}$ is fed back to the transmitter with accumulated channel estimation errors, quantization errors, and feedback delay errors (as in Chapter 1, (1.7)) represented in the Gaussian random matrix $\mathbf{\Xi} \in \mathcal{C}\ \mathcal{N}(0, \sigma^2_{\mathbf{\Xi}}\mathbf{I})$, where $\sigma^2_{\mathbf{\Xi}}$ is the variance of the error [68]. This updates (2.28), according to (1.7), to be

$$\mathbf{H} = (\mathbf{H}_w + \mathbf{\Xi})\, \mathbf{R}_{\mathrm{t}}^{1/2} \,. \tag{2.29}$$

In the following, we discuss the impact of knowing the CSI at the transmitter and how this can be exploited to increase the system throughput and enhance the performance.

2.2.2 Closed-loop MIMO Systems

Let us consider a general MIMO channel matrix $\mathbf{H} \in \mathbb{C}^{N_R \times N_T}$ which is perfectly known at both transmitter and receiver, i.e., $\sigma^2_{\mathbf{\Xi}} = 0$. If a vector $\mathbf{x} \in \mathbb{C}^{N_T}$ is transmitted, the received vector $\mathbf{y} \in \mathbb{C}^{N_R}$ is given by

$$\mathbf{y} = \mathbf{H}\mathbf{x} + \mathbf{n} \qquad \text{and} \qquad \mathbf{x} = \mathbf{F}\mathbf{s} \,, \tag{2.30}$$

where $\mathbf{n}$ is the additive white Gaussian noise, $\mathbf{s}$ is the vector of uniformly distributed modulated symbols such that $\mathrm{E}[\mathbf{s}\mathbf{s}^*] = \mathbf{I}_{N_T}$, and $\mathbf{F}$ is a precoding matrix, such that

$$\mathbf{F} = \mathbf{U_T}\mathbf{P}^{\frac{1}{2}} \,, \tag{2.31}$$

where $\mathbf{P}$ is a diagonal matrix containing the power values (also called spatial-shaping matrix) and $\mathbf{U_T}$ is the beamforming (beam-steering) unitary matrix [69].

The beamforming matrix $\mathbf{U_T}$ is selected to match the channel spatial signature to fulfil certain criteria, e.g., to maximize the signal-to-interference and noise ratio (SINR) or minimize the mean-square error [59]. Figure 2.7 depicts the MIMO closed-loop communication, where the pre-coder matrix is $\mathbf{F}$ and the post-coder (linear equalizer) is $\mathbf{W}$. The CSI is assumed to be fed back through a limited/quantized separate feedback channel with a certain delay τ_d. The adaptive algorithm is asumed to be located at the transmitter, which acts as a base-station in a down-link scenario. This algorithm is supposed to adapt the bit and power allocation as well as the precoding matrix. In the following, we will especially discuss the MIMO channel diagonalization, maximizing the mutual information, and designing the optimum receiver.

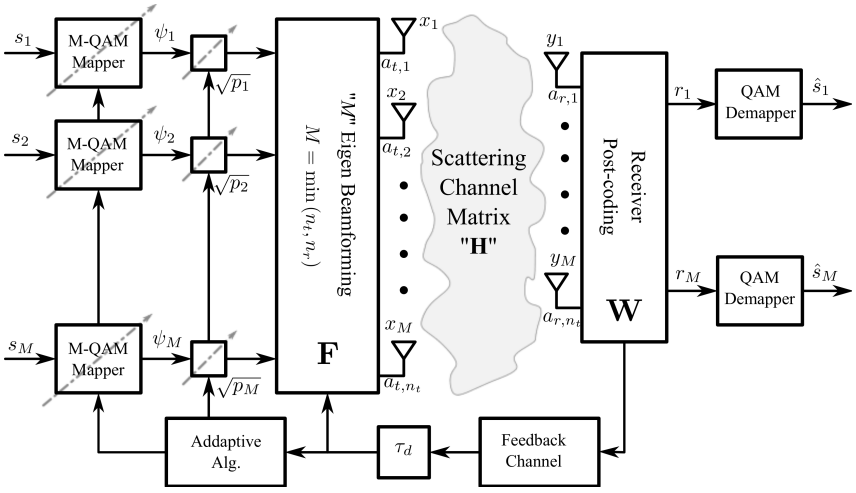

Figure 2.7: Closed-loop MIMO system with different CSI qualities

2.2.2.1 Diagonalizing the MIMO channel

In order to realize an adaptive MIMO communication, the channel matrix $\mathbf{H}$ has to be diagonalized in order to resolve the channel gains into non-interfering links, i.e., to adapt each link separately. From matrix theory, one can easily obtain the singular value decomposition (SVD) of any general (non-square) channel matrix $\mathbf{H}$ as follows

$$\mathbf{H} = \mathbf{U}\mathbf{\Sigma}\mathbf{V}^* \,, \tag{2.32}$$

where $\mathbf{U} \in \mathbb{C}^{\mathbf{N_R}\times\mathbf{N_R}}$ and $\mathbf{V} \in \mathbb{C}^{\mathbf{N_T}\times\mathbf{N_T}}$ are unitary matrices, such that $\mathbf{U}^*\mathbf{U} = \mathbf{I}_{N_R}$ and $\mathbf{V}^*\mathbf{V} = \mathbf{I}_{N_T}$. $\mathbf{\Sigma} \in \mathbb{R}^{\mathbf{N_R}\times\mathbf{N_T}}$ is a diagonal matrix containing the singular values of $\mathbf{H}$, which are the square-roots of the eigenvalues of the Hermitian matrix $\mathbf{H}^*\mathbf{H}$. In this case, $\mathbf{H}$ has R eigenbeams, where $R \leq \min(N_R, N_T)$. In order to diagonalize the total channel matrix, one has to multiply it by $\mathbf{V}$ and $\mathbf{U}*$ from the right and the left hand side, respectively. This means to multiply by $\mathbf{V}$ at the transmitter and $\mathbf{U}*$ at the receiver [24], i.e., $\mathbf{U_T} = \mathbf{V}$ and $\mathbf{W} = \mathbf{U}^*$. Thereby, Eqn. (2.30) can be written as

$$\begin{aligned} \mathbf{r} &= \mathbf{W}\mathbf{y} = \mathbf{U}^*\left(\mathbf{H}\mathbf{V}\mathbf{P}^{\frac{1}{2}}\mathbf{s}\right) + \mathbf{n} \\ &= \mathbf{U}^*\mathbf{U}\mathbf{\Sigma}\mathbf{V}^*\mathbf{V}\mathbf{P}^{\frac{1}{2}}\mathbf{s} + \mathbf{U}^*\mathbf{n} \\ &= \mathbf{\Sigma}\left(\mathbf{P}^{\frac{1}{2}}\mathbf{s}\right) + \hat{\mathbf{n}} \,, \end{aligned} \tag{2.33}$$

where $\hat{\mathbf{n}} = \mathbf{U}^*\mathbf{n}$, which can still be considered white (non-colored) noise, since $\mathbf{U}$ is a unitary matrix. However, if a digital amplitude modulation, e.g., QAM, is used, the decision borders of the detector (for more than 2 bits/symbol) will be very sensitive to the channel gain or the singular values in $\mathbf{\Sigma}$. Therefore, one has to scale (2.33) by $\mathbf{\Sigma}^{-1}$. This means that the optimum receiver in this case is a zero-forcing (ZF) receiver, which maintains orthogonality. However, the diagonalization is destroyed when the channel is not perfectly known at both sides, i.e., transmitter and receiver. Thus, the weak singular values will limit the overall performance due to noise enhancement. This can be avoided using an optimum adaptive scheme that suppresses the weak singular values (called also eigenchannels).

Another very important advantage in the SVD MIMO scheme, even without further power allocation, is its scalable diversity gain. As known in literature, Alamouti in [58], succeeded to formulate a 2×2 MIMO system that achieves a full-rate (rate-1) full-diversity without any CSI at the transmitter. However, it is not easily expanded to more antennas. Therefore, an SVD MIMO scheme with dominant eigen-beam transmission, i.e., transmitting over the strongest value in $\mathbf{\Sigma}$, can achieve a better performance with transmit-diversity and MRC at the receiver.

Figure. 2.8 shows a performance gain of 2.3 dB for the SVD scheme over the Alamouti space-time block-code (STBC). However, this requires a perfect CSI at the transmitter. Even a 10% error in the CSI will result in an unavoidable error floor.

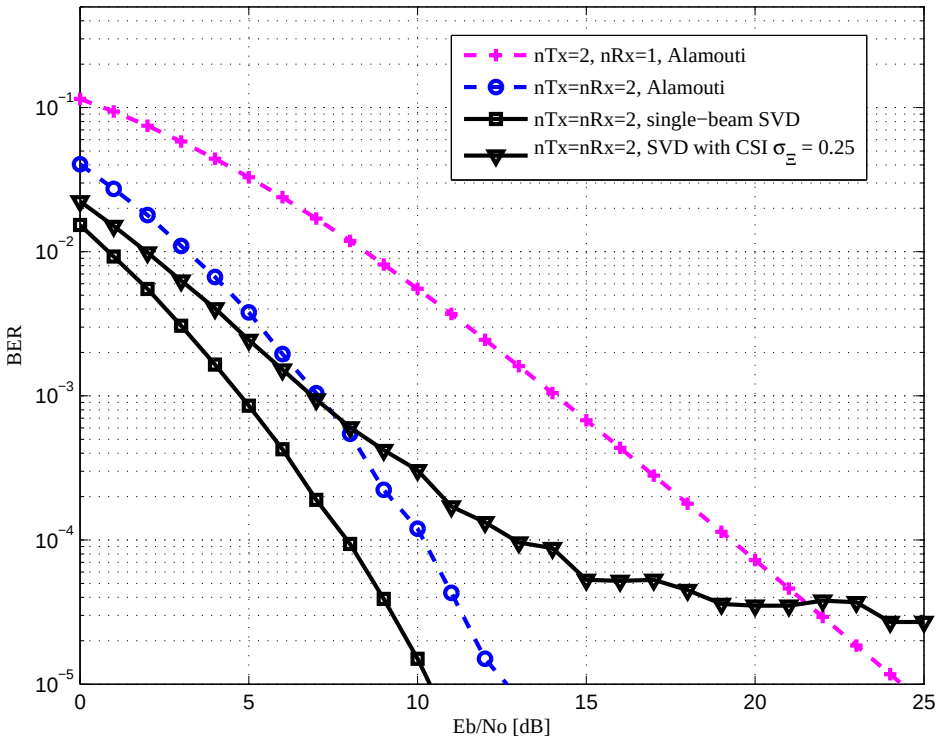

Figure 2.8: BER for BPSK modulation using Alamouti STBC and single-beam SVD MIMO

2.2.2.2 Optimum receiver design and achieving channel capacity

Knowing that the input power across the transmitted beams is the covariance matrix $\mathbf{Q_x}$ of the input vector $\mathbf{x}$, i.e., determined by $\mathbf{Q_x} = \mathrm{E}[\mathbf{x}\mathbf{x}^*]$, such that

$$\mathrm{Tr}\left(\mathbf{Q_x}\right) = \mathrm{Tr}\left(\mathrm{E}\left[\mathbf{F}\mathbf{F}^*\right]\right) = P_T \ , \tag{2.34}$$

where $\mathrm{Tr}(\mathbf{A})$ denotes the trace of a matrix $\mathbf{A}$ and P_T is the maximum allowed transmit power from the N_T antennas. If the output power is uniformly distributed, the diagonal elements of $\mathbf{P}$ are constant and equal to P_T/N_T.

In [67], the MIMO channel capacity is determined by maximizing the mutual information between the input vector $\mathbf{x}$ and the output vector $\mathbf{y}$, i.e., $\max I(\mathbf{x};\mathbf{y})$, given that the trace of the covariance matrix is P_T. This results in

$$C = \max_{\mathrm{Tr}(\mathbf{R_x})=P_T} \log_2 \left[\det \left(\mathbf{I}_{N_R} + \frac{1}{\sigma_n^2} \mathbf{H} \mathbf{Q_x} \mathbf{H}^* \right) \right] , \tag{2.35}$$

where $\det(\mathbf{A})$ denotes the determinant of matrix $\mathbf{A}$. In order to maximize the mutual information given a maximum transmit power constraint, the following optimization problem needs to be solved with respect to $\mathbf{Q_x}$

$$\begin{aligned} \text{maximize} \qquad & \log_2 \left[\det \left(\mathbf{I}_{N_R} + \frac{1}{\sigma_n^2} \mathbf{H} \mathbf{Q_x} \mathbf{H}^* \right) \right] \\ \text{subject to} \qquad & \mathrm{Tr}\left(\mathbf{Q_x}\right) = P_T \quad \text{and} \quad \mathbf{Q_x} \succeq 0 \, , \end{aligned} \tag{2.36}$$

where $\mathbf{Q_x} \succeq 0$ defines it as positive semidefinite matrix. The proof of (2.36) is given in Appendix F. The problem defined in (2.36) can be solved similar to the classical water-filling in (2.16) by exploiting the fact that $\det(\mathbf{I}+\mathbf{XY}) = \det(\mathbf{I}+\mathbf{YX})$ and $\mathbf{Q_x} = \mathbf{FF}^*$. Now, similar to the problem formulation in (2.17), we can reformulate (2.36) to be

$$\begin{aligned} \text{minimize} \qquad & -\log_2 \left[\det \left(\sigma_n^2 \mathbf{I}_{N_T} + \mathbf{F}^* \mathbf{H}^* \mathbf{H} \mathbf{F} \right) \right] \\ \text{subject to} \qquad & \mathrm{trace}\left(\mathbf{Q_x}\right) = P_T \quad \text{and} \quad \mathbf{Q_x} \succeq 0 \, , \end{aligned} \tag{2.37}$$

where the value inside the determinant is the reciprocal of the mean-square error (MSE) of a MIMO channel [70] (see Appendix F for more detail). Maximizing the mutual information is equivalent to minimizing $\log_2(\det[\mathbf{E}])$, where $\mathbf{E}$ is the MSE of (2.30) (as stated in Appendix F, Section F.4) and is defined as

$$\mathbf{E} = \left(\sigma_n^2 \mathbf{I}_{N_T} \beta + \mathbf{F}^* \mathbf{H}^* \mathbf{H} \mathbf{F} \right)^{-1} , \tag{2.38}$$

where $\beta = 1$ indicates an MSE case and $\beta = 0$ indicates zero-forcing case. Hence, for $\beta = 1$, the optimum receiver is an MMSE receiver matrix (Wiener filter) $\mathbf{W}$ in Fig. 2.7), where $\mathbf{W}$

$$\begin{aligned} \mathbf{W} &= \left[\mathbf{H} \mathbf{F} \left(\sigma_n^2 \mathbf{I}_{N_R} + \mathbf{H} \mathbf{F} \mathbf{F}^* \mathbf{H}^* \right)^{-1} \right]^* \\ &= \left(\sigma_n^2 \mathbf{I}_{N_T} + \mathbf{F}^* \mathbf{H}^* \mathbf{H} \mathbf{F} \right)^{-1} \mathbf{F}^* \mathbf{H}^* \, . \end{aligned} \tag{2.39}$$

Therefore, (2.33) can be written as

$$\mathbf{r} = \mathbf{W}\mathbf{y} = \left(\sigma_n^2 \mathbf{I}_{N_T} \beta + \mathbf{F}^* \mathbf{H}^* \mathbf{H} \mathbf{F} \right)^{-1} \mathbf{F}^* \mathbf{H}^* \left(\mathbf{H}\mathbf{F}\mathbf{s} + \mathbf{n} \right) \, . \tag{2.40}$$

In this case, the only sources of interference are the other transmitted beams. Therefore, we have to keep these beams parallel to maintain orthogonality and to maintain low MSE. This is simply achieved by diagonalizing the MSE cost function $(\sigma_n^2 \mathbf{I}_{N_T} \beta + \mathbf{F}^* \mathbf{H}^* \mathbf{H} \mathbf{F})$[3]. By decomposing the Hermitian matrices $\mathbf{H}^*\mathbf{H}$ using the eigenvalue decomposition (EVD), we obtain

$$\mathbf{H}^*\mathbf{H} = \mathbf{V}\ \mathbf{D}\ \mathbf{V}^*, \tag{2.41}$$

[3] which is not exactly achieved due to the cross-talks arise from the constant $\sigma_n^2 \mathbf{I}_{N_T}$, i.e., $\beta = 1$

where $\mathbf{D} = \text{diag}\{\lambda_0, \cdots, \lambda_{R-1}\}$, λ_s are the eigenvalues $\forall s = 0..R-1$, and $\mathbf{V}$ is the unitary matrix that contains (on its columns) the eigenvectors of $\mathbf{H}^*\mathbf{H}$. Now, by selecting $\mathbf{F} = \mathbf{U_T P}^{1/2} = \mathbf{V P}^{1/2}$, $\mathbf{E}$ is converted into a pure diagonal matrix as follows

$$\begin{aligned}\mathbf{E} &= \left(\sigma_n^2 \mathbf{I}_{N_T}\beta + \mathbf{F}^*\mathbf{H}^*\mathbf{H}\mathbf{F}\right)^{-1} \\ &= \left(\sigma_n^2 \mathbf{I}_{N_T}\beta + \mathbf{P}^{1/2}\mathbf{V}^*\mathbf{V}\mathbf{D}\mathbf{V}^*\mathbf{V}\ \mathbf{D}\ \mathbf{V}^*\mathbf{F}\right)^{-1} \\ &= \left(\sigma_n^2 \mathbf{I}_{N_T}\beta + \mathbf{P}^{\frac{1}{2}}\mathbf{D}^2\mathbf{P}^{\frac{1}{2}}\right)^{-1} . \end{aligned} \tag{2.42}$$

After substituting (2.42) in (2.40), the detected vector $\mathbf{r}$ is given by

$$\mathbf{r} = \mathbf{W}\mathbf{y} = \left(\sigma_n^2 \mathbf{I}_{N_T}\beta + \mathbf{P}\mathbf{D}^2\right)^{-1} \mathbf{P}\mathbf{D}^2\mathbf{s} + \tilde{\mathbf{n}} , \tag{2.43}$$

where $\tilde{\mathbf{n}} = \mathbf{W}\mathbf{n}$ is a colored noise vector due to the Wiener filter. Since a MMSE receiver is used, the inter eigen-interference is not completely suppressed. In order to have (2.43) as a purely diagonal matrix, β should be set to zero, i.e., $\mathbf{W}$ is converted into a ZF spatial equalizer to have

$$\mathbf{W} = \mathbf{P}^{-1/2}\mathbf{D}^{-1} . \tag{2.44}$$

The results in (2.44) is used to convert (2.37) into parallel channels. In this case, the water-filling for perfectly diagonalized ZF receiver is achieved by solving the Lagrangian equation corresponds to (2.36), which is converted using (2.44) and the matrix properties in Appendix G ($\log_2\left[\det(\mathbf{A})\right] = \log_2 \prod_i \lambda_{A_i}$) to

$$\begin{aligned} &\text{maximize} \quad \log_2\left[\prod_{s=0}^{R-1}\left(1 + p_s\lambda_s/\sigma_n^2\right)\right] \\ &\quad \text{or} \\ &\text{maximize} \quad \sum_{s=0}^{R-1}\log_2\left[\left(1 + p_s\lambda_s/\sigma_n^2\right)\right] \\ &\text{subject to} \quad \sum_{s=0}^{R-1} p_s = P_T \quad \text{and} \quad p_s \geq 0\ , \forall\ s = 0..R-1 . \end{aligned} \tag{2.45}$$

The KKT conditions in this case is similar to (2.18), except for that the summation here runs over R only (not N). Thus, we get the water-filling power values across the eigenbeams s as

$$p_s = \max\left(0, \mu - \frac{\sigma_n^2}{\lambda_s}\right), \tag{2.46}$$

where p_s are the diagonal elements of $\mathbf{P}$ in (2.44), σ_n^2 is the noise variance, and μ is the water-level in case of ZF using perfect CSI at the transmitter [67].

For MMSE receiver, the cross-talk are not perfectly eliminated due to the constant $\sigma_n^2\mathbf{I}_{N_T}$. Thus, we expect another power allocation that solves the following optimization (starting from (2.37)

and knowing that $\log_2\left[\det(\mathbf{A})\right] = \log_2 \prod_i \lambda_{A_i}$)

$$\begin{aligned} &\text{minimize} \quad -\log_2\left[\prod_{s=0}^{R-1}\left(\sigma_n^2 + p_s\lambda_s\right)\right] \\ &\quad\text{or} \\ &\text{minmize} \quad -\sum_{s=0}^{R-1}\log_2\left[\left(\sigma_n^2 + p_s\lambda_s\right)\right] \\ &\text{subject to} \quad \sum_{s=0}^{R-1} p_s = P_T \quad \text{and} \quad p_s \geq 0\ ,\forall\ s = 0..R-1\ . \end{aligned} \tag{2.47}$$

Therefore, water-filling-like power allocation can be found as in Appendix E, (D.33), as follows

$$p_s = \left(0, \mu\frac{\sigma_n}{\sqrt{\lambda_s}} - \frac{\sigma_n^2}{\lambda_s}\right)\ . \tag{2.48}$$

where p_s are the diagonal element of $\mathbf{P}$ in (2.43).

2.2.2.3 Capacity of MIMO channel using imperfect CSI

Throughout this thesis, we assume an ergodic channel, where its statistical properties (such as its mean (ensemble average) and variance) can be deduced from a sufficiently long realization [34]. Thus, the ergodic capacity for a MIMO system is the expectation (ensemble average) of (2.35). In general, for imperfect CSI with an arbitrary error variance $\sigma_{\boldsymbol{\Xi}}^2$ (as in (1.7)) and antenna correlation at the transmitter that results in an error covariance matrix $\mathbf{I} + \sigma_{\boldsymbol{\Xi}}^2\mathbf{I}$ (as given in Appendix F (F.26)), the average channel capacity is given by [24][4]

$$\begin{aligned} C &= \mathrm{E}\left[\max_{\mathrm{Tr}(\mathbf{R_x})=P_T} \log_2\left[\det\left(\mathbf{I}_{N_R} + \frac{1}{\sigma_n^2\left(1+\sigma_{\boldsymbol{\Xi}}\mathrm{Tr}(\mathbf{Q_x})\right)}\mathbf{H}\mathbf{Q_x}\mathbf{H}^*\right)\right]\right] \\ &= \mathrm{E}\left[\max_{\sum_{s=0}^{R-1} p_s = P_T} \sum_{s=0}^{R-1}\log_2\left[\left(1 + \frac{p_s\lambda_s}{(1+\sigma_{\boldsymbol{\Xi}}^2 P_T)\sigma_n^2}\right)\right]\right]\ , \end{aligned} \tag{2.49}$$

where $\mathrm{Tr}(\mathbf{Q_x}) = P_T$, i.e., assuming uncorrelated antennas at both sides. If $\sigma_{\boldsymbol{\Xi}}^2 = 0$, i.e., perfect CSI, the capacity formula in (2.49) is equivalent to (2.35).

Figure 2.9 depicts the performance of a perfect CSI (solid lines) and imperfect CSI with a dominant delay/quantization error equal to 10% of the instantaneous channel variance (dashed lines). The dotted lines refer to a higher correlation channel, taken from [71]. Therefore, it is clear that the highly correlated channels have significantly lower capacity, as it turns down the rank of the Gaussian channel matrix.

Besides feeding back the instantaneous channel values or the delayed/quantized values (with the error matrix $\boldsymbol{\Xi}$), there are other feedback methods that depend on the channel statistics. The channel mean feedback [44] is a low-rate feedback scheme which is suitable for slow fading channels that vary arround a certain mean K, e.g., Rician fading in (1.9). However, if the channel has no mean or the variations are much faster than the feedback rate, the input covariance

[4] see derivation in Appendix F, Section F.4

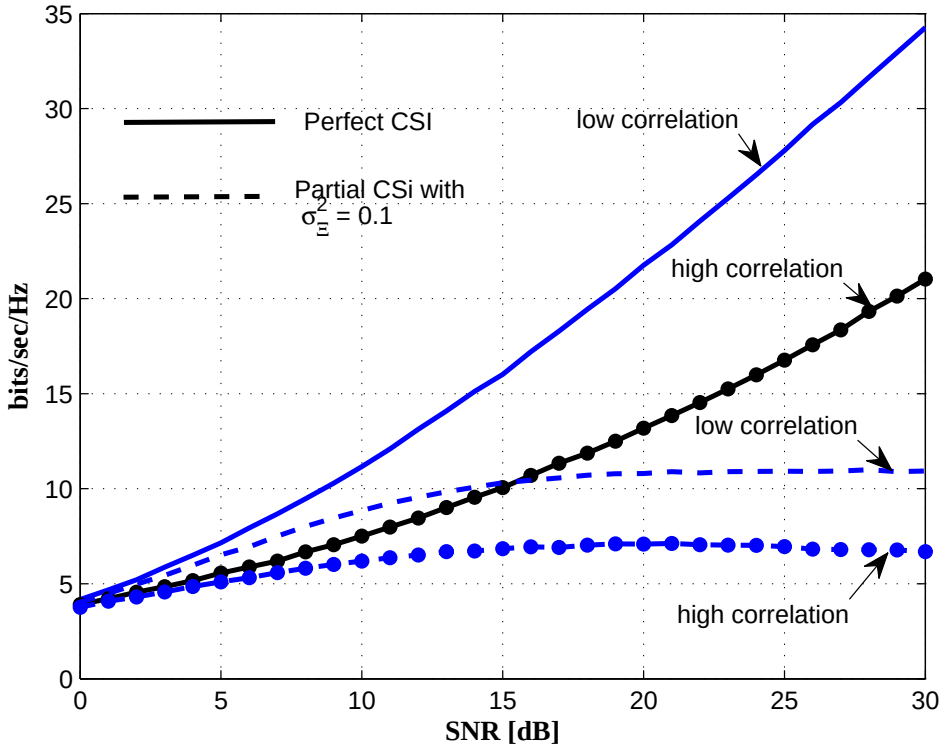

Figure 2.9: The ergodic capacity of a 4×4 MIMO system considering perfect CSI, imperfect CSI, and antenna correlation

matrix $E(\mathbf{x}\mathbf{x}^*) = \mathbf{R_t}$ knowledge can still enhance the channel capacity [72]. Since $\mathbf{R_t}$ depends only on the spatial information, it is not required to have extra feedback along the spectral or the temporal indices, i.e., the spatial covariance information for every frequency is sufficient for adaptation.

2.2.3 Adaptive MIMO with Prioritized Transmission

Utilizing the previous diagonalization in MIMO channels, i.e., across the spatial indices, allows for adapting each eigenbeam separately. Thus, one can allocate power and bits to each of these eigenbeams, independently, according to their eigenvalues. Moreover, the variations of these eigenvalues, i.e., from one channel realization to another, enriches the chance of devoting different data with different priority. In MIMO-OFDM, one can even think of each subcarrier as a new channel realization. This gives the freedom to realize adaptive modulation in frequency and space. In Chapter 5, we will discuss the possibilities of adapting the transmission link to the different channel values in order to realize different bit loads with different priorities.

2.3 Multiuser Adaptive MIMO System

A multiuser system divides the given *multiuser channel* resources amongst different users. The problem in the previous sentence is the word "divide", where appropriate division means to track the users channel quality and their required QoS. Traditionally, when the users' CSI had not be considered in the old mobile system, e.g. global system mobile (GSM) [34], the multiuser channels have been divided into equal time and frequency slots; named as time division multiple access (TDMA) and frequency division multiple access (FDMA), respectively. Another dimension has been added to the previous two, during the cellular mobile era as well, which is code-division multiple access (CDMA) [34]. In CDMA, the users' data are sent simultaneously in time and frequency, however, encoded with unique special codes associated with each user. These codes are chosen to be orthogonal or even quasi-orthogonal such that, every user's data is assumed to be a useful information for him and a noise to the others applying the multiuser interference (MUI) concept [15]. However, in this case, the MUI is assumed to have a white Gaussian distribution, i.e., white Gaussian noise. Figure 2.6 shows a multiuser shared system (Fig. 2.6.a), where only one user (at a time or frequency) is scheduled for transmission and other users remain idle.

In order to minimize the MUI in CDMA, a restricted transmit-power control (TPC) is applied at the transmitter of each user. The duty of the TPC is to adjust the emitted power of the user in order to maximize the quality of reception, which is related to the SINR. The overall emitted power and the power of each user is adjusted according to an overall power constraint and the user's required QoS, respectively. In the downlink scenario, the power adaptation is straightforward [24]. However, it is more complicated in uplink transmission, since each user will take an arbitrary position to the base-station and to his neighboring users. Hence, assuming an uplink with N_u interfering users, the SINR for the u^{th} is given by

$$\text{SINR}_u = \frac{g_u p_u}{\sigma_n^2 + \rho \sum\limits_{j \neq j}^{N_u} g_j p_j} , \quad u = 0, ..., N_u - 1 , \tag{2.50}$$

where g_u and p_u are the channel gain and the transmitted power of the u^{th} user, respectively. ρ is the interference reduction factor, where $\rho = 0$ in TDMA or FDMA case and $\rho \leq 1$ in CDMA case. Hence, p_u can be adapted such that SINR_u is higher than or equal to a required SINR_T (threshold).

2.3.1 Spatial Beamforming and Capacity Maximization

Smart antenna arrays can help in directing the transmitted power simultaneously towards different users, where each user receives a distinct amount of the total transmitted power according to his unique spatial signature. This is denoted as spatial division multiple access (SDMA), which increases both the reliability (due to transmitting multiples versions of the original signal in the space) and the throughput of the system by maximizing the multiplexing gain utilizing the distinct spatial signatures. Figure 2.10.b depicts an SDMA scheme, where all users are allowed to transmit simultaneously in the direction of their spatial signature.

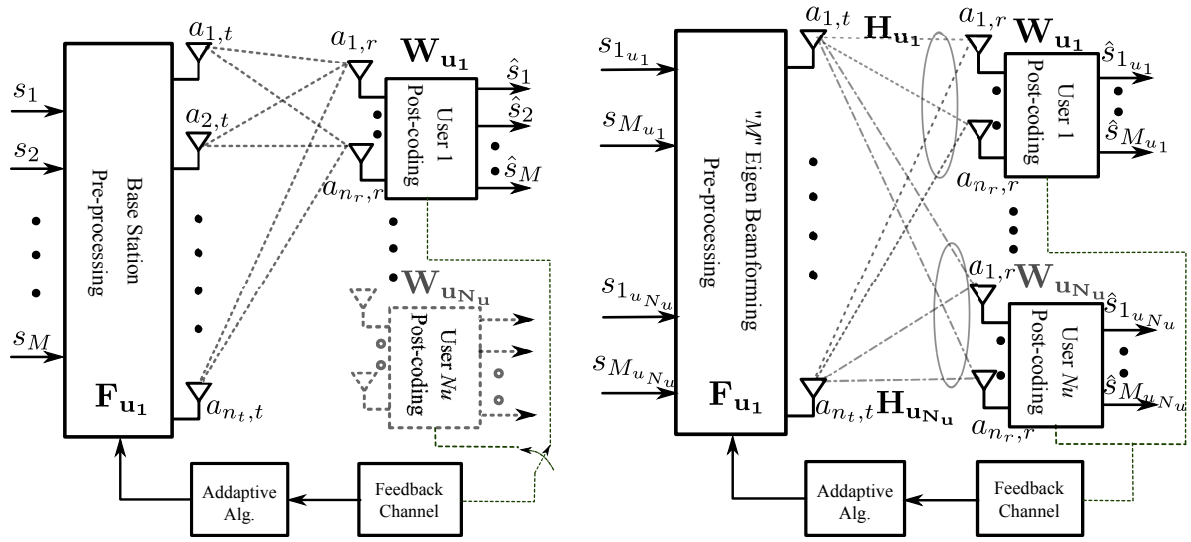

(a) T/FDMA MU-MIMO approach (b) SDMA MU-MIMO approach

Figure 2.10: Multiuser multiple access block-diagram

2.3.1.1 Multiuser MIMO

MIMO spatial multiplexing can be exploited for providing simultaneous data transmission towards different users, i.e., an SDMA multiuser (MU) MIMO system. In MU-MIMO system, the geographically distributed users (together with the BS) act as a "virtual" MIMO system with huge antenna spacing, though, less correlation. However, the main performance limiting factor in this case is the colored MUI. Therefore, MU-MIMO is characterized as an interference limited communication system. The key challenge in such a case is to design an optimum transmit filter, i.e., beamforming, to suppress the undesired interference. This can be performed by either null steering [29] (by enabling parallel spatial pipes that achieve full spatial multiplexing) or minimize the undesired signal at the desired user direction [73]. Applying MU-MIMO in combination with OFDM technique gives the freedom to schedule users across spatial dimensions (if feasible as in [31]) as well as frequency and time[5] domains . Figure 2.11 depicts the available shared resources, where users are scheduled across frequency, time, and/or space.

2.3.1.2 Multiuser beamforming in MIMO channels

Unlike the scalar AWGN broadcast channel (BC), MIMO BC are in general non-degraded [74]. This means that the users in MIMO cases cannot be sorted according to their channel gains as in the scaler AWGN channels[6]. Thus, the capacity region [75] of the MIMO broadcast channel is not even known in general. However, the MIMO multiple access channel (MAC) capacity can be easily achieved using a successive MUI cancellation using ordered users. In order to find the capacity region in case of MIMO BC, one can either implement a successive non-ordered

[5] to avoid channel correlations or long burst fades

[6] This is known from the characteristic of the degraded broadcast channel (DBC) [26].

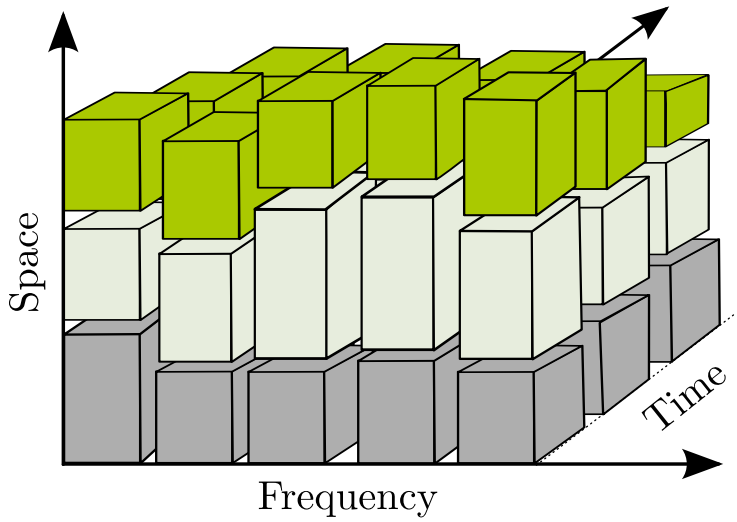

Figure 2.11: Scheduling in space, time, and frequency

pre-cancellation for MUI, e.g., dirty paper code (DPC)[7] [27], or implement an optimum linear MU beamforming. Non-linear successive techniques and DPC are not in the scope of this thesis, however, the reader is directed to [27, 76]. In contrast, linear beamformers are studied due to its suitability for transforming the non degraded BC into a degraded one, consequently, achieving feasible SDMA for different users.

A straight-forward solution for this problem has been proposed by Khaled, N. et al in [29], which is known as block-diagonalization. In this case, each user is allowed to transmit on the null-space (along the direction (eigenvectors) of the zero eigenvalues) of the other users. This is assumed to approach the sum capacity of the BC MU-MIMO as well as the MAC MU-MIMO by completely mitigating the MUI [28]. However, this comes at the expense of the transmit-receive antenna-size restricted constraint [29]. Another important downside of this beamforming technique is that it requires an accurate CSI knowledge at the transmitter. To relief this transmit-receive antenna-size constraint, a non-diagonal beamforming exploiting the duality between uplink and downlink is required [31, 77]. Further details are discussed in the following sections.

2.3.2 Multiuser Channel Block Diagonalization

The algorithm in [29] proposes to use SVD, similar to single-user MIMO case, in order to achieve a diagonalized or a block-diagonalization (BD) in the downlink scenarios. This is also known in literature as channel inversion or zero-forcing (ZF) approach. In this case, the optimal transmitter and receiver matrices are computed such that the inter-user interference is canceled out leaving each user with his equivalent, hence, diagonalizable single-user MIMO channel. This can be seen as a block-diagonalized matrix with equivalent single-user matrices along its diagonal. This can be seen as a diagonal SDMA MIMO system, if the smaller channel blocks can be diagonalized using SVD as well.

[7] The transmitter first picks a codeword for the 1^{st} user and subtract it from the codeword of the 2^{nd} user. Therefore, user 2 does not see the 1^{st} codeword as interference.

Diagonal SDMA, however, imposes a strict condition on the dimension of the MU MIMO system, such that number of transmit antennas at the base-station must be greater than or equal to the total number of receive antennas on all users, i.e., $N_T \geq N_u \times N_R$ assuming an equal number of receive antennas N_R. This condition makes it impractical in some scenarios with higher number of users unless both frequency and time can be utilized for scheduling users to minimize the size of the transmitter antenna array. As said before, diagonalization using SVD requires full knowledge of the CSI at both sides, the transmitter (for adaptation) and the receivers (for equalization). Thus, any channel uncertainty will lead to inter-user interference and intra-user interference due to the inefficient diagonalization using imperfect CSI. The solution in [29] proposes a transmit filter based on a null space constraint which projects each user onto the zero-eigenvalues of the other users virtual MIMO channel. Hence, this results in a complete cancellation to the inter-user interference. The general model of this diagonal SDMA is similar to the one in Fig. 2.10.b, i.e., downlink scenario.

In this model, we consider a BC scenario with N_u users, where the data symbols of all users are collected in the column vector $\mathbf{x} = [\mathbf{x}_0, ..., \mathbf{x}_{N_u-1}]^T$. In this scenario, the base-station has N_T antennas and each user has N_R receive antennas. This results in the individual channel matrix $\mathbf{H}_u \in \mathbb{C}^{N_R \times N_T}$ seen at the u^{th} user receive antennas. The overall $N_u N_R \times N_T$ channel matrix $\mathbf{H}$ is given by $\mathbf{H} = \left[\mathbf{H}_0^T, ..., \mathbf{H}_u^T, ..., \mathbf{H}_{N_u-1}^T\right]^T$, i.e., concatenating all users' channel matrices. The global transmit filter $\mathbf{F} \in \mathbb{C}^{N_T \times N_T}$ is obtained by stacking N_u transmit filters as follows $\mathbf{F} = [\mathbf{F}_0, ..., \mathbf{F}_{N_u-1}]$, where $\mathbf{F}_u \in \mathbb{C}^{N_T \times N_R}$ is the precoding matrix at the BS. Let us assume that $\mathbf{F}_u = \mathbf{U}_{\mathbf{T}u}\mathbf{Q}_{\mathbf{T}u}$, where $\mathbf{U}_{\mathbf{T}u}$ is a unitary beamforming matrix and $\mathbf{Q}_{\mathbf{T}u}$ is a power spatial shaping diagonal matrix, such that

$$\mathrm{Tr}\left(\mathbf{Q}_{\mathbf{T}}\right) = P_T \ , \tag{2.51}$$

is $\mathbf{Q}_{\mathbf{T}} \in \mathbb{R}_+^{N_T \times N_T}$ is the global spatial-shaping diagonal matrix for all users. Similar to $\mathbf{F}$, $\mathbf{U}_{\mathbf{T}} = [\mathbf{U}_{\mathbf{T}1}, ..., \mathbf{U}_{\mathbf{T}N_u}] \in \mathbb{C}^{N_T \times N_T}$. Accordingly, user u receives the following vector

$$\mathbf{y}_u = \mathbf{H}_u\mathbf{U}_{\mathbf{T}}\mathbf{Q}_{\mathbf{T}}\mathbf{x} + \mathbf{n}_u, \tag{2.52}$$

where $\mathbf{n}_u$ represents the AWGN at the u^{th} user terminal and $\mathbf{Q}_{\mathbf{T}}$ is the spectral shaping (power loading) for all users, which is a diagonal matrix. The post-processing at the u^{th} receiver using the $\mathbf{W}_u$ receive filter results in

$$\mathbf{r}_u = \mathbf{W}_u\mathbf{H}_u\mathbf{F}\mathbf{Q}_{\mathbf{T}}\mathbf{x} + \mathbf{W}_u\mathbf{n}_u \ , \tag{2.53}$$

where $\mathbf{x} \in \mathbb{C}^{N_u N_R \times 1}$ contains $N_u N_R$ symbols (for all users). Thus, to avoid inter-user interference completely, $\mathbf{H}_u\mathbf{F}$ must be block diagonalized, i.e., no inter-user (inter-block) interference. Furthermore, to avoid any user inter-eigen interference, the blocks along the reultant diagonal (sub-MIMO channels) needs to be diagonalized as well, i.e., using extra precoding and zero-forcing approach as in (2.43).

2.3.2.1 Transmit/receive filter design and full channel diagonalization

Precoding with block diagonalization completely suppresses the MUI by projecting, orthogonally, each user onto the null-space of the others [29, 28], i.e., $\mathbf{H}_{i\neq u}\mathbf{F}_u = \mathbf{0}$. This means that $\mathbf{F}_u^{(N_T \times N_R)}$

spans the $M_u \leq N_R$ null spaces (zero eigenvalues) of the matrix formed by concatenating all the users matrices except the one of our user of interest. This matrix is given by

$$\mathbf{H}_u^{\text{null}} = \left[\mathbf{H}_{i=0}^T \cdots \mathbf{H}_{i\neq u}^T \cdots \mathbf{H}_{i=N_u-1}^T\right]^T \ \forall\ i \neq u\ , \tag{2.54}$$

where $M \leq N_R$. Hence, the system is reduced to an equivalent single-user MIMO case. Therefore, the authors in [29] suggested to adapt the spectral shaping ($\mathbf{Q}_{\mathbf{T}u} = \text{diag}(p_{u,1}, ..., p_{u,M_u})$) in order to minimize the MSE (MMSE). As with (2.48), $p_{u,s}$ is the known MMSE water-filling-like solution [29], which is given by

$$p_{u,s} = \left[\mu \frac{\sigma_n}{\Sigma_{u,s}^{\star}} - \frac{\sigma_n^2}{\Sigma_{u,s}^{2\star}}\right]^+ \ ,\ \forall\ s = 0 \cdots M_u - 1 \tag{2.55}$$

where $[x]^+$ denotes that $x \geq 0$, μ is a Lagrangian multiplier that can be found iteratively such that $\sum_{u=0}^{N_u-1}\sum_{s=0}^{M_u-1} p_{u,s} = P_T$, and $\Sigma_{u,s}^{\star}$ are the singular values of the new resultant channel $\mathbf{H}_u^{\star} = \mathbf{H}_u\mathbf{F}_u$, such that SVD($\mathbf{H}_u^{\star}$) = $\mathbf{U}_u^{\star}\mathbf{\Sigma}_u^{\star}\mathbf{V}_u^{*star}$. Thereafter, we can be derived using SVD, similar to single-user case, in order to achieve a full diagonalization to the matrix block received by every user, i.e., $\mathbf{H}_u^{\star}$, extra precoding matrix $\mathbf{V}_u \in \mathbb{C}^{N_R \times N_R}$ and power loading $\mathbf{P}_u \in \mathbb{R}_+^{N_R \times N_R}$ diagonal matrix have to be used for every user knowing the SVD of his equivalent channel $\mathbf{H}_u^{\star}$. Accordingly, the overall block-diagonal channel matrix matrix is given by

$$\begin{aligned} \mathbf{H}^{\text{eq}} &= \mathbf{H}\mathbf{U}_{\mathbf{T}}\mathbf{Q}_{\mathbf{T}}\mathbf{V}\mathbf{P}^{1/2} \\ &= \begin{bmatrix} \mathbf{H}_0\mathbf{U}_{\mathbf{T}0}\mathbf{Q}_{\mathbf{T}0}\mathbf{V}_0\mathbf{P}_0^{1/2} & \cdots & 0 \\ \vdots & \ddots & \vdots \\ 0 & \cdots & \mathbf{H}_{N_u-1}\mathbf{U}_{\mathbf{T}N_u-1}\mathbf{Q}_{\mathbf{T}N_u-1}\mathbf{V}_{N_u-1}\mathbf{P}_{N_u-1}^{1/2} \end{bmatrix}, \end{aligned} \tag{2.56}$$

where $\mathbf{H}_u^{\text{eq}} = \mathbf{H}_u\mathbf{U}_{\mathbf{T}u}\mathbf{Q}_{\mathbf{T}u}\mathbf{V}_u\mathbf{P}_u^{1/2} \in \mathbb{C}^{N_R \times N_R}$. Since MMSE criterion is the target optimum receiver, $\mathbf{W}_u$ has to satisfy the MMSE solution of $\mathbf{H}_u^{\text{eq}}$ as in (2.42).

In case of CSI uncertainty, $\hat{\mathbf{H}}_u$ is introduced as the erroneous channel matrix that is deviated from the instant channel values by $\mathbf{\Xi}_u$, i.e., $\hat{\mathbf{H}}_u = \mathbf{H}_i - \mathbf{\Xi}_u$. Accordingly, the pre-processing null-space matrices are the erroneous ones $\hat{\mathbf{U}_{\mathbf{T}}}_u$ and $\hat{\mathbf{Q}_{\mathbf{T}}}_u$. Thus, they are not capable of achieving a full block-diagonal channel any more. For instance, the received symbol is

$$\begin{aligned} \mathbf{y}_u &= \mathbf{H}_u\hat{\mathbf{U}}_{\mathbf{T}}\hat{\mathbf{Q}}_{\mathbf{T}}\hat{\mathbf{V}}\hat{\mathbf{P}}^{1/2}\mathbf{x} + \mathbf{n}_u \\ &= \left(\hat{\mathbf{H}}_u + \mathbf{\Xi}_u\right)\hat{\mathbf{U}}_{\mathbf{T}}\hat{\mathbf{Q}}_{\mathbf{T}}\hat{\mathbf{V}}\hat{\mathbf{P}}^{1/2}\mathbf{x} + \mathbf{n}_u \\ &= \hat{\mathbf{H}}_u\hat{\mathbf{U}}_{\mathbf{T}_u}\hat{\mathbf{Q}}_{\mathbf{T}_u}\hat{\mathbf{V}}_u\hat{\mathbf{P}}_u^{1/2}\mathbf{x}_u + \overbrace{\mathbf{\Xi}_u \sum_{i=0,i\neq u}^{N_u-1} \hat{\mathbf{U}}_{\mathbf{T}_i}\hat{\mathbf{Q}}_{\mathbf{T}_i}\hat{\mathbf{V}}_i\hat{\mathbf{P}}_i^{1/2}\mathbf{x}_i}^{\text{residual MUI}} + \mathbf{n}_i\ . \end{aligned} \tag{2.57}$$

In case of sever channel uncertainties, (2.57) cannot be approximated as a single-user, i.e., the residual MUI is relatively high. Accordingly, neither ZF nor MMSE are the optimal receivers any more. Therefore, successive interference cancellation or space-time block codes can be used as an alternative, which is beyond the scope of this thesis. Moreover, a more robust schemes can be considered which includes the channel uncertainty matrix $\mathbf{\Xi}_u$ into the optimization process. Although these schemes do not diagonalize the multiuser channel, we are still able to construct a kind of virtual orthogonalization as discussed in the rest of this chapter.

2.3.2.2 MAC-BC duality

In single-user MIMO system, the downlink and the uplink are almost identical in their structure. However, in multiuser systems, i.e., in the MAC, the base-station performs a joint reception from all users, which is not a valid solution in the BC case assuming a non-cooperative scheme. The other important issue in BC is its non-degraded characteristic that leads to a very complex alternative formulation, e.g., using the non-linear DPC formulation. Hence, the *duality* between the MAC and the BC scenarios has been exploited to simplify the mathematical structure in the BC. In the first place, this duality can be exploited to reformulate the capacity region of the BC ($\mathcal{C}_{\text{BC}}$), with a fixed power constraint P_T and a channel matrix $\mathbf{H}^*$[8], in terms of the union of all MAC individual capacity regions with an equivalent sum-power constrain, i.e., $\sum(p_0, ..., p_{N_u-1}) = P_T$. This can be expressed (similar to [74]) as

$$\mathcal{C}_{\text{BC}}\left(P_T, \mathbf{H}^*\right) = \bigcup_{\sum(p_0,...,p_{N_u-1})=P_T} \mathcal{C}_{\text{MAC}_{\text{dual}}}\left(p_0, ..., p_{N_u-1}, \mathbf{H}\right) \ . \tag{2.58}$$

However, the capacity region of the MAC can also be found using virtual BC scenarios (with their DPC regions). In this case, the $\mathcal{C}_{\text{MAC}}$ is given by

$$\mathcal{C}_{\text{MAC}}\left(P_T, \mathbf{H}\right) = \bigcap_{(w_0,...,w_{N_u-1})>0} \mathcal{C}_{\text{BD}^{\text{DPC}}_{\text{dual}}}\left(\frac{p_0}{w_0}, ..., \frac{p_{N_u-1}}{w_{N_u-1}}, \mathbf{H}^* = \sqrt{w_0}\mathbf{H}^*{}_0, ..., \sqrt{w_{N_u-1}}\mathbf{H}^*{}_{N_u-1}\right) \ , \tag{2.59}$$

where the scaling by w models the near-far effect of those uniformly distributed users. Figure 2.12 illustrates the original BC (in Fig. 2.12.a) and its dual (or virtual) MAC in (Fig. 2.12.b).

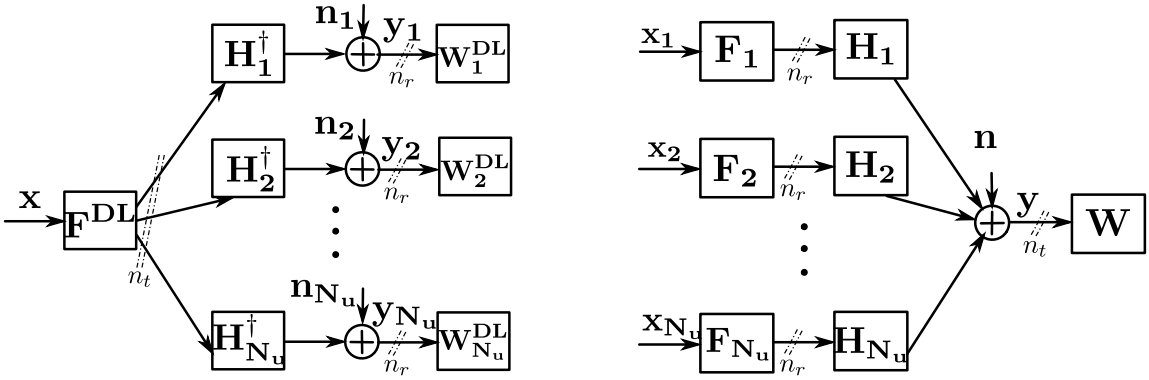

(a) MU-MIMO original-BC (downlink)

(b) MU-MIMO dual-MAC (uplink)

Figure 2.12: MU MIMO system block diagram shows the MAC-BC duality

Independent from these previous capacity results, the same duality characteristic, even the same duality structure as in Fig. 2.12, has also been exploited to simplify the optimal transmission strategies by finding the optimal beamformer filters. Thus, the derivation complexity and the computational complexity of the BC transmit filters have been reduced utilizing this MAC-BC duality in MIMO systems. An early study by Boche et al. has been considering an SINR constraint in order to realize the BC beamformers [31]. However, a second type of this duality,

[8]The conjugate here is used to interchange between the transmit and receive antennas.

which is the MSE-duality, has been introduced in [77, 78, 79]. The main assumption in that case is that the MSE of the BC and its dual MAC are identical. Hence, the beamformers and the receive filters can be optimally found using pure convex optimization approaches [31, 77]. The main advantage here is that a global optimum is achieved, however, with enormous computational complexity. One of the main reasons behind these optimum approaches being impractical, is the use of the general purpose optimization solvers rather than building their own specific optimizers. Currently, the more practical ideas are considering the traditional Lagrangian iterative dual method [80, 78, 79]. These iterative methods succeed in diminishing the overall complexity. However, they can only guarantee achieving local minima instead of the global one [80]. However, they can easily achieve a multilevel QoS based transmission.

2.3.2.3 Multiuser with individual QoS constraints

In order to realize different QoSs amongst dfferent users, Schubert et al. discussed the feasibility region assuming a constrained SINR value ($\mathrm{SINR_T}$) [31]. Thus, this system is said to be feasible if the achievable $\min \mathrm{SINR}_u$ is greater than or equal a certain $\mathrm{SINR_T}$, i.e., $\min \mathrm{SINR}_u/\mathrm{SINR_T} \geq 1$. Therefore, it is required to maximize this ratio such that

$$\begin{aligned} \underset{p_u}{\text{maximize}} \quad & \min_{0\leq u\leq N_u-1} \frac{\mathrm{SINR}_u}{\mathrm{SINR_T}} \\ \text{subject to} \quad & \sum_{u=0}^{N_u-1} p_u = P_T \ . \end{aligned} \tag{2.60}$$

Figure 2.13.a illustrates the previous monotonically increasing SINR feasibility. Using the analogy between the SINR and the MSE, the authors in [81] considered another QoS constrained transmission, however, with respect to the minimum MSE (MMSE) of the u^{th} user. The MMSE in this case is given as a function of the users SINR_u and the transmit filter $\mathbf{F}_u$ as

$$E_u = f\left(1/\mathrm{SINR}_u(\mathbf{F_u})\right) \ . \tag{2.61}$$

In other words, maximizing the SINR will certainly leads to minimizing E_u. This, in general, aims at optimizing the overall performance, e.g., maximizing the throughput. Moreover, optimizing the MSE is very suitable for switching off arbitrary users, or even data-streams, if they are facing poor channel qualities or very low SINR.

Generally speaking, the optimum resource allocation based on MSE optimization can be handled using the following strategies:

A- Best overall system performance: where it is required to minimize the summation the users' MSE such that

$$E^{\mathrm{opt}} = \underset{\mathbf{F}^*\mathbf{F}}{\text{minimize}} \quad \sum_{u=0}^{N_u-1} E_u \ , \tag{2.62}$$

where $\mathbf{F}^*\mathbf{F}$ is all the feasible power loading matrix of the MSE E_i. In general, the minimization of the sum-MSE (2.62) yields an excellent un-coded SER [79], which is

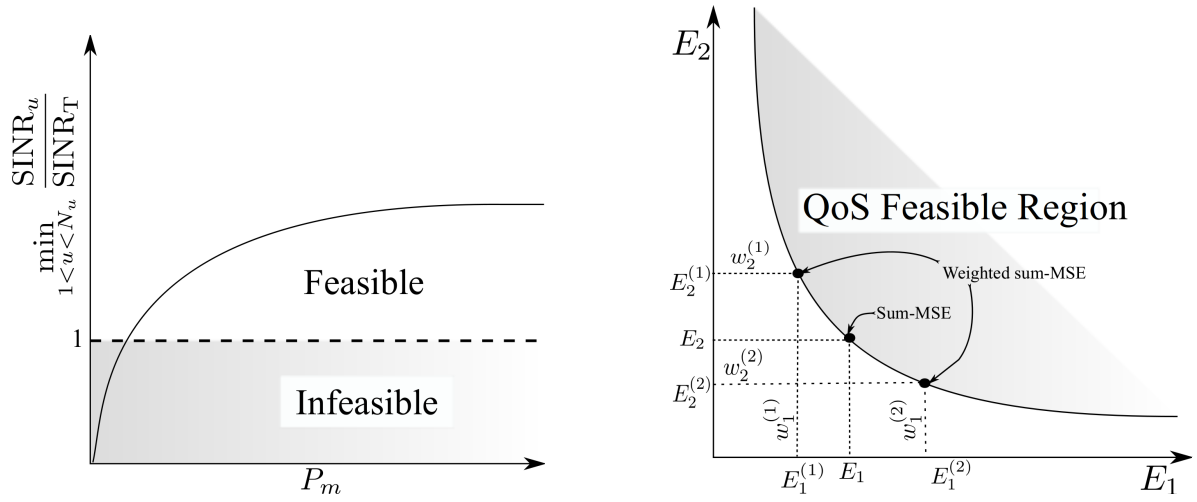

(a) Non-linear SINR monotonicity in P_T

(b) Sum-MSE $E_i + E_j$ or weighted sum-MSE $(w_i^{(k)} E_i^{(k)} + w_j^{(k)} E_j^{(k)})$

Figure 2.13: Feasibility region for optimum resource allocation

mandatory for the analysis in this thesis. Thus, the convexity of the feasibility region (in Fig. 2.13.b) is mandatory to achieve the minimum point.

B- Weighted sum-MSE (prioritized user allocation): this scheme aims at minimizing the sum-MSE in (2.62) multiplied by a weighting vector $\mathbf{w} = [w_0, .., w_{N_u-1}]$, where $\mathbf{1} \cdot \mathbf{w} = 1$. $\mathbf{w}$ can be chosen in order to realize unequal error protections (UEP) among the given users [81]. The optimization problem is given by

$$E^{\text{opt}} = \underset{\mathbf{F}^*\mathbf{F},\mathbf{w}}{\text{minimize}} \quad \sum_{u=0}^{N_u-1} w_u E_u \ . \tag{2.63}$$

Optimizing the sum-MSE or the weighted sum-MSE can be unfair, i.e., resources are not distributed equally, since achieving this minimum sum-MSE may result in switching off users with weaker channel gains and, instead, concentrate the power towards the user with the strong channels, i.e., similar to the greedy adaptive method [81].

C- Minimize the maximum fairness: In order to achieve a fair system, the maximum MSE E_u has to be minimized. In other words, this means to keep all $E_u \ \forall \ u = 0..N_u - 1$ at roughly the same level. The optimization problem is given by

$$E^{\text{opt}} = \underset{\mathbf{F}^*\mathbf{F}}{\text{minimize}} \left(\max_{\forall u=0..N_u-1)} E_u \right) \ . \tag{2.64}$$

This scheme is only useful when users are relying on emergency services or delay-sensitive applications (like video and audio conversation).

Throughout this thesis, we deal with the different QoS (or the prioritized) transmission, e.g., using the weighted sum-MSE as in (2.63) (published in [1]).

2.3.2.4 Minimizing the MSE and throughput maximization

The previous MSE minimization does not guarantee fully independent users (as in BD), which is our main goal in order to realize adaptive prioritized transmission. Even more, streams are not jointly optimized and, hence, cannot be used directly by any rate adaptive algorithm. Therefore, it is required to minimize the MSE of each stream separately. However, the question here will be: can we still make these streams independent (as in the BD scheme)? This, on the one hand, is a very complex optimization approach. On the other hand, if even complexity is not an issue, it is not an optimum solution from the capacity point of view. The reason for sub-optimality is the non-convexity of (2.63) in $\{\mathbf{F}_u, \mathbf{W}_u\}$ [82], which results into local minima. Therefore, it is required to imitate the diagonalization in, e.g., the BD, scheme. This can be achieved by considering the MMSE as a reasonable metric for channel adaptation. This is also practical since the MMSE is distinct for each user. Additionally, it gives an average performance for all streams, i.e., one can allocate these streams equally. The standard sum rate expression for the streams for user u is given in [30], however, using the $\mathrm{SINR}_{u,s}$ as

$$\sum_{s=0}^{M_u-1} R_i = \sum_{s=0}^{M_u-1} \log_2\left(1+\mathrm{SINR}_{u,s}\right) \ , \tag{2.65}$$

where M_u is the number of streams for user u. In order to break the dependency on each stream s, (2.65) is modified to use the MMSE instead of the SINR. Therefore, we use the relation between MMSE and SINR which is given, using the bijective [81] mapping, by

$$\mathrm{MMSE}_u = \frac{1}{1+\mathrm{SINR}_u} \ . \tag{2.66}$$

Hereto, the per-user sum rate is simply given by

$$R_u = -\log_2\left(\mathrm{MMSE}_u\right) \ , \tag{2.67}$$

where MMSE_u is the summation of the MMSEs of all streams used by user u. Accordingly, we can allocate bits equally to all streams for a given subcarrier, i.e., considering OFDM transmission. However, the number of bits may vary from subcarrier to another according to the calculated MMSE for each user.

Certainly, we can only achieve the users rate region using the non-linear DPC. However, in this thesis, we consider only the sub-optimal linear preceding approaches. Thus, for solving (2.63), we can user either a semidefinite programing (SDP) solver [77] or Lagrangian iterative methods [78]. In Chapter 6, we present a complete algorithm that allocates bits and multiplex users (using weighted MMSE criterion) with different QoS iteratively.

2.3.3 Adaptive MU MIMO with QoS

In the previous subsections, we discussed the possibilities of attaining diagonalization across different users and across their different streams. This has been made easy due to the assumption that the CSI is known perfectly or partially at the transmitter. In OFDMA, this diagonalization

can be achieved by exploiting the orthogonal subcarriers. Thus, it is sufficient to know the carrier gain-to-noise ratio (CGNR) of the user's individual subcarriers to adapt modulation and power.

Afterwards, we discussed the possibilities of multiplexing different users using a diagonalizable SDMA technique, e.g., using BD, assuming a perfect CSI. Moreover, the CSI knowledge helped us to further diagonalize the individual user's streams using SVD, as with single user MIMO transmission. Thus, adaptation can similarly be achieved.

Finally, we described a non-diagonal SDMA transmission, which is carried out by minimizing the induced MUI, i.e., minimizing the MSE. In this case, modulation and power adaptation can be realized by exploiting the users' individual MSE or the SINR. Furthermore, maximizing the sum rate can easily be obtained by minimizing either the sum MSE , i.e., achieving the MMSE or, equivalently, maximize the SINR.

In Chapter 6, we will describe some algorithms that can efficiently devote different numbers of bits to these independent resources based on their qualities and the users' QoSs. We will also discuss the possibilities of realizing prioritized data transmission across the users' different streams.

Chapter 3

UEP Adaptive Modulation

Historically, in single-link single-priority communication, a number of algorithms have been introduced to adapt the multicarrier transmission system to the varying channel conditions. The classical Hughes-Hartogs algorithm is well known in literature as the optimum bit-loading algorithm. It is based on a "greedy optimization method" that aims at finding a global optimum by adding a single bit to the subcarrier that requires the minimum incremental power at each iteration [83]. Therefore, it is optimal for minimizing the energy or maximizing the system margin, by reallocating the leftover power. However, due to complex search operations in Hughes-Hartogs, less complex (and also sub-optimal) methods where proposed later. Campello bit-loading proposed in [33], which is a linear representation of the Levin bit-loading algorithm [84], is a simple alternative to the Hughes-Hartogs bit-loading. It achieves almost the same optimum power allocation, despite requiring only a fraction of the complexity. The simplification here lies in the quantization of the channel-gain-to-noise ratio (CGNR) $\mathcal{G}_k$ and combining similar levels of $\mathcal{G}_k$ into L groups, where L is much smaller than the number of subcarriers N. Thereafter, the number of bits are computed based on the quantized Shannon's capacity formula as shown in [32]. Using the CGNR and subcarrier grouping make Campello's bit-loading a practical solution for limited or quantized channel feedback systems by achieving a sub-optimal bit load. However, to satisfy a given target bit-rate B_T, the algorithm continues subtracting/adding bits using the same greedy fashion known from Hughes and Hartogs.

Prior to Campello's algorithm, the adaptive bit-rate scheme by Chow et al. in [32] allocates bits according to the subcarriers CGNR and the required total target sum rate (B_T) using Shannon's capacity formula and an introduced adaptive noise margin γ. This is mainly based on the so called "gap approximation" (introduced in Chapter 2) which states that

$$B = \sum_{k=0}^{N-1} \log_2 \left(1 + p_k \frac{\mathcal{G}_k}{\Gamma \gamma_m} \right) , \tag{3.1}$$

where p_k is the allocated power on each subcarrier which is assumed to be unity before bit-loading, and $\mathcal{G}_k$ is the CGNR for the k^{th} subcarrier. γ_m is the noise margin that is utilized later to realize different QoS and Γ is the **gap** approximation factor introduced by Forney for integer constellations, i.e., PAM or QAM [32]. However, in this thesis we assume that $\Gamma = 1$, hence, we only allocate bits according to the required QoS by tuning the noise margin γ_m [2].

Later, Fischer et al. succeed to minimize the symbol-error rate (SER) using a Lagrangian optimization approach subject to a total power constraint. Frankly speaking, the Fischer algorithm is another implementation of the gap approximation. It maximizes the squared Euclidean distance to the decision threshold relative to the noise variance per dimension (SNR_0). Thus, changing the bit-rate with respect to a constant CGNR and a fixed power constraint leads to lowering SNR_0, i.e., reducing the Euclidean distance. This is equivalent to decreasing the noise margin in the Chow algorithm. In this chapter, we show that approximating the bit-loading formula used by Chow et al. defines a variable noise margin in Fischer's adaptive formula.

All the previous algorithms have been considering a single priority transmission class. However, in modern communications, unequal error protection (UEP) transmission with different (prioritized) SERs are required in order to deliver scalable qualities of services (QoSs), e.g., scalable video and multimedia transmission and prioritized communication for single and multiple users. In this chapter, we give an overview of the traditional bit-loading algorithms. Thereafter, we describe different algorithms that realize UEP transmission by modifying some of the pre-existing equal error protection (EEP) bit-loading algorithms.

3.1 Bit-loading State-of-the-Art

In multicarrier modulation, narrow-band noise, narrow-band interference, and deep channel fading are generally hitting a small number of the given subcarriers while other subcarriers are kept unaffected. Thus, the number of bits on each subcarrier is adapted to fit the different channel conditions. Accordingly, subcarriers with high CGNR are loaded with a higher power and larger number of bits, while the subcarriers with lower CGNR may be loaded with fewer, or even no, bits. This process is called *bit* and *power allocation*. Bit loading has been investigated mainly for DMT systems used in the wireline application, i.e., in DSL. These algorithms have exploited the easiness and the steadiness of measuring the channel coefficients.

A number of algorithms have been proposed to solve the bit-loading problem in the DSL environment but not in varying wireless channels. Thus, the early wireless LAN (WLAN) modems did not include any adaptive modulation module. However, the recent bit-rate demanding wireless applications are pushing towards more efficient and simpler adaptive algorithms, which are mainly based on the pre-existing ones known from DSL literature. However, they have to be much faster and less complex in order to adapt to the fast-varying channel conditions [85].

According to our literature survey, we classify the algorithms as follows:

I – **Rate-Adaptive (RA) criterion:** in this case, the number of bits required to be loaded has to be maximized subject to a given (strictly fixed) power constraint, i.e.,

$$\begin{aligned} \text{maximize} \quad & \sum_{k=0}^{N-1} \log_2\left(1 + p_k \frac{\mathcal{G}_k}{\gamma_m}\right) , \\ \text{subject to} \quad & \sum_{k=0}^{N-1} p_k = P_T \, . \end{aligned} \tag{3.2}$$

II – **SER Minimization (SM) criterion:** in this case, the SER $\mathcal{P}$ is required to be strictly fulfilled under a fixed power constraint, i.e.,

$$\begin{aligned} &\text{minimize} \quad \mathcal{P} \ , \\ &\text{subject to} \quad \sum_{k=0}^{N-1} p_k \leq P_T \ . \end{aligned} \tag{3.3}$$

III – **Margin-Adaptive (MA) criterion:** the total power is minimized such that a target bit-rate B_T is fulfilled.

$$\begin{aligned} &\text{minimize} \quad \sum_{k=0}^{N-1} p_k \ , \\ &\text{subject to} \quad \sum_{k=0}^{N-1} \log_2 \left(1 + p_k \frac{\mathcal{G}_k}{\gamma_m}\right) = B_T \ . \end{aligned} \tag{3.4}$$

If the power threshold P_T is exceeded before fulfilling the target rate B_T, the total bit load can still be forced to B_T, however, by virtually exceeding the P_T limit, i.e., assume $\sum_{k=0}^{N-1} p_k \geq P_T$. Thereafter, the power per subcarrier is rescaled to maintain the overall P_T, i.e., the margin is equivalently reduced. However, if B_T is fulfilled before exceeding the power threshold P_T, the remaining power maybe redistributed over all subcarriers. In this case, the margin is maximized. This is known as **(IV-) margin-maximization (MM) criterion**.

In the next section, we introduce some bit-loading examples based on the greedy (or the semi-greedy) method, which are said to be optimum since they are able to satisfy their constraints using only the integer bit values [33]. We also show the straightforward approach that truncates the non-integer (approximate) bit load values computed in (3.1). These algorithms can be summarized as follows:

1. **Optimum Loading Algorithms (Greedy Bit-Loading)**

   - Hughes, Hartogs [83],
   - Levin-Campello [33]
   - George, Amrani. [86]

2. **Sub- Loading Algorithms (Finite Granularity Bit-Loading)**

   - Chow, Cioffi, Bingham [32],
   - Fischer, Huber [87]
   - Yu, Willson [88]

3.1.1 Optimal Loading Algorithms – Greedy Methods

3.1.1.1 The Hughes-Hartogs algorithm

The first and also the oldest bit-loading algorithm was developed by Hughes and Hartogs in [83], which was applied first in the early voice-band modems (Telebit). This algorithm achieves a margin adaptive solution, where the power is minimized given a constant SER and a target total power P_T. Hence, bits are distributed successively, placing one bit at a time, to minimize the total power consumption.

The algorithm needs to compute every incremental power for each bit placement in order to select the subcarrier with the lowest incremental power. Thus, intensive searching and sorting operations are required, which make it a very computationally complex algorithm. As mentioned before, the Hughes-Hartogs algorithm starts with a margin adaptive (MA) criterion, which can be changed to a rate adaptive (RA) criterion if it is required to allocate a fixed number of bits B_T, however, with a higher SER. Moreover, when there is still left-over power and $B_{\max}$ is already achieved, the margin can be increased (achieving margin maximization (MM) criterion) by redistributing the left-over power.

3.1.1.2 Campello algorithm

The main drawback of the Hughes-Hartogs algorithm has been addressed by Campello de Souza [33]. This algorithm does not directly follow the greedy bit-loading, however, it allocates first an approximate number of bits using the given CGNR values. This is designed to be a lower bound for the required final bit loads. Furthermore, the actual target sum rate is achieved by brute-force the remaining bits using a single bit addition or removal following the greedy method proposed by Hughes and Hartogs. This, in turn, minimizes the total power. Thus, the closer the approximate bit load is to the target rate, the less complex this algorithm becomes. In order to compute an energy-efficient bit loads, the following quantized logarithmic CGNR is computed using a floor operator (to guarantee the minimum bit loads)

$$\mathbb{G}_k = \lfloor \log_2(\lambda_k/\sigma^2) \rfloor = \lfloor \log_2 \mathcal{G}_k \rfloor \ , \tag{3.5}$$

where λ is the channel coefficient squared $|h|^2$ and σ_n^2 is the noise variance. The floor operator in the previous equation, together with neglecting the "1" in (3.4), guarantees the allocation of the minimum possible number of bits to the weak subcarriers during the early iterations. Hence, the approximate number of bits b_k is given by

$$b_k = \{\mathbb{G}_k + i_B\}_0^{b_{max}} = \begin{cases} b_{max}, & b_{max} < \mathbb{G}_k + i_B \\ \mathbb{G}_k + i_B, & 0 \leq \mathbb{G}_k + i_B(k) \leq b_{max} \\ 0, & \mathbb{G}_k + i_B(k) < 0 \ , \end{cases} \tag{3.6}$$

where $i_B \in \mathbb{Z}$ is added to (3.5) in order to move the total sum rate ($\sum_k^N b_k$) towards the final target rate in order to minimize the computational complexity. The remaining bits are then

added/removed according to the incremental power on each subcarrier. The power required to allocate b_k bits on the k^{th} subcarrier with CGNR= $\mathcal{G}_k$ is given (using the capacity formula) as

$$p_k(b_k) = \frac{(2^{b_k}-1)}{\mathcal{G}_k}\,, \tag{3.7}$$

such that $p_k(b_k) \leq p_k(b_k+1)$. Therefore, the incremental power needed for allocating one extra bit is given by

$$\begin{aligned}\Delta p_k(b_k+1) &= p_k(b_k+1) - p_k(b_k) \\ &= \frac{2^{b_k}}{\mathcal{G}_k} = \frac{2^{b_k}}{2^{\mathbb{G}_k}} = 2^{(b_k-\mathbb{G}_k)}\,.\end{aligned} \tag{3.8}$$

According to the previous formula and to [33], one can easily notice that the main goal of this algorithm is just to find an optimum i_B in order to reduce intensive search and sorting in the Hughes-Hartogs sense. Additionally, the complexity is reduced by finding groups of subcarriers that have roughly the same quantized logarithmic CGNR $\mathbb{G}$. Furthermore, $\mathbb{G}_k$ are normalized to positive values by subtracting their minimum value. Thereafter, the subcarrier indices are stored in the 2-dimension array $\mathcal{M}_l$, where the columns represent these L quantized levels and the rows store the subcarrier indices corresponding to each of these L levels, i.e.,

$$\mathcal{M}_l = \{k = \{0,1,2,\cdots,N-1\} : \{\mathbb{G}_k = l\}\}\,, \quad l = 0,\ldots,L-1\,. \tag{3.9}$$

Algorithm 3.1 Original Campello MA bit-loading algorithm

Initialize: i_B, b_k, p_k and Δp_k with all zeros and $\mathbb{G}_k = \lfloor \log_2(\lambda_k/\sigma^2) \rfloor = \lfloor \log_2 \mathcal{G}_k \rfloor$
Input: $\mathbb{G}_1, \mathbb{G}_2, \ldots, \mathbb{G}_N, L, N, B_T$
Output: bit load b_k and power allocation p_k for every subcarrier
Require: $\sum_{k=0}^{N-1} b_k \leq B_{\max}$

```
Find M_l according to G_k.
repeat
    increment i_B by 1
    calculate b_k using (3.6)
    calculate the sum rate Σ_{k=0}^{N-1} b_k(i_B)
until Σ_{k=0}^{N-1} b_k(i_B) ≈ B_T
repeat
    if (Σ_{k=0}^{N-1} b_k < B_T) then
        iteratively increment the subcarriers with the minimum Δp_k(b_k + 1)
    else if Σ_{k=0}^{N-1} b_k > B_T then
        iteratively decrement the subcarriers with the maximum Δp_k(b_k − 1)
    end if
until Σ_{k=0}^{N-1} b_k = B_T or the maximum number of iterations is reached
```

Clustering of the N given subcarriers into L groups will certainly reduce the searching and sorting complexity to be only $\mathcal{O}(N)$. This makes it amongst the fastest bit-loading algorithm. Even more, due to the strict quantization on the CGNR, it is easily realized using fixed-point processors, which has a superior advantage for practical implementations.

3.1.1.3 The George-Amrani bit-loading algorithm

Conventional bit-loading algorithms intend to achieve a constant SER for all subcarriers. This may not be required, when channel coding is in place, since it will have some averaging effect over the frequency subcarriers. The George-Amrani [86] algorithm points into this direction. The basic idea of this algorithm is to fully utilize a constant power spectral density (PSD). Hence, bits are allocated, in a greedy fashion, to the subcarriers with the minimum incremental SER, i.e., according to their quantized CGNRs. Accordingly, this algorithm leads to a variable SER along the subcarriers, however, the average SER is minimized for a given B_T.

The main drawback of this method is the allocation of fixed power to every subcarrier and even the weakest ones. This can be useful in some applications with relatively strong channel [89]. However, for weak channel conditions (low SNR), this strictly violates the water-filling criterion, which aims at maximizing the overall capacity by not allocating power to the very weak subcarriers; see Chapter 2 for more details about water-filling. Since we are not assuming constant PSD applications, we will not consider this algorithm to realize UEP bit-loading.

3.1.2 Sub-optimum Loading Algorithms – Finite Granularity

3.1.2.1 The Chow-Cioffi-Bingham algorithm

Sub-optimal solutions were proposed to reduce the complexity of greedy algorithms. Based on Shannon's capacity formula, Chow, Cioffi, and Bingham proposed a sub-optimal bit-loading scheme [32] that allocates the subcarriers according to their CGNR and a certain noise margin, γ_m using a modified Shannon capacity formula with the gap approximation. Therefore, the margin γ_m is adapted to fulfill the required target sum rate B_T. Based on the finally computed bit loads, the power is allocated. The Chow-Cioffi-Bingham algorithm is typically implemented in existing wireline modems, e.g., ADSL and VDSL, where their channels typically only vary slowly. However, in wireless applications, the channels vary much faster than in the wireline case. Therefore, more simplifications are required to implement adaptive modulation in wireless communications. The algorithm by Chow et al. does not guarantee a fast convergence to the required B_T. In order to understand their sub-optimal bit-loading algorithm, it is divided into three parts:

I- find the optimal γ_m given the target sum rate B_T and the CGNR for each subcarrier;

II- if the number iterations is not sufficient, use brute-force bit-loading to fulfill B_T;

III- adjust the subcarrier power allocation according the loaded bits b_k and the CGNR.

The resulting transmit power distribution will typically not be flat; it will rather have a saw-tooth-like shape with approximately 3 dB peak-to-peak variation due to the integer bit constellations. The height of the saw-tooth may exceed 3 dB for smaller non-square constellations as depicted in Figure 3.1.

Algorithm 3.2 Original RA algorithm proposed by Chow et al.

Input: Required symbol-error probability $\mathcal{P}$, target power P_T, total number of subcarriers N, target sum rate B_T, and the maximum number of iterations "MaxCount"

Initialize: CGNR $\mathcal{G}_k = \lambda_k/\sigma^2$, $\forall k = 0..N-1$, $N_{\text{used}} = N$, IterateCount $= 0$, and $\gamma_m = 0$ dB

Output: bit load b_k, power allocation p_k, γ_m, and N_{used}

Require: $\sum_{k=0}^{N-1} b_k \leq B_T$

1: **while** $\sum_{k=0}^{N-1} b_k \ncong B_T$ and IterateCount $\leq$ MaxCount **do**

2: Compute b_k using

$$b_k = \log_2\left(1 + \frac{\mathcal{G}_k}{\gamma_m}\right) \tag{3.10}$$

3: Compute the quantized bit-load values $\hat{b}_k = \lfloor b_k + 0.5 \rfloor$.

4: The quantization error Δb_k is the difference between b_k and $\hat{b}_k$, i.e., $\Delta b_k = b_k - \hat{b}_k$.

5: If $\hat{b}_k = 0$, eliminate the subcarrier index k from the used subcarriers set N_{used}.

6: **if** $(\sum_{k=0}^{N-1} \hat{b}_k = 0)$ **then**

7: declare "bad channel" and **break** this loop

8: **end if**

9: Update γ_m using $\gamma_{m,\text{new}} := \gamma_{m,\text{old}} \cdot 2^{\frac{\sum_k^N \hat{b}_k - B_T}{N_{\text{used}}}}$

10: IterateCount $\Leftarrow$ IterateCount $+ 1$

11: **end while**

12: brute-force bit-loading to the target sum rate

13: **repeat**

14: **if** $(\sum_{k=0}^{N-1} \hat{b}_k > B_T)$ **then**

15: $\hat{b}_k \Leftarrow \max(\hat{b}_k - 1, 0)$ at the k^{th} subcarrier with the smallest quantization error Δb_k

16: **else if** $\sum_{k=0}^{N-1} \hat{b}_k < B_T$ **then**

17: $\hat{b}_k \Leftarrow \min(\hat{b}_k + 1, b_{\max})$ at the k^{th} subcarrier with the highest quantization error Δb_k

18: **end if**

19: **until** $\sum_{k=0}^{N-1} \hat{b}_k = B_T$

20: Calculate the subcarrier power p_k according to the desired bit-error probability[1] (see Appendix F)

$$p_k = \frac{2\,(2^{b_k} - 1)}{3\,\mathcal{G}_k}\left[\text{erfc}^{-1}\left(\frac{\mathcal{P}\; b_k\; \sqrt{2^{\hat{b}_k}}}{2\,(\sqrt{2^{\hat{b}_k}} - 1)}\right)\right]^2 \tag{3.11}$$

where $\mathcal{P}$ is the SER erfc is the complementary Gaussian error function.

21: Compute $P_\Sigma = \sum_{k \in N_{used}} p_k$ and modify the power allocation according to

$$p_k := \frac{P_T}{P_\Sigma} \cdot p_k \tag{3.12}$$

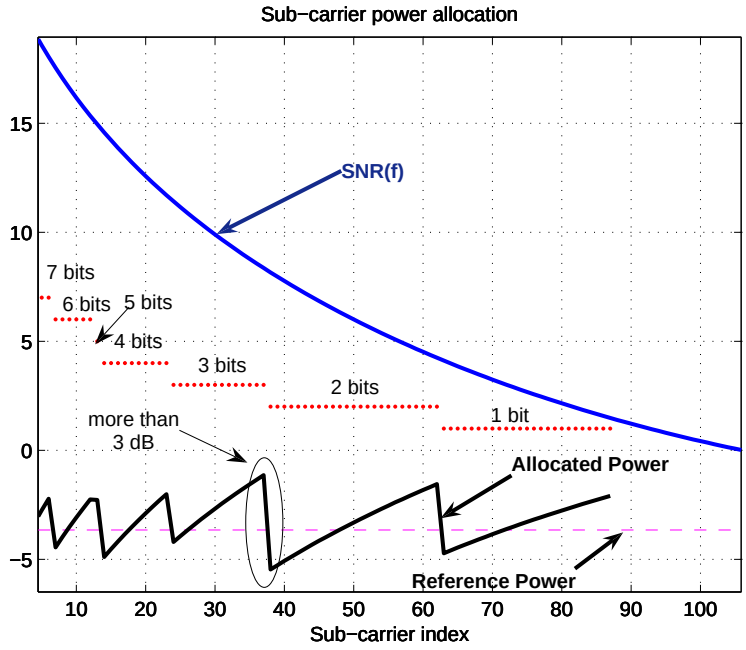

Figure 3.1: Bit loading and power allocation

This algorithm has a lower complexity than the one proposed by Hughes and Hartogs. The complexity in the worst case of this algorithm is proportional to $\mathcal{O}(\text{MaxCount} \cdot N + 2N)$ basic computational operations (add, subtract, and multiply) [32]. However, the algorithm still suffers from some disadvantages. First, the power allocation is separated from the bit-loading, which does not ensure power optimization. Second, starting from an arbitrary γ_m does not necessarily guarantee convergence for every channel. A possible solution is proposed later in this chapter.

3.1.2.2 The Fischer-Huber algorithm

The Fischer-Huber algorithm [87] distributes fixed number of bits and power in order to minimize the SER using a Lagrangian optimization approach subject to a total power constraint. This is achieved by maximizing the squared Euclidean distance to the decision threshold (relative to the noise variance per dimension) SNR_0. That is why one can see it as an algorithm that can achieve some sort of compromise between RA and SM criteria. Additionally, it is required that the SER per each subcarrier is roughly constant. Thus, for QAM modulation (see Appendix F), it is required that

$$\mathcal{P}(k) = 2\left(1 - \frac{1}{\sqrt{M}}\right)\text{erfc}\left(\sqrt{\frac{3}{2}\frac{p_k}{(M-1)}\mathcal{G}_k}\right) \approx 2\left(1 - \frac{1}{\sqrt{M}}\right)\text{erfc}\left(\sqrt{\frac{3}{2}\frac{d_k^2}{2}\mathcal{G}_k}\right) \simeq \text{const}\ , \tag{3.13}$$

where d_k is the minimum Euclidean distance between signal points, and $\mathcal{G}_k$ is the CGNR, $M = 2^{b_k}$. From (3.13), it is clear that

$$d_k^2\mathcal{G}_k = \text{SNR}_0 \simeq \text{const}\ , \tag{3.14}$$

where SNR_0 is the SNR related to neighboring points. It inherently represents the symbol-error probability. Hence, maximizing SNR_0 means maximizing the squared minimum Euclidean distance of the signal points at the receiver side d_k^2, which minimizes the SER.

Accordingly, solving (3.14) for d_k results in the following transmit power [90]

$$p_k = \mathrm{SNR}_0 \frac{2^{b_k}}{\mathcal{G}_k} \,, \tag{3.15}$$

where SNR_0 is given by

$$\mathrm{SNR}_0 = \frac{P_T}{\sum_{k=0}^{N_{\mathrm{used}}-1} 2^{b_k}/\mathcal{G}_k} \,, \tag{3.16}$$

which is only maximized when the denominator is minimized subject to these additional constraints:

CONSTR. 1- $B_T = \sum_k b_k \simeq \mathrm{const}$

CONSTR. 2- $P_T = \sum_k p_k \simeq \mathrm{const.}$

Introducing the Lagrangian multiplier μ for CONSTR. 1 and solving these Karush-Kuhn-Tucker (KKT) conditions, we obtain the following Lagrange-optimization [90]

$$\overset{\text{Fischer}}{\mathcal{L}} = \sum_{k=0}^{N_{\mathrm{used}}-1} \frac{2^{b_k}}{\mathcal{G}_k} - \mu \left(\sum_{k=0}^{N_{used}-1} b_k - B_T \right) \,. \tag{3.17}$$

Differentiating the previous equation with respect to b_k results in

$$\frac{2^{b_k}}{\mathcal{G}_k} \simeq \mathrm{const}, \quad \forall k = 0..N_{\mathrm{used}} - 1 \,. \tag{3.18}$$

Using CONSTR. 1 and (3.18), we find that

$$(\mathrm{const})^{N_{used}} = \left(\frac{2^{b_k}}{\mathcal{G}_k} \right)^{N_{used}} = 2^{B_T} \cdot \Pi_{l=1}^{N_{used}} \frac{1}{\mathcal{G}_k} \,. \tag{3.19}$$

Therefore,

$$\frac{2^{b_k}}{\mathcal{G}_k} = \sqrt[N_{used}]{2^{B_T} \cdot \Pi_{l=1}^{N_{used}} \frac{1}{\mathcal{G}_k}} \,. \tag{3.20}$$

Finally, the bit load values are given by

$$\begin{aligned} b_k &= \frac{B_T}{N_{used}} - \frac{\sum_{l=1}^{N_{used}} \log_2 \mathcal{G}_l}{N_{used}} + \log_2 \mathcal{G}_k = \overbrace{\frac{B_T}{N_{used}} - \frac{\sum_{l=1}^{N_{used}} \mathbb{G}_l}{N_{used}}}^{\text{const.}} + \mathbb{G}_k \\ &= \overline{b} - \overline{\mathbb{G}} + \mathbb{G}_k \,, \end{aligned} \tag{3.21}$$

where $\overline{b}$ is the average number of bits/carrier for the given target sum rate B_T, $\overline{\mathbb{G}}$ is the average of the logarithmic CGNR. Hence, the number of bits of the k^{th} subcarrier is essentially determined by the logarithm of the CGNR $\mathcal{G}_k$ plus a certain constant. Thus, this constant mainly depends on the number of evacuated subcarriers, i.e., the subcarriers with negative bit loads. In the previous equation, the summation over every subcarrier is performed using floating point summation,

exactly like what is done inside the $\log_2$ in the Chow algorithm (3.10). However, omitting the "1" from (3.10) simplifies the calculations further, where the logarithmic values can be computed only during initialization. Hence, removing this "1" from (3.10) and finding the sum over the used subcarriers N_{used} and comparing it to (3.16), we find γ_m to be

$$\gamma_m = \frac{P_T}{\sum_{k=0}^{N_{\text{used}}-1} 2^{b_k}/\mathcal{G}_k} = \text{SNR}_0 \ . \tag{3.22}$$

This means that both algorithms are computationally identical and the maximum noise margin is achieved in the Chow algorithm by omitting this "1". However, this "1" addition in (3.10) guarantees $b_k \geq 0$.

The bit load values in (3.21) are not necessarily positive. Therefore, the subcarriers with $b_k < 0$ are omitted from the total used subcarriers N_{used}. This increases both $\overline{b}$ and $\overline{\mathbb{G}}$ by decreasing the common denominator and excluding some of the negative values in $\overline{\mathbb{G}}$. Therefore, we cannot predict if the constant $\overline{b} - \overline{\mathbb{G}}$ is monotonically increasing or decreasing at every iteration, which makes controlling the convergence here not a simple task, since (3.21) may still deliver negative b_k in the next iterations depending on the CGNR itself.

Finally, when (3.21) converges, i.e., no more negative bit load is found, it will only guarantee fulfilling B_T, if the floating-point bit loads b_k are used. However, this may be very far from the correct answer after quantization, i.e., $\hat{b}_k = \lfloor b_k + 0.5 \rfloor$. This is not the case in the Chow algorithm, where the sum of the quantized bit loads are forced to be as close as possible to B_T. In the following, we present the steps of the Fischer-Huber algorithm.

Algorithm 3.3 Original Fischer-Huber bit-loading algorithm

Input: CGNR $\mathcal{G}_k$ for every subcarrier position $k = 0..N-1$, total number of subcarriers N, and target sum rate B_T

Output: bit load b_k for every subcarrier and the used subcarriers N_{used}

Initialize: $N_{\text{used}} = N$ and the set of usable subcarriers $\mathcal{M} = 0..N-1$

Require: $\sum_{k=0}^{N-1} b_k \leq B_T$

1: **repeat**
2: determine the bit load $b_k < 0$ using (3.21)
3: find the locations of $b_k < 0$ and remove them from $\mathcal{M}$
4: update N_{used}
5: compute the power using (3.22), such that

$$p_k = \frac{2^{b_k}/\mathcal{G}_k}{\sum_i^{N_{\text{used}}} 2^{b_i}/\mathcal{G}_i} P_T \tag{3.23}$$

6: **until** $\sum_{k=0}^{N-1} b_k = B_T$
7: **if** ($\sum_{k=0}^{N-1} \hat{b}_k \neq B_T$, where $\hat{b} = \lfloor b_k + 0.5 \rfloor$) **then**
8: use the brute-force approach as in the Chow's algorithm until $\sum_{k=0}^{N-1} \hat{b}_k = B_T$
9: **end if**

3.1.2.3 Yu-Willson UEP bit-loading

All the previous bit-loading algorithms assume that the whole bit stream has equal priority, which is not the case for some applications, e.g., multimedia. The Yu-Willson [88] algorithm is one of the first algorithms that considered implemented UEP-loaded frames. The main idea in this algorithm is to have N_g different classes of services inside the same multicarrier frame. These classes are allocated to N_g different subcarrier sets $\mathcal{M}_{j=0..N_g-1}$ and not just a single class as in the previously discussed algorithms. Each of these N_g classes has to be loaded with a different number of bits T_j and allows for different SERs $P_{e,j}$ according to the required UEP profile. Let $b_{k,j}$ be the bit load and $p_{k,j}$ be the allocated power on the k^{th} subcarrier in the j^{th} group. Following the Fischer-Huber's Lagrange cost function (3.17) with a modification to the class index j, the new cost function is rewritten as

$$\overset{\text{Yu-Willson}}{\mathcal{L}} = \sum_{j=0}^{N_g-1} \sum_{\mathcal{M}_j} \frac{2^{b_{k,j}}}{\mathcal{G}_{k,j}} - \sum_{j=0}^{N_g-1} \mu_j \left(\sum_{\mathcal{M}_j} b_{k,j} - T_j \right) , \tag{3.24}$$

where $T_j = \sum_{\mathcal{M}_j} b_{k,j}$ and $B_T = \sum_{j=0}^{N_g-1} T_j$. We know that the SER for each group $\mathcal{P}_j$ is constant, as in Fischer et al. and Chow et al. algorithms, which is given by [15]

$$\mathcal{P}_j = \frac{K_{k,j}}{2} \text{erfc} \left(\sqrt{\frac{3}{2} \frac{p_{k,j}\mathcal{G}_{k,j}}{(2^{b_{k,j}} - 1)}} \right) , \tag{3.25}$$

where $K_{k,j} = (1 - \frac{1}{\sqrt{2^{b_{k,j}}}}) \approx 4$ for higher order constellations. Now, performing a Lagrange minimization of $\mathcal{L}$, exactly as in the Fischer-Huber algorithm, however, for N_g classes, we obtain

$$b_{k,j} = \frac{T_j}{L_{\mathcal{M}_j}} - \frac{\sum_{\mathcal{M}_j} \log_2 \mathcal{G}_{k,j}}{L_{\mathcal{M}_j}} + \log_2 \mathcal{G}_{k,j} = \overline{b}_j - \overline{\mathbb{G}}_j + \mathbb{G}_{k,j} . \tag{3.26}$$

$L_{\mathcal{M}_j}$ is the number of subcarriers in the j^{th} class, $\overline{b}_j$ is the average number of bits in the j^{th} class, and $\overline{\mathbb{G}}_j$ is the j^{th} class mean logarithmic CGNR, i.e., $\log_2 \mathcal{G}_{k,j}$. However, $\mathcal{M}_j$ itself and the border lines between the classes are still unknown. Therefore, the authors of [88] assume a set of assumptions to achieve $L_{\mathcal{M}_j}$, which are

1. the channel is almost constant within each class and, hence, the average number of bits/subcarrier in each class $\overline{b}_j$ is given by

$$\overline{b}_j \approx \frac{T_j}{L_{\mathcal{M}_j}} , \tag{3.27}$$

2. the power on every subcarrier within the same class is fixed and the power even does not change among classes. Using (3.25) and (3.27), this power is given by

$$\overline{p}_j \approx \frac{2}{3} \frac{2^{\overline{b}_j}}{\left(\Pi_{\mathcal{M}_j} \mathcal{G}_{k,j} \right)^{1/L_{\mathcal{M}_j}}} \left[\text{erfc}^{-1} \left(\frac{\mathcal{P}_j}{2} \right) \right]^2 \approx \overline{p} , \tag{3.28}$$

where $\overline{p}_j$ and $\overline{b}_j$ are the average power and the average number of bits for class j, respectively. $\overline{\mathcal{G}}_j = \left(\Pi_{\mathcal{M}_j} \mathcal{G}_{k,j} \right)^{1/L_{\mathcal{M}_j}}$ is the geometric mean of $\mathcal{G}_{k,j}$ of the j^{th},

3. using the Chernoff bound[2], the approximate symbol error probability and a better approximate average bit load are given as

$$\mathcal{P}_j \approx \exp\left[-\frac{3}{2}\frac{\overline{p}_j\overline{\mathcal{G}}_j}{2^{\overline{b}_j}}\right] \quad \text{and} \quad \overline{b}_j \approx \log_2\left(-\frac{3}{2}\frac{\overline{p}_j\overline{\mathcal{G}}_j}{\ln\mathcal{P}_j}\right) , \tag{3.29}$$

respectively. Herewith, using (3.27), an intermediate value for $L_{\mathcal{M}_j}$ is given by

$$L_{\mathcal{M}_j} \approx \frac{T_j}{\overline{b}_{k,j}} , \tag{3.30}$$

4. finally, the algorithm considers the same overall number of non-zero subcarriers N_{used} as the one given by the non-UEP Fischer-Huber case. Thus, the assumption is that

$$N_{\text{used}} = \sum_{j=1}^{N_g} L_{\mathcal{M}_j} . \tag{3.31}$$

Substituting (3.29) in (3.30) and the result into (3.31) we get

$$N_{\text{used}} = \sum_{j=1}^{N_g} \frac{T_j}{\log_2\left[\underbrace{\frac{-3}{2}\overline{p}_j}_{x}\cdot\frac{\overline{\mathcal{G}}_j}{\ln\mathcal{P}_j}\right]} . \tag{3.32}$$

After solving (3.32)[3] for x, where the non-approximate $x = -3\overline{p}_j/2$, the obtained $\overline{p}_j$ can be substituted in (3.29) to find the an approximate number of bit $\overline{b}_j$. Hence, a more accurate $L_{\mathcal{M}_j}$ is found using (3.30). Finally, this $L_{\mathcal{M}_j}$ is used to compute the more accurate $b_{k,j}$ using (3.26). Thereafter, the quantized $\hat{b}_{k,j}$ is computed and, hence, a more accurate $L_{\mathcal{M}_j}$ is found accordingly. This results can be even enhanced iteratively, until B_T and T_j are fulfilled or using the common brute-force method[4]. Our conclusion is that Yu-Willson proposed the idea for realizing UEP using only bit-loading. However, there algorithm is far too complected and even not clear enough. From computationally complexity point of view, this algorithm is of $\mathcal{O}(\text{mean}(L_{\mathcal{M}_{j=0..Ng-1}})^{N_g} + N \cdot X_{\#\text{ of counts needed to adjust } x})$ operations. In this chapter, we are presenting a more efficient methods to realize the subcarrier partitioning problem.

[2]It gives exponentially decreasing bounds on tail distributions of sums of independent random variables [91].

[3]The authors assume that x can be obtained in closed form. However, we are sure that it has to be computed using a few number of iterations.

[4]The quantization step is not clear in the Yu-Willson paper at all.

3.2 UEP Bit-loading and Power Allocation

The source encoders of some applications, like multimedia, deliver data of different importance levels, i.e., different data requires different levels of protections. Such applications are demanding UEP, in which important data is protected better against errors. In order to realize UEP in such systems, it is necessary to design new techniques that adapt the resources unequally in order to realize a certain UEP profile.

Unequal error protection (UEP) channel coding would be one possible solution together with the current loading algorithms. However, the earlier physical transport components can allow for easier implementation of UEP transmission that can reduce the effort and the redundancy bits used in channel coding. For example, modulation levels can be adapted for devoting different numbers of bits according to the given UEP profile. This is practically valid when OFDM (DMT) is used, where the different channel conditions can be allocated to different numbers of bits with different error protections. Hence, we propose a set of iterative UEP bit-loading algorithms which are capable of realizing different noise margins γ_j for different priority classes j in the same data frame. This is done by allocating different data parts, e.g., different streams, to different subcarriers (with different bit-rate and error probabilities).

In [3]-[2], we succeeded in modifying the traditional bit-loading algorithms, e.g., the ones by Hughes-Hartogs, Campello, Chow-Cioffi-Bingham [32], and Fischer-Huber [87] to realize UEP. This was based on a simple subcarriers partitioning. In here, we present three different approaches for solving this problem. The first approach aims at finding the hypothetical thresholds between classes using the fastest possible search technique, which is a binary search. This technique has a complexity $O(N \log_2(N))$, where N is the number of subcarriers. However, in every iteration, the sum rate of all subcarriers in each group has to be computed. Therefore, the second approach [4] aims at minimizing searching complexity using a cumulative summation (CUMSUM) process. The CUMSUM stops adding the bits of each groups once it approaches the desired sum rate for each group. In order to simplify the role of our CUMSUM, we derive "almost" accurate initial conditions. The third approach [3] succeeds in finding these hypothetical thresholds with one (or at most two) iterations. In the following, we sketch the designed UEP bit-loading algorithms. First, we start with the simple subcarrier partitioning using binary search and integer summation. Next, we present the second approach with a floating-point summation approximation. Finally, we discuss a single iteration partitioning scheme that replaces the greedy bit-loading algorithms.

3.2.1 Subcarrier Sorting and Partitioning

In order to realize UEP transmission, it is required to sub-divide the given subcarriers among the required N_g protection classes. This can be achieved by setting hypothetical thresholds, τ_j, which are modified to fulfill UEP requirements, thereby, changing the number of subcarriers for each class. In practice, the carriers will initially be ordered according to $\mathcal{G}_k$ before introducing thresholds. Robust sorting tends to allocate the most important data, with the higher γ_j, to

lower CGNR subcarriers and the least important data to higher CGNR subcarriers.

Allocating important data to weaker subcarriers will protect them in case of non-stationary noise, e.g., impulse-like noise, since the SNR may not vary that much. Another advantage of combining such 'robust sorting' and the UEP bit-loading is spreading the important data over many subcarriers. This results in reducing the impact of harmful narrow-band interference if the important data are subject to these interference locations. The opposite scheme, when the most important data are allocated to the subcarriers with the highest CGNR, is referred to as 'intuitive sorting'. Figure 3.2 models a special case of ordered CGNRs composed of three protection classes (Class_0, Class_1, and Class_2), where Class_0 is the highest protected class in both schemes.

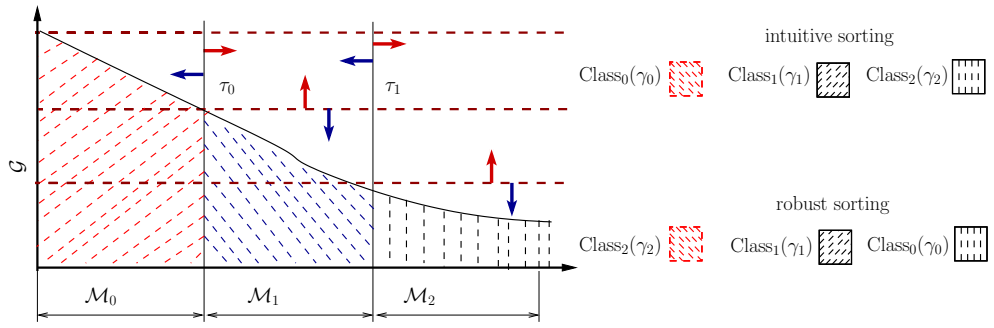

Figure 3.2: SNR thresholds for different sorting schemes

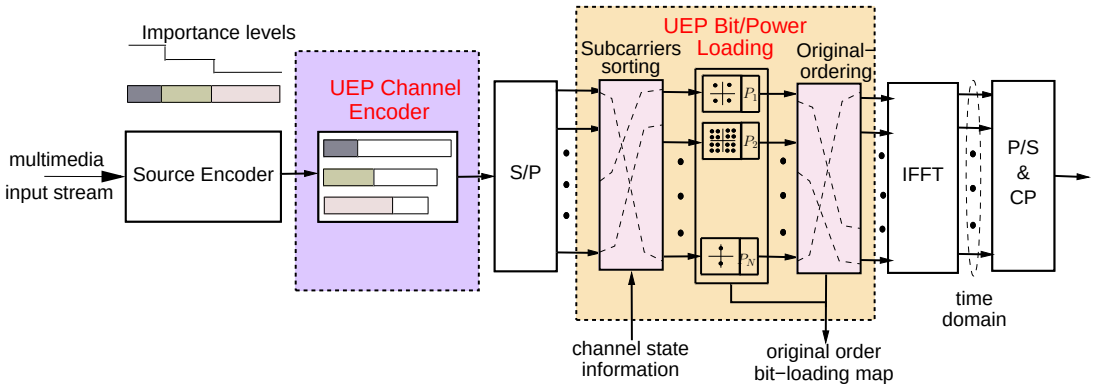

Figure 3.3: Transmitter block diagram showing the UEP/adaptive process

3.2.2 Chow-like UEP Bit-loading

In [4, 2, 5], we adopt different noise margins γ_j for j protection levels instead of a single noise margin. Assuming N_g protection levels, our algorithm is flexible to adapt modulation and power in order to realize arbitrary noise margin separations between these classes. In this method, we modify the bit-loading formula (originally given by Chow et al.) given by (3.10). Thus, the modified UEP (quantized) bit-loading formula is given by [6]

$$\hat{b}_{k,j} = \lfloor b_{k,j} + 0.5 \rfloor_0^{b_{\max}} = \left\lfloor \log_2 \left(1 + \frac{\mathcal{G}_{k,j}}{\gamma_j} \right) + \frac{1}{2} \right\rfloor_0^{b_{\max}}, \tag{3.33}$$

with quantization errors

$$\Delta b_{k,j} = b_{k,j} - \hat{b}_{k,j} \ , \tag{3.34}$$

where γ_j is the noise margin and, again, $\mathcal{G}_{k,j} = \lambda_{k,j}/\sigma_n^2$. Without loss of generality, the γ_j are assumed to have constant spacing. Throughout this thesis, we stick to margin separations of 3 dB. Figure 3.3 depicts the proposed block diagram of the prioritized adaptive transmitter.

In the following, we presents two developed approaches to realize UEP. The first uses an iterative method to subdivide the subcarriers among the classes. The second uses a faster searching approach with a more accurate initial noise margin.

3.2.2.1 UEP Chow-like bit-loading - first approach

The following is the complete pseudo-code of our algorithm.

Algorithm 3.4 UEP Chow-like RA UEP bit-loading – first approach

Input: CGNR $\mathcal{G}_k = \lambda_k/\sigma_n^2$,$\forall k = 0..N-1$, N_g, B_T, T_j, P_T, the maximum outer iterations "MaxCnt$_1$", the maximum inner iterations "MaxCnt$_2$", and $\Delta\gamma = 3$ dB

Output: γ_j, average probability of error $\mathcal{P}_j$, and bit allocation

Initialize: total number of subcarriers N, target sum rate B_T, outer counter $\text{Cnt}_1 = 0$, inner counter $\text{Cnt}_2 = 0$, and $\gamma_{m_{\text{init}}} = 1$

1: sort the subcarriers in a descending order according to the subcarriers CGNR
2: **repeat**
3: the ordered subcarrier indices are stored in the set $\mathcal{M}_j$, where $j = 0..N_g - 1$ and $\mathcal{M}_j$ initially divides the subcarriers equally
4: γ_0 may initially be set to $\gamma_{m_{\text{init}}}$ and is iteratively adjusted to fulfill the UEP requirements and the required individual number of bits T_j. Let γ_0 denote the highest protection level. The others are computed as $\gamma_j = \gamma_0 - j \cdot \Delta\gamma$ in dB
5: **repeat**
6: $b_{k,j}$ is calculated using (3.33)
7: the number of subcarriers in $\mathcal{M}_j$, $\forall\ j \in [0, N_g - 1)$ is adjusted using a binary search as described in Appendix A. This process is equivalent to sliding the hypothetical thresholds τ_j in Fig 3.2.
8: $\text{Cnt}_2 \Leftarrow \text{Cnt}_2 + 1$
9: **until** $\sum_{\mathcal{M}_j} b_{k,j} = T_j$ or $\text{Cnt}_2 = \text{MaxCnt}_2$
10: γ_0 is recalculated using $\gamma_{0,new} = \gamma_{0,old} \cdot 2^{\frac{\sum_k^N b_k - B_T}{N}}$; $\gamma_j = \gamma_0 - j \cdot \Delta\gamma$; and $\text{Cnt}_1 \Leftarrow \text{Cnt}_1 + 1$
11: **until** $\sum_k^N b_k = B_T$ or $\text{Cnt}_1 = \text{MaxCnt}_1$
12: **if** IterateCount = MaxCount and $B_{tot} \neq B_T$ **then**
13: If the maximum number of iterations is approached without achieving B_T, brute-force measures, as in Algorithm 3.2 from line 14 to line 18, are taken. Dependent on $\Delta b_{k,N_g-1}$ bits are added to the least protected class at locations of maximum $\Delta b_{k,N_g-1}$ or bits are removed at locations of minimum $\Delta b_{k,N_g-1}$ until the target bit-rate is fulfilled.
14: **end if**

Based on the Chow algorithm, we define N_g groups with different required target rates T_j and the total target bit-rate is given by $B_T = \sum_{j=0}^{N_g-1} T_j$. According to (3.33), the numbers of bits $b_{k,j}$ are truncated to the nearest integer $\hat{b}_{k,j}$, where $\Delta b_{k,j}$ is the 'quantization error', and $b_{\max}$ is the maximum allowed number of bits per subcarrier. We consider constant noise margin steps $\Delta\gamma_j$ between the groups, which, of course, can be generalized to different step sizes. Finally, the power is allocated using the symbol-error rate formula as in Algorithm 3.2, line 20, and scaled up (or down) based on the target power P_T as in line 21.

The analysis of Algorithm 3.4

Our results are generated assuming an application that only requires three different protection classes. Each class requires different target-rates, T_j, and a fixed noise margin step size, $\Delta\gamma$, between these classes. $\Delta\gamma$ needs to be selected according to application requirements, and here it is assumed to be fixed at 3 dB. Thus, the symbol-error rate curves would be separated by 3 dB. The pure Chow-Cioffi algorithm [32] without UEP (non-UEP) bit-loading is chosen as a reference. In this approach, the robust sorting is an additional ingredient which has not been taken into account in [88]. Otherwise, high protected data will be extremely vulnerable to non-stationary channel conditions, like impulse noise and deep fading conditions. However, there is a price to be payed if robust sorting is blindly applied. In order to study these effects more, we subdivide the analysis into two independent studies, with and without non-stationary noise.

Channel with stationary noise only: Figure 3.4 shows the effect of stationary background noise for both sorting schemes, with intuitive and robust sorting. All the curves show the desired spacing of 3 dB. Furthermore, we added the corresponding performance curve for of a non-UEP bit allocation for comparison. As expected, this curve represents an average performance relative to the UEP curves with equal margin separations and different individual rates. However, the non-UEP scheme performs closer to the least priority class for the case when $T_0 < ... < T_{N_g-1}$. From Fig. 3.4, we see that there is a drawback when blindly applying robust sorting. It shows a worse performance in a stationary environment by almost 1.7 dB. This is due to the large quantization steps in power needed for allocating bits of the highest-priority class. This may result in having quite some non-used subcarriers at low SNRs, since these subcarriers were only devoted to high-priority bits, which cannot be placed there any more. One could allow for mixed allocation of additional lower priority bits on these unused low-SNR subcarriers.

Channel with impulse noise in addition to background noise: Here, we studied real measured impulse noise. In order to compute a pseudo PSD, the frequency domain of the impulse noise signal was calculated by an FFT assuming it to be a stationary event, which is, of course, not true (see Chapter 1, Section 1.3.1, for more details). Figure 3.5 shows the symbol-error rate curves due to impulse noise plus stationary noise. In this case, the system with robust sorting performs dramatically better than the intuitive sorting. It can also be shown that intuitive sorting SER performances are even turned upside down such that the best protected class will be having the worst SER. One could also allow for a switching between robust sorting and intuitive sorting depending on the presence/absence of non-stationary noise on the channel.

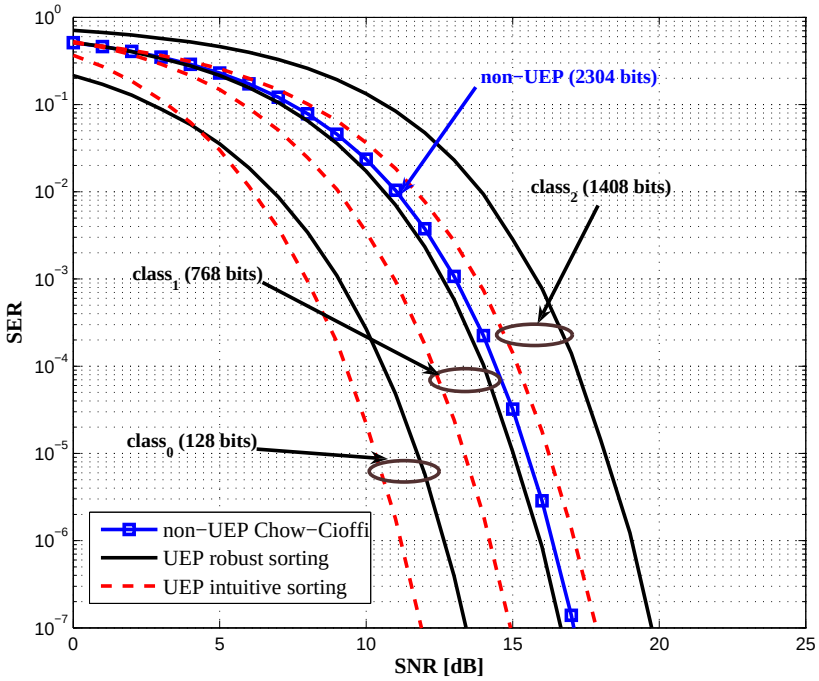

Figure 3.4: SER for UEP using intuitive sorting (without impulse noise), with a sum rate of $B_T = 2304$ bits/DMT-frame with 512 subcarriers under T1/HDSL NEXT disturbers using an Austrian 0.4-mm cable of length 2 km

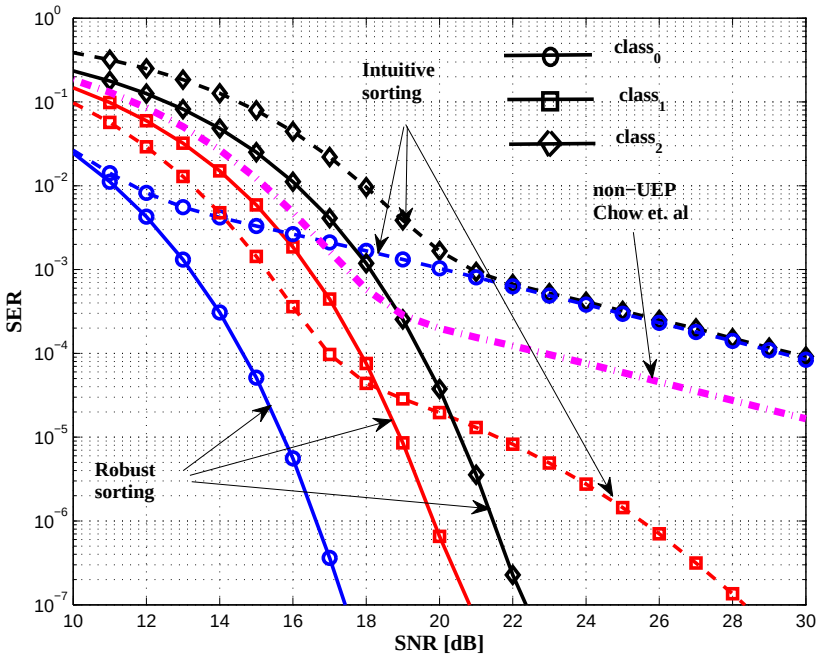

Figure 3.5: UEP using robust and intuitive sorting under the effect of impulse noise assuming sum rate $B_T = 2304$ for 512 DMT subcarriers under T1/HDSL NEXT disturber and the impulse noise described in Chapter 1 using an Austrian 0.4-mm cable of length 2 km

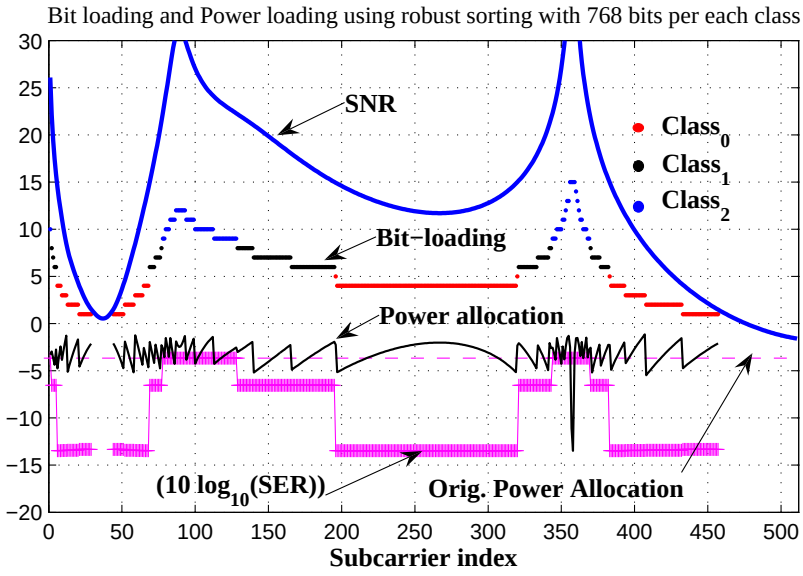

Figure 3.6: Robust sorting for a sum rate $B_T = 2304$ bits/DMT-frame with 512 subcarriers using a MAR model impulse response of a 2 km 0.4 mm loop and 10-T1/10-HDSL NEXT disturbers

Bit and Power Loading: Figure 3.6 shows the UEP bit and power loading for the robust sorting mode for the defined channel parameters and stationary noise at 512 subcarriers (FFT length 1024), it also shows (with some normalization to fit the given coordinate scale) SER varies for each UEP level. As of robust sorting, high protected data will be put on low-SNR subcarriers with a correspondingly very low bit load, i.e., small QAM constellations. This ensures a strong protection against non-stationary noise and varying channel conditions.

Due to the lower bit load values and the resulting data spread over a large number of subcarriers for the highest protected class, narrow-band interference can only hit a few of these carriers, which are carrying only a small number of bits. This make it also robust against narrow-band interference. Figure 3.7 shows the loading with the 'intuitive sorting'. Unlike the robust sorting scheme, the highest protected data will be placed in the highest-CGNR subcarriers with a high number of bits. Consequently, this concentrates the important data in fewer subcarriers, which makes the system vulnerable to non-stationary distortion and narrow-band interference. Despite of that, the intuitive sorting improves the subcarrier utilization and optimize the power allocation.

3.2.2.2 UEP Chow-like bit-loading SER analysis - second approach

In the previous approach, the dependence on an arbitrary initial γ_m leads to a very slow convergence to the target rates. However, in [4], we proposed another Chow-like UEP bit-loading which achieves the target rates in a very small time. The main reason for this fast convergence is the accurate computation of an initial margin γ_m, which is computed using a starting average noise margin $\gamma_{m_{\text{init}}}$ that is further enhanced using a single floating-point summation. Hence, for an odd number of classes[5], we can show that the middle class m performs very similar

[5] Assuming equal margin separations and equal individual target rates.

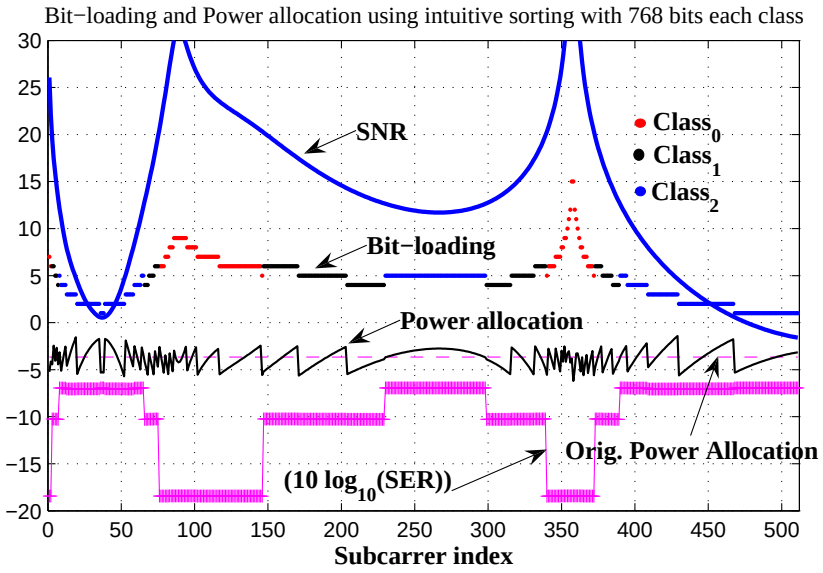

Figure 3.7: Intuitive sorting assuming the same sum rate $B_T = 2304$ for 512 subcarriers for MAR model of a 2 km 0.4 mm loop and 10-T1/10-HDSL NEXT disturbers

to a non-UEP bit-loading that allocates an equivalent total sum rate B_T using the same N subcarriers, e.g., as in Fig. 3.4. The initial average noise margin $\gamma_{m_{\text{init}}}$ is approximated using the average CGNR $\overline{\mathcal{G}}$ and the average number of bits/subcarrier B_T/N, i.e., assuming a non-UEP bit-loading and uniform CGNR (e.g., as assumed by Yu and Willson). Thus, such that

$$\gamma_{m_{\text{init}}} = \frac{\overline{\mathcal{G}}}{2^{B_T/N}} \ . \tag{3.35}$$

Thereafter, we enhance this value using the following steps.

1. compute the total sum rate using $\gamma_m = \gamma_{m_{(\text{init})}}$ as:

$$\begin{aligned} B_T &= \sum_{k=0}^{N-1} \log_2\left(1 + \frac{\mathcal{G}_k}{\gamma_m}\right) = \sum_{k=0}^{N-1} \log_2\left(\frac{\gamma_m + \mathcal{G}_k}{\gamma_m}\right) \\ &= \sum_{k=0}^{N-1} \log_2\left(\gamma_m + \mathcal{G}_k\right) - N_s \log_2 \gamma_m \ , \end{aligned} \tag{3.36}$$

2. assuming that $\gamma_m << \mathcal{G}_k$, the addition inside the $\log_2$, i.e., $(\gamma_m + \mathcal{G}_k)$, is less sensitive to γ_m. Thus, it is helpful to express γ_m in (3.36) as a function of $\mathcal{G}_k$ and γ_m as follows

$$N_s \log_2 \gamma_m = \sum_{k=0}^{N-1} \log_2\left(\gamma_m + \mathcal{G}_k\right) - B_T \ .$$

3. Consequently, a new and a more enhanced version of γ_m can be computed using the old value $\gamma_{m_{\text{old}}}$[6] using a summation of floating-point values as follows

$$\begin{aligned} \log_2 \gamma_m &= \frac{\sum_{k=0}^{N-1} \log_2\left(\gamma_{m_{\text{old}}} + \mathcal{G}_k\right) - B_T}{N} \\ \therefore \quad \gamma_m &= 2^{\frac{\sum_{k=0}^{N-1} \log_2\left(\gamma_{m_{\text{old}}} + \mathcal{G}_k\right) - B_T}{N}} \ . \end{aligned} \tag{3.37}$$

[6] $\gamma_{m_{\text{old}}}$ may initially be set to $\gamma_{m_{\text{init}}}$

Accordingly, the noise margins of the other class are computed using Δ_γ as

$$\gamma_{j+1} = \gamma_j / \Delta_\gamma \ . \tag{3.38}$$

The main idea behind the approximation in (3.37) is the floating-point summation in (3.36), which deals with the accumulation of the floating-point bit loads that results from the $\log_2$ operator. The floating point summation has been known for its difficult implementation on the outdated digital signal processors (DSPs). However, this approach is applicable in most of the modern fixed-point DSPs, which are capable of realizing mixed fixed-point widths, i.e., 16, 32, or even 64, in their main computational unit (multiply and accumulate unit (MAC))[7]. Therefore, they are capable of realizing different precision and accuracies using only binary additions with fixed-point representation. This is as easy as the integer addition, e.g., in [32, 87], except for the effort needed for controlling overflows, which are already minimized using a mixed fixed-point widths architecture [92].

Moreover, relying on the quantized summation inside the adaptation loops may lead to error propagation due to the quantization error. Additionally, starting from an arbitrary γ_m, which has not been proved in [32] to guarantee convergence at all, is increasing the chance for error propagation, i.e., when a false bit-loading values are computed using the inaccurate γ_m. Thus, the previous floating-point summation helps to limit the error propagation. Furthermore, the proposed floating-point summation results in an accurate (or almost accurate) γ_m that satisfies the target sum rate using the floating-point bit loads.

Bit-loading and subcarrier grouping

As a straightforward approach for allocating the different N_g classes, the subcarriers are also sorted in descending order (according to their CGNR). Thus, the data in the highest priority class $j = 0$ are allowed to consume the stronger subcarriers first, i.e., assuming intuitive sorting. Hence, the bits in class $j = 0$ are allocated using Eqn. (3.33) and the computed γ_0. Thereafter, a hypothetical threshold is set to the subcarrier location that satisfies the individual target rate T_0. This can be performed using the same binary search method in the first approach. Keeping into mind that the binary search requires $N \log_2 N$ iterations and each of this iterations requires the sum rate for each group to be computed, which is, indeed, a huge complexity at the end. Therefore, we introduce a novel scheme that performs a sequential summation for all bit loads using the so-called cumulative summation[8]. Simply, the cumulative summation is composed of an adder and a shift register (initially set to zero), where the output of the adder is saved into this shift register and then moved again to the input of the adder after an appropriate delay. Thereafter, the value in the delay element is inserted to the adder input and added to the input stream as in shown Fig. 3.8. Hence, for an arbitrary input array $\mathbf{x}$, where $\mathbf{x} = \{\alpha_0, \alpha_1, \alpha_2, \alpha_3, ..., \alpha_{N-1}\}$, the cumulative summation output $\mathbf{y}$ is defined as the following

$$\mathbf{y}(i) = \text{cumsum}(\mathbf{x}) = \sum_{n=0}^{n=i} \alpha_n \ , \ \forall \ i = 0..N-1 \ .$$

[7] modern fixed-point DSP acquire 16-bits data and perform their arithmetic operations on 32 and/or 64 bits MAC unit as, e.g., in the Analog Devices Blackfin DSP [92]

[8] cumulative summation in Matlab [93] and Octave [94] is known as the function *cumsum*()

This accumulation is done sequentially until we achieve the given target sum rate, thus, we stop accumulating. Moreover, we proposed a tapped bridge cumsum (as in Fig. 3.8) where we can decide to stop at the current output, i.e., $\sum_{i=0}^{n-1} \mathbf{x}(i)$ or the previous summation at $n-1$, if the current summation is bigger than the required rate. Hence, for sorted channel gains, as in Fig. 3.2, the hypothetical threshold, e.g., of the first class τ_0, can be found such that the sum rate is slightly greater than or equal T_0. Consequently, the next classes are allocated using their individual bit loads $b_{k,j}(\gamma_j)$ and target rates T_j. However, the accumulation starts from the subcarrier next to the previous hypothetical threshold τ_{j-1}. Finally, if the total target rate B_T is not fulfilled, the overall γ_m has to be readjusted using an outer loop which forces to calculate the initial γ_m once more. Hence, the whole procedure has to be recomputed.

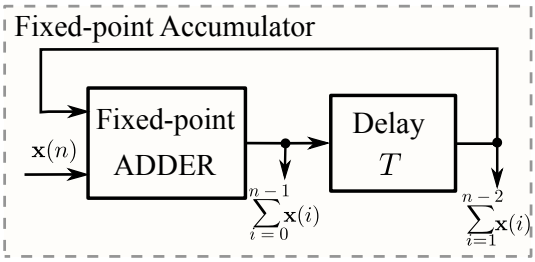

Figure 3.8: The proposed cumulative summation with two bridge taps

If the total power $\sum_{k=0}^{N-1} p_k$ computed from (3.39) is lower than the target power P_T, the scaling in Line 16 is equivalent to a margin maximization (MM) criterion. However, in general, this step guarantees adapting the margin to the current channel conditions. The main drawback of this approach is the need for two nested loops. An inner loop which adjusts the individual classes sum rate T_j (as binary search is used) and an outer loop which is responsible for adjusting the over all sum rate B_T. Therefore, we present another approach that aims adjusting the individual rates using a sequential addition of the sorted bit-loading values.

The analysis of Algorithm 3.5

Figure 3.9 shows the performance of the modified Chow et al. algorithm assuming multicarrier modulation with 2048 subcarriers. In this case, we considered a wireless channel which is subject to a multipath Rayleigh fading with addition to AWGN. We considered the channel power delay profile of 9 delayed taps that results in a frequency selective frequency response (see Chapter 1 for more details about wireless channels). Accordingly, bits are allocated depending on the sorted CGNR of all subcarrier, the target sum rate for every class, and the required margin separations between classes. We assumed the same margin separations between each two classes to be 3 dB. As expected, the algorithm preserves the designed 3 dB margin separation for any given sum rate or individual rates. However, it is clear in this figure, and similar to previous results in Fig. 3.4, that the performance deteriorates when adding more bits to the first class (see the second scenario with target rate of each class fixed to T_j =2048 bits).

Convergence of Algorithm 3.5

We studied the convergence of the original Chow et al. algorithm (first approach) using two

Algorithm 3.5 UEP Chow-like RA UEP bit-loading – second approach

Input: CGNR $\mathcal{G}_k = \lambda_k/\sigma_n^2$,$\forall k = 0..N$, N_g, B_T, T_j, the maximum number of iterations "MaxCnt$_1$", and $\Delta\gamma = 3$ dB

Output: γ_j, power allocation p_k, average probability of error $\mathcal{P}_j$, and bit loads

Initialize: start index $\mathcal{I} = 0$, $\tau_j = N \ \forall \ j = 0..N_g - 1$, target power P_T, total subcarriers N, target sum rate B_T, counter $\text{Cnt}_1 = 0$, and $\gamma_{m,\text{old}} = \gamma_{m_{\text{init}}} = \frac{\overline{\mathcal{G}_k}}{2^{B_T/N}}$

1: sort the subcarriers in a descending order according to the subcarriers CGNR
2: **repeat**
3: compute γ_m for the middle class m using (3.37). Thereafter, the other γ_j are computed using the relation (3.38)
4: **repeat**
5: $\hat{b}_{k,j}$ is calculated as in (3.33) using γ_j starting from $\mathcal{I}$
6: using the cumsum operator $\hat{b}_k \ \forall k = 0..N-1$ values, the number of subcarriers for each priority class are selected such that T_j is fulfilled.
7: set τ_j to the location where the cumsum stops
8: $\mathcal{I} \Leftarrow \tau_j + 1$
9: $j \Leftarrow j + 1$
10: **until** $j = N_g$
11: γ_m is recalculated using the following adjustment, as in Algorithm 3.4, $\gamma_{m,\text{new}} = \gamma_{m,\text{old}} \cdot 2^{\frac{B_{tot}-B_T}{N}}$
12: $\gamma_j = \gamma_m + (m-j)\cdot\Delta\gamma$
13: $\gamma_{m_{\text{init}}} = \gamma_m$
14: $\text{Cnt}_1 \Leftarrow \text{Cnt1} + 1$
15: **until** $\sum_j^{N_g}\sum_{\mathcal{M}_j} b_{k,j} = B_T$ or $\text{Cnt}_1 = \text{MaxCnt}_1$
16: **if** $\sum_j^{N_g}\sum_{\mathcal{M}_j} b_{k,j} \neq B_T$ **then**
17: further tuning based on the quantization error (3.34) is performed as in [32]
18: **end if**
19: power is allocated from the capacity formula, i.e., $b_{k,j} = \log_2(1 + \frac{p_{k,j}\mathcal{G}_{k,j}}{\gamma_j})$, such that

$$p_{k,j} = \left(2^{b_{k,j}} - 1\right)\frac{\gamma_j}{\mathcal{G}_{k,j}} \ . \tag{3.39}$$

20: power is rescaled such that $p_{k,j} = p_{k,j} \cdot \sum_k^N p_k / P_T$.

different methods: starting with a fixed arbitrary margin of 3 dB and a uniformly distributed random margin $\in [0.1, 10)$. Furthermore, we studied our second approach using the initial margin using (3.35) with a single floating-point summation enhancement (as in (3.36)). In order to simplify our comparison, we assumed a single priority class that requires the total target rate of 2304 bits/OFDM symbol (a non-UEP bit-loading). The channel for every iteration has been generated randomly using the Rayleigh fading parameters in the discussed second approach, while the SNR of the AWGN has been randomly selected between -5 and 15 dB. In Fig. 3.10, it is clear that starting from a random (or even fixed margin) does not suite every channel and every CGNR. However, computing the margin efficiently, as in our second approach, leads to

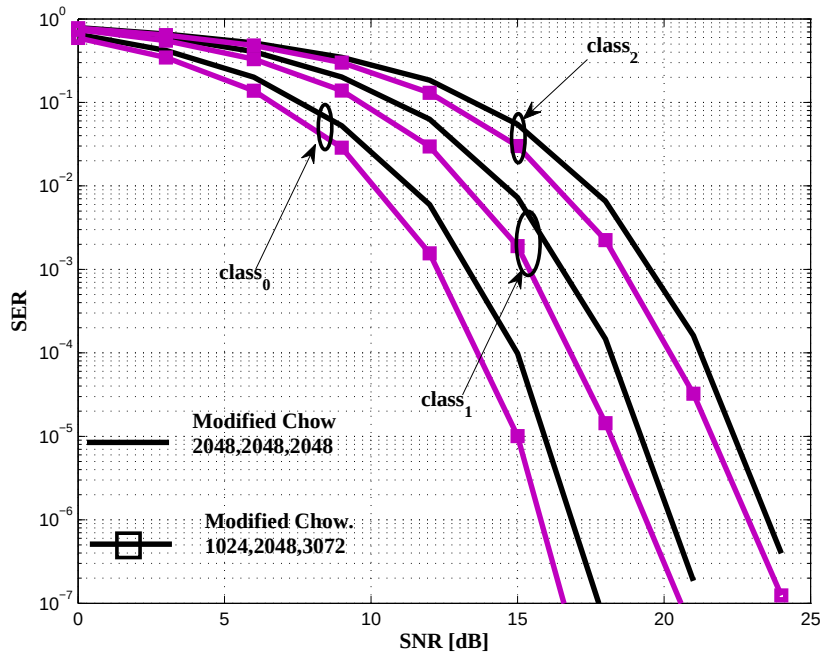

Figure 3.9: Intuitive sorting Chow-like UEP bit-loading, second approach, allocating 2048 subcarriers assuming two scenarios: T_0=1024, T_1=2048, T_2=3072, and $T_{j=0..2}$=2048 bits

almost instantaneous convergence, i.e., results achieved at the second or the third iteration.

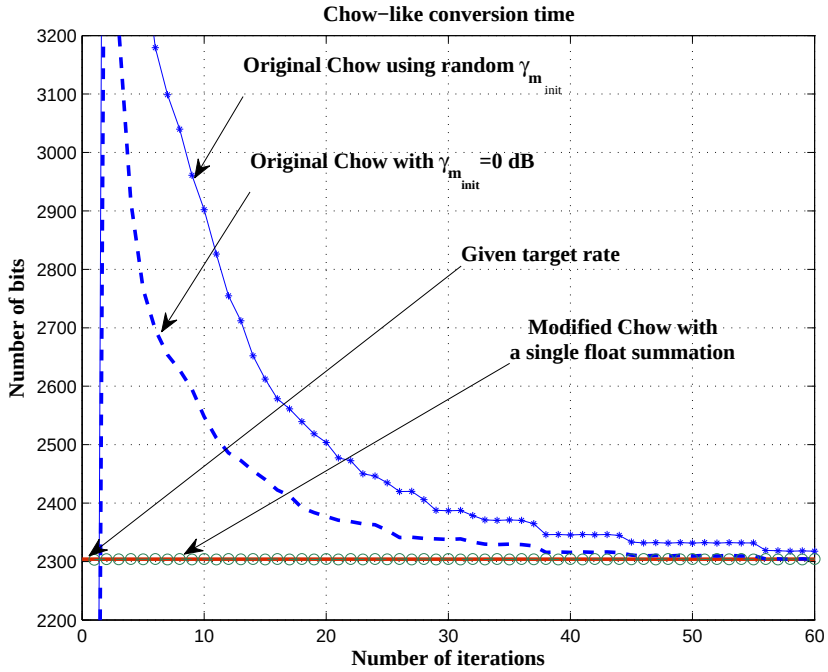

Figure 3.10: Chow-like convergence time using the first and the second approach

3.2.3 Fischer-like UEP Bit-loading

In this algorithm, we discuss the possibilities of modifying the Fischer-Huber algorithm [87] for realizing UEP. As mentioned in Section 3.1.2.3, Yu and Willson have already studied the Fischer algorithm and the possibilities to realize UEP. However, we are revisiting this algorithm using our sorting-partitioning approach proposed earlier in this chapter, Section 3.2.1. Finally, we propose a new floating-point adaptation that guarantees faster convergence to the required overall target sum rate B_T and the individual bit-rate T_j. The main advantage of the Fischer-Huber algorithm is the linear representation of the bit-loading equations. Accordingly, the modified UEP bit-loading formula of the Fischer algorithm (3.21) (for N_g classes) can be written as

$$b_{k,j} = \frac{T_j}{L_{\mathcal{M}_j}} - \frac{1}{L_{\mathcal{M}_j}} \sum_{\mathcal{M}_j} \log_2 \mathcal{G}_{k,j} + \log_2 \mathcal{G}_{k,j} = \bar{b}_j - \overline{\mathbb{G}}_j + \mathbb{G}_{k,j} \ , \tag{3.40}$$

where, again, $\mathbb{G}_{k,j}$ is the $\log_2$ value of the channel-to-noise gain $\mathcal{G}_{k,j}$, and $\overline{\mathbb{G}}_{k,j}$ represents its geometric mean. Thus, Fischer-like UEP bit-loading is also allocating bits according to $\bar{b}_j - \overline{\mathbb{G}}_j$ which is only dependent on the number of used subcarriers and does not change significantly between classes, unless we know the subcarrier set in each class $\mathcal{M}_j$. That is why Yu and Willson try first to adjust $\mathcal{M}_j$ before knowing the exact bit load values. Indeed, this method is very difficult to implement. However, if we use the first approximate values for $\mathcal{M}_j$ with an adaptive margin that changes iteratively (as in the Chow algorithm), we can adapt much faster to the final quantized bit loads. Therefore, we derive here the relation between (3.40) and Chow's noise margin in (3.33) (after omitting the "1" inside the $\log_2$) to be

$$\overbrace{b_{k,j}}^{\text{Chow-like}} = \log_2(\mathcal{G}_{k,j}/\gamma_j) = \mathbb{G}_{k,j} + \log_2(1/\gamma_j) \tag{3.41}$$

$$\overbrace{b_{k,j}}^{\text{Fischer-like}} = \mathbb{G}_{k,j} + \frac{T_j}{L_{\mathcal{M}_j}} - \overline{\mathbb{G}}_{k,j} \ . \tag{3.42}$$

Now, equating (3.42) to (3.41), we get

$$\frac{T_j}{L_{\mathcal{M}_j}} - \overline{\mathbb{G}}_{k,j} = \log_2 1/\gamma_j \ , \tag{3.43}$$

where γ_j is the j^{th} class noise margin. Hence, the steps of Algorithm 3.4 can directly be applied to realize UEP with different Δ_{γ_j} using an iterative method, i.e., Section 3.2.3.1. Similar to Algorithm 3.5, we develop a faster version of the modified Fischer-Huber Algorithm in Section 3.1.2.2

3.2.3.1 Fischer-like UEP bit-loading – iterative method

To modify the bit-loading (in (3.40)), to realize the different margin separations Δ_γ, we have to find the relation between the noise margin and the error probability which is then inserted it in

the Yu-Willson system equations. As in (F.4), Appendix F, the SER for M-ary QAM is

$$\begin{aligned}\mathcal{P}_j &= 2\left(1-\frac{1}{\sqrt{2^{b_{k,j}}}}\right)\operatorname{erfc}\left(\sqrt{\frac{3}{2}\frac{\overline{p}\mathcal{G}_{k,j}}{(2^{b_{k,j}}-1)}}\right)\\ &\approx 2\operatorname{erfc}\left(\sqrt{\frac{3}{2}\frac{\overline{p}\mathcal{G}_{k,j}}{(2^{b_{k,j}}-1)}}\right)\ ,\end{aligned} \tag{3.44}$$

where $(1-1/\sqrt{2^{b_{k,j}}}) \approx 1$ for higher order modulation, $\overline{p}$ is the average signal power[9], and $\mathcal{G}_{k,j}$ is the CGNR of the j^{th} class and the k^{th} subcarrier. Thus, from (3.33) we get the relation between $\mathcal{G}_{k,j}$ and γ_j for different bit load values to be

$$\mathcal{G}_{k,j} = \gamma_j\left(2^{b_{k,j}}-1\right)\ . \tag{3.45}$$

Now, substituting (3.45) into (3.44), we obtain

$$\mathcal{P}_j \approx 2\operatorname{erfc}\left(\sqrt{\frac{3\gamma_j}{2}}\right)\ . \tag{3.46}$$

Therefore, the noise margin for class j can be written as

$$\gamma_j \approx \frac{2}{3}\left[\operatorname{erfc}^{-1}\left(\frac{\mathcal{P}_j}{2}\right)\right]^2\ , \tag{3.47}$$

where $\gamma_j = \gamma_0$,for $j=0$ or $\gamma_j = \gamma_0/(j\cdot\Delta_\gamma)$,$\forall\ j = 0..N_g-1$. Thus, if the SER for each class is given and the final individual bit-rates T_j, one can compute the equivalent noise margin γ_j directly using (3.47). Hence, the exact bit load values in (3.42) can be directly computed in order to satisfy the given SER. However, γ_j is computed independent of the given rates. Thus, they cannot guarantee the required T_j. Hence, the bit loads of the most important class is first computed using the stronger subcarriers; the hypothetical threshold is set accordingly, such that T_0 is fulfilled. The next classes may consume the remaining subcarriers until their individual bit-rates are fulfilled or no more subcarriers are left. Certainly, the hypothetical thresholds can be found using either the binary search (as in Algorithm 3.4) or the "cumsum" method in the second approach. In this case, we start searching for the hypothetical thresholds from the first subcarrier index. Nevertheless, one can follow the Yu-Willson algorithm to find an approximate value for the number of subcarriers in each group to narrow down searching. This is done using the average number of bits for each class $\overline{b}_j$ such that $L_{\mathcal{M}_j} = T_j/\overline{b}_j$. In this case, $\overline{b}_j$ can directly be computed from (3.41) and (3.47), however, using the $\overline{\mathcal{G}}_j$, as follows

$$\overline{b}_j = \overline{\mathbb{G}}_j - \log_2\gamma_j = \log_2\left(\frac{3}{2}\overline{\mathcal{G}}_j\left[\operatorname{erfc}^{-1}\left(\frac{\mathcal{P}_j}{2}\right)\right]^{-2}\right)\ , \tag{3.48}$$

which is used to obtain a better approximate $L_{\mathcal{M}_j}$. Thereafter, bits are computed using (3.42) until the individual target rates T_j are fulfilled, however, assuming a floating-point (non-quantized) bit loads. Thus, further quantization step is required, which may not be able to fulfill the target $\mathcal{P}_j$. Therefore, the power values on each subcarrier are forced to follow the required γ_j (computed from $\mathcal{P}_j$ as in (3.47)), the final $b_{k,j}$, and $\mathcal{G}_{k,j}$ using (3.44) to be

$$p_{k,j} \approx \frac{2}{3}\frac{\left(2^{\hat{b}_{k,j}}-1\right)}{\mathcal{G}_{k,j}}\left[\operatorname{erfc}^{-1}\left(\frac{\mathcal{P}_j}{2}\right)\right]^2 = \frac{2}{3}\frac{3}{2}\frac{\left(2^{\hat{b}_{k,j}}-1\right)}{\mathcal{G}_{k,j}}\gamma_j\ , \tag{3.49}$$

[9]Here we assume that the power is the same on every subcarrier, which is also the assumption by Fischer and Yu et al..

where $\hat{b}_{k,j} = \lfloor b_{k,j} + \frac{1}{2} \rfloor$. In the following, we discuss the complete pseudo-code of the algorithm.

Algorithm 3.6 Fischer-like using UEP bit-loading based on the modified Yu-Willson algorithm

Input: CGNR $\mathcal{G}_k = \lambda_k / \sigma_n^2$,$\forall\ k = 0..N-1$, N_g classes, target sum rate B_T, individual rates for each class T_j, target power P_T, $\mathcal{P}_0$, and $\Delta\gamma = 3$ dB

Output: $\mathcal{P}_j$ (computed using γ_j, Δ_γ, and (3.46)), power allocation $p_{k,j}$, and bit loads $b_{k,j}$

Initialize: $j = 0$ and $\gamma_0 = \frac{2}{3}\left[\text{erfc}^{-1}\left(\frac{\mathcal{P}_0}{2}\right)\right]^2$

1: sort the subcarriers in a descending order according to the subcarriers CGNR
2: find $\bar{b}_j$ using (3.48) and compute the approximate value for $L_{\mathcal{M}_j}$ such that $L_{\mathcal{M}_j} = \frac{T_j}{\bar{b}_j}$
3: according to $L_{\mathcal{M}_j}$, the subcarrier indices are addressed in the sets $\mathcal{M}_j$
4: **repeat**
5: compute the accurate γ_j using γ_0 and Δ_γ
6: calculate $b_{k,j}$ for each k subcarrier in $\mathcal{M}_j$ using (3.42)
7: compute the quantized $\hat{b}_{k.j} = \lfloor b_{k,j} + \frac{1}{2} \rfloor$
8: adjust $\mathcal{M}_j$ iteratively using sequential[10] until $\sum_{\mathcal{M}_j} b_{k,j} \approx T_j$, where a few bits may be left to the brute-force steps as in Algorithm 3.2 (Line 14 to Line 18)
9: $j \Leftarrow j + 1$
10: $\gamma_j = \gamma_0 - j \cdot \Delta\gamma$
11: **until** $j = N_g$ or no more subcarriers left
12: the power is allocated and scaled similar to Algorithm 3.5, Line 19 and Line 20

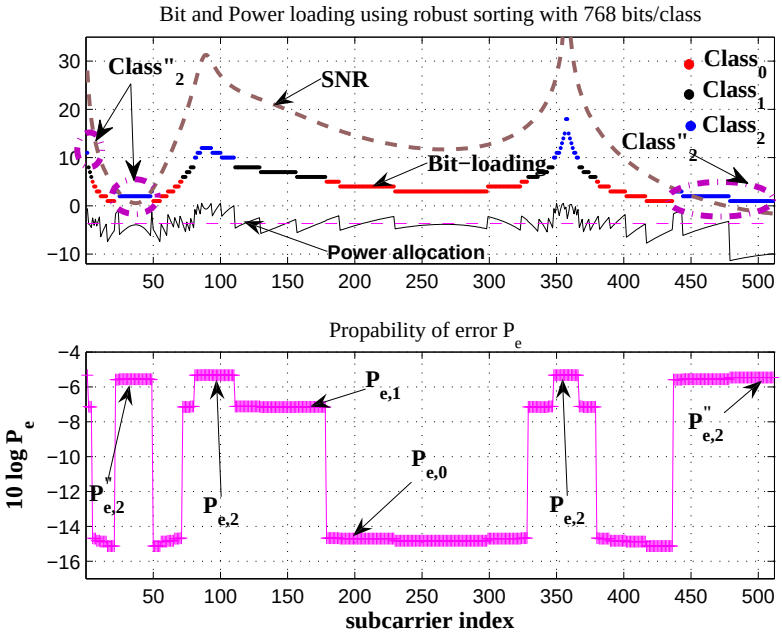

Figure 3.11: UEP Fischer-like using robust sorting

Figure 3.11 depicts the robust sorting scheme proposed in Section 3.2.1, where the most important bits are allocated to the weaker subcarriers first. The least important data are allowed to be placed on the good subcarriers and still use the leftover weak subcarriers from allocating the

highest priority class. Figure 3.12 depicts the bit-loading results for the intuitive sorting case. In both figures, the bit load values are quantized and the power is allocated according to the required $\mathcal{P}_j$. From both figures, we notice that the SER of the robust sorting is slightly worse

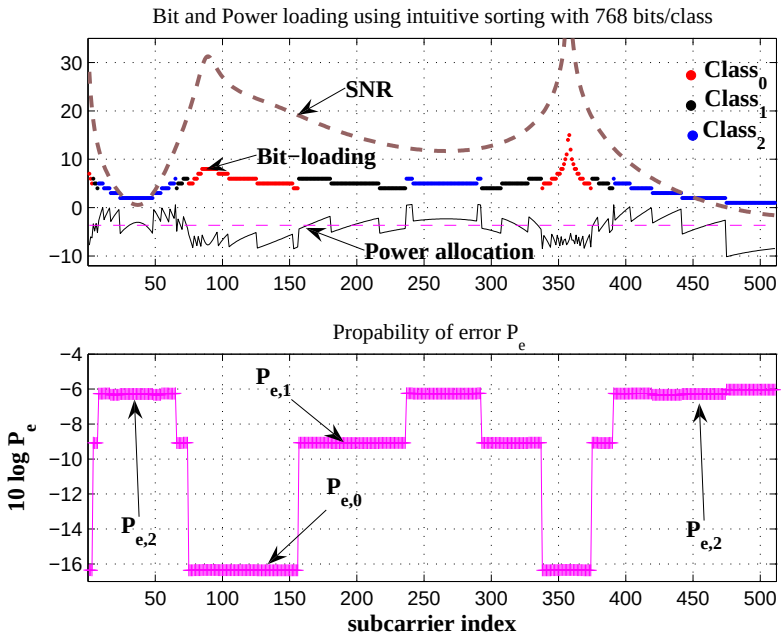

Figure 3.12: UEP Fischer-like using intuitive sorting

than the intuitive bit-loading. This can be due to congesting the bits of the least priority class to a few number of subcarriers, i.e., consuming higher power. Similarly, the weaker subcarriers are reserved for the highest priority data with high power consumption.

3.2.3.2 UEP Fischer-like bit-loading – fast method

If a target sum rate B_T is required to be fulfilled for N_g individual classes with T_j individual target rates on each class, the algorithm turns to be rate-adaptive. Hereto, the margin in (3.42) has to be calculated according to the given rates and to the current channel $\mathcal{G}_k$. As mentioned in Section 3.1.2, the main drawback of the Fischer algorithm is its slow evacuation of the negative subcarriers. As a solution, we propose a generic adaptive margin which is added to (3.42) in order to adapt the total target rate and the individual rates. This margin is adapted similar to the Chow et al. method and using the quantized positive bit loads by

$$\gamma_m^{\text{new}} \quad = \quad \gamma_m^{\text{old}} \cdot 2^{\frac{\sum_k^N \hat{b}_{k,j} - B_T}{N}} \,, \tag{3.50}$$

where the total number of used subcarriers is assumed to be N. Therefore, the $-\log_2 \gamma$ in (3.42) is computed to be

$$-\log_2 \gamma_m^{\text{new}} \quad = \quad -\log_2 \gamma_m^{\text{old}} - \frac{\sum_k^N \hat{b}_{k,j} - B_T}{N} \,. \tag{3.51}$$

In order to adapt each of the N_g different classes, their margin separations have to be considered in (3.51), i.e., by adding $-\log_2 \gamma_m - \log_2 ((m-j)\Delta_\gamma)$ to the bit load of the j^{th} class. Assuming

equal number of bits on each of these N_g classes makes the middle class equivalent to non-UEP bit-loading with the total sum rate B_T[11]. Therefore, $\gamma_m \equiv \gamma_{\text{middle}}$, which is used in order to compute every other γ_j. In the following, we list the required steps for this algorithm assuming an odd number of classes.

Algorithm 3.7 Fischer-like UEP bit-loading based on the Chow-like algorithm

Input: CGNR $\mathcal{G}_k = \lambda_k/\sigma_n^2$,$\forall k = 0..N-1$, N_g classes, target sum rate B_T, individual rates for each class T_j, target power P_T, and $\Delta\gamma = 3$ dB

Output: power allocation $p_{k,j}$ and the exact quantized bit load $\hat{b}_{k,j}$

Initialize: $j = 0$, starting index $\mathcal{I} = 0$, $\tau_j = N$, $-\log_2 \gamma_m = \frac{T_j}{L_{\mathcal{M}_j}} - \overline{\mathbb{G}}_{k,j}$, and $m = \frac{N_g - 1}{2}$

1: compute the logarithm of $\mathcal{G}_k$, $\mathbb{G}_k$,$\forall\ k = 0..N-1$

2: sort the subcarriers in a descending order according to $\mathbb{G}_k$ in a set $\mathcal{M}$

3: **repeat**

4: **repeat**

5: Calculate the quantized bit loads of the j^{th} class $\hat{b}_{k,j}$ for each subcarrier in $\mathcal{M}_j$ as

$$\hat{b}_{k,j} = \lfloor \overbrace{\mathbb{G}_{k,m} - \log_2\left((m-j)\Delta_\gamma\right) + \frac{1}{2}}^{\text{const}} - \log_2 \gamma_m \rfloor_0^{b_{\max}} ,$$

where $\mathcal{M}_j \in \mathcal{M}(\mathcal{I}+1 : \tau_j)$

6: find a more accurate τ_j using "cumsum", such that $\sum_{\mathcal{M}_j} b_{k,j} \approx T_j$

7: change the starting index $\mathcal{I}$ such that $\mathcal{I} \Leftarrow \tau_j$

8: **until** $j = N_g$ or no more subcarriers left

9: update γ_m such that $-\log_2 \gamma_m = -\log_2 \gamma_m - \frac{\sum_k^N \hat{b}_{k,j} - B_T}{N}$

10: $j \Leftarrow j + 1$

11: **until** $\sum_k^N \hat{b}_{k,j} \approx B_T$

12: power is allocated according to the bit-loading and $\mathcal{G}_k$ as in Algorithm 3.5, Section 3.2.2.2.

Analysis of Algorithm 3.7

As expect, from Fig. 3.13, the Fischer-like algorithm performs similar to the Chow-like proposed in the previous section. However, it has a slightly better performance for the least protected class assuming intuitive bit-loading. This is clear since the removal of the "1" in the capacity formula protects from allocating the very weak subcarriers and, therefore, improves the power allocation.

Convergence of Algorithm 3.7

In herein, we study the convergence of the modified Fischer-like UEP bit-lading, which is required to allocate 3 classes with 3 dB margin separations. Each of these classes is allocated with 768 bits, i.e., 2304 bits/OFDM in total. We see from Fig. 3.14 that the algorithm is also converging in almost 3 iterations. This fast convergence here is due to the use of the floating point margin

[11] If $T_0 < T_1 < ... < T_{N_g-1}$, it is most likely that we select one of the last classes to resemble the average noise margin γ_m.

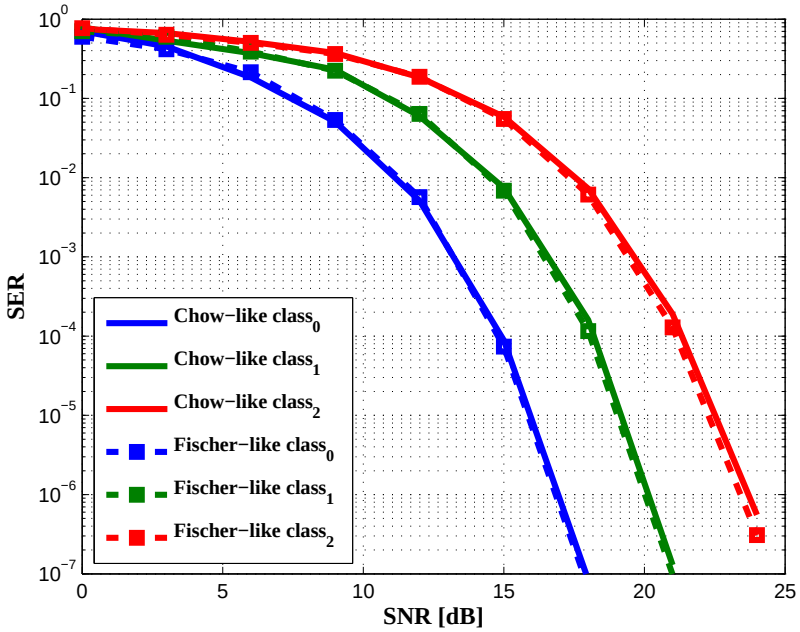

Figure 3.13: Chow-like vs Fischer-like UEP bit-loading using 2048 subcarriers and 2048 bits/class

adaptation, i.e., without the early and the slowly evacuation of the negative-load subcarriers. However, a residual oscillation can be seen on either the least priority class or, equivalently, the final target rate. This oscillation results form discarding the brute-force process at all (which has to be implemented in the last class). However, it is oscillating by a small number of bits, i.e., only ± 2 of the required target rate for this particular scenario.

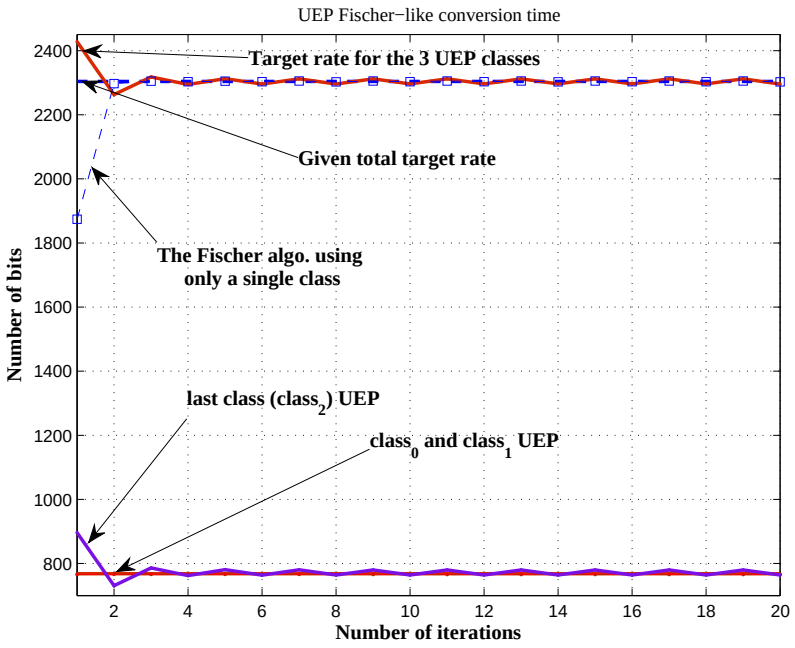

Figure 3.14: Convergence time of the Fischer-like algorithm

3.2.4 UEP Bit Allocation Based on the Greedy Method

The previous simple partitioning scheme allocates different parts of the data stream to different subcarriers (with different bit-rates and error probabilities) according to the required QoSs. This is very suitable for bit-loading schemes which rely on allocating bits according to the quantized Shannon capacity. However, for greedy methods and the algorithms that follow the power-minimization criterion, the partitioning schemes proposed in the previous sections becomes a very complex and impractical approach. Thus, we developed a partitioning scheme that efficiently approximates the number of subcarriers required for each priority class exploiting the relation between the required QoS, the target bit-rate, and the given number of subcarriers. First, we modify the heaviest -and the optimum- greedy bit-loading algorithm developed by Hughes-Hartogs [83]. Therein, the required target rates are only allowed to allocate the pre-calculated subcarrier partitions. Second, we modify the less complex (and sub-optimal) algorithm by Campello in [33] using the same method.

3.2.5 Modified Hughes-Hartogs Algorithm for UEP Bit-loading

Hughes-Hartogs' bit-loading algorithm cannot follow the partitioning scheme in [7, 2]. The reason is that the greedy algorithms allocate bits to the subcarriers with the minimum incremental power first. Therefore, we approximate the number of subcarriers required for each class by finding a hypothetical threshold between the current class and the successive classes as will be discussed later. Our approach follows the margin-adaptive criterion discussed early in this chapter. Accordingly, the maximum system margin is given by

$$\gamma_{\max} = \frac{P_T}{\sum_k^N p_k} \ . \tag{3.52}$$

3.2.5.1 Partitioning scheme

Based on the required SER and the target bit rates T_j for each class, we compute equivalent bit rates B_{T_j} (discussed later), assuming that each class can freely allocate the entire number of subcarriers separately, i.e., $B_{T_j} > T_j$. However, the selection of these B_{T_j} have to preserve or 3 dB margin separations between the classes. Once B_{T_j} for all classes are computed, we can start accumulating bits for the first class, $j = 0$, until its target rate T_0 is fulfilled, i.e., at a certain subcarrier index. This index is set as a hypothetical threshold for this class. For the next class, we start accumulating bits from the next subcarrier position and stop at the position where the accumulated number of bits gives T_{j+1}. In Appendix B, Example 1, we calculate the equivalent number of bits for an odd number of priority classes, when each class is assumed to allocate all the N subcarriers. Assume that the subcarriers are sorted in descending order and assume that it is required to allocate an equivalent number of bits, B_{T_j}, on each class, such that the SER is similar to the case when T_j is allocated to $\mathcal{M}_j$ only. According to Appendix B, assuming a fixed margin separation of 3 dB, the first, the second, and the third priority classes allocates an equivalent number of bits equals to $B_T - N$, B_T, and $B_T + N$ bits, respectively.

The following are the steps for allocating the given subcarriers to the required classes without extra iterations:

(a) Assume that each priority class is allowed to consume all the N subcarriers (sorted in descending order) to allocate B_{T_j} bits simultaneously.

(b) As in Fig. 3.15 (Part a), the first, the second, and the third priority classes will allocate $B_{T_0} = B_T - N$, $B_{T_1} = B_T$, and $B_{T_2} = B_T + N$ bits, respectively (Appendix B, Example 1).

(c) Starting from the first class and the highest SNR subcarrier, bits are accumulated using a cumulative summation (*cumsum*) process.

(d) The cum-sum will stop accumulating bits when the output is greater than or equal T_0. Hence, the current subcarrier will be the hypothetical threshold subcarrier θ_1.

(e) For the next class, the cum-sum will accumulate the bits of the second class starting from $(\theta_1 + 1)$ and continue accumulating until the output $\geq T_1$ as in Fig. 3.15. (Part b).

(f) The same steps are repeated for the remaining classes, see Fig 3.15 (Part c), to find θ_j.

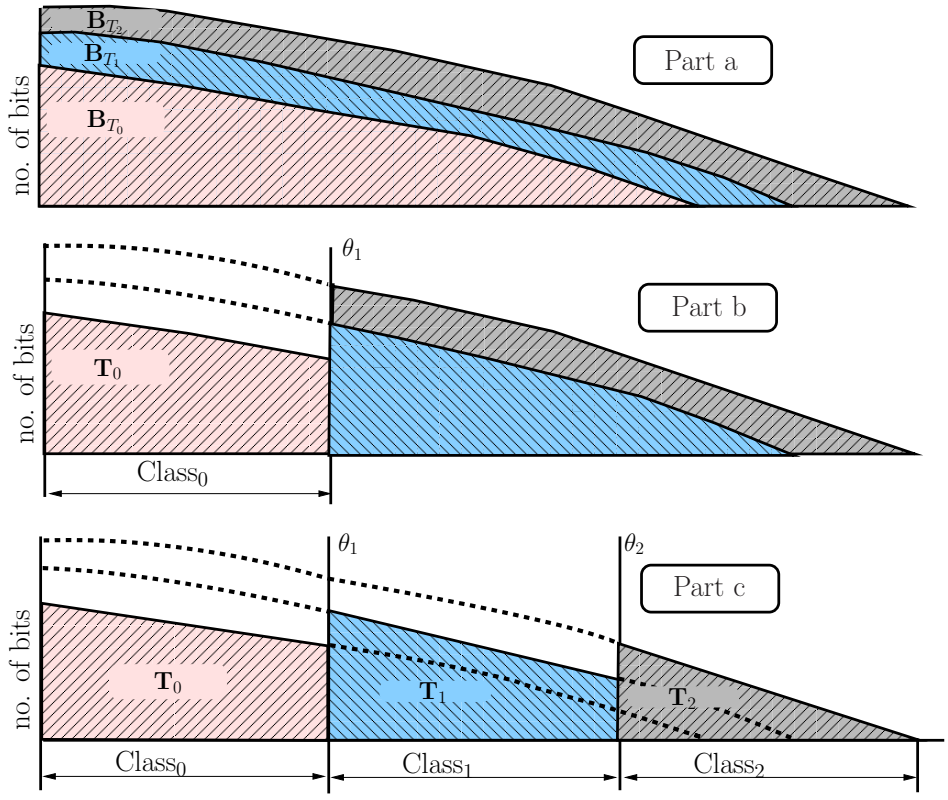

Figure 3.15: Partitioning using our approximation, cum-sum, and the calculated B_{T_j}

3.2.5.2 UEP Bit-loading steps based on Hughes-Hartogs algorithm

The complete Hughes-Hartogs-like bit-loading algorithm steps are as follows:

Algorithm 3.8 Hughes-Hartogs-like margin adaptive UEP bit-loading

Input: CGNR $\mathcal{G}_k = \lambda_k/\sigma_n^2$, $\forall k = 0..N-1$, N_g classes, target sum rate B_T, individual rates for each class T_j, the equivalent rates B_{T_j} (Appendix B), and target power P_T

Output: the power allocation $p_{k,j}$ and the exact discrete bit-loading values $\hat{b}_{k,j}$

Initialize: the zero matrices $\mathbf{B}$ (bits) and $\mathbf{E}$ (power) with N rows and N_g columns (for adapting each class with its B_{T_j}), $j = 0$, and the starting index $\mathcal{I} = 0$

1: sort the subcarriers in a descending order according to $\mathbb{G}_k$ in a set $\mathcal{M}$
2: **repeat**
3: **repeat**
4: compute the incremental power steps $\Delta p_{k,j}$ for M given classes in case of incrementing each subcarrier by only one bit as in [8]

$$\begin{aligned}\Delta p_{k,j} &= \frac{\frac{2}{3}\left[\text{erfc}^{-1}\left(\frac{\mathcal{P}_0}{2}\right)\right]^2}{\mathcal{G}_k \Delta_{\gamma_j}} \overbrace{\left(2^{\mathbf{B}(k,j)+1} - 2^{\mathbf{B}(k,j)}\right)}^{\text{bit increment}} \\ &= \frac{\frac{2}{3}\left[\text{erfc}^{-1}\left(\frac{\mathcal{P}_0}{2}\right)\right]^2}{\mathcal{G}_k \Delta_{\gamma_j}} \left(2^{\mathbf{B}(k,j)}\right) , \end{aligned} \tag{3.53}$$

where $\mathcal{P}_0$ is the probability of error of the first class.
5: find k with the minimum $\Delta p_{k,j}$ among all subcarriers in each class
6: increment $\mathbf{B}(k,j)$ by one bit such that it does not exceed the maximum $b_{\max}$
7: increment the power of the k^{th} subcarrier by $\Delta p_{k,j}$, i.e., $p_{k,j} = p_{k,j} + \Delta p_{k,j}$
8: update $\mathbf{E}(k,j)$ such that $\mathbf{E}(k,j) = p_{k,j}$
9: **until** $\sum_k^N b_k^j \approx B_{T_j}$
10: find τ_j such that $\sum_{\mathcal{M}_j} b_k = T_j$, see Fig. 3.15 (Part a) for more details.
11: find the set of subcarriers in each group such that $\mathcal{M}_j \in \mathcal{M}(\mathcal{I}+1 : \tau_j)$
12: increment class index $j \Leftarrow j+1$ and the starting index $\mathcal{I} \Leftarrow \tau_j$
13: **until** $j = N_g$ or $\tau_j = N$
14: rescale the allocated power such that

$$p_{k,j} = p_{k,j} \frac{\sum_N p_k}{P_T} . \tag{3.54}$$

3.2.6 Modified Campello Algorithm for UEP Bit-loading

We developed in [8] a sub-optimal bit loading algorithm based on the one described by Campello in [33] in order to realize an adaptive hierarchical modulation (which is discussed in the next chapter). This has been done to avoid the iterative QoS based partitioning in [7, 2]. However, since we are now able to perform a simple QoS partitioning as discussed before, it is easier to

modify the same sub-optimal bit-loading algorithm to realize UEP using a non-hierarchical modulation. This will be simpler and more efficient than the previous greedy bit-loading algorithm. The simplification here lies in the quantization of the channel-gain-to-noise ratio $\mathcal{G}_k$, gathering similar levels of $\mathcal{G}_k$ into L groups, where L is much smaller than the number of subcarriers N. We simplified it further by introducing a linear solver that computes the approximate bit load for these L levels, instead of the consecutive logical iterations in the original algorithm [33]. The discrete bit-loading $b \in \mathbb{Z}_0^{b_{\max}}$ is said to be energy-efficient, assuming two different subcarriers n & m, if

$$\max_n \Delta p_n(b_n) < \min_m \Delta p_m(b_m + 1) \;\; \forall \; n, m = 1, ..., N \; . \tag{3.55}$$

This means that the maximum incremental power achieved (to place b_n bits) is less than the minimum power required to add an extra bit on any other subcarrier ($\min_m \Delta p_m(b_m + 1)$). As in [8], the approximate discrete bit-allocation $\hat{b}_{k,j}$ that satisfies (3.55) is given by [33]

$$\hat{b}_{k,j} = \left[\lfloor \log_2 \mathcal{G}_{k,j} \rfloor + i^j_{B_{\text{opt}}} \right]_0^{b_{\max}} \; , \tag{3.56}$$

where $i^j_{B_{\text{opt}}} \in \mathbb{Z}$ is selected such that $\sum_k \hat{b}_{k,j} \leq B_{T_j}$[12] and $\mathcal{G}_{k,j} = \mathcal{G}_k / \Gamma_j$ is the gain-to-noise ratio with the gap Γ_j of each class j. In [33], the value $i^j_{B_{\text{opt}}}$ guarantees only a local optimum. Therefore, in [8], we relaxed this expression to include $i^j_{B_{\text{opt}}}$, $i^j_{B_{\text{opt}}} + 1$, and $i^j_{B_{\text{opt}}} - 1$. The one that approaches the target rate is selected. This reduces the total number of iterations required for brute-force steps (as in Algorithm 3.2) to achieve a strict target rate. Γ_j, as in [95], is defined as

$$\Gamma_j = \frac{2}{3} \left[\text{erfc}^{-1} \left(\frac{\mathcal{P}_{\text{j}}}{2} \right) \right]^2 \; . \tag{3.57}$$

The floor operator ensures, first, a lower bound for the bit load and second, that subcarriers with different real $\mathcal{G}_{k,j}$ are allocated to the same number of bits $\bar{b}_i$, where i is the index of the similar bit-loading. Assuming that the number of identical bit load is R_N; let $\mathbf{V}$ be a vector of length R_N, where each index contains a pointer V_i^j to a vector $\mathbf{u}_i^j$ which contains the subcarriers with similar bit-loading such that for class j, each index in $\mathbf{V}^j$ is

$$V_i^j \Rightarrow \{ \mathbf{u}_i^j : \lfloor \log_2 \mathcal{G}_{u_i,j} \rfloor = \bar{b}_i \} \; . \tag{3.58}$$

Since $\log_2 \mathcal{G}_{k,j}$ can result in negative values, one has to scale it by the minimum value $\log_2 \mathcal{G}_j^{\min}$ such that

$$\hat{\mathbb{G}}_i^j = \lfloor \log_2 \mathcal{G}_{k,j} - \log_2 \mathcal{G}_j^{\min} \rfloor \; , \tag{3.59}$$

are all positive values. The quantization error due to the floor operator is

$$\Delta_k^j = \{ \log_2 \mathcal{G}_{k,j} - \log_2 \mathcal{G}_j^{\min} \} - \hat{\mathbb{G}}_i^j \; . \tag{3.60}$$

The total bit-rate (computed using (3.56)) is

$$\sum_{k=0}^{N-1} \hat{b}_{k,j} = \sum_{i=0}^{L-1} \left[\hat{\mathbb{G}}_i^j V_i + i^j_{B_{\text{opt}}} V_i \right]_0^{b_{\max}} \; . \tag{3.61}$$

[12] the equivalent number of bits if the j^{th} class consumes the N subcarriers

After relaxing i_B in (3.61) to be $\in \mathbb{R}$, the proposed values for computing $i^j_{B_{\text{opt}}}$ can be computed as follows

$$i_B = \left\lfloor \frac{B_{T_j} - \sum_{i=0}^{L-1} \hat{\mathbb{G}}_i^j V_i^j}{L_j} \right\rfloor \tag{3.62}$$

$$\mathbf{i}_B^j = \begin{pmatrix} i_B - 1 \\ i_B \\ i_B + 1 \end{pmatrix} \in \mathbb{Z} \,, \tag{3.63}$$

where the floor operation guarantees that we are always a sum rate less than or equal B_T, i.e., we need only to decrement the bit load values to achieve the exact B_T. Hence, $i^j_{B_{\text{opt}}}$ is selected from these three values in order to minimize

$$\min_{\mathbf{i}_B^j} \quad B_{T_j} - \sum_{k=0}^{N_j-1} \hat{b}_{k,j} \,, \tag{3.64}$$

where $\hat{b}_{k,j}$ is finally computed using (3.56).

The 1st method using quantization errors only:
This method is similar to the brute-forcing done by Chow et al. in Algorithm 3.2. One has, however, to consider two issues while brute-forcing using the quantization error only:

1. the quantization error on each subcarrier can only be used once, i.e., since only the first time minimizes the energy for sorted subcarriers [33].

2. the quantization error on weak subcarriers may lead to allocate non-feasible subcarriers or over-load others, which may lead to a huge power consumption.

Algorithm 3.9 Campello-like margin adaptive UEP bit-loading

Input: CGNR $\mathbb{G}_k$, $\forall k = 0..N-1$, N_g classes, target sum rate B_T, individual rates for each class T_j, and target power P_T

Output: power allocation $p_{k,j}$ and the bit-loading values $\hat{b}_{k,j}$

Initialize: the zero matrices $\mathbf{B}$ (bits) and $\mathbf{E}$ (power) with N rows and N_g columns, $j = 0$, the starting index $\mathcal{I} = 0$, and the quantization error vector Δ with all zeros.

1: sort the subcarriers in a descending order according to $\mathbb{G}_k$ in a set $\mathcal{M}$

2: **repeat**

3: compute $\hat{\mathbb{G}}_i^j \ \forall \ i = 0..R_N - 1$ using (3.59), then find $i_{B_{\text{opt}}}$ using (3.63) and B_{T_j} in the previous algorithm; compute the bit-loading $\hat{b}_{k,j}$ using (3.56) and fill $\mathbf{B}(k,j) = \hat{b}_{k,j}$

4: find the quantization error using (3.60), such that

$$\Delta_k^j = \{\mathbb{G}_{k,j} - \mathbb{G}_j^{\min}\} - \hat{\mathbb{G}}_i^j$$

5: **repeat**

6: increment find k with the highest Δ_k

7: $\hat{b}_k \Leftarrow= \hat{b}_k + 1$; and fill $\mathbf{B}(k,j) = \hat{b}_{k,j}$

8: $\Delta_k = -1$, so as not to use it again.

9: **until** $\sum_{k=0}^{N-1} \mathbf{B}(k,j) \approx B_{T_j}$

10: find the set of subcarriers in each group such that $\mathcal{M}_j \in \mathcal{M}(\mathcal{I}+1 : \tau_j)$

11: increment class index $j \Leftarrow j+1$ and the starting index $\mathcal{I} \Leftarrow \tau_j$

12: **until** $j = N_g$ or $\tau_j = N$

13: calculate the power for the k^{th} subcarrier and the j^{th} class and update $\mathbf{E}$ using

$$p_{k,j} = \frac{\frac{2}{3}\left[\text{erfc}^{-1}\left(\frac{\mathcal{P}_0}{2}\right)\right]^2}{\mathcal{G}_k}\left(\frac{2^{\mathbf{B}(j,k)}-1}{\Delta_{\gamma_j}}\right) \tag{3.65}$$

14: rescale the allocated power such that

$$p_{k,j} = p_{k,j}\frac{\sum_N p_k}{P_T} \tag{3.66}$$

2nd method using the minimum incremental power

We implement the same steps as before except for Line 6. Instead, we followed the Hughes-Hartogs approach. This modification needs to fulfill Eq. (3.55) as follows

6: find k with the minimum $\Delta p_{k,j}$ (computed using (3.53)) among all subcarriers in each class; decrement (increment) the k^{th} subcarrier that comes with the maximum (minimum) incremental power, i.e., $\max \Delta p_k(b_k - 1)$ ($\min \Delta p_k(b_k + 1)$). Thereafter, update Δp_k such that $\Delta p_k = \Delta p_k - \max \Delta p_k(b_k - 1)$ or $\Delta p_k = \Delta p_k + \min \Delta p_k(b_k + 1)$, respectively.

The results of algorithms 3.8 and 3.9

To evaluate our algorithm, we consider three priority classes with three different priorities. As can be seen from Fig. 3.16, assuming 2048 bits per class, the 3 dB margin separation in case of perfect channel state information is preserved with almost no difference in performance between the modified Hughes-Hartogs and the modified Campello algorithms.

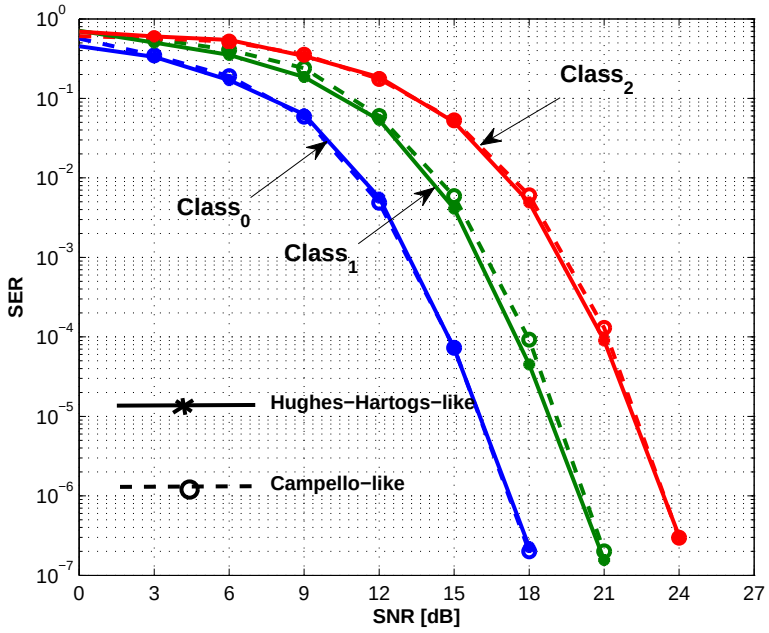

Figure 3.16: Adaptive UEP OFDM with $\Delta_\gamma = 3$ dB, 2048 subcarriers, and 2048 bits/class

For channel uncertainties, we adopted the uncertainty model in Chapter 1, Section 1.3.2 (1.7), where a Rayleigh channel with complex components, each real and imaginary is assumed to be a Gaussian variable with zero mean and variance equal 1, i.e., $\mathbb{C}\mathcal{N}(0,1)$. The errors are assumed to be Gaussian as well with zero mean and 25% deviation from the channel variance, i.e., the channel correlation coefficient square $|\rho_c|^2 = 1/4$. In Fig. 3.17, the performance of our modified Campello algorithm with channel uncertainties at both sides transmitter (bit-loading errors) and receiver (equalization errors). One can see that that reducing the overall rate by 25% can enhance the performance, while still not sufficient.

The difference between the proposed methods can be seen in Fig. 3.18. In this figure, the upper plot represents the Campello-like UEP bit-loading using 1$^{\text{st}}$ method, the middle plot represents the 2$^{\text{nd}}$ method, and lower plot is depicting the Hughes-Hartogs-like UEP bit-loading. Comparing the upper and the middle plot, one can notice that the quantization error alone is not sufficient to determine the brute-force final bit distribution at the low-SNR values, i.e., the 1$^{\text{st}}$ method allocates more the weaker subcarriers. Comparing the Campello-like 2$^{\text{nd}}$ method to the Hughes-Hartogs-like, one can directly notice that the latter algorithm does not fulfill the water-filling criterion and, hence, spreads more over the total number of subcarriers.

We further verify this issue by plotting the power allocation of these three schemes in Fig. 3.19. From this figure, it becomes clear that the 1$^{\text{st}}$ method of Campello-like UEP bit-loading consumes

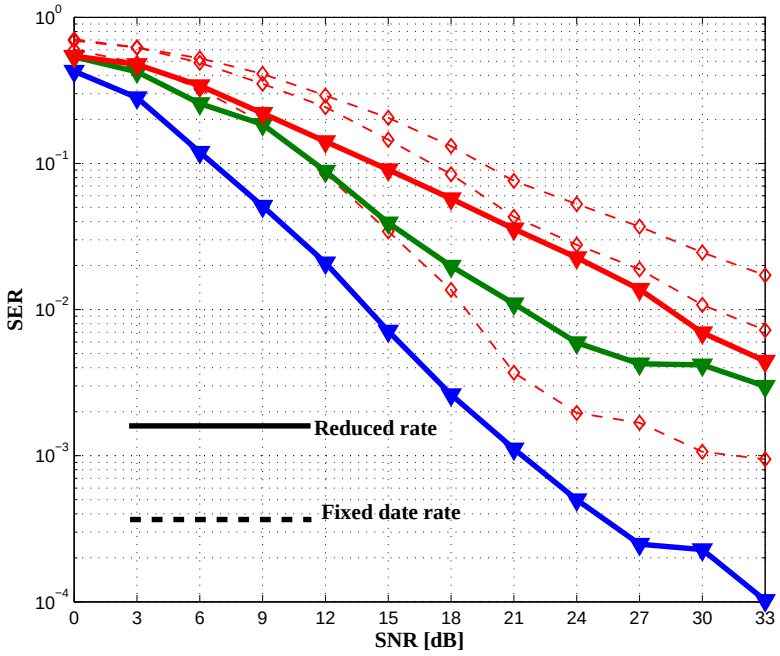

Figure 3.17: Adaptive UEP with 25% channel uncertainty using the Campello-like algorithm, 2^{nd} method

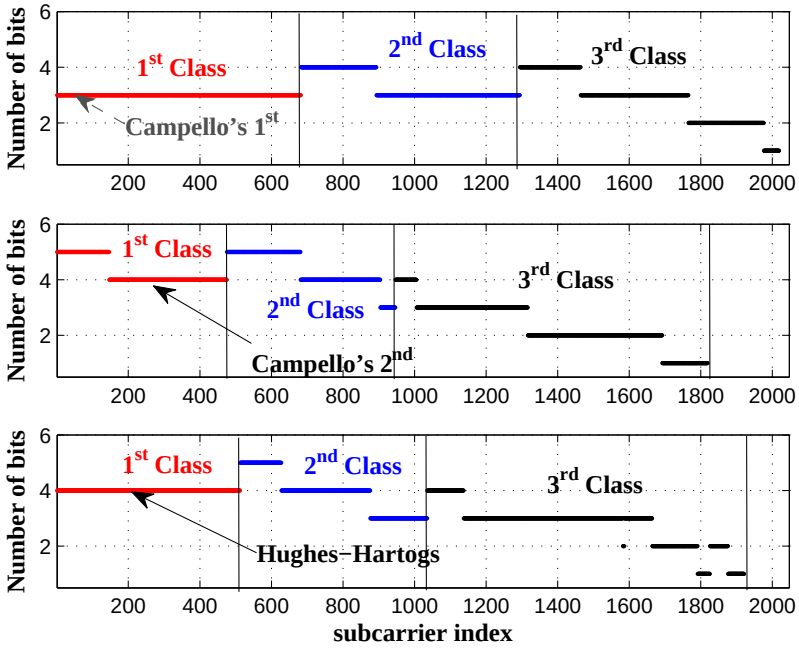

Figure 3.18: UEP bit-loading using Campello-like (1st and 2nd method) vs. the Hughes-Hartogs-like for sorted subcarriers at SNR = 5 dB

more power at the weaker subcarriers (see jumps at the second and the third classes). However, Hughes-Hartogs-like and Campello-like, using the 2^{nd} method, are distributing the power more efficiently. In these two schemes, a jump by a factor of 3 dB is seen at any bit-loading transition. It is clear also (from this figure with sorted subcarriers) that the Campello-like UEP bit-loading (2^{nd} method) follows water-filling-like effect which comes due to quantizing of the channel capacity formula.

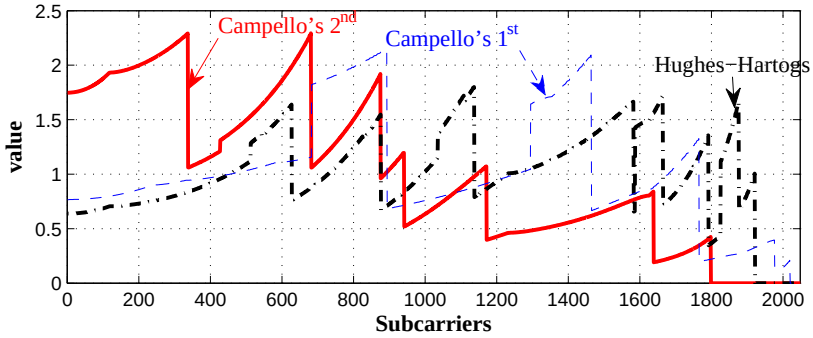

Figure 3.19: Power allocation using Hughes-Hartogs and Campello like algorithm for sorted subcarriers at SNR = 5 dB

Chapter 4

Adaptive UEP Multilevel Modulation

The recent era of fast and high-definition (HD) multimedia broadcasting has evolved from considering a single priority transmission to multilayer transmission with different reliabilities. This is achieved by utilizing the channel degradation, where the sub-channels (assuming multicarrier or multiuser system) can be sorted according to their attenuation [26]. Hence, all the spatial, temporal, and spectral sub-channels have to be allocated based on their carriers gain-to-noise ratio and the required QoSs. One solution is to use UEP bit-loading as proposed in Chapter 3, where the given resources are divided according to the prioritized data. However, in some applications, the mandatory data have to be equally decoded by all receivers at the same time and the extra data are only interpreted by the higher definition ones. For example, in HD video broadcasting, images recorded using the HD resolution 720p, i.e., 1280×720 pixels[1] [97], are required to be screened on either old or new featured receivers. In this case, the extra pixels needed for HD resolution have to be transmitted together with the traditional standard definition (SD) resolution on the same resources.

As a solution for this dilemma, hierarchical modulation has been introduced in the modern multimedia standards, e.g., the digital video broadcasting – terrestrial (DVB-T) [98] and the ultra mobile broadband (UMB) [99] standards. Thus, hierarchical modulation (also known as embedded modulation [100]) uses constellations with non-uniformly spaced signal points. Hence, two or more modulation schemes, for two or more different data symbols, are mapped onto the same constellation set. One of these schemes has a higher modulation order, which can only be interpreted by more advanced receivers or the ones which are close enough to the transmitter. The other modulation scheme has a lower modulation order. Nevertheless, it can be decoded by every receiver in the network.

There are different hierarchical constellation constructions in literature. In [98, 100, 99] proposes the constellation in Fig. 4.1.a. It implements the lower modulation order (4-QAM) using the cloud formed by the higher modulation order (16-QAM) with different Euclidean distance. In

[1]The pixel is the smallest addressable screen element and the smallest unit of a picture [96].

other words, the 4-QAM is formed by the cloud of another smaller four 4-QAM, i.e., each of these 4-QAMs is located in a single quadrant (see Fig. 4.1.a). The Euclidean distance between the neighboring points of the smaller constellation is d_1. However, the distances between the centers of each two neighboring clouds (the Euclidean distance of the virtual lower modulation order) is d_0. The main drawback of this model is that the minimum Euclidean distance[2] decreases monotonically with increasing the number of levels or for every single bit addition. In contrast, we select the hierarchical constellation proposed in [101] and illustrated in Fig. 4.1.b. In this case, the minimum Euclidean distance between any two clouds of the j^{th} class is kept the fixed during bit allocation; this equal to d_{j-1}. However, after allocating all possible bits, the overall constellation size will, of course, shrink to keep the same average energy. This means that the average symbol energy needs certainly to be computed for every new class addition and, even, for each single bit addition.

In order to compute proper SER values for all possible cases, the authors in [101] suggest to calculate the average power for all possible constellations analytically, as a clossed form expression is not too handy. However, we computed the average power numerically (using MATLAB/Octave) for all possible cases. This can be done easily by calculating the energy of each constellation point (the average of the distances to the origin of each possible realization). Finally, these values are stored in a simple lookup table, which make it an efficient approach, especially, in practical real-time applications.

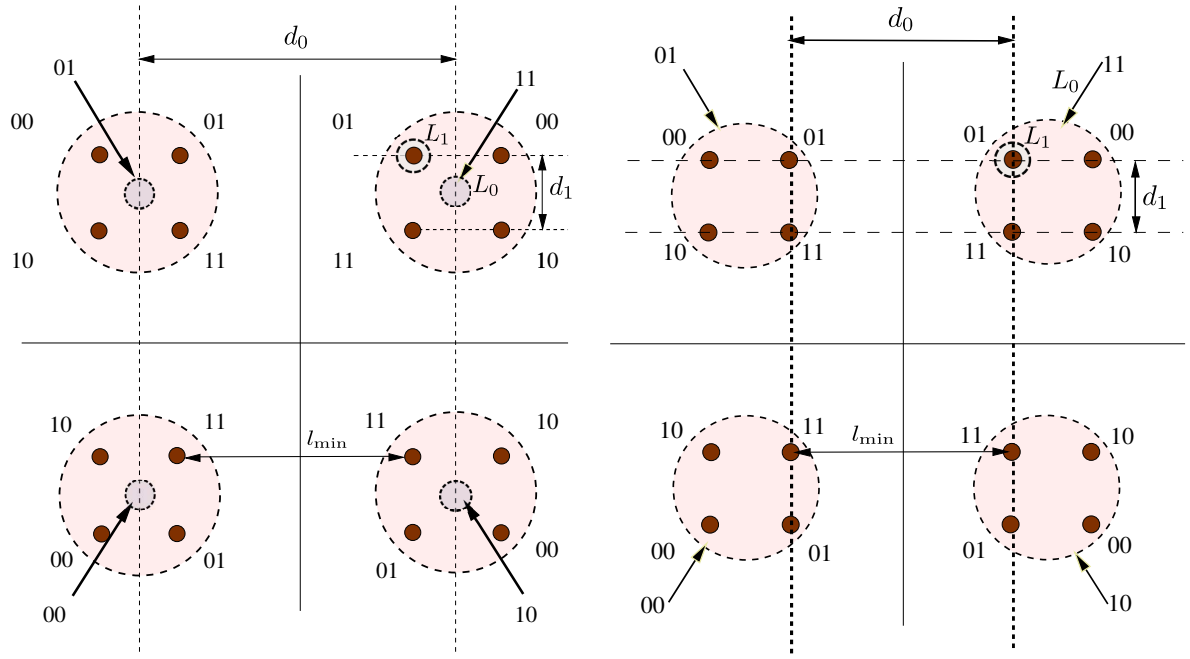

(a) a virtual 4-QAM (L_0) is embedded in a 16-QAM (L_1) using the fixed average power constellation

(b) a 4-QAM cloud (L_0) is embedded in a 16-QAM (L_1) using the fixed minimum distance

Figure 4.1: Hierarchical quadrature amplitude modulation 4/16-QAM

Adjusting the Euclidean distances between different constellations is capable of delivering UEP. Thus, for realizing N_g priority classes, one has to realize N_g different Euclidean distances d_j

[2] $l_{\min}$, which is the distance between the nearest two neighboring points of two adjacent clouds

($\forall\ j\ \in\ \{0..N_g - 1\}$). Here, we first present prioritized transmission using a non-adaptive hierarchical modulation which implies different Euclidean distances. Thereafter, we introduce an adaptive hierarchical modulation scheme that realizes an adaptive multilevel (hierarchical and non-hierarchical) modulation which depends on the CGNR of each carrier in a multicarrier transmission.

In this chapter, we use two different bit-loading algorithms to give a flavor of possible options, although we will not study all the proposed UEP bit-loading algorithms again, which we know from Chapter 3. However, extensions to these algorithms are always straightforward. Therefore, in this chapter we stick to the greedy bit-loading approach which is modified to adopt multi-level embedded (or hierarchical) modulation to achieve UEP in OFDM transmission [9, 10].

4.1 UEP with Hierarchical Modulation

In hierarchical (or embedded) modulation, the margin separations between N_g given classes with different Euclidean distances d_j can easily be adjusted modifying the ratios between constellation distances, i.e., $\frac{d_j}{d_i}$, where i and j are two different classes. In Fig. 4.2, we assume the same prioritized transmission profile as with Chapter 3, i.e., assuming the same 3 different classes ($\mathrm{L}_j,\ j \in \{0, 1, 2\}$) with a 3 dB margin separations, such that

$$d_0/d_1 = d_1/d_2 = \sqrt{2}\,. \tag{4.1}$$

Thus, for every single bit addition, the power is calculated using the average symbol energy in the lookup table and the margin separations given by the relation in (4.1) .

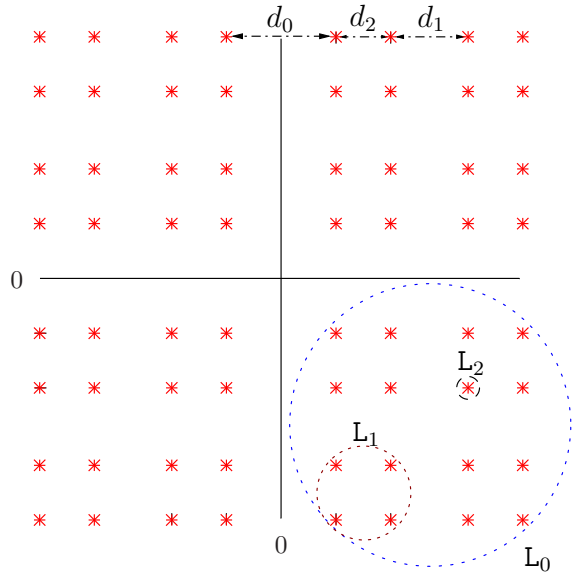

(a) A 4-QAM (L_0) is embedded in a 16-QAM (L_1) which is embedded in a 64-QAM (L_2)

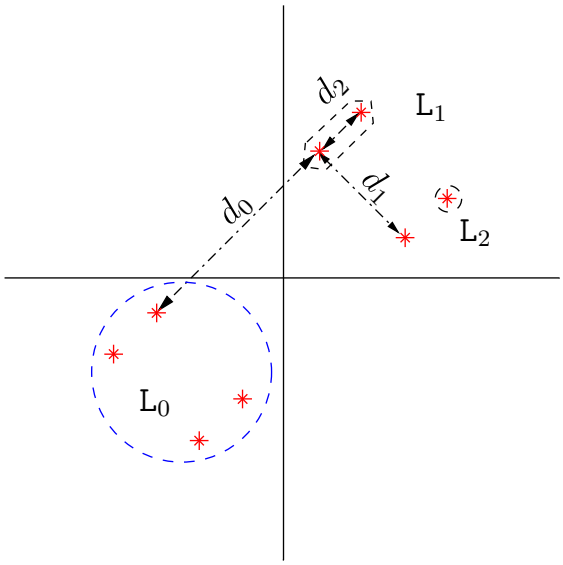

(b) A BPSK (L_0) is embedded in a 4-QAM (L_1) which is embedded in a non-square 8-QAM (L_2)

Figure 4.2: Hierarchical quadrature amplitude modulation: (a) 4/16/64-QAM and (b) 2/4/8-QAM

In this hierarchical modulation scheme, we assume to have square, cross, and the sub-optimal rectangular constellations, i.e., a single bit addition can alternate between them. We depict two different constellations, first, a square constellation that realizes a 4/16/64-QAM (Fig. 4.2.a) and, second, a rectangular constellation that is denoted as 2/4/8-QAM (Fig. 4.2.b).

4.1.1 Non-adaptive Hierarchical Modulation

In herein, we show the performance of a non-adaptive hierarchical modulation which preserves an arbitrary margin separation of 3 dB. Figure 4.3 depicts the symbol-error ratios in case of AWGN using a fixed hierarchical modulation equivalent to 2/4/8-QAM (as defined in Fig. 4.2.b). Figure 4.3 also shows the comparison between AWGN and a Rayleigh fading channel (using the same multipath fading channel used in Chapter 3 and Chapter 1). It is clear form this figure that the 3-dB margin is strictly preserved in the AWGN case, only. In Rayleigh fading channels, this margin separation becomes wider, almost 6 dB at a SER (symbol-error ratio) of $2 \cdot 10^{-3}$. Nevertheless, the order of the classes and the relative margin separations are roughly preserved.

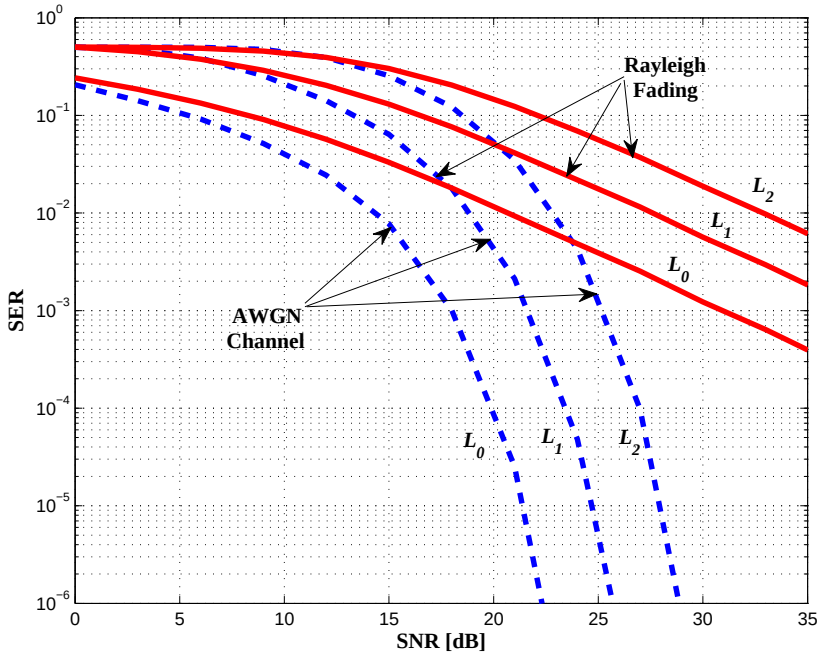

Figure 4.3: SER for 2/4/8 hierarchical QAM (defined in Fig. 4.2.b) assuming 3 different classes with a margin separation of 3 dB, i.e., in total, 6144 bits were placed on 2048 subcarriers

In case of Rayleigh channel, the overall system performance deteriorates compared to the AWGN channel. This is due to the fixed modulation size and the fixed power allocation under the varying channel gains. Hence, further adaptation to channel conditions, using adaptive modulation and power allocation, is a very important to keep the margin separation preserved and to enhance the performance by adapting to the channel conditions.

4.1.2 Adaptive Multilevel Modulation

The UEP bit-loading algorithms discussed in Chapter 3 are relying mainly on subdividing the total number of subcarriers into a given number of classes. That was, to a certain extend, a complex iterative process. Yet, we opt for hierarchical modulation to realize UEP classes together with bit-allocation instead of the subcarrier grouping, since it realizes different classes more efficiently without tedious binary searching or sub-optimal subcarrier grouping. This can be achieved by allowing coexistence between non-hierarchical and hierarchical (multilevel) constellations.

4.2 Hughes-Hartogs-like Multilevel Adaptive Modulation

We extend our work further to realize UEP using adaptive hierarchical modulation starting from the greedy bit-loading by Hughes-Hartogs. Assuming an intuitive sorting, the highest priority class first consumes the good-CGNR subcarriers with the minimum incremental power (calculated based on the maximum allowed symbol-error rate $\mathcal{P}_0$ (SER) and the channel coefficients). Thereafter, the bits of the following classes are allowed to be allocated to either already used subcarriers in a hierarchical fashion or to yet free subcarriers depending on the minimum power increment. Free subcarriers are used then based on the same given margin separation $\Delta\gamma_j$, which is identical to the one given by the hierarchical modulation Euclidean spacing.

Hence, the only required information to establish our algorithm now is the SER of the first class $\mathcal{P}_0$, the subcarriers CGNR $\mathcal{G}_k$, and the required margin separations $\Delta\gamma_j$. The initial margin γ_0 is computed using only the knowledge of $\mathcal{P}_0$ by applying the approximated relation between the given $\mathcal{P}_0$ and the required margin in (3.47) (Chapter 3 - Section 3.2.3). Hence, the other margins γ_j of the less important data are computed using the given margin separation $\Delta\gamma_0$, such that $\gamma_j = \gamma_0/(j \cdot \Delta_\gamma)\ , \forall\ j \in \{1..N_g - 1\}$. Thereafter, the other SER $\mathcal{P}_j$ are calculated using the computed margins γ_j and the inverse relation in (3.46).

In the following, we propose the modified UEP Hughes-Hartogs bit-loading algorithm (originally defined in Chapter 3, Section 3.1) using hierarchical modulation. The system margin is always adapted according to the total target power P_T and the allocated power to the each subcarrier P_k. Thus, the maximum system margin is given by

$$\gamma_{\max} = \frac{P_T}{\sum_k^N P_k}\ . \tag{4.2}$$

In this algorithm, the matrix $\mathbf{B}$ has N_g hierarchy levels as its columns and N subcarriers as its rows. Non-allocation of leading column(s) means that first protection level data have not been put on the corresponding carrier. Nevertheless, lower-priority classes may still realize hierarchical modulation using smaller hierarchical signal sets. However, if only one class is able to allocate bits on a certain subcarrier k, this subcarrier will have a homogeneous constellation. The number of bis and the power allocated to such subcarriers are controlled in order to preserve the margin separation $\Delta\gamma_j$.

Algorithm 4.1 Hughes-Hartogs-like margin adaptive UEP multilevel bit-loading

Input: CGNR $\mathcal{G}_k$, N_g classes, target sum rate B_T, individual rates for each class T_j, the maximum required $\mathcal{P}_0$, and target power P_T. The maximum allowed number of bits on each class $b^j_{\max}$, and the maximum number of bits per carrier $b_{\max}$.

Output: $p_{k,j}$ and the exact discrete bit-loading values $\hat{b}_{k,j}$

Initialize: set $j = 0$, allocate $N \times N_g$ zeros to the bit-loading matrix $\mathbf{B}$ and N zeros to the power loading vector $\mathbf{P}$ and the incremental power vector $\Delta\mathbf{P}$

1: **repeat**
2: **repeat**
3: compute the incremental power ΔP_k, for every subcarrier assuming a single bit addition, using the following approximate equation (assuming non-hierarchical as in (3.53)):

$$\Delta\mathbf{P}(k) = \frac{\frac{2}{3}\left[\text{erfc}^{-1}\left(\frac{\mathcal{P}_0}{2}\right)\right]^2}{\mathcal{G}_k \Delta\gamma_j} 2^{\sum_{l=0}^{j}\mathbf{B}(k,l)} , \tag{4.3}$$

where $\Delta\gamma_j$ is the margin difference between the first priority class margin γ_0 and the j^{th} class margin γ_j. $\sum_{j=0}^{N_g-1}\mathbf{B}(k,j)$ is the total number of bits on the k^{th} subcarrier allocated by classes $j, j-1, ..., 0$, i.e., the current number of bits on this subcarrier.
4: $\Delta\mathbf{P}(k) = \Delta P_k$
5: find the subcarrier index k that corresponds to the minimum incremental power in $\Delta\mathbf{P}$
6: **if** $\mathbf{B}(k,j) + 1 \leq b^j_{\max}$ and $\sum_{l=0}^{j}\mathbf{B}(k,j) + 1 \leq b_{\max}$ **then**
7: $\mathbf{B}(k,j) \Leftarrow \mathbf{B}(k,j) + 1$
8: $\mathbf{P}(k) \Leftarrow \mathbf{P}(k) + \Delta\mathbf{P}(k)$
9: **end if**
10: **until** $\sum_{k=0}^{N-1}\mathbf{B}(k,j) = T_j$
11: $j \Leftarrow j + 1$
12: **until** $j = N_g$
13: rescale the allocated power such that $p_k = p_k \frac{P_T}{\sum_{k=0}^{N-1}\mathbf{P}(k)} = p_k\gamma_{\max}$.

Equation (4.3) approximates the multilevel overlapping incremental power to an equivalent incremental power of a homogenous modulation, assuming the same number of bits. In Appendix C, we show that this approximation results in a lower bound of the incremental power. This means that the computed incremental power in (4.3) is slightly less than the exact incremental power. This induces more subcarriers with hierarchical that it should be. Thus, we admit that this is a suboptimal solution, which results in worse performance. However, we can exactly compute the factor between the incremental power of the homogeneous and the non-homogeneous modulation as discussed in Appendix C.

Figure 4.4 depicts the performance of the modified Hughes-Hartogs algorithm for two cases. The first case, when allocating 1024 bits to the first, 2048 bits to the second, and 3072 bits to the least priority class. The second case, when all classes are allocated equally with 2048 bits. In our simulation, we assume the number of subcarriers to be 2048 and $b^j_{\max}$ of each modulation layer to be 6 bits. First of all, it is clear from Fig. 4.4 that the 3 dB spacing is better preserved

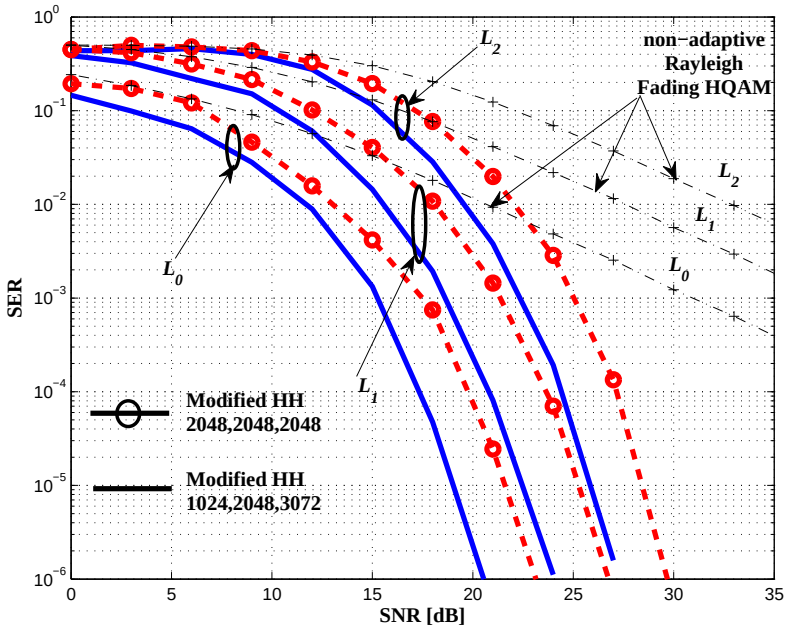

Figure 4.4: SER in Rayleigh fading for the Hughes-Hartogs-like algorithm with adaptive hierarchical QAM assuming 3 different classes with Δ_γ 3 dB. In total, this figure has 6144 bits on 2048 subcarriers with two scenarios: T_0=1024, T_1=2048, T_2=3072, and T_j=2048, $j = 0..2$

in the case of the Rayleigh channel using adaptive modulation than the non-adaptive case. We also observe the same performance degradation as in the modified Chow algorithm using non-hierarchical UEP bit-loading (Chapter 3, Section 3.2.2), when adding more bits to the first class.

4.3 Campello-like Multilevel Adaptive Modulation

We also modify Campello's bit-loading algorithm following the same footprints of Algorithm 5 to realize UEP with adaptive hierarchical modulation. This algorithm allocates T_0 bits (of the first class) to the entire number of subcarriers using the channel CGNR $\mathcal{G}_k$ and the constant $i^j_{B_{\text{opt}}}$ using (6.21) in Chapter 3, Section 3.2.6. Hence, the resulting bit-loading of this priority level is computed and saved in the bit-loading matrix $\mathbf{B}_{k,0}$. The power is computed accordingly using (3.7), i.e., $\Delta\gamma_0 = 1$. The priority class $j = 1$ is also allowed to consume the total number of subcarriers, however, to allocate a target sum rate $T_0 + T_1$ this time. Similarly, the bit loads for $j = 1$ are computed and saved in the bit-loading matrix at the next position, i.e., $\mathbf{B}_{k,1}$.

Thereafter, the computed bit loads of the first class, which is stored in $\mathbf{B}_{k,0}$, is subtracted from the bit load values of the second class, i.e., $\mathbf{B}_{k,1} = \mathbf{B}_{k,1} - \mathbf{B}_{k,0}$[3]. Now, the power allocation of the second class is ready to be computed as in (3.53) using the current bit load values in $\mathbf{B}_{k,1}$, $\mathcal{P}_0$, and $\Delta\gamma_1$. The other classes are allocated similarly, where each priority class allocates its target rate in addition to the target rate of all the previous higher classes. Later, the accumulated bit

[3]This only true assuming $\gamma_0 > \gamma_1 > ... > \gamma_{N_g}$

loads of the higher $j-1$ classes, $\sum_{l=0}^{j-1} T_l$, are subtracted from the computed bit-loading and power is calculated accordingly. Finally, the bit loads in each column of $\mathbf{B}$ is related to a specific modulation layer forming a multilevel hierarchical modulation. Algorithm 4.2 shows the details of this approach.

Algorithm 4.2 Campello-like UEP multilevel adaptive modulation:

Input: CGNR $\mathcal{G}_k$, N_g classes, target sum rate B_T, individual rates for each class T_j, the maximum allowed SER $\mathcal{P}_0$, and target power P_T. The maximum allowed number of bits on each class $b^j_{\max}$, and the maximum number of bits per carrier $b_{\max}$.

Output: $p_{k,j}$ and the exact discrete bit-loading values $\hat{b}_{k,j}$

Initialize: set $j=0$, the accumulated rate to $T_j^{\text{temp}} = \sum_{l=0}^{j} T_l$, allocate $N \times N_g$ zeros to the bit-loading matrix $\mathbf{B}$ and to the power loading matrix $\mathbf{P}$, and N zeros to the vector $\Delta\mathbf{P}$.

1: **repeat**

2: compute $\hat{\mathbb{G}}_k^j \ \forall\ j = 0..R-1$, where R is the number of groups with similar bit-loading (as in Algorithm. 3.9), compute $i_{B_{\text{opt}}}$ using (3.63). Thereafter, compute the accumulated number of bits (of the j classes) $\mathbf{B}(k,j)$ using (3.56) and the incremental power $\Delta\mathbf{P}(k)$, using (4.3), for a single bit addition

$$\mathbf{B}(k,j) = \left[\lfloor \log_2 g_k^j \rfloor + i_{B_{\text{opt}}}\right]_0^{b_{\max}} \text{ and } \Delta\mathbf{P}(k) = \frac{\frac{2}{3}\left[\text{erfc}^{-1}\left(\frac{\mathcal{P}_0}{2}\right)\right]^2}{\mathcal{G}_k}\left(\frac{2^{\mathbf{B}(k,j)}}{\Delta_{\gamma_j}}\right) \tag{4.4}$$

3: **repeat**

4: **if** $(\mathbf{B}(k,j) - \mathbf{B}(k,j)+1) \le b^j_{\max}$ and $(\mathbf{B}(k,j)+1) \le b_{\max}$ **then**

5: increment $\mathbf{B}(k,j)$ corresponds to the subcarrier with the smallest $\Delta\mathbf{P}(k)$

6: **end if**

7: **until** $T_j^{\text{temp}} \le \sum_k \mathbf{B}(k,j)$,

8: **if** $j \ge 1$ **then**

9: subtract the bit-loading of the $j-1$ class(es) from the current accumulated b_k, thereby, the bit-loading for each class is $b_{k,j} = b_{k,j} - \sum_j b_{k,j-1}$

10: **end if**

11: the energy is recalculated similar to Eqn. (3.65) and following the same assumption in (4.3), i.e., compute the power only for the bits in the j^{th} class, as follows

$$\mathbf{P}(k,j) = \frac{\frac{2}{3}\left[\text{erfc}^{-1}\left(\frac{\mathcal{P}_0}{2}\right)\right]^2}{\mathcal{G}_k \Delta_{\gamma_j}}\left(2^{\mathbf{B}(j,k)} - 2^{\mathbf{B}(j-1,k)}\right)$$

12: $j \Leftarrow j+1$

13: **until** $j = N_g$

14: the energy is accumulated such that the resultant energy is given by $P_k = \sum_{j=0}^{Ng-1} \mathbf{P}(k,j)$

15: rescale the allocated power such that $p_k = p_k \frac{P_T}{\sum_{k=0}^{N-1}\sum_{j=0}^{N_g-1}\mathbf{P}(k)} = p_k \gamma_{\max}$.

In Fig. 4.5, we plot the SER curves of the proposed Campello-like hierarchical adaptive modulation versus the Campello-like adaptive UEP bit-loading with non-hierarchical modulation, proposed in Chapter 3. In both cases, we assume a Rayleigh fading wireless channel using OFDM transmission with 2048 subcarriers. The total number of bits required to be allocated in each of these cases is 2048 subcarrier for each class; assuming 3 classes with 3 dB margin separations. Hence, we find that the performance of the non-hierarchical Chow-like algorithm outperforms the hierarchical Campello-like bit loading. This is mainly due to the power-inefficiency of hierarchical constellations.

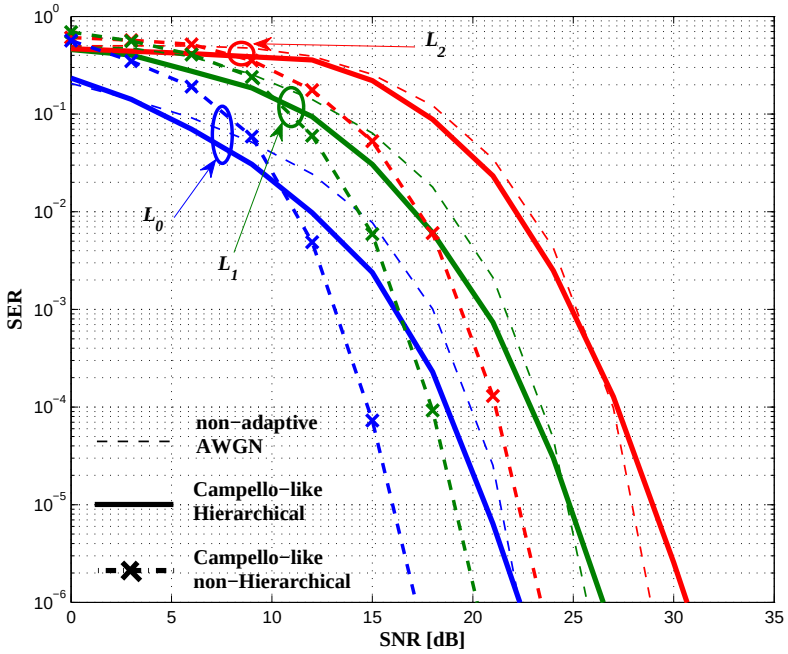

Figure 4.5: AWGN 2/4/8-QAM vs Chow-like vs Campello-like (hierarchical modulation) with T_j=2048, $j = 0..2$

For comparison, in Fig. 4.5, we also plot the SER curves of the non-adaptive hierarchical modulation with AWGN (the thin dashed lines) using the same number of bits/subcarrier as in the adaptive case, i.e., 3 bits/subcarrier or 1-bit for each class which results in 2/4/8-QAM (similar to Fig. 4.3). We see that the adaptive modulation outperforms the non-adaptive AWGN reference curves at low SNR. This is very clear since the adaptive modulation allocates bits only to the good-SNR subcarriers and also switches to non-hierarchical modulation at very weak subcarriers.

Finally, in Fig. 4.6, we show the comparison between Campello-like and Hughes-Hartogs-like adaptive hierarchical modulation using the same target rates and the same channel conditions. From this comparison, we see that the Campello-like algorithm outperforms the Hughes-Hartogs-like one only at the high priority classes. Strictly speaking, the first priority class is even better than the second class compared to the Hughes-Hartogs-like performances. However, the Hughes-Hartogs-like third class performs better than the Campello-like algorithm with steeper

performance at high SNR. This is due to the fact that the Hughes-Hartogs-like algorithm tends to spread more over the given subcarriers in order to consume all the minimum incremental power positions. In contrast, the Campello-like algorithm congests more bits to the good subcarrier at low-SNR conditions. This is also a convenient clarification to the decrease of this performance gap at high SNRs.

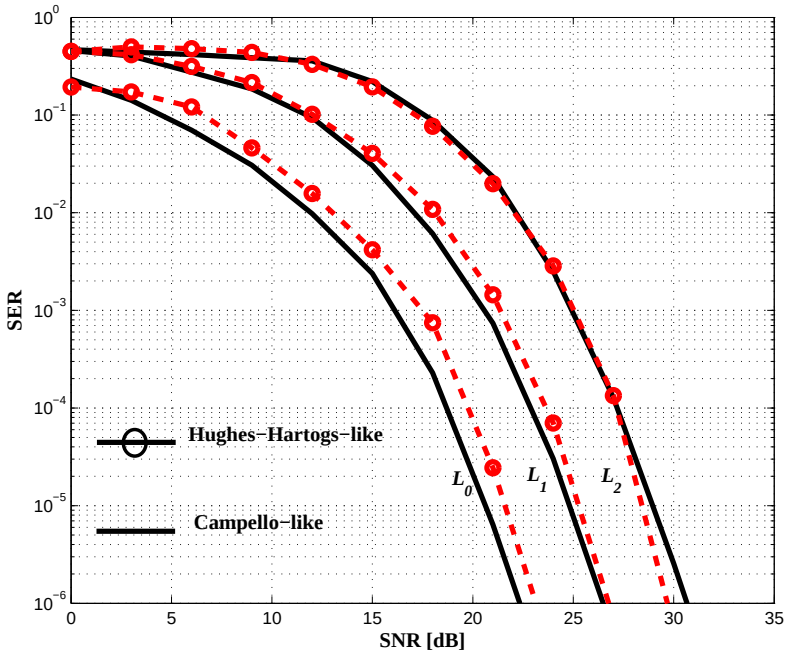

Figure 4.6: SER performance of the Hughes-Hartogs-like hierarchical modulation vs the Campello-like one assuming T_j=2048, $j = 0..2$.

Chapter 5

Multiple-Input, Multiple-Output Channel with Prioritized Transmission

As discussed in Chapter 2, the MIMO channels can easily be decomposed into different eigenchannels[1] with different gains. These distinct eigenchannels can be used as the underlying structure for transmitting adaptive modulation with different priorities. Therefore, it is necessary to design techniques that allocate these spatial resources and adapt the modulation scheme such that the overall performance satisfies the required QoS. In frequency-selective channels, the MIMO performance deteriorates, seriously. This could effectively be resolved by cutting down the whole bandwidth into smaller subcarriers, such that the channel appears to be flat within these narrow subcarriers. Thus, multicarrier techniques, e.g., OFDM, are used in conjunction with the existing MIMO systems to transfer such frequency selective channels into N narrower flat sub-bands. Additionally, the MIMO-OFDM combination takes advantages of simple frequency domain equalization and channel adaptation capabilities along the spectral domain. Generally, this is achievable using closed-loop transmission (with feedback to the transmitter) and utilizing the individual subcarriers and the individual eigenchannels.

Accordingly, the transmission can be adapted to the channel variations. However, to achieve the optimum performance, the complete channel state information (CSI) would need to be known *accurately* at the transmitter. However, a perfect CSI knowledge is indeed a rather impractical assumption due to estimation errors, limited feedback conditions, channel feedback delays, and/or quantization errors. Hence, a partial CSI at the transmitter is a more realistic assumption between the two extremes, perfect CSI [102] and no-CSI [44]. There are two main partial feedback schemes: the channel quantized/delayed (or channel mean) feedback $\hat{\mathbf{H}}$ [7, 11] and the channel covariance feedback $\mathbf{R}_{\mathbf{H}} = E\{\mathbf{H}^{*}\mathbf{H}\}$ [12].

Since the decomposition of the instantaneous channel (using SVD) varies from that of the delayed or the inaccurate CSI, the transmission orthogonalization cannot be guaranteed any more.

[1] also known in literature, for every subchannel, as eigenbeams [44]

Thus, CSI inaccuracy induces an inter-eigen interference (IEI), which results in performance deterioration. Hence, to compensate for the orthogonality distortion, we consider implementing different pre- and post-processing units at the transmitter and the receiver, respectively [102][2]. We refer to the pre-processing at the transmitter as eigen-beamforming or shortly beamforming, which is a steering unitary matrix that rotates the transmission beam to the direction of the eigenvectors of the MIMO channel. The post-processing at the receiver can be considered as a linear spatial equalizer using the zero-forcing (ZF) or the minimum-mean square error (MMSE); see Chapter 2, Section 2.2, for more details about eigen-beamforming and linear spatial equalizers. However, the limitations of linear equalizers to combat severe interference and noise enhancements (due to some weak channels) necessitate the need for non-linear equalization [15]. Thus, we propose to use a successive interference cancellation technique based on the well-known V-BLAST non-linear spatial equalizer.

Based on the algorithms proposed in Chapter 3 and 4, we also extended the UEP adaptation to the MIMO-OFDM case. Thus, bits and power are allocated along the different subcarriers and their eigenchannels. This changes the bit and power loading process into a two-dimensional (space and frequency) problem. We also realize UEP by fulfilling arbitrary performance margins between the given protection classes. Additionally, the adaptive UEP multilevel hierarchical modulation, proposed in Chapter 4, is extended to the multiple antenna case.

Finally, we investigate the impact of a more practical limited CSI, which is the channel correlation (or channel covariance) feedback, i.e., $\mathbf{R_H} = E\{\mathbf{H}^*\mathbf{H}\}$. This kind of CSI is more suitable in the case of rapid channel variations, where the transmitter cannot keep track on the instantaneous channel values [72]. As in [12], we compare this technique to the quantized/delayed feedback with the UEP bit-loading proposed in [7, 11]. The only limitation of this feedback model is that it requires channels with a limited number of scatterers, i.e., where the antennas are considered to be correlated following the separable Kronecker antenna correlation model. See Chapter 2 for more details about the MIMO channel correlation models .

In our simulation model, we consider both the perfect and the imperfect CSI as in [7, 8, 11, 12]. Furthermore, different spatial correlation scenarios are considered in order to examine the performance of the robust and the intuitive sorting proposed in Chapter 3.

5.1 MIMO Channel Model

In our simulation model, we consider a MIMO-OFDM system deploying N_T transmit antennas (with N_T IFFTs), N_R receiver antennas (with N_R FFTs), and N subcarriers as in Fig. 5.1. In order to model the two dimensions of the MIMO-OFDM (space and frequency) which are used in our UEP bit-loading, we consider a MIMO channel matrix $\tilde{\mathbf{H}}_k \in \mathbb{C}^{N_R \times N_T}$ for each subcarrier k. For rich-scattering environments, the elements of $\tilde{\mathbf{H}}_k$ can be considered as i.i.d. with a zero mean circularly symmetric complex Gaussian (ZMCSCG) distribution (as in Chapter 2 – Section 2.2.1). Thus, the normalized channel (scaled to the number of transmit antennas

[2] assuming N_T antennas at the transmitter and N_R antennas at the receiver

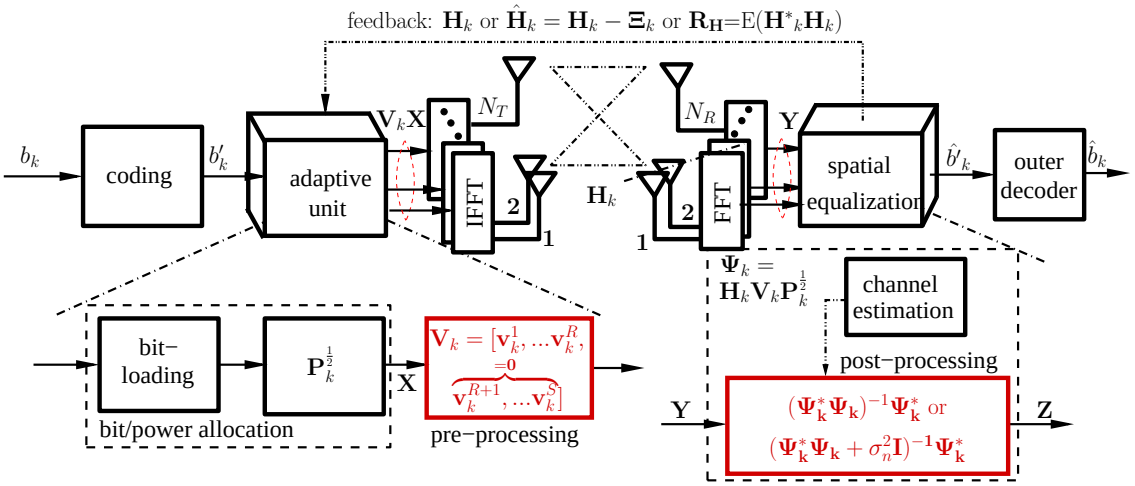

Figure 5.1: MIMO-OFDM bit and power allocation

N_T) is given by $\tilde{\mathbf{H}}_k \in \mathbb{CN}(\mathbf{0}, \sigma^2_{\tilde{\mathbf{H}}}\mathbf{I})$, where the rich-scattering assumption guarantees to have a diagonal covariance matrix $\sigma^2_{\tilde{\mathbf{H}}}\mathbf{I}$. However, if the channel is assumed to be a non-zero mean, e.g., Rician fading channel with a direct LoS, $\mathbf{H}_k \sim \mathbb{CN}(\overline{\mathbf{H}}_k, \sigma^2_{\mathbf{H}}\mathbf{I})$, where $\overline{\mathbf{H}}_k$ is related to the Rician fading factor K (see Chapter 2 – Section 2.2.1). In limited-scattering environments, the resultant covariance matrix is not diagonal any more. Thus, $\mathbf{H}_k \sim \mathbb{CN}(\overline{\mathbf{0}}_k, \mathbf{R_H})$, where the channel covariance matrix is given by

$$\mathbf{R_H} = E\{\mathbf{H}^*_k\mathbf{H}_k\} \, . \tag{5.1}$$

Therefore, in OFDM transmission, the covariance matrix $\mathbf{R_H}$ can easily be estimated at the receiver by performing an ensemble average over a sufficient number of subcarriers, i.e., assuming no correlation between the neighboring subcarriers.

In order to simplify the channel correlation parameters, we follow the separable Kronecker correlation model discussed in Chapter 2, which can easily separate between the correlation presents near the transmitter and the correlation at the receiver side. Accordingly, one can write the equivalent correlated channel matrix $\mathbf{H}_k$ as

$$\mathbf{H}_k \equiv \mathbf{R}_R^{1/2}\tilde{\mathbf{H}}_k\mathbf{R}_T^{1/2} \, , \tag{5.2}$$

where the elements of $\tilde{\mathbf{H}}_k$ are assumed to be i.i.d. with ZMCSGC distribution, $\mathbf{R}_T \in \mathbb{C}^{N_T \times N_T}$ is the transmit correlation matrix, and $\mathbf{R}_R \in \mathbb{C}^{N_R \times N_R}$ is the receive correlation matrix [64]. For mathematical convenience, we assume no correlation at the receiver side, i.e., $\mathbf{R_R} \approx \mathbf{I}$. This is a reasonable assumption when the receiver is located in a rich-scattering environment (indoor), while the transmitter is in a limited-scattering environment (outdoor) [71]. Consequently, the MIMO channel matrix in (5.2) is reduced to

$$\mathbf{H}_k = \tilde{\mathbf{H}}_k\mathbf{R}_T^{1/2} \, . \tag{5.3}$$

Hence, the correlation matrix $\mathbf{R_H}$ in (5.1) is further simplified according to (5.3) to be

$$\mathbf{R_H} = E\{\mathbf{H}^*_k\mathbf{H}_k\} = \mathbf{R}_T^{*,1/2}E\{\tilde{\mathbf{H}}^*_k\tilde{\mathbf{H}}_k\}\mathbf{R}_T^{1/2} \equiv \mathbf{R}_T \, , \tag{5.4}$$

where $E\{\tilde{\mathbf{H}}^*_k\tilde{\mathbf{H}}_k\} = \mathbf{I}$. Therefore, estimating the transmit antenna correlation $\mathbf{R}_T$ is sufficient to envisage link adaptation based on spatial correlation.

5.2 Limited Feedback Regimes

Throughout this thesis, we consider a perfect CSI together with limited (or partial) feedback regimes that only allow for feeding the transmitter with subsets of the estimated channel at the receiver, i.e., quantized or delayed feedback [11, 8]. We also consider the channel covariance feedback, which varies much slower than either the instantaneous channel or the limited one. Accordingly, the partial CSI is achieved by feeding back either A or B:

A - **a deficient channel version $\hat{\mathbf{H}}_k$**, which could either be the channel statistical mean in case of Rician fading channels or the outdated/delayed/quantized channel estimate. To minimize the complexity of the feedback channel, one can consider $\hat{\mathbf{H}}$ as the actual channel matrix, however, deviating from the instantaneous $\mathbf{H}$ by the error matrix $\mathbf{\Xi}_k$, which define as

$$\mathbf{\Xi}_k = \mathbf{H}_k - \hat{\mathbf{H}}_k,\ k = 0..N-1\ , \tag{5.5}$$

where $\mathbf{\Xi} \in \mathbb{C}\mathcal{N}(0, \sigma^2_{\mathbf{\Xi}}\mathbf{I})$. Thus, the variance of the outdated channel is given by

$$\sigma^2_{\hat{\mathbf{H}}}\mathbf{I} = \left(\sigma^2_{\mathbf{H}} - \sigma^2_{\mathbf{\Xi}}\right)\mathbf{I}\ . \tag{5.6}$$

B - **the channel correlation $\mathbf{R_H} = E\{\mathbf{H}^*\mathbf{H}\}$**, for the case where the channel variations are much faster than the quantized feedback rate. In such feedback schemes, the bit-rate and the power values are only allocated to the directions of the maximum eigenvalues without any further spectral dependency, i.e., using the transmitter correlation matrix $\mathbf{R}_T$.

5.2.1 Quantized or Delayed Channel Feedback

In this thesis, we only consider the limited feedback scheme given by either the quantized or the outdated (delayed) $\hat{\mathbf{H}}_k$ (as in scheme A). The SVD of $\hat{\mathbf{H}}_k$ and the EVD of the Hermitian matrix $\hat{\mathbf{H}}^*_k\hat{\mathbf{H}}_k$ are given by

$$\hat{\mathbf{U}}_\mathbf{k}\hat{\mathbf{D}}^{1/2}_k\hat{\mathbf{V}}^*_\mathbf{k} \ \text{ and } \ \hat{\mathbf{V}}_\mathbf{k}\hat{\mathbf{D}}_\mathbf{k}\hat{\mathbf{V}}^*_\mathbf{k}\ , \tag{5.7}$$

respectively, where $\hat{\mathbf{V}}_k$ and $\hat{\mathbf{U}}_k$ are unitary matrices and $\hat{\mathbf{D}}_k$ is a diagonal matrix with the eigenvalues of $\hat{\mathbf{H}}^*_k\hat{\mathbf{H}}_k$. As discussed in Chapter 2, the optimum beamforming can be preserved at the transmitter by knowing $\hat{\mathbf{V}}_k$ or only R of its columns that corresponds to the R highest eigenbeams. Thus, our CSI error model, adopted from [44], is stated as $\mathbf{H}_k = \hat{\mathbf{H}}_k + \Xi_k$, where $\mathbf{H}_k$ is the instantaneous channel model and the estimated CSI at the receiver (assuming a perfect CSI at the receiver side). $\mathbf{\Xi}_k \sim \mathbb{C}\mathcal{N}(0, \sigma^2_{\mathbf{\Xi}})$ represents the CSI error. Hence, the received vector $\mathbf{Y}_k$ of the k^{th} subcarrier, after applying the precoding matrix $\hat{\mathbf{V}}_k$ and the power loading matrix $\mathbf{P}^{1/2}_k$ similar to Chapter 2, Section 2.2.2, can be written as

$$\begin{aligned}
\mathbf{Y}_k &= \mathbf{H}_k\hat{\mathbf{V}}_k\mathbf{P}^{1/2}_k\mathbf{X}_k + \mathbf{n}_k \\
&= \mathbf{U}_k\mathbf{D}^{1/2}_k\overbrace{\mathbf{V}^*_k\hat{\mathbf{V}}_k}^{\widetilde{\mathbf{V}}_k}\mathbf{P}^{1/2}_k\mathbf{X}_k + \mathbf{n}_k \\
&= \overbrace{\mathbf{U}_k\mathbf{D}^{1/2}_k\widetilde{\mathbf{V}}_k\mathbf{P}^{1/2}_k}^{\mathbf{\Psi}_k}\mathbf{X}_k + \mathbf{n}_k\ ,
\end{aligned} \tag{5.8}$$

where $\mathbf{X}_k$ is the transmitted vector and $\mathbf{n}_k \sim \mathbb{C}^{N_R \times 1}\mathcal{N}(0, \sigma_n^2)$ is an additive white Gaussian noise vector and $\widetilde{\mathbf{V}}_k$ is simply a new unitary matrix results from multiplying two unitary matrices, i.e., $\mathbf{V}_k^*$ and $\hat{\mathbf{V}}_k$. $\mathbf{\Psi}_k$ represents the aggregated channel matrix and $\mathbf{P}_k^{1/2}$ is a diagonal matrix containing the allocated power values, which is also a part of $\mathbf{\Psi}_k$. An estimate of $\mathbf{\Psi}_k$ is sufficient for knowing the power allocation at the receiver [103]. In perfect CSI, i.e., $\sigma_{\underline{\Xi}}^2 = 0$ and $\widetilde{\mathbf{V}}_k = \mathbf{I}_{N_T}$, we obtain

$$\mathbf{\Psi}_k = \mathbf{U}_k \mathbf{\Lambda}_k \ , \tag{5.9}$$

where $\mathbf{U}_k$ is a unitary matrix and $\mathbf{\Lambda}_k$ is the diagonal matrix $\mathbf{D}_k^{1/2}\mathbf{P}_k^{1/2}$. However, in the imperfect CSI case, $\widetilde{\mathbf{V}}_k$ is a general (non-diagonal) matrix and thus

$$\mathbf{\Psi}_k = \mathbf{U}_k \mathbf{D}_k^{1/2} \widetilde{\mathbf{V}}_k \mathbf{P}_k^{1/2} \ . \tag{5.10}$$

Eigen-beamforming based on quantized/delayed CSI

In this case, the eigen-beamforming is implemented at the transmitter by multiplying the antenna array by a pre-coding matrix. This matrix maximizes the received power by directing the transmitted power to the directions of the eigenbeams. As mentioned in the previous section, the optimum pre-coding matrix is the unitary matrix $\hat{\mathbf{V}}_k$, i.e., the rightmost unitary matrix in (5.7) [44]. Moreover, weaker eigenbeams can still be suppressed to avoid performance deterioration, e.g., noise enhancement and inter-eigen interference (IEI) [103]. This is achieved by switching off the columns of $\hat{\mathbf{V}}$ corresponding to weaker eigenbeams. Thus, if the rank of $\hat{\mathbf{H}}_k$ is n and the maximum allowed beamforming is R, where $0 < R < n$, we achieve a reduced-order beamforming. This we denote as R-dimension or R-D beamforming. For instance, we split the beamforming matrix $\hat{\mathbf{V}}_k$ into two parts, such that

$$\hat{\mathbf{V}}_k = [\hat{\mathbf{v}}_k^{(1)} \hat{\mathbf{v}}_k^{(2)}] \ ,$$

where $\hat{\mathbf{v}}_k^{(1)} = [v_k^{(1)}, ..., v_k^{(R)}]$ and $\hat{\mathbf{v}}_k^{(2)} = [0, .., 0]$. As soon as $n = R$, the system realizes a full eigen-beamforming. This is not necessarily the best case when the channel is highly correlated, i.e., has some weak eigenchannels.

5.2.2 Channel Covariance Feedback

In contrast to the delayed/quantized channel feedback, we assume here that the eigenvalues and the eigenvectors of $\mathbf{R_H}$ are the only available information at the transmitter. However, a perfect CSI is assumed to be readily at the receiver where it is used to deploy a linear equalizer, e.g., ZF or MMSE equalizer. Moreover, perfectly uncorrelated receive antennas are assumed. Thence, the optimal beamforming and bit-loading can be obtained using the eigen-decomposition of $\mathbf{R}_T$ [72]. This is a positive definite Hermitian matrix, where one can directly decompose it using EVD as in (5.7) to be

$$\begin{aligned} \mathbf{R}_T &= \mathbf{U}_T \mathbf{D}_T \mathbf{U}_T^* \quad \text{or} \\ \mathbf{R}_T^{1/2} &= \mathbf{U}_T \mathbf{D}_T^{1/2} \mathbf{U}_T^* \ , \end{aligned} \tag{5.11}$$

where $\mathbf{U}_T$ is a unitary matrix containing N_T eigenvectors which can be used for realizing the optimum beamforming at the transmitter. $\mathbf{D}_T$ is a diagonal matrix of the eigenvalues of $\mathbf{R}_T$ that determine the bit and the power allocation[3].

Since the decomposition of $\mathbf{R}_T$ does not vary with frequency, all subcarriers that belong to the same eigenchannel are allocated identically, i.e., using their unique spatial gains. However, the UEP bit-loading algorithms proposed in Chapter 3 can still vary the bit-loading, across the spectral domain, according to the different noise margins γ_j for each class j, i.e., if we have different classes allocating the same eigenchannel. The received vector $\mathbf{Y}_k$ of the k^{th} subcarrier can be written as

$$\mathbf{Y}_k = \mathbf{H}_k \mathbf{R}_T^{1/2} \mathbf{U}_T \mathbf{P}^{1/2} \mathbf{X}_k + \mathbf{n}_k \ , \tag{5.12}$$

where $\mathbf{H}_k \sim \mathbb{C}^{N_R \times N_T} \mathcal{N}(0, \sigma_{\hat{\mathbf{H}}} \mathbf{I})$, $\mathbf{P}^{1/2}$ is independent of the number of subcarriers, i.e., fixed for all subcarriers, $\mathbf{X}_k$ is the transmitted vector, and $\mathbf{n}_k \sim \mathcal{CN}(0, \sigma_n^2)$ is the additive white Gaussian noise vector. Using the EVD in (5.11), one can rephrase (5.12) to be

$$\mathbf{Y}_k = \overbrace{\underbrace{\mathbf{H}_k \mathbf{U}_T}_{\widetilde{\mathbf{H}}_k} \mathbf{D}_T^{1/2} \underbrace{\mathbf{U}_T^* \mathbf{U}_T}_{\mathbf{I}} \mathbf{P}^{1/2}}^{\mathbf{\Psi}_k} \mathbf{X}_k + \mathbf{n}_k \ , \tag{5.13}$$

where $\mathbf{\Psi}_k$ represents the aggregated channel matrix that could be estimated at the receiver and $\widetilde{\mathbf{H}}_k$ has the same distribution as $\mathbf{H}_k$. Similar to the quantized/delayed feedback, the power loading matrix $\mathbf{P}$ is implicitly estimated during the estimation of the aggregated channel $\mathbf{\Psi}_k$. If $\mathbf{R}_T$ is perfectly estimated[4], then (5.13) reduces to

$$\mathbf{Y}_k = \overbrace{\widetilde{\mathbf{H}}_k \mathbf{\Delta}_T}^{\mathbf{\Psi}_k} \mathbf{X}_k + \mathbf{n}_k \ , \tag{5.14}$$

where the diagonal matrix $\mathbf{\Delta}_T = \mathbf{D}_T^{1/2} \mathbf{P}^{1/2}$. If the estimation of $\mathbf{R}_T$ is not performed perfectly, we will get an erroneous correlation matrix $\hat{\mathbf{R}}_T = \hat{\mathbf{U}}_T \hat{\mathbf{D}}_T \hat{\mathbf{U}}_T^*$. Thus, $\mathbf{U}_T^* \hat{\mathbf{U}}_T = \widetilde{\mathbf{U}}_k^*$ is not an identity matrix; rather a unitary one. Nevertheless, the distribution of $\mathbf{\Psi}_k$ will not be changed.

Channel Covariance Eigen-beamforming

The eigen-beamforming based on the channel covariance feedback is used to maximize the received power along the eigenvectors of the transmit correlation matrix. Hereto, the optimum beamforming is realized by multiplying the transmit antennas by the unitary pre-processing matrix $\mathbf{U}_T$, which results from decomposing $\mathbf{R}_T$ as in (5.11).

For spatially correlated channels, we propose using a reduced eigen-beamforming to enhance the performance [12]. As with the previous partial CSI technique, we realize the reduced eigen-beamforming by allocating zeros to the columns of $\mathbf{U}_R$ corresponding to the weak eigenbeams.

[3] The matrix square-root has no effect on the left and the right unitary matrices [104].

[4] $\mathbf{R}_T$ is estimated by averaging out $\mathbf{H}_k^* \mathbf{H}_k$ using insufficient number of subcarriers.

5.3 Equalization for Diagonalized MIMO

The post-combiner at the receiver is designed to be a spatial equalizer in order to mitigate the IEI caused by the MIMO channels. For perfect CSI, one can still prove that the linear ZF spatial equalizer is the optimum solution (as proposed in Chapter 2, Section 2.2), as it diagonalize the resultant channel matrix at the equalizer output[5]. This completely mitigates the IEI. For more details about channel diagonalization in MIMO case, the reader is referred to Chapter 2.

If we are dealing with imperfect CSI, the diagonalization cannot be guaranteed any more. In this case, ZF equalization introduces its well-known drawback, noise enhancement, besides a residual amount of noise superposition or, namely, IEI[6]. In this case, we consider a linear MMSE to combat the noise enhancement, however, without further reduction of the noise superposition that results in IEI. In order to reduce the remaining IEI in the resulting channel $\mathbf{\Psi}$, we propose to use a non-linear successive interference cancellation, e.g., the V-BLAST technique introduced in Chapter 2.

5.3.1 Zero-forcing Linear Spatial Equalizer

The ZF equalizer is a linear equalizer that uses the inverse of the overall MIMO channel response matrix $\mathbf{\Psi}_k$ without considering the noise effect. Thus, in case of rank-deficient channel matrices, the Moore-Penrose generalized inverse (pseudo-inverse) of the channel matrix $\mathbf{\Psi}_k$ is used, which uses SVD such that

$$\mathbf{\Psi}_k^{\dagger} = \mathbf{U}_{\mathbf{\Psi},k}\mathbf{D}_{\mathbf{\Psi},k}^{\dagger/2}\mathbf{V}_{\mathbf{\Psi},k}^{*} \, , \tag{5.15}$$

where $\mathbf{D}_{\mathbf{\Psi}}^{\dagger/2} = \mathrm{diag}\{1/\sqrt{\lambda_0}, 1/\sqrt{\lambda_1}, ..., 1/\sqrt{\lambda_s}, ..., 1/\sqrt{\lambda_n}\}$, λ_s are the eigenvalues of $\mathbf{\Psi}_k^{*}\mathbf{\Psi}_k$, and n is its rank. Thus, if $n < \min\{N_r, N_t\}$, the remaining diagonal elements are replaced with zeros to suppress any noise enhancement due to weak eigenchannels. As in Fig. 5.1, the equalizer output is given by

$$\mathbf{Z}_k = \mathbf{W}_k\mathbf{Y}_k \, , \tag{5.16}$$

where the equalizing matrix $\mathbf{W}_k \in \mathbb{C}^{N_T \times N_R}$ for the ZF equalizer is given by

$$\mathbf{W} = \mathbf{\Psi}_{\mathbf{k}}^{\dagger} = \{\mathbf{\Psi}_{\mathbf{k}}^{*}\mathbf{\Psi}_{\mathbf{k}}\}^{\dagger}\mathbf{\Psi}_{\mathbf{k}}^{*} \, . \tag{5.17}$$

Therefore, $\mathbf{Z}_k$ in (5.16) after substituting with (5.8) is given by

$$\begin{aligned} \mathbf{Z}_k &= \mathbf{W}_k\left(\mathbf{\Psi}_k\mathbf{X}_k + \mathbf{n}_k\right) \\ &= \overbrace{\{\mathbf{\Psi}_k^{*}\mathbf{\Psi}_k\}^{\dagger}\mathbf{\Psi}_k^{*}\mathbf{\Psi}_k}^{\mathbf{\Phi}_k}\mathbf{X}_k + \overbrace{\{\mathbf{\Psi}_k^{*}\mathbf{\Psi}_k\}^{\dagger}\mathbf{\Psi}_k^{*}}^{\mathbf{W}_k}\mathbf{n}_k \, , \end{aligned} \tag{5.18}$$

where $\{\mathbf{\Psi}_k^{*}\mathbf{\Psi}_k\}$ is a square (non-diagonal) matrix, $\mathbf{\Psi}_k \in \mathbb{C}^{N_R \times N_T}$, and $\mathbf{\Phi}_k = \mathbf{I}_{N_T}$. However, if $\{\mathbf{\Psi}_k^{*}\mathbf{\Psi}_k\}$ is a full-rank matrix and its inverse exist[7], the pseudo-inverse in (5.17) can be safely

[5] similar to multicarrier modulation, where the optimum equalization is also ZF when ICI is avoided

[6] In ZF equalization, the interference is completely forced to be zero. However, the noise values at different positions are superimposed on the desired symbol. This we also refer as IEI in this chapter.

[7] mostly the case when $N_R > N_T$

replaced by a normal matrix inverse, such that

$$\mathbf{W}_k = \mathbf{\Psi}_k^{\dagger} = \{\mathbf{\Psi}_k^* \mathbf{\Psi}_k\}^{-1} \mathbf{\Psi}_k^* \, . \tag{5.19}$$

In perfect CSI similar to (5.9), the equalizing matrix in (5.19) is reduced to be $\mathbf{W}_k = \mathbf{\Lambda}_k^{\dagger/2} \mathbf{U}_k^*$. Hence, one can rewrite (5.18) as

$$\mathbf{Z}_k = \mathbf{X}_k + \mathbf{\Lambda}_k^{\dagger/2} \tilde{\mathbf{n}}_k \, , \tag{5.20}$$

where $\tilde{\mathbf{n}}_k = \mathbf{U}_k^* \mathbf{n}_k$ is also white Gaussian noise[8] and multiplied by a diagonal matrix $\mathbf{\Lambda}_k$. However, for imperfect CSI, $\mathbf{\Psi}_k$ is given as (5.10), which means that $\mathbf{W}_k$ is a full matrix leading to noise enhancement due to the weak eigenbeams of $\mathbf{\Psi}_k^* \mathbf{\Psi}_k$. Furthermore, for rank-deficient channel matrices or with reduced eigen-beamforming, the pseudo-inverse automatically allocates zeros to these locations. This automatically reduces the noise enhancement.

5.3.2 Minimum-mean Square Error Linear Equalizer

The linear minimum-mean square error (MMSE) equalizer succeeds in mitigating the noise enhancement by considering the noise value during the inversion of $\{\mathbf{\Psi}_k^* \mathbf{\Psi}_k\}$. Hence, the MMSE linear equalizer matrix is given by

$$\mathbf{W} = \{\mathbf{\Psi}^* \mathbf{\Psi} + \sigma_{\mathbf{n}}^{\mathbf{2}} \mathbf{I}\}^{-\mathbf{1}} \mathbf{\Psi}^* \, . \tag{5.21}$$

However, at low σ_n^2 (high SNR) the equalizing matrix in (5.21) becomes similar to (5.17), which makes their performances very close to each other. Therefore, the linear MMSE also suffers from the same non-avoidable IEI as in the case of ZF. It is, hence, necessary to eliminate the remaining interference using successive interference reduction methods, i.e., non-linear equalization.

5.3.3 Successive Interference Cancellation using V-BLAST

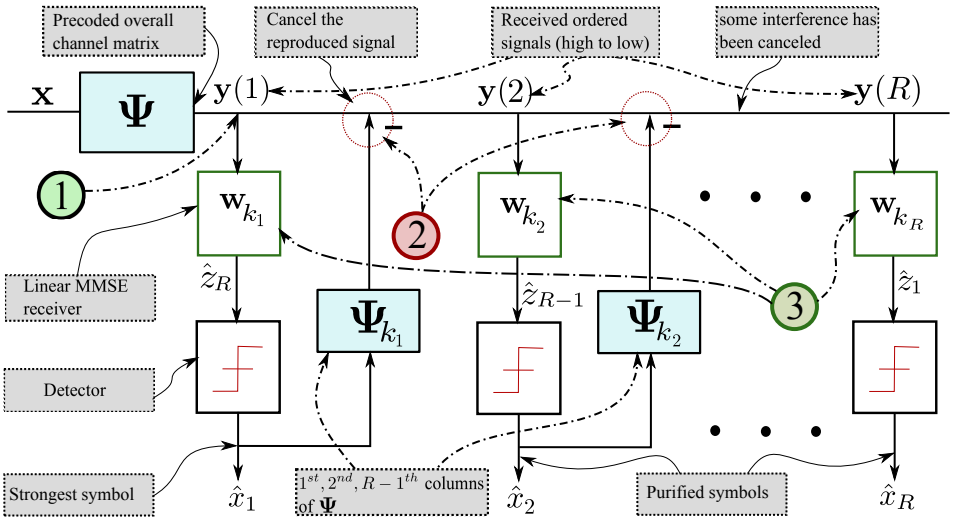

Figure 5.2: MIMO UEP bit-loading

[8] since the unitary matrix does not change the noise power

The well-known V-BLAST, also known as vertical Bell Laboratories Layered Space-Time method, is a successive interference cancellation (SIC) receiver. This technique consists of data being transmitted from different transmit antennas onto the space forming different layers [61]. These layers are successively decoded at the receiver, where the interference is successively canceled. Certainly, the order of detecting the symbols affects the overall performance. Thus, our modified V-BLAST utilizes the precoded (preordered) overall channel $\mathbf{\Psi}$ to avoid the iterative search-and-sort process used in the original algorithm in [61]. In this case, the first column of $\mathbf{\Psi}$ represents the strongest received signal while its last column is the weakest one[9]. Hence, the 3 main steps (marked with *circles* in Fig. 5.2) to perform a SIC are given as:

1. Detect the strongest symbol sorted symbols $\mathbf{y}(k_i),\ k = 1..R$, using the appropriate MMSE.
2. Interference is canceled using the previously regenerated symbol (after hard-detection).
3. The remaining interference is nulled from each symbol using ZF or MMSE.

Here we consider implementing V-BLAST on the resulting channel matrix $\mathbf{\Psi}_k$ after bit-loading, power allocation, and beamforming for imperfect CSI. Thus, if bits are allocated using one of our UEP approaches for intuitively sorted subcarriers, we always get the most important data on the higher eigenchannel, i.e., let us name it index k_i. Consequently, the detection of the strongest symbol is carried out without considering the minor interference of the weaker eigenchannels. Moreover, the weaker eigenchannels are purified from the stronger eigenchannel using SIC [13]. In the following, we present the modified V-BLAST-MMSE algorithm (also depicted in Fig 5.2):

Algorithm 5.1 V-BLAST for adaptive systems with distorted diagonalization

Initialize: $i \Leftarrow 1$, $k_i \Leftarrow i$ (strongest column), $\mathbf{W} = (\mathbf{\Psi}_i^* \mathbf{\Psi}_i + \sigma_n^2 \mathbf{I})^{-1} \mathbf{\Psi}_i^*$, and $\mathbf{\Psi}_i = \mathbf{\Psi}$

repeat
  if the normalized CSI error variance $\sigma_{\mathbf{\Xi}}^2 \leq 0.5$ **then**
    set the equalizer minimum MSE row $k_i = i$, i.e., minimum MSE
  else
    find the minimum row $k_i = \arg\min_m \parallel \mathbf{W}(m,:) \parallel^2,\ m = 1..R$
  end if
  compute the MMSE (nulling) row: $\mathbf{w}_{k_i} = \mathbf{W}(:, k_i)$
  implement the MMSE interference nulling: $z_{k_i} = \mathbf{w}_{k_i} \mathbf{y}_i$, where $\mathbf{y}_i$ has less interference
  detect the symbol: $\hat{x}_{k_i} = \text{detect}(z_{k_i})$
  perform the cancellation of the detected component: $\mathbf{y}_{i-1} = \mathbf{y}_i - \mathbf{\Psi}(:, k_i)\hat{x}_{k_i}$
  if the normalized CSI error variance $\sigma_{\mathbf{\Xi}}^2 > 0.5$ **then**
    set the columns k_i of $\mathbf{\Psi}_i$ to all zeros, i.e., for not selecting it again
    compute the new equalize matrix for the i^{th} iteration: $\mathbf{W} = (\mathbf{\Psi}_i^* \mathbf{\Psi}_i + \sigma_n^2 \mathbf{I})^{-1} \mathbf{\Psi}_i^*$
  end if
  go to the next column: $i \Leftarrow i + 1$
until $i = 0$

[9] However, for very high CSI errors, one has to do search-and-sort technique, iteratively, as in [61].

ℹ In Line 10, the original overall matrix $\mathbf{\Psi}$ is used to regenerate the detected symbols.

From the previous steps, one can deduce the similarities between the V-BLAST and the decision feedback equalizer (DFE), albeit with ordered symbols. The importance of ordering is that it permits detecting and nulling the interference of the strongest signal first, i.e., the symbol with least susceptibility to interference. This limits the error propagation to the weaker symbols.

5.4 UEP Bit-loading for MIMO-OFDM

As mentioned in the previous section, in order to adapt the MIMO-OFDM transmission, we require at the transmitter either the instantaneous channel matrix $\mathbf{H}_k$ or the partial channel matrix $\hat{\mathbf{H}}_k$ or, at least, the transmit covariance matrix $\mathbf{R}_T$. Herewith, the eigenbeams for all subcarriers, i.e., eigenchannels, are used to allocate bits and powers. The eigenchannels on every subcarrier are sorted according to their eigenbeam values realized by SVD or EVD. Thus, to realize different UEP classes, the hypothetical thresholds proposed in Chapter 3 divides the sorted eigenchannels in both dimensions, space and frequency, in order to allocate N_g classes with different margin separation $\Delta\gamma_j$. We are also using the same sorting mechanisms proposed in Chapter 3, which are:

I- the intuitive sorting: where the subcarriers with the highest eigenbeams are allocated to the important data and

II- the robust sorting: which uses the lowest eigenchannels for allocating the most important data and the highest eigenchannels for the less important data.

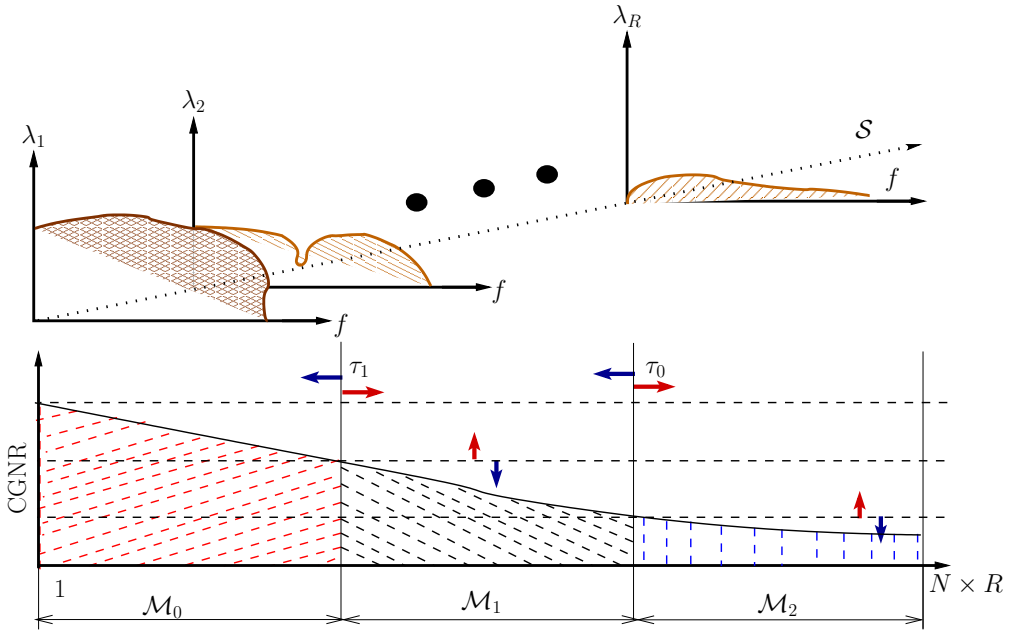

Figure 5.3: Hypothetical thresholds separating eigenchannels for three protection classes assuming the index 0 stands for the highest protected one

In order to proceed with either method I or II, all subcarriers of all eigenbeams have to be combined in a long buffer, i.e., assuming an equivalent SISO case with a buffer $\mathcal{M} \in \mathbb{Z}^{1\times NR}$. The sorting algorithms have to go sequentially through this buffer in order to satisfy the two-dimensional sorting (see Figure 5.3). Furthermore, τ_j are set within this buffer such that the UEP requirements are fulfilled by modifying these thresholds, thereby changing the number of subcarriers of each class. However, the limited/partial channel feedbacks are expected to result in performance degradations. These limitations are described extensively using the SER performance in our results and analysis section assuming different scenarios. Now, we proceed with the bit-loading schemes for MIMO-OFDM transmission.

Figure 5.4 depicts the spatial-spectral channel gains (Fig 5.4.a) together with the bit-loading (Fig 5.4.b) using the robust sorting scheme. It is clear from this figure that the robust sorting already spans a huge number of subcarriers for the first class leaving only a few eigenchannels where the other classes can be allocated.

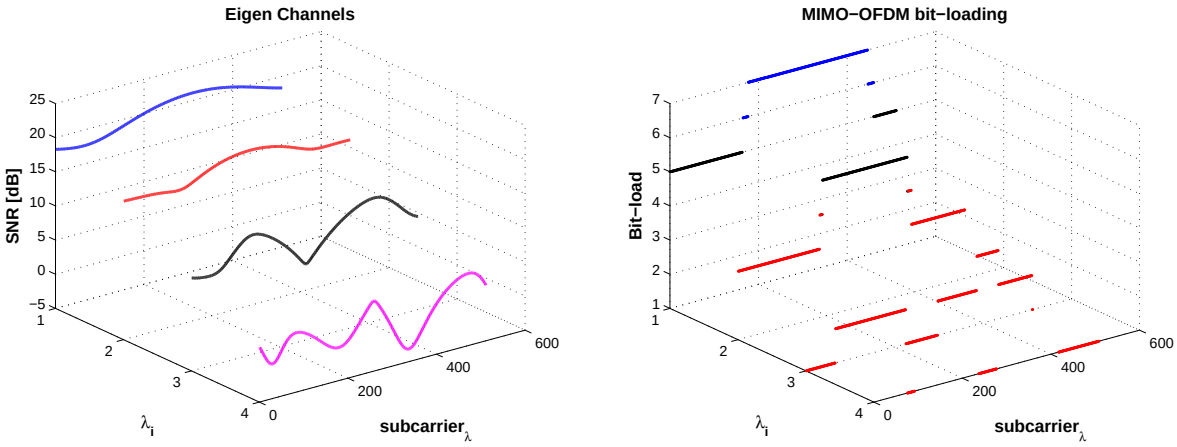

(a) Eigen channel gains

(b) red (highest priority) and blue (least priority)

Figure 5.4: MIMO adaptive modulation using robust sorting

5.4.1 UEP using Adaptive Non-hierarchical Modulation

In this section, we briefly discuss the realization of UEP by modifying the bit and power allocation algorithm (Algorithm 3.5), proposed in Chapter 3for a MIMO-OFDM system with either perfect or partial channel feedback. In this case, we assume the number of eigenchannels R to be less than or, at most, equals to the channel matrix rank n. This means that a 4×4 MIMO channel matrix, has a maximum allowed spatial size of 4-D. However, we can still consider a reduced number of eigenchannels to reduce the IEI, e.g., 2-D, which means to consider only the highest 2 eigenchannels. In the following, we summarize the required steps to realize UEP bit-loading for perfect CSI, $\mathbf{H}$, or partial (quantized/delayed) CSI, $\hat{\mathbf{H}}$, in Algorithm 5.2 based on Algorithm 3.5. Thereafter, in Algorithm 5.3, we show the modifications needed for changing Algorithm 5.2 in order to realize UEP using the given channel covariances feedback without any spectral dependencies.

5.4.1.1 Using perfect/delayed/quantized feedback

Algorithm 5.2 UEP adaptive MIMO using the Chow-like bit-loading – second approach

Input: perfect channel matrix $\mathbf{H}_k$ or quantized channel matrix $\hat{\mathbf{H}}_k, k = 0..N-1$, the channel rank or the maximum eigenbeams R, the total eigenchannels NR, the maximum number of iterations "MaxCnt", target power P_T, target sum rate B_T, and $\Delta\gamma = 3$ dB

Output: γ_j, the SER $\mathcal{P}_j$, the power $p^j_{s,k}$, and bit allocation $\hat{b}^j_s$, where s is the spatial index.

Initialize: the subcarriers indices $\mathcal{M} \in \mathbb{Z}^{1\times NR}$, the equivalent subcarrier indices v, and the start index $\mathcal{I}$ with all zeros. $\tau_j = N\ ,\ j = 0..N_g - 1$, and the counter Cnt = 0

1: decompose the Hermitian channel $\mathbf{H}^*_k\mathbf{H}_k$ for every subcarrier k using EVD, such that

$$\mathbf{H}^*_k\mathbf{H}_k = \mathbf{V}_k\mathbf{D}_k\mathbf{V}^*_k\ , \tag{5.22}$$

where $\mathbf{D}_k = \text{diag}\{\lambda_{1,k}, \lambda_{2,k}, ..., \lambda_{s,k}, ..., \lambda_{R,k}\}\ ,\ k = 0..N-1$; compute $\mathcal{G}_{s,k} = \lambda_{s,k}/\sigma^2_n$.

2: sort the NR eigenchannels in a descending order according to $\mathcal{G}_{s,k}$; map $\{s,k\} \multimap \mathcal{M}$

3: find the mean CGNR $\overline{\mathcal{G}} = \frac{\sum_{k=0}^{N-1}\sum_{s=0}^{R-1}\lambda s,k}{NR\sigma^2_n}$, then $\gamma_{m_{\text{init}}} = \frac{\overline{\mathcal{G}}}{2^{B_T/N}}$

4: **repeat**

5: find γ_m of the middle class m using (3.36) and (3.37) (Chapter 3) together with $\gamma_{m_{\text{init}}}$

6: **repeat**

7: compute the individual γ_j using the relation (3.38) and Δ_γ

8: calculate $\hat{b}^j_v$ as in (3.33) using γ_j starting from $\mathcal{I}$, where v is the running index of $\mathcal{M}$

9: use the cumsum to accumulate $\hat{b}^j_v\ ,\ v = 0..N-1$; stop accumulating when T_j is fulfilled.

10: set τ_j to the location where the cumsum stops, i.e., $\sum_{v=\mathcal{I}}^{\tau_j}\hat{b}^j_v = T_j$

11: update $\mathcal{I} \Leftarrow \tau_j + 1$ and $j \Leftarrow j + 1$.

12: **until** $j = N_g$

13: γ_m is recalculated using the same adjustment as in Chapter 3 – Algorithm 3.4, such that $\gamma_{m,new} = \gamma_{m,old} \cdot 2^{\frac{B_{tot}-B_T}{N}}$

14: update $\gamma_j = \gamma_m + (m-j)\cdot\Delta\gamma$ [dB]; where m is the middle class.

15: Cnt $\Leftarrow$ Cnt + 1

16: **until** $\sum_{v\in\mathcal{M}} b^j_v \approx B_T$ or Cnt = MaxCnt

17: **if** $\sum_{v\in\mathcal{M}} b^j_v \neq B_T$ **then**

18: brute-force based on the quantization error (3.34) as in Chapter 4 – Algorithm 3.4

19: **end if**

20: invert the mapping in Line 2, i.e., $\{s,k\} \multimap \mathcal{M}$

21: power is allocated using $p^j_{s,k} = \left(2^{b^j_{s,k}} - 1\right)\frac{\gamma_j}{\mathcal{G}^j_{s,k}}$.

22: power is rescaled such that $p^j_{s,k} = p^j_{s,k}/P_T \cdot \left(\sum_{s=0}^{R-1}\sum_{k=0}^{N-1} P_{s,k}\right)$.

Note: $\multimap$ is a multi-mapping that maps a vector or a matrix into another vectorized form; $\multimap$ is the opposite

5.4.1.2 Using channel covariance feedback

In this algorithm, the number of bits on all subcarriers (belongs to the same eigenbeam s) is the same, i.e., bit-loading only varies between classes and spatial layers. Hence, we need to compute the exact number of subcarrier (and on which layer s) that should be allocated to class j, i.e., without any spectral dependency. The following algorithm states this idea.

Algorithm 5.3 UEP adaptive MIMO using channel covariance feedback

Input: $\mathbf{R}_T$, eigenchannels R, maximum iterations "MaxCnt", and $\Delta\gamma = 3$ dB.

Output: γ_j, $\mathcal{P}_j$, p_s^j and bit allocation $\hat{b}_s^j$, where s is the spatial index $\sim \{1..R\}$.

Initialize: the number of subcarriers matrix $\boldsymbol{\Upsilon} \in \mathbb{Z}^{R \times N_g}$ with zeros, $\mathbf{d} \in \mathbb{Z}^{R \times 1}$ with all N , an auxiliary bit counter $B_c = 0$, spatial counter $s = 0$, $j = 0$, and iteration counter Cnt $= 0$.

decompose $\mathbf{R}_T$ using (5.11), to have the sorted eigenvalues $\mathbf{D}_T = \text{diag}\{\lambda_1, \lambda_2, ..., \lambda_s, ..., \lambda_R\}$
$\mathcal{G}_s = \lambda_s/\sigma_n^2$ (similar $\forall\ k$), $\overline{\mathcal{G}}_s = \left(\sum_{s=0}^{R-1} \lambda_s/\sigma_n^2\right)/R$, and $\gamma_{m_{\text{init}}} = \frac{\overline{\mathcal{G}}_s}{2^{B_T/N}}$; find γ_m
repeat
  set the starting spatial index s to "0"
  repeat
    re-enhance γ_j, as with Algorithm 5.2, then compute $\hat{b}_s^j$,$\forall\ s$ using (3.33) (same $\forall\ k$)
    repeat
      if T_j is not fulfilled after considering allocating $\hat{b}_s^j$ to all subcarriers of the eigenbeam s, i.e., $\left(\mathbf{d}(s) \cdot \hat{b}_s^j \leq T_j - B_c\right)$ **then**
        class j consumes all subcarriers of s: $\boldsymbol{\Upsilon}(s, j) = \mathbf{d}(s)$
        save the current sum rate $B_c = \mathbf{d}(s) \cdot \hat{b}_s^j$
        $s \Leftarrow s + 1$
      else if $\left(N \cdot \hat{b}_s^j + B_c > T_j\right)$ **then**
        compute the exact number of subcarries needed as $\boldsymbol{\Upsilon}(s, j) = \left\lceil \frac{T_j - B_c}{\hat{b}_s^j} \right\rceil$
        update the remaining subcarriers for the next class $\mathbf{d}(s) = N - \boldsymbol{\Upsilon}(s, j)$
        reset $B_c = 0$; increment $j \Leftarrow j + 1$; **break** this loop
      end if
    until $s \geq R$ or $\sum_{s=0}^{R-1} \boldsymbol{\Upsilon}(s, j)\hat{b}_s^j \approx T_j$ (which can not be guaranteed to be equal)
  until $j \geq N_g$
until $\sum_{j=0}^{N-g-1} \sum_{s=0}^{R-1} \boldsymbol{\Upsilon}(s, j)\hat{b}_s^j \approx B_T$ or Cnt++ = MaxCnt
if $\sum_{s=0}^{R-1} \boldsymbol{\Upsilon}(s, j)\hat{b}_s^j \neq B_T$ **then**
  increment/decrement random subcarriers of the last priority class, i.e., $j = N_g - 1$, until B_T is fulfilled.
end if
power is allocated using the eigenvalues λ^s and the quantized bit-loading $\hat{b}_s^j$ as $p_s^j = \left(2^{\hat{b}_s^j} - 1\right)\frac{\sigma_n^2}{\lambda_s}$ and rescaled such that $p_s^j = p_s^j \frac{P_T}{\sum_{s=0}^{R-1} \sum_{j=0}^{N_g-0} \boldsymbol{\Upsilon}(\mathbf{s},\mathbf{j}) p_s^j}$.

To consider the robust sorting scheme in this case, the eigenchannels with the lowest λ_s, i.e., the lower eigenvalues of $\mathbf{R}_T$, are selected for the important data. However, the intuitive loading starts from the highest eigenvalue λ_0, assuming sorted eigenvalues.

5.4.2 UEP using Adaptive Hierarchical and Multilevel Modulation

Similar to Chapter 4, the simple subcarrier partitioning used in Section 5.4.1 has been replaced by an adaptive multilevel modulation, albeit using MIMO-OFDM. This scheme omits the borders between eigenchannels by embedding them on each other in a hierarchical fashion. This is an easier approach if the power-minimization is the target criterion, i.e., searching for subcarriers with low incremental power (performed by the least priority classes) is not limited between hypothetical thresholds. Again, only partial CSI is assumed to be available at the transmitter, e.g., the quantized/outdated $\hat{\mathbf{H}}_k$. Similar to Algorithm 5.2, bits and power values are allocated according to the eigenvalues of $\hat{\mathbf{H}}^*\hat{\mathbf{H}}$ according to (5.7). Furthermore, the total power is steered in space using the unitary matrix $\hat{\mathbf{V}}_k$.

In order to implement UEP bit-loading in this case, the highest priority class first consumes the eigenchannels with the minimum incremental power, i.e., assuming intuitive sorting. Thereafter, the next classes are allowed to be superimposed on already used eigenchannels (using hierarchical modulation) or the free ones leading to a multilevel (hierarchical and non-hierarchical) modulation as described in Chapter 4. Similarly, an arbitrary margin separation is kept constant by using a fixed ratio between the inter-constellation distances d_j for each level j, as shown in Fig. 4.2 (Chapter 4), defined by the margin separations between classes, e.g., $\Delta_\gamma = 3$ dB.

In the following, we present the modifications to the Hughes-Hartogs and the Campello-like algorithms in order to realize UEP in MIMO-OFDM system using multilevel modulation. In both algorithms, we assume either perfect or quantized/delayed CSI.

5.4.2.1 UEP using Hughes-Hartogs-like adaptive multilevel modulation

Based on the Hughes-Hartogs-like bit-loading in Algorithm 4.1 (Chapter 4), the incremental power is calculated based on the maximum allowed SER of the first class $\mathcal{P}^0$ and the channel eigenbeams $\lambda_{s,k}$ $k = 0..N-1$ and $s = 0..R-1$. Assuming an intuitive sorting, where the most important data are allowed to consume first the eigenchannels that require the minimum incremental power (using the given SER P_{e_0}). Accordingly, the next classes are allocated using hierarchical and non-hierarchical modulation as discussed before.

The SERs $\mathcal{P}^j$ of the less important data are calculated using the given margin separations γ_j and the given $\mathcal{P}^0$. In the following, we modify Algorithm 4.1 to be ready for adapting MIMO-OFDM systems. In this case, we are allowed only to increment bits according to a preselected vector $\mathbf{Z}_b \in \mathbb{Z}$. In this vector, we deliberately drop the inefficient constellation sizes, i.e., the BPSK (1-bit/symbol) and the power inefficient 8-QAM (with 3 bits/symbol).

Algorithm 5.4 UEP multilevel MIMO bit-loading using the Hughes-Hartogs-like algorithm

Input: channel matrix $\mathbf{H}_k$, $k = 0..N-1$, number of subcarriers N, required eigenchannels R, i.e., total eigenchannels NR, maximum allowed SER of the first class $\mathcal{P}^0$, and $\Delta\gamma = 3$ dB.

Initialize: $j = 0$, the bit-loading matrix $\mathbf{B}$ with $NR \times N_g$ zeros, NR zeros to the power loading vector $\mathbf{P}$ and the incremental power vector $\Delta\mathbf{P}$, $\mathbf{Z}_b = \{0, 2, 4, 5, .., b^j_{\max}\}$, and the bit index counter $c_v = 0$, $v = 0..NR-1$, i.e., c_v is a counter inside $\mathbf{Z}_b$, where $0 \leq c_v \leq \text{length}(\mathbf{Z}_b)$.

Output: the average $\mathcal{P}^j$, and bit allocation matrix $\mathbf{B} \in \mathbb{Z}^{NR \times N_g}$.

1: decompose $\mathbf{H}^*_k\mathbf{H}_k$ similar to Algorithm 5.2

2: concatenate the NR eigenchannels $\mathcal{G}_v = \lambda_v/\sigma^2_n$, $v = 0..RN-1$) also as in Algorithm 5.2, however, without sorting. Thereafter, save the mapping $\{s, k\} \multimap v$ (unsorted).

3: **repeat**

4: **repeat**

5: compute the incremental power steps $\Delta\mathbf{P}(v)$, for every eigenchannel v, using the approximate equation (based on (3.53) in Chapter 3 and Appendix C)

$$\Delta\mathbf{P}(v) = \frac{\frac{2}{3}\left[\text{erfc}^{-1}\left(\frac{\mathcal{P}^0}{2}\right)\right]^2}{\Delta\gamma_j\mathcal{G}_v}\left(2^{\mathbf{Z}_b(c_v+1)} - 2^{\mathbf{Z}_b(c_v)}\right)$$

6: find v with the smallest incremental power $\Delta\mathbf{P}(v)$

7: increment the bit-loading index: $c_v \Leftarrow c_v + 1$

8: update the bit-loading matrix: $\mathbf{B}(v, j) = \mathbf{Z}_b(c_v + 1)$

9: update the power allocation vector: $\mathbf{P}(v) \Leftarrow \mathbf{P}(v) + \Delta\mathbf{P}(v)$

10: **until** $\sum_{v=0}^{RN-1}\mathbf{B}(v, j) = T_j$

11: $j \Leftarrow j + 1$

12: **until** $j = N_g$

13: rescale the allocated power such that $\mathbf{p}^s(k) = \mathbf{p}^s(k)\frac{P_T}{\sum_{v=0}^{RN-1}\mathbf{P}(v)}$

14: invert the mapping in Line 2 such that $\{s, k\} \multimap v$.

In the following, we modify the less complex Campello algorithm in order to realize UEP.

5.4.2.2 UEP using the Campello-like adaptive multilevel modulation

Based on the Campello-like UEP bit-loading algorithm proposed in Chapter 4 (Algorithm 4.2), we propose similar modifications to realize different QoS in MIMO-OFDM using multilevel modulation. As with Algorithm 5.2, the subcarriers of all eigenbeams are combined and sorted together in a descending order (based on their eigenvalues) assuming intuitive sorting. However, we also consider the robust scheme which provides an embedded multiplexing-diversity trade-off, i.e., by automatically reducing the number of eigenbeams according to the MIMO channel gains, that enhances the performance in case of non-perfect channel conditions.

Algorithm 5.5 UEP multilevel MIMO bit-loading using the Campello-like algorithm

Input: similar to Algorithm 5.2

Initialize: set $j = 0$, the accumulated rate to $T_j^{\text{temp}} = \sum_{l=0}^{j} T_l$, allocate $NR \times N_g$ zeros to the bit-loading matrix $\mathbf{B}(v, j)$ and to the power loading matrix $\mathbf{P}(v, j)$, NR zeros to the vector $\Delta\mathbf{P}(\mathbf{v})$, $\mathbf{Z}_b = \{0, 2, 4, 5, .., b_{\max}^j\}$, and the bit index counter $c_v = 1$, $v = 0..NR - 1$.

Output: the average $\mathcal{P}^j$, the bit allocation matrix $\mathbf{B}$, and the power loading matrix $\mathbf{P}$.

1: decompose $\mathbf{H}_k^* \mathbf{H}_k$ similar to Algorithm 5.2; sort the NR eigenchannels in a descending order according to $\mathcal{G}_v$ (store the mapping between $\{s, k\} \multimap v$).

2: compute $\mathbb{G}_\mu = \lfloor \log_2(\lambda_v/\sigma_n^2) \rfloor$, $\mu = 0..\rho - 1$, where ρ is the number of groups with similar bit load (as in Algorithm 4.2), i.e., map $v \multimap \mu$.

3: **repeat**

4: compute $i_{B_{\text{opt}}}^j$ using (3.63), then compute $\mathbf{B}(v, j)$ as in (6.21), where

$$\mathbf{B}(v \multimap \mu, j) = \left[\mathbb{G}_\mu + i_{B_{\text{opt}}}^j \right]_0^{b_{\max}}$$

5: read the index of $\mathbf{Z}_b$ equivalent to $\mathbf{B}(v, j)$, i.e., $c_v = \text{index}\left(\mathbf{Z}_b = \mathbf{B}(v, j)\right)$

6: compute the increment power vector (as in Algorithm 5.4)

$$\Delta\mathbf{P}(v) = \frac{\frac{2}{3}\left[\text{erfc}^{-1}\left(\frac{\mathcal{P}^0}{2}\right)\right]^2}{\Delta\gamma_j \mathcal{G}_v} \left(2^{\mathbf{Z}_b(c_v+1)} - 2^{\mathbf{Z}_b(c_v)}\right)$$

7: **while** $\sum_{v=0}^{RN-1} \mathbf{B}(k, j) = T_j^{\text{temp}}$ **do**

8: update $\mathbf{B}(v, j) = \mathbf{Z}_b(c_v + 1)$, where v is the index of the smallest incremental power $\Delta\mathbf{P}(v)$

9: **end while**

10: **if** $j \geq 1$ **then**

11: subtract the bit-loading of the $j - 1$ class(es) (T_{j-1}^{temp}) from the current bit-loading $\mathbf{B}(v, j)$, thereby, the bit-loading for each class is $\mathbf{B}(v, j) = \mathbf{B}(v, j) - \sum_{l=0}^{j-1} \mathbf{B}(v, l)$

12: **end if**

13: $\mathbf{P}(v)$ is calculated similar to (3.65), i.e., $\mathbf{P}(v) = \frac{\frac{2}{3}\left[\text{erfc}^{-1}\left(\frac{\mathcal{P}^0}{2}\right)\right]^2}{\mathcal{G}_k \Delta_{\gamma_j}} \left(2^{\mathbf{B}(v,j)} - 1\right)$

14: $j \Leftarrow j + 1$

15: **until** $j = N_g$

16: the energy is accumulated such that the resulting energy is given by

$$P_v = \sum_{j=0}^{Ng-1} \mathbf{P}(v)$$

17: rescale the allocated power such that $P_v = P_v(\sum_{v=0}^{NR-1} P_v)/P_T = P_v \gamma_{\max}$

18: invert the mapping in Line 1 such that $\{s, k\} \multimap v$.

5.5 UEP MIMO-OFDM –Results and Analysis–

In our simulation, we model a 4×4 MIMO-OFDM transmission system with $N = 512$ subcarriers for each eigenbeam. Thus, the total average power for each eigenchannels equals $P_T/4$, where P_T is the maximum permissible power emission from the transmitter. All the MIMO channels are assumed to undergo a Rayleigh fading channel with 9 equally spaced delayed paths and the same parameters used in Chapter 2 and 3. Here, we assume a MIMO channel with 3 different correlation models:

- the perfectly scattered channel where $\mathbf{R}_T = \mathbf{I}$ which means that the channels between the scatterers around the transmitter and its antennas are perfectly uncorrelated,
- the limited-scattering environment [71] with $\text{diag}(\mathbf{D}_T) = [7.0, 4.3, 2.7, 1.9]$, and
- the highly correlated (indoor-to-outdoor) with $\text{diag}\,(\mathbf{D}_T) = \text{diag}(15.81, 2.81 \times 10^{-1}, 1.7 \times 10^{-2}, 6 \times 10^{-4})$ as in [64].

Our results are generated assuming an application that requires three different protection classes, i.e., $N_g = 3$. Each class requires a different individual sum rate T_j and an arbitrary noise margin step size $\Delta\gamma$ between these classes. T_j and $\Delta\gamma$ needs to be selected according to application requirements. Throughout this thesis, $\Delta\gamma$ is assumed to be fixed at 3 dB. Thus, the margin of the other classes are computed according to $\gamma_j = \gamma_0 + j\Delta_j$, where γ_0 stands for the highest priority class, i.e., $j = 0$. The maximum allowed number of bits per subcarrier is $B_{\max} = 8$ (with homogeneous modulation). However, the maximum number of bits for hierarchical modulation is 12 bits, with a maximum of 6 bits for each modulation layer j, i.e., $b^j_{\max}$.

We propose two scenarios with different target rates for each individual class, The first scenario allocates $T_j = 1024$ bits/class which means in total 3072 bits for the 3 classes. This is equivalent to 6 bits/subcarrier in an equivalent SISO case with 512 subcarriers. The second scenario assumes twice the number of bits/class, i.e., $T_j = 2048$. This results in an equivalent SISO channel with 12 bits/subcarrier, which is more than the maximum allowed number of bits/subcarrier, i.e., $b_{\max}$. We compare the first scenario with the equivalent SISO case using Algorithm 3.5. In these two scenarios, we consider both sorting schemes, the intuitive and the robust.

To verify our simulations, we present the analytical solution for perfect and partial (erroneous) CSI. In this case, our MIMO-OFDM setup is implemented similar to the simulation model. However, the SER is computed by substituting the calculated bit loads $b^j_{s,k}$ and the power values $p^j_{s,k}$ in the exact SER formula derived in Appendix F.

Moreover, we compare the adaptive MIMO-OFDM using quantized/delayed feedback [7, 11] to the channel covariance feedback results [12] using linear MMSE or linear ZF equalization. For comparison, we consider the non-linear VBLAST successive interference cancellation for both quantized and covariance feedback. Finally, we show the results of adaptive hierarchical modulation using algorithms 5.4 and 5.5.

[9]The transmitter $\mathbf{R}_T$ has antenna separations of 10λ, angle of arrival (AoA) 20^o, and angular spread of 5^o

5.5.1 Adaptive MIMO-OFDM with Limited CSI – Algorithm 5.2

For generating our results, we assume an instantaneous channel with an error matrix $\mathbf{\Xi}_k$. The variance of this error matrix is $\sigma_{\Xi}^2\mathbf{I}$, where σ_{Ξ}^2 takes the values $\{0, 0.1, 0.25\}$, i.e., $\sigma_{\Xi}^2 = 0$ indicates the perfect CSI case. In this case, the erroneous channel matrix $\hat{\mathbf{H}}_k$ is deviating from $\mathbf{H}$ by the error matrix $\mathbf{\Xi}_k = \mathbf{H}_k - \hat{\mathbf{H}}_k$, where $\mathbf{\Xi} \in \mathbb{C}\mathcal{N}(0, \sigma_{\Xi}^2\mathbf{I})$ as defined in Section 5.2, Scheme A. However, the distinct MIMO eigenvalues of $\hat{\mathbf{H}}$ can still offer the chance for realizing UEP.

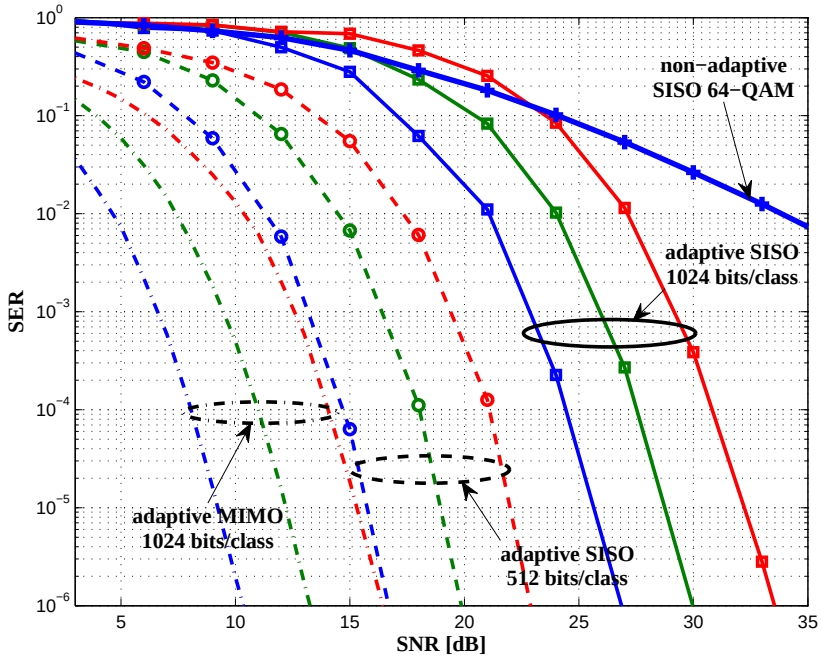

Figure 5.5: MIMO channel with perfect CSI and 1024 bit/subcarrier versus the equivalent SISO case

Figure 5.5 depicts the SER for a linear ZF MIMO transmission with 1024 bits/class assuming a perfect CSI ($\sigma_{\Xi}^2 = 0$). The equivalent SISO case with 512 bits/class and 1024 bits/class are depicted as well. In the case of MIMO-OFDM, the bits and power values are allocated using Algorithm 5.2. However, in the case of SISO, we select the equivalent adaptive technique from Chapter 3, i.e., Algorithm 3.5. Additionally, the non-adaptive homogeneous modulation with 6 bits/symbol (64-QAM), i.e., for the same OFDM parameters, is shown in the same figure.

Figure 5.6 depicts the UEP bit and power loading across the MIMO concatenated eigenchannels using Algorithm 5.2 and assuming perfect CSI with intuitive sorting. In this figure, λ_s , $s = 1..4$ represents the four eigenchannels of this channel. The power is allocated as in Line 21 in Algorithm 5.2. It is clear from this figure that the first and the second priority classes consume (almost) the first and the second highest eigenbeams, respectively, using the entire number of subcarriers, i.e., 512. Notice that the power level varies between subcarriers according to the number of bits and the eigenchannel gains. This make the saw-tooth shape more visible at the lower eigenchannels due to the strong bit-loading fluctuations.

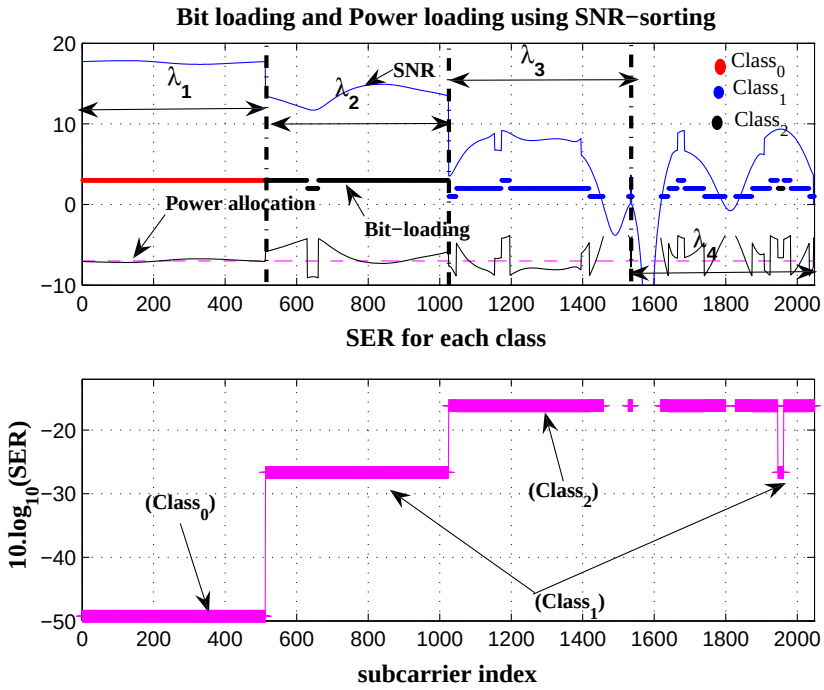

Figure 5.6: UEP bit-loading with intuitive sorting and 512 subcarriers 4×4 MIMO-OFDM

5.5.1.1 Analytical SER for UEP adaptive modulation – perfect CSI

Here we present the analytical SER results assuming UEP bit-loading based on Algorithm 5.2 with perfect CSI. It is known from Chapter 3 that the SER formula for the AWGN channel for M-ary quadrature amplitude modulation (QAM) is given by (as in Appendix F)

$$\mathcal{P}_M(\hat{b}_k) = 2\left(1 - \frac{1}{\sqrt{2^{\hat{b}_k}}}\right) \operatorname{erfc}\left(\sqrt{\frac{3}{2}\frac{E_s/N_o}{\left(2^{\hat{b}_k}-1\right)}}\right) , \tag{5.23}$$

where $E_s/N_o = 1/\sigma_n^2$ allocating equal power (unity), i.e., $E_s = 1$. Formula (5.23) is sufficient for only square and cross constellations with high-modulation order. However, a more exact SER formula is given in Appendix F.

Assuming perfect CSI, i.e., perfect diagonalization and perfect equalization, for frequency-nonselective[10] situations, the channel gains result in multiplicative distortions to the transmitted symbols. In case of ZF equalization, the noise is scaled by this multiplicative gain[11], which we denote here as α_s^2. Thus, for slowly fading channels, this multiplicative distortion may be regarded as a constant gain for any symbol k at least for one signaling interval [15]. Hence, the instantaneous SNR at the ZF equalizer output is given by

$$\rho_s^{\mathrm{ZF}} = \alpha_s^2 E_s/N_0 = \alpha_k^2 P_s/\sigma_n^2 \equiv P_s \mathcal{G}_k \ , \tag{5.24}$$

where P_s is the power on each eigenchannel s and α_s^2 is the channel coefficient squared which has a chi-square distribution with two dimensions of freedom. To obtain the exact SER, we have to

[10] OFDM always guarantees flat-fading on every subcarrier, see Chapter 2.

[11] If the channel entries h_k are assumed to be ZMCSCG, then $\alpha_s^2 \equiv |h_s|^2$ follow a Chi-square distribution with two degrees of freedom.

average $\mathcal{P}_M(\hat{b}_k, \rho_r)$ for every bit load $\hat{b}_k$ by computing the following integration over the exact SNR ranges of $\hat{b}_k$, e.g., $0 \rightarrow \rho_{\hat{b}_1}, \rho_{\hat{b}_1} \rightarrow \rho_{\hat{b}_1}, ..., \rho_{b_{\max}} \rightarrow \infty$, similar to [105]. Accordingly,

$$\begin{aligned} \mathcal{P}_{\rho_r}^{\mathrm{ZF}} &= \frac{\hat{b}_1}{\bar{b}} \cdot \int_0^{\rho_{\hat{b}_1}} \mathcal{P}_M(\hat{b}_1, \rho_s^{\mathrm{ZF}}) p(\rho_s^{\mathrm{ZF}}) d(\rho_s^{\mathrm{ZF}}) + \frac{\hat{b}_2}{\bar{b}} \cdot \int_{\rho_{\hat{b}_1}}^{\rho_{\hat{b}_2}} \mathcal{P}_M(\hat{b}_2, \rho_s^{\mathrm{ZF}}) p(\rho_s^{\mathrm{ZF}}) d(\rho_s^{\mathrm{ZF}}) + ... \\ &+ \frac{\hat{b}_{\max}}{\bar{b}} \cdot \int_{\rho_{b_{\max}}}^{\infty} \mathcal{P}_M(\hat{b}_{\max}, \rho_s^{\mathrm{ZF}}) p(\rho_s^{\mathrm{ZF}}) d(\rho_s^{\mathrm{ZF}}) \,, \end{aligned} \tag{5.25}$$

where $\bar{b}$ is the average number of bits/subcarrier, $p(\rho_s^{\mathrm{ZF}})$ is the probability density function (PDF) of $P_s\alpha_k^2/\sigma_n^2$ which has also a Chi-square distribution assuming a fixed noise levels. The authors of [105] also assumed P_k to be constant for different bit values in order to compute (5.25) similar to [15, Chapter 14]. However, this is not effective in the case of UEP bit-loading as the power allocation varies significantly between classes and between different subcarriers. Another complication in (5.25) is that its integral limits have to be created for every number of bits and for every class j, i.e., results in $b_{\max} \times N_g$ integral ranges.

For this reason, we consider the instantaneous SER by compute (5.23) using the instantaneous values of $b_{s,k}^j$ and $p_{s,k}^j$ for every class j, spatial index s, and subcarrier k, which are all computed using Algorithm 5.2. These values are directly inserted into (5.24) and (5.23) in order to find the instantaneous SER. Thus, we accept all the SNR value used for every bit load, i.e., instead of computing the integral range separately. Using Mont-Carlo computer, the SERs values are average for every bit load. This is also repeated for every class j, assuming that all classes allocate the same number of subcarriers.

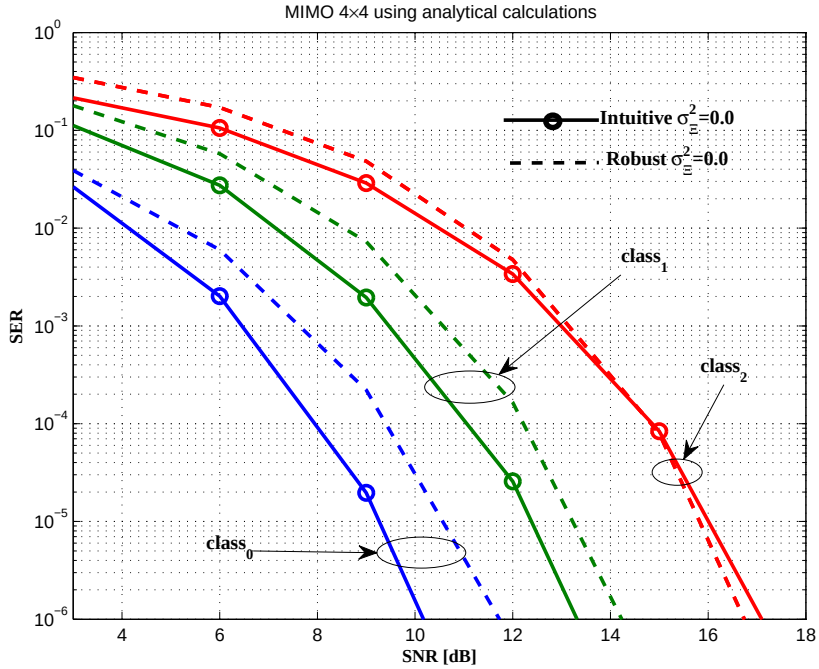

Figure 5.7: MIMO channel with perfect CSI and 1024 bit/subcarrier using intuitive and robust sorting.

Figure 5.7 depicts the SER performance assuming $\sigma_{\Xi}^2 = 0.25$ for different sorting schemes using our analytical scheme only. We also found from this figure that robust sorting almost realizes a

2-D eigen-beamforming. This is the reason for the 2 dB performance degradation between the robust and the intuitive. The comparison between our simulation model[12] and the analytical one[13], using Algorithm 5.2, is shown in Fig. 5.8. Both results are comparable, except for the lowest priority class where we believe that this is inaccurate due to the brute-force process, which is only implemented in this class.

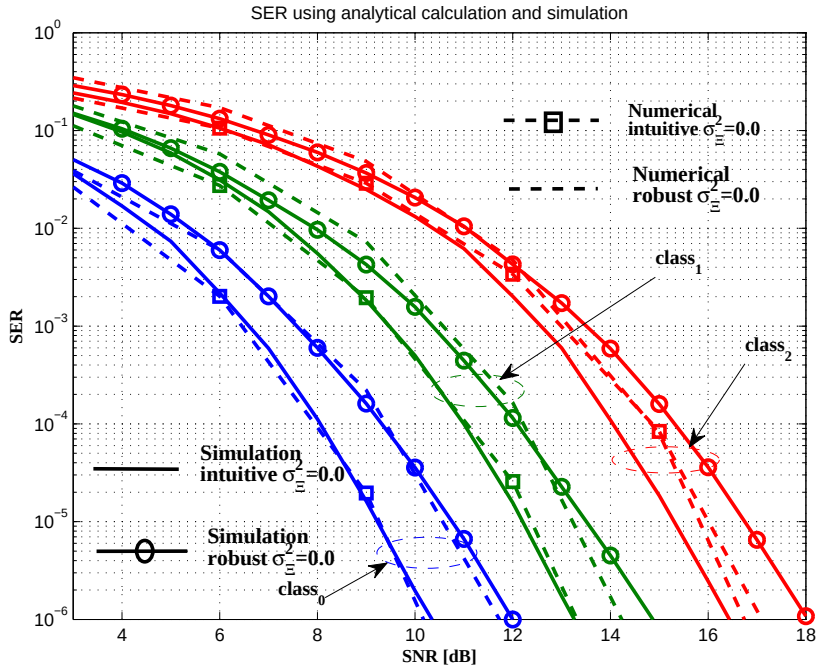

Figure 5.8: MIMO with perfect CSI and 1024 bit/subcarrier using numerical results versus simulations.

5.5.1.2 Analytical SER for UEP adaptive modulation – partial CSI

In this section, we consider an imperfect CSI that results from channel quantization, delays, or feedback channel imperfection. As in the previous sections, this error is assumed to be Gaussian with a zero mean and a variance of σ^2_{Ξ}. According to Appendix F and similar to [70], the SER is proved to be a function of the SINR by proving that $\frac{1}{2}\text{erfc}^2$ (SINR) is convex (decreasing) in all the SINR range, where it is sufficient to show that its first and second derivative are negative and positive, respectively. The proof of is given in Appendix F. Hereto, the relation between the MMSE value and the equivalent SINR, known from [106, 107], is given by[14]

$$\text{SINR} \quad = \quad \frac{1}{\text{MMSE}} - 1 \, . \tag{5.26}$$

Knowing the MMSE for every eigenchannel s to be (as in Appendix F)

[12] using 1024 bits and 512 subcarriers with a 4×4 MIMO-OFDM which transmit QAM symbols

[13] using the same simulation parameters and performing SER averaging using Mont-Carlo simulations of (5.25)

[14] This relation is obvious for ZF equalizers as the SINR= $\frac{1}{\mathbf{H}^*\mathbf{H}}$. However, for MMSE receivers, it is derived from (5.21) in Appendix F.

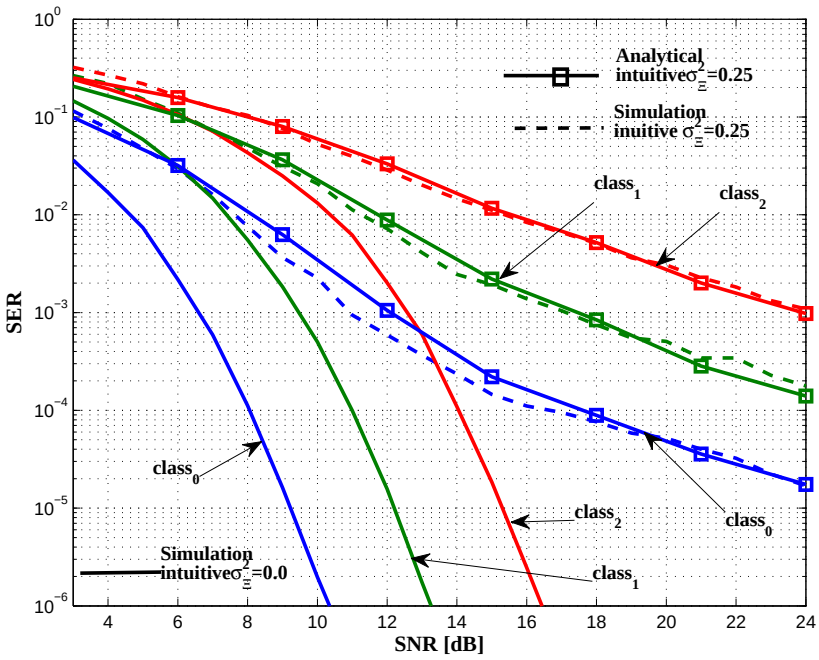

Figure 5.9: MIMO numerical SER versus simulations for intuitive sorting.

$$\mathrm{MMSE}_s = \left[\mathbf{I}_{N_T} + \frac{1}{\sigma_n^2}(\mathbf{H}\hat{\mathbf{V}}\mathbf{P}^{1/2})^* \left(\mathbf{I}_{N_R} + \sigma_{\mathbf{\Xi}}^2 \mathbf{I}_{N_R}\right)^{-1} \mathbf{H}\hat{\mathbf{V}}\mathbf{P}^{1/2}\right]_{s,s}^{-1}, \tag{5.27}$$

the equalizer $\mathrm{SINR}_{s,k}$ for the outdated channel at the transmitter is given by

$$\begin{aligned} \rho_{s,k} &= \frac{1}{\mathrm{MMSE}_{s,k}} - 1 \\ &= \frac{1}{\left[\mathbf{I}_{N_T} + \frac{1}{\sigma_n^2}(\mathbf{H}\hat{\mathbf{V}}\mathbf{P}^{1/2})^* \left(\mathbf{I}_{N_R} + \sigma_{\mathbf{\Xi}}^2 \mathbf{I}_{N_R}\right)^{-1} \mathbf{H}\hat{\mathbf{V}}\mathbf{P}^{1/2}\right]_{s,s}^{-1}} - 1 \,. \end{aligned} \tag{5.28}$$

Thus, $\rho_{s,k}$ can be used as in the perfect CSI (using (5.23)) after computing $b_{s,k}^j$ and $p_{s,k}^j$ using Algorithm 5.2. The complete proof of (5.28) is given in Appendix F – Section F.4.

The SER curves for partial CSI with $\sigma_{\mathbf{\Xi}}^2 = 0.25$ for intuitive and robust sorting are given in Fig. 5.9 and Fig. 5.10, respectively. Also a comparison to the simulated results is given in these figures in order to verify our partial CSI simulation model.

5.5.2 Spatial Equalizers and Imperfect CSI

As described in Section 5.3.1, a ZF equalizer is capable of diagonalizing the channel at the receiver in case of perfect CSI. However, for the partial CSI case, the diagonalization is not perfectly maintained. This results in residual IEI and noise enhancement. Therefore, we propose the alternative linear MMSE equalizer. The equalization matrices $\mathbf{W}_k$ for MMSE and ZF are given by (5.21) and (5.17), respectively. Here, we compare the MMSE and ZF equalizers under different CSI errors $\sigma_{\mathbf{\Xi}}$ and different sorting schemes.

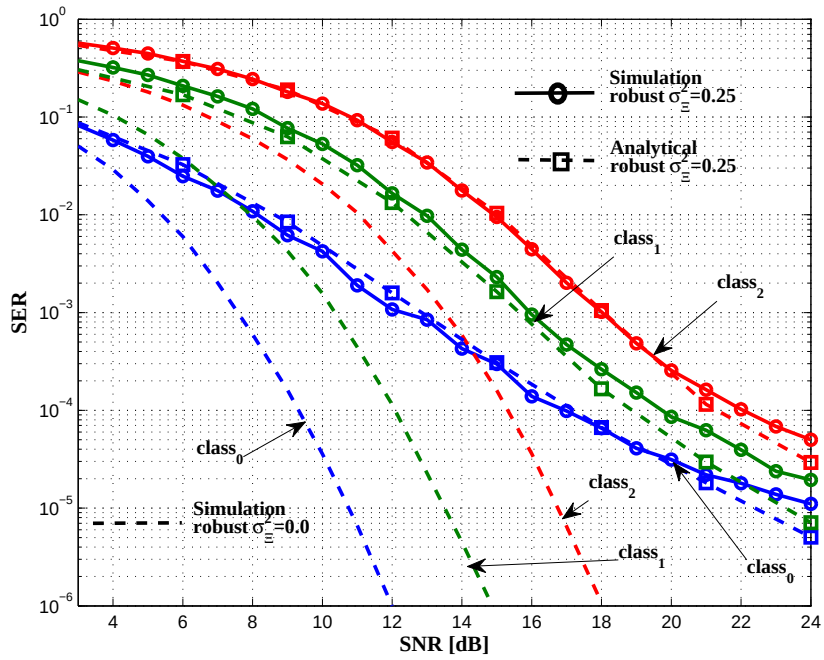

Figure 5.10: MIMO numerical SER versus simulations for robust sorting.

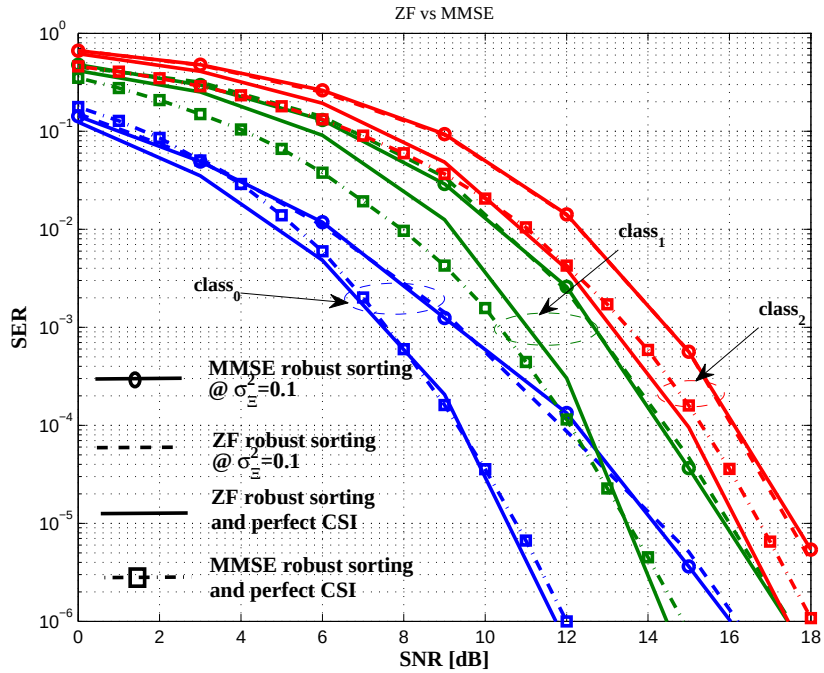

Figure 5.11: 4-D MIMO robust sorting for ZF versus MMSE receivers @ $\sigma_{\Xi} = 0.10$.

5.5.2.1 Full eigen-beamforming

Figure 5.11 shows the performance of UEP bit-loading Algorithm 5.2 under a small amount of CSI errors, i.e., $\sigma_{\Xi}^2 = 0.1$, using ZF with a robust sorting, where the important data is allocated to the weaker eigenchannels. Therefore, the performance of the important data deteriorates

more than the least priority data which comes only behind the perfect CSI by just 0.8 dB.

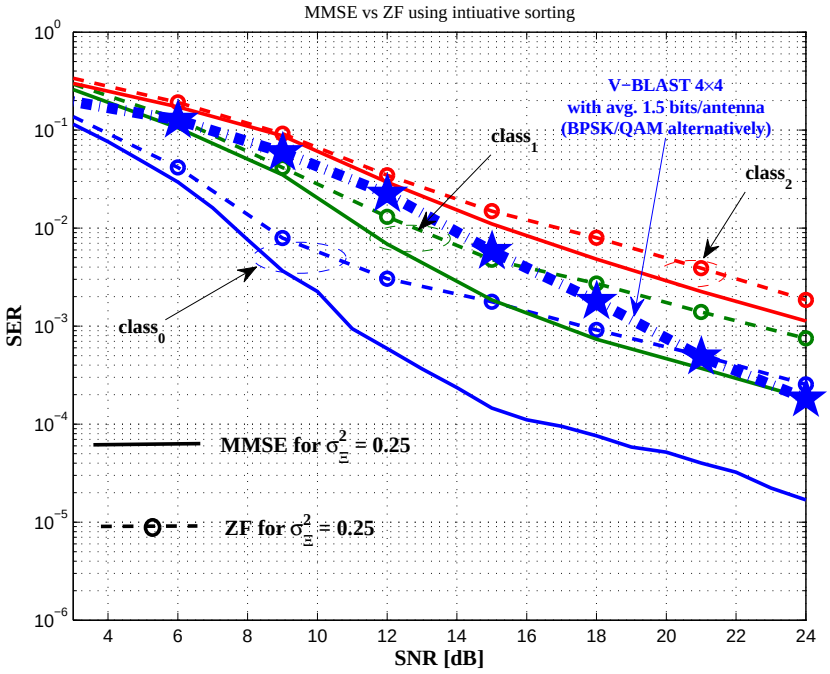

Figure 5.12: 4-D MIMO intuitive sorting for ZF versus MMSE receivers @ $\sigma_{\Xi} = 0.25$.

It is clear from Fig. 5.12 that the MMSE (presented in Section 5.3.2) outperforms the ZF assuming full eigen-beamforming 4-D. Furthermore, a comparison to the tradition V-BLAST (with MMSE nulling as in Section 5.3.3) shows that the performance of adaptive modulation (even under CSI uncertainties with $\sigma^2_{\Xi} = 0.25$) outperforms the non-adaptive V-BLAST case assuming the same number of bits. See the difference between the middle class using MMSE (which is similar to a non-UEP adaptive modulation) and the VBLAST performance (thick-line with pentagon star); the middle class outperforms the V-BLAST.

Figure 5.13 compares the ZF performance against the MMSE assuming 4-D beamforming using robust sorting. It is clear from this figure (compared to Fig. 5.12) that the robust sorting outperforms the intuitive sorting. The reason behind this performance enhancement is that the robust sorting defines an implicit multiplexing-diversity trade-off. Since the weaker eigen-Channels are already suppressed, it is noticeable that there is a similarity between the results of MMSE and ZF. Also in this figure, we depict the performance of the V-BLAST using non-adaptive modulation. In this case, we assume the same OFDM parameters (as used in the adaptive schemes) with 1.5 bits/subcarrier, which is achieved by alternating BPSK and 4-QAM on the given subcarriers. Here, the V-BLAST performance is worse than all the linear equalizer cases with partial CSI.

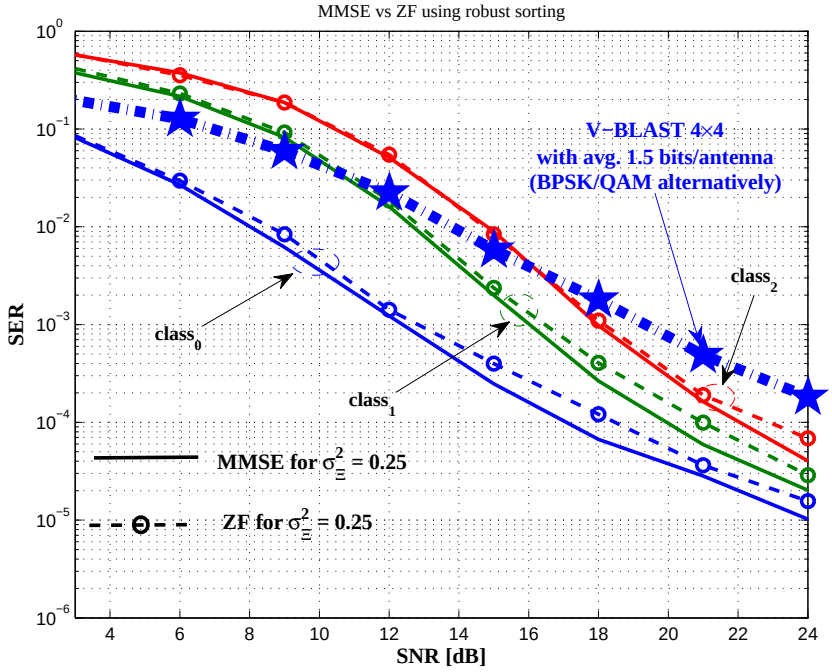

Figure 5.13: 4-D MIMO robust sorting for ZF versus MMSE receivers @ $\sigma_{\Xi} = 0.25$.

5.5.2.2 Reduced eigen-beamforming

We consider the same amount of CSI errors and the same number of bits with a reduced eigen-beamforming using 2-D only, i.e., suppress the weaker eigenchannels such that the MIMO channel is resized to an equivalent 2×4, however, still utilizing the strong eigen-channels.

If we compare Fig 5.11 to the 2-D beamforming in Fig. 5.14, we can see a considerable improvement due to suppressing the weakest eigenchannels. It is clear that the performances of the ZF and the MMSE are equivalent. The non-adaptive V-BLAST comes behind all our scenarios.

In Fig. 5.15, the 2-D beamforming reduces the gap between the perfect CSI and the partial case to almost 3 dB (for robust sorting). The intuitive sorting is performing slightly worse (∼0.9 dB) than the intuitive scheme in this case. Nevertheless, the SER curves show no error-floor at high SNRs and full compliance with the proposed UEP profile.

5.5.2.3 Highly correlated channels

The performance of the highly correlated channels in Fig. 5.16 is not reliable for realizing an efficient MIMO-OFDM adaptation using this target sum rate, i.e., 3072 bits. However, the mandatory information, i.e., highest priority class, and the order of the classes are kept safe. The correlated channels are going to be very interesting if we realize a single eigen-beamforming (1-D). Frankly speaking, using water-filling for power pre-allocation (as discussed in Chapter 2) will dynamically allocate zeroes to the weaker eigenchannels, which automatically realizes a 1-D eigen-beamformer. It is clear from the figure, that the highest priority class of robust sorting

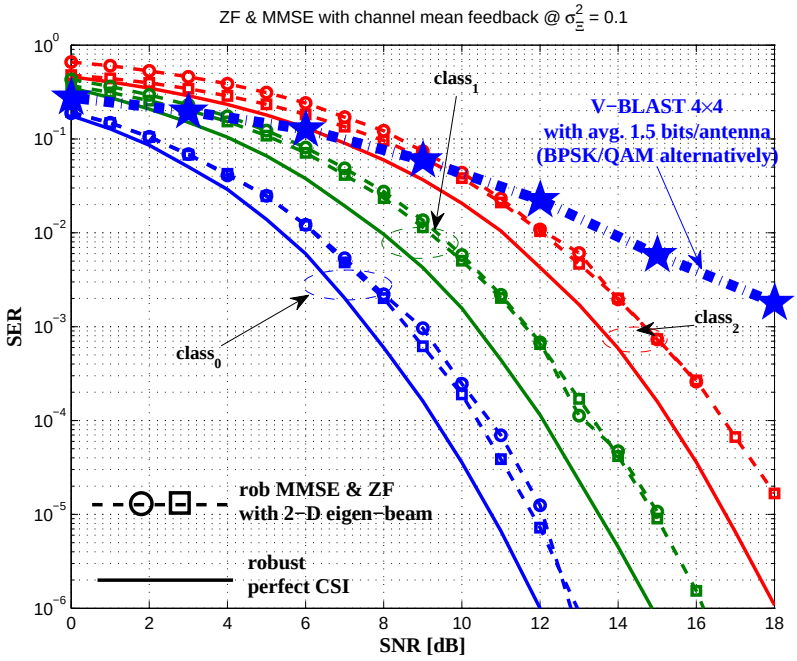

Figure 5.14: 2-D MIMO channel with different ZF and MMSE @ $\sigma_{\Xi} = 0.10$

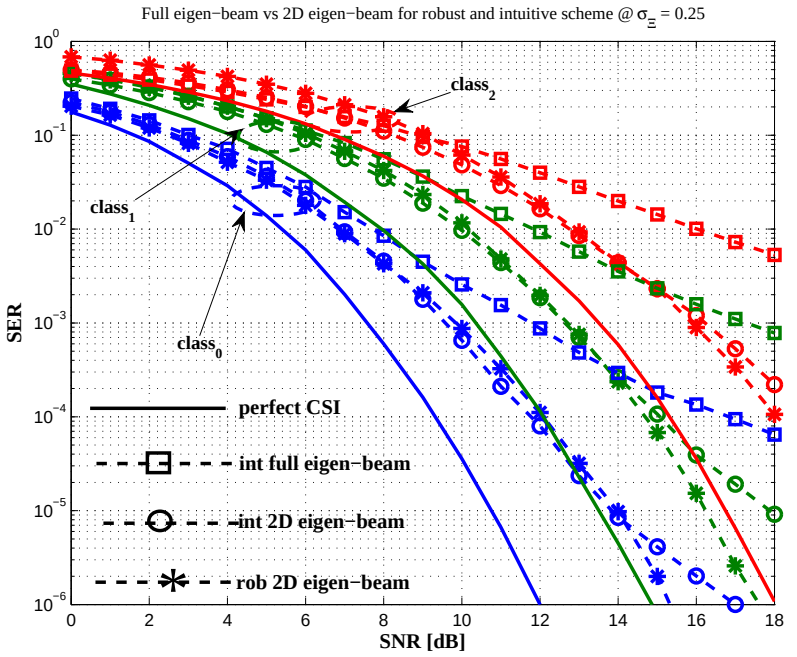

Figure 5.15: 2-D MIMO channel with different ZF and MMSE @ $\sigma_{\Xi} = 0.25$

(with partial CSI) is only 1 dB worse than the perfect CSI. However, it sacrifices the lower protected classes, which could be compensated by reducing the target sum rate. The intuitive scheme preserves the performance of the other classes with a noticeable error floor at the highest priority class.

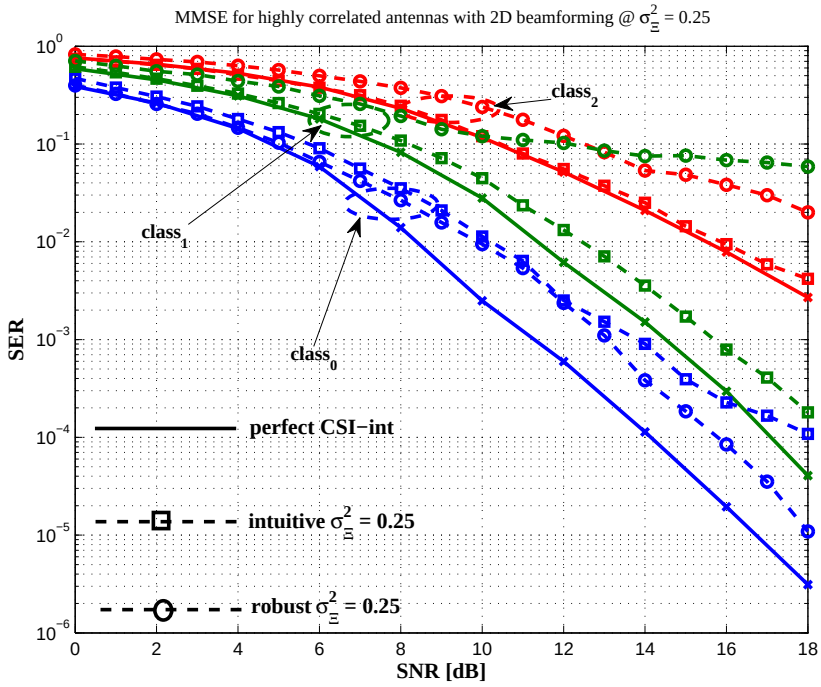

Figure 5.16: MIMO channel with different ZF and MMSE @ $\sigma_\Xi = 0.25$

5.5.3 UEP Bit-loading with Channel Correlation Feedback

We assume that the channel correlation matrix $\mathbf{R}_T$ is estimated at the receiver using a sufficient number of subcarriers. Here we consider the same channel correlation models described early in Section 5.5. The total number of bits for each class T_j is chosen to be 1024 bits, i.e., the total target sum rate = 3072 bits. As a reference, a non-adaptive 1×4 SIMO transmission with 64-QAM and V-BLAST with 1.5 bits/antenna are simulated.

Low correlated channel models:

Figure 5.17 depicts the results for UEP bit-loading Algorithm 5.3 using a 4-D eigen-beamforming. Unlike the perfect CSI, the proposed margin separation (3 dB) is not strictly fulfilled; it is rather 3.9 dB in this case. The channel mean feedback leads to a better performance. However, the margin steps are getting wider. In each case, the performance degradation is due to the wide range of channel uncertainties at the weaker eigenchannels. Nevertheless, the order of the classes is kept the same. We can also show that the robust bit-loading outperforms the intuitive bit-loading by more than 8 dB at symbol error rates (SER) of 10^{-5} (for the highest priority class). This is again due to suppressing the weak eigenchannels and utilizing the good eigenchannels. Accordingly, there is an interesting observation from Fig. 5.18 where a 2-D beamforming method shows exactly the same performance as the 4-D robust method. This means that the robust scheme reduces the MIMO system, automatically, to the effective spatial dimensions.

It is also clear from the figures 5.17 and 5.18 that the adaptive schemes outperform the equivalent non-adaptive scheme, i.e., 1×4 SIMO with 64QAM, at low-to-moderate SNRs. However, we can

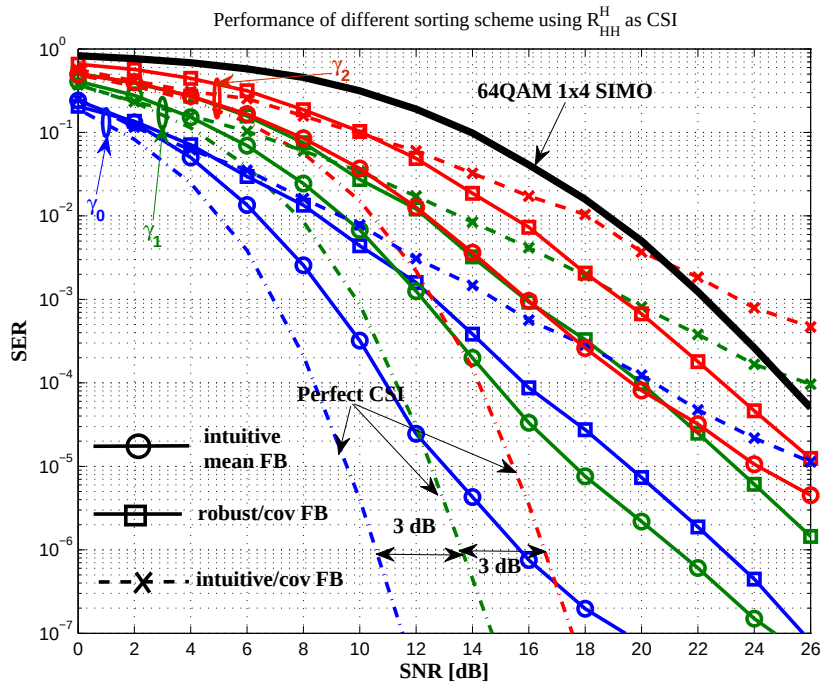

Figure 5.17: Different sorting schemes for UEP vs EEP and non-adaptive scheme

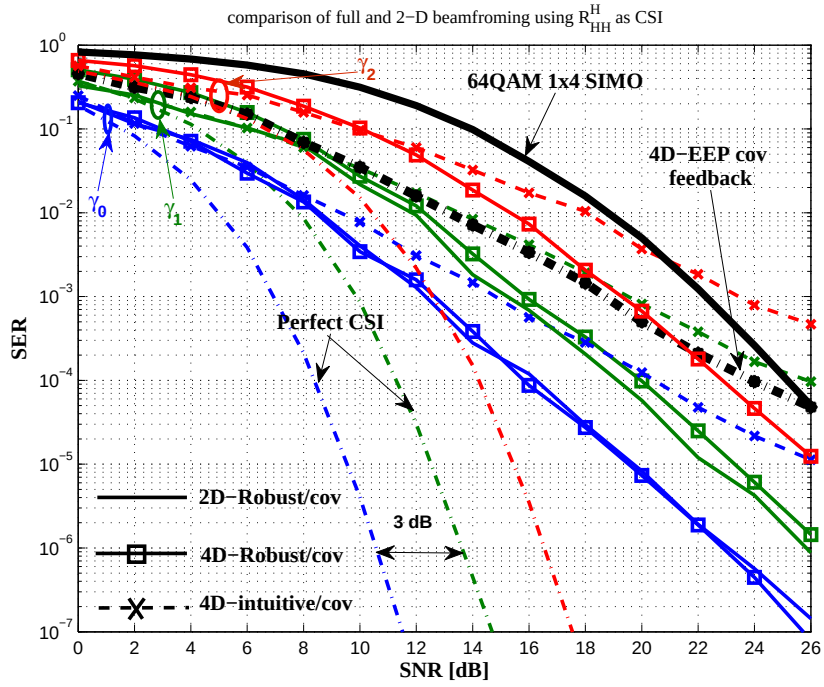

Figure 5.18: Full vs 2-D beamforming with adaptive EEP comparison

see a considerable performance enhancement at SNR $>$ 20 dB (due to absence of interferences). Moreover, an equal error-protection (EEP) scheme, shown in Fig. 5.18 with exactly the same parameters, shows an average performance when compared to the 4-D intuitive method.

Highly correlated channel:

Figure 5.19 depicts the performance of two different channel correlation models, the weakly and the strongly correlated. The correlated channel shows a slight performance gain compared to the less correlated channel at high SNR. This is due to power concentration towards a single eigenchannel using the proposed eigen-beamforming matrix $\mathbf{U}_T$. This is not the case for a weakly correlated channel, where the power is still utilizing weaker eigenchannels. Moreover, the highest priority class (for the single eigen-beamforming of the highly correlated channel model) achieves a gain of 10 dB compared to either non-adaptive SIMO with 64-QAM or non adaptive V-BLAST (at an SER of 10^{-4}). This gain is convenient to envisage the utilization of our UEP adaptation for correlated channels. Furthermore, the robust scheme using the correlation CSI better preserves the performance of every class and keeps the separations near to the designed value, i.e., 3 dB, as in the perfect CSI.

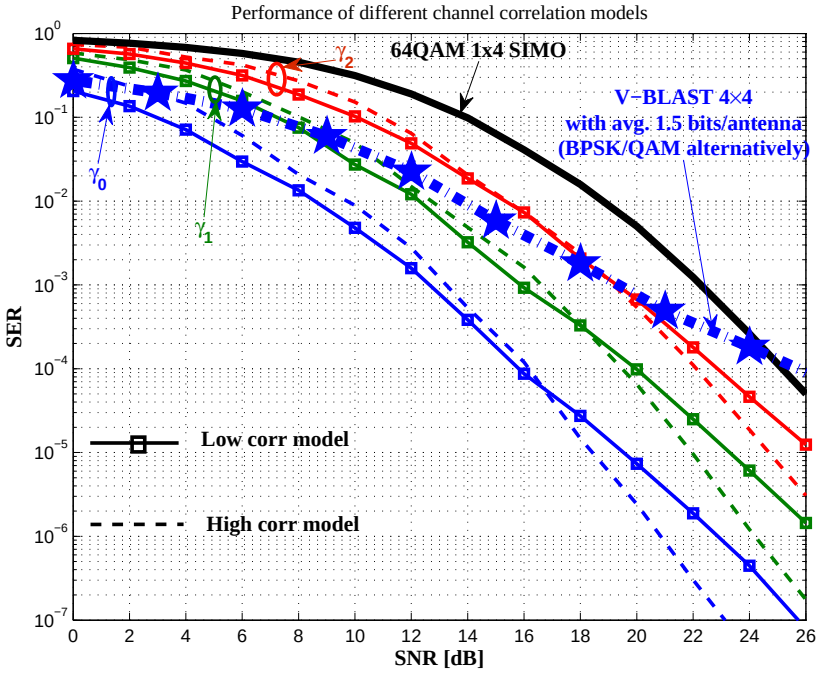

Figure 5.19: Different channel correlation models with robust loading

5.5.4 Compensating Channel Uncertainties Using Non-linear Equalizers

In Fig. 5.20, we depict the performance of a linear MMSE equalizer versus the performance of an adaptive V-BLAST proposed in Section 5.3.3. For intuitive sorting with 4-D eigen-beamforming, our proposed adaptive V-BLAST outperforms the MMSE with almost 12 dB at an SER of 10^{-5}. Additionally, the V-BLAST is only 5 dB worse than the perfect CSI using 4-D eigen-beamforming, comparing the results of Fig. 5.20 with Fig. 5.5 at an SER of 10^{-6}. Since the V-BLAST already sorts the symbols according to their channel gains, the algorithm starts with the least priority data in case of robust sorting, which has the highest SER. Therefore, error propagates to the highest priority data resulting in the error floor seen at high-SNR.

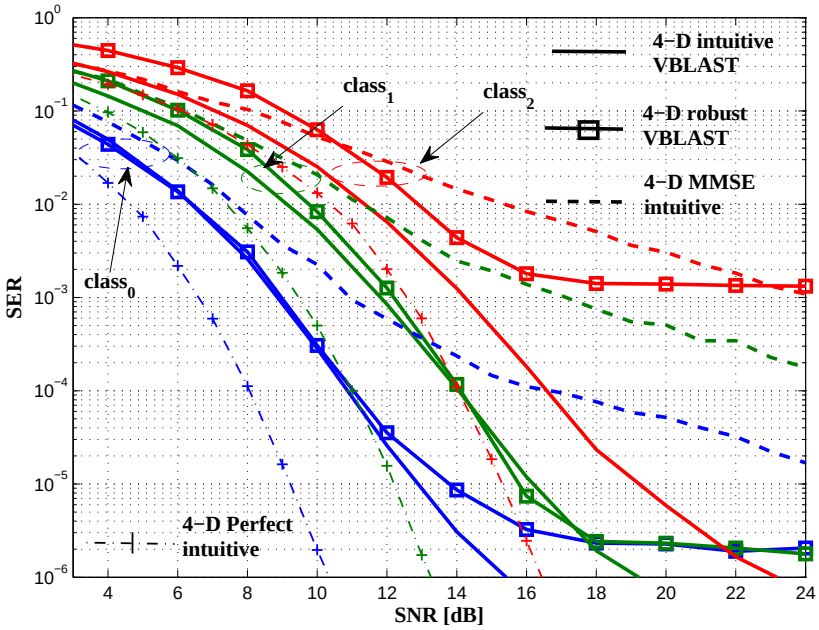

Figure 5.20: 4-D VBLAST vs MMSE with intuitive sorting for $\sigma^2_{\underline{\underline{\Xi}}} = 0.25$

Figure 5.21 depicts the reduced eigen-beamforming case using linear MMSE and VBLAST with MMSE nulling receiver to adapt 1024 bits/class. As expected, our adaptive V-BLAST using intuitive sorting also outperforms the equivalent linear MMSE spatial equalizer and performs very close to perfect CSI conditions with only a loss of 1.8 dB. The reason for this significant improvement is that we started with the most protected symbol, i.e., fewer errors to propagate. In Fig. 5.22, using channel covariance feedback adaptive MIMO-OFDM, i.e., implementing Algorithm 5.3, we show that the adaptive V-BLAST with intuitive sorting performs better than the equivalent intuitive sorting using a linear MMSE equalizer (see Fig. 5.18). The order of the classes is kept safe due to utilizing the channel correlation matrix eigenvalues and eigenvectors. However, the MMSE case with a robust sorting is performing slightly better than the V-BLAST case. As a final conclusion here, the adaptive V-BLAST results in a performance gain (slightly more than 7.4 dB) compared to the non-adaptive V-BLAST, even with channel correlation feedback.

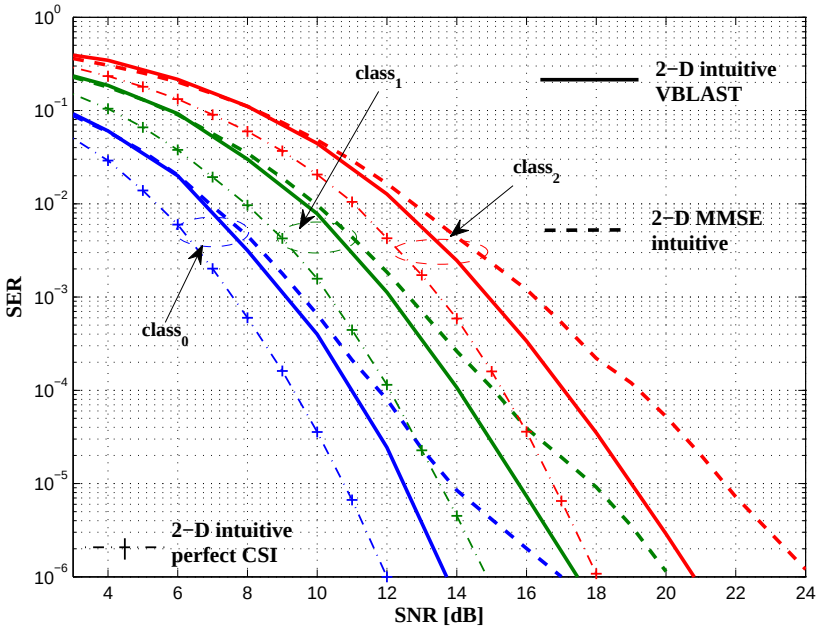

Figure 5.21: 2-D VBLAST vs MMSE with intuitive sorting for $\sigma^2_{\underline{\underline{\Xi}}} = 0.25$

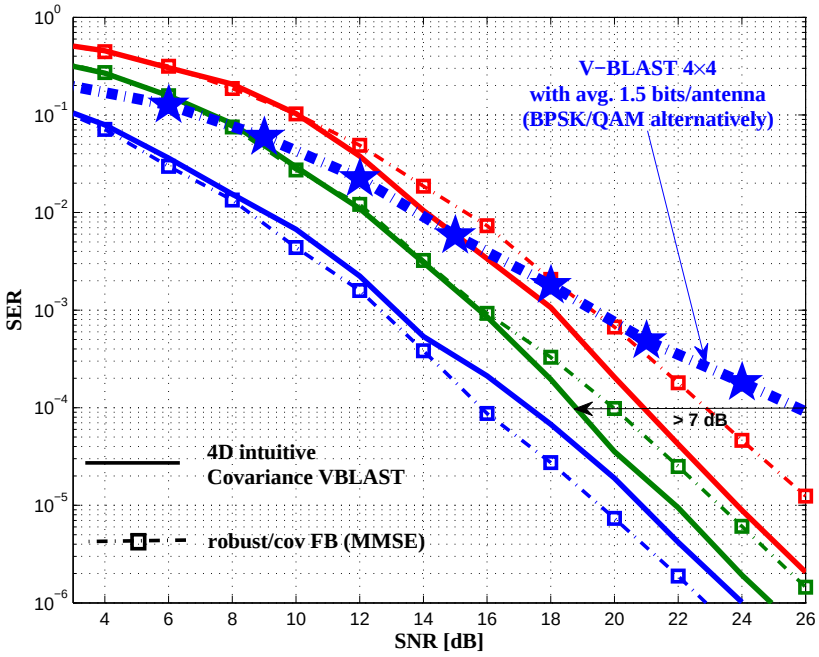

Figure 5.22: Covariance feedback VBLAST vs MMSE with intuitive sorting

5.5.5 Campello- and Huges-Hartogs-like Adaptive Multilevel Modulation

Here, we present the performance of the UEP multilevel (hierarchical and non-hierarchical) adaptive modulation using the Huges-Hartogs-like bit-loading (Algorithm 5.4) and the Campello-like (Algorithm 5.5) using MIMO-OFDM transmission. Assuming a total individual sum rate for each class of $T_j = 1024$ and CSI with an error variance $\sigma^2_{\Xi} = 0.25$, on can notice from Fig. 5.23 that the performance of the 2-D eigen-beamforming using the Campello-like UEP bit-loading (with multilevel modulation) is worse than the equivalent Chow-like UEP (non-hierarchical) bit-loading (Algorithm 5.2) using an intuitive sorting, a 2-D beamforming and the same CSI error variance. From the same figure, we notice that the Campello-like UEP bit-loading (Algorithm 5.5) with 2-D outperforms the 4-D eigen-beamforming by only 2 dB (assuming the same CSI uncertainties).

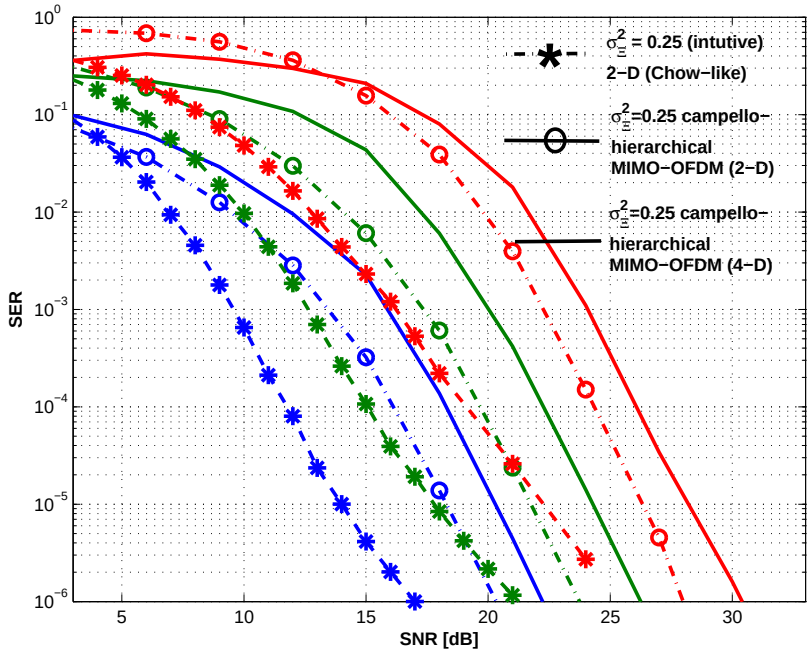

Figure 5.23: MIMO intuitive sorting @ $\sigma_{\Xi} = 0.25$ and 2048 bits/class.

In Fig. 5.24, we depicts the 4-D eigen-beamforming using Campello-like multilevel adaptive modulation compared to the Chow-like (non-hierarchical) MIMO-OFDM using only $T_j = 1024$. From these results, it is clear that the non-hierarchical modulation outperforms the hierarchical (multilevel) modulation by almost 6 dB (for perfect CSI), i.e., similar to the results in Chapter 4, Fig. 4.5. This is due to the inefficient power allocation of the hierarchical modulations.

However, in Fig. 5.25, using 2-D eigen-beamforming and imperfect CSI, Algorithm 5.5 is worse than the perfect CSI (using $T_j = 1024$) by only 3 dB.

Figure 5.26 depicts the SER of the Huges-Hartogs-like UEP bit-loading (Algorithm 5.4). As can be seen in this figure, the two-dimensional beamforming (the third case with CSI errors) outperforms the full eigen-beamforming. Certainly, this is also due to suppressing the weaker

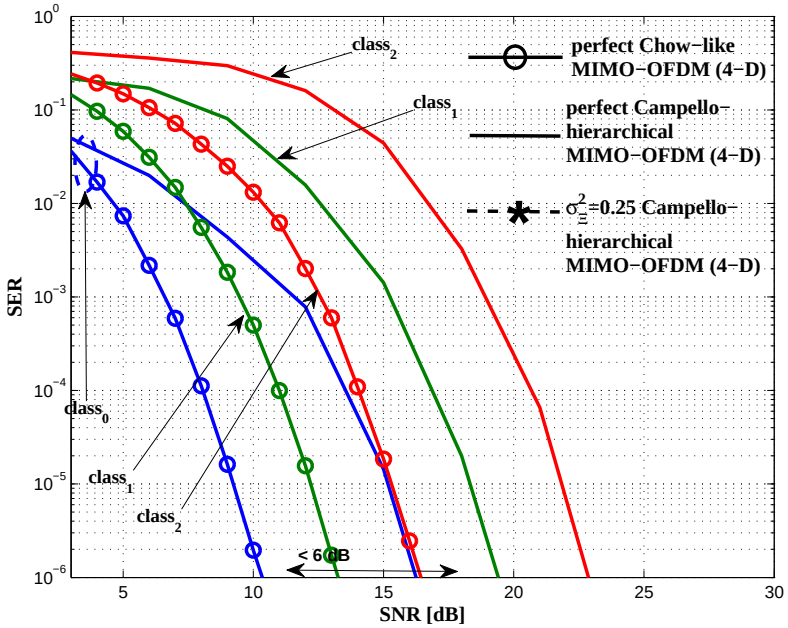

Figure 5.24: 4-D MIMO Campello hierarchical modulation @ $\sigma_{\Xi} = 0.25$ using 1024 bits/class.

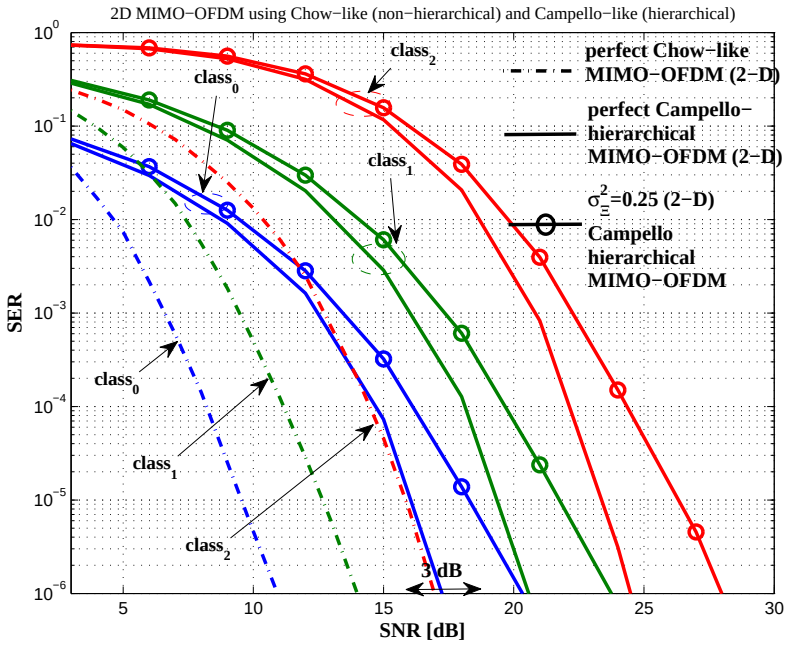

Figure 5.25: 2-D MIMO Campello hierarchical modulation @ $\sigma_{\Xi} = 0.25$ using 1024 bits/class.

eigenbeams, which are more susceptible to the inter-eigen interference caused by the CSI errors[15]. Furthermore, this indicates that the 4×4 MIMO channel is, practically, not more than 2×4. From the same figure, one can see that the margin separation is strictly fulfilled in case of perfect CSI and the reduced eigen-beamforming with partial CSI. However, the gap is getting wider in case of full eigen-beamforming with CSI errors. The power allocation of the proposed

[15]Weaker eigenchannels are also introducing interference on the stronger ones.

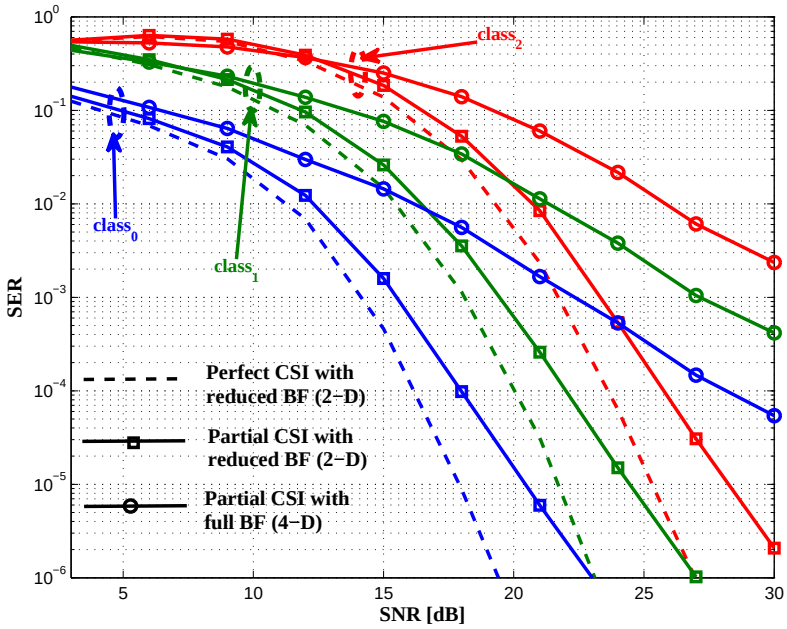

Figure 5.26: UEP Adaptive hierarchical modulation with CSI errors with a variance = 0.25.

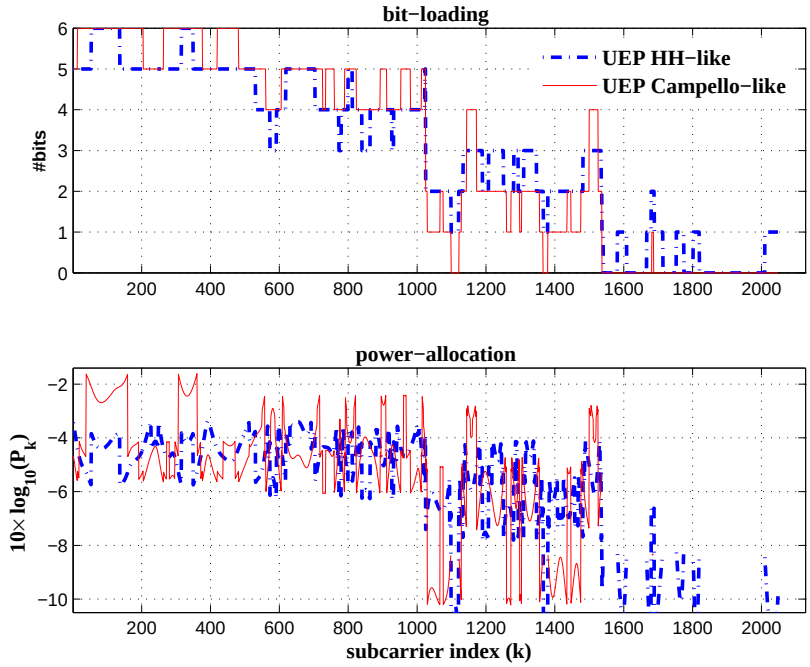

Figure 5.27: The accumulated bit-loading and power allocation of the 3 hierarchical layers using the Campello-like and the Hughes-Hartogs(HH)-like UEP bit-loading.

algorithms is investigated in Fig. 5.27. From this figure, it is clear that the floor operation used in the Campello algorithm forces the weaker eigenvalues to be evacuated; leaving their power to the stronger ones. This results in a performance gain of almost 6 dB over the Hughes-Hartogs UEP bit-loading in case of full eigen-beamforming (see Fig. 5.28). One may consider Algorithm 5.5 to be more protecting against channel uncertainties. However, both algorithms

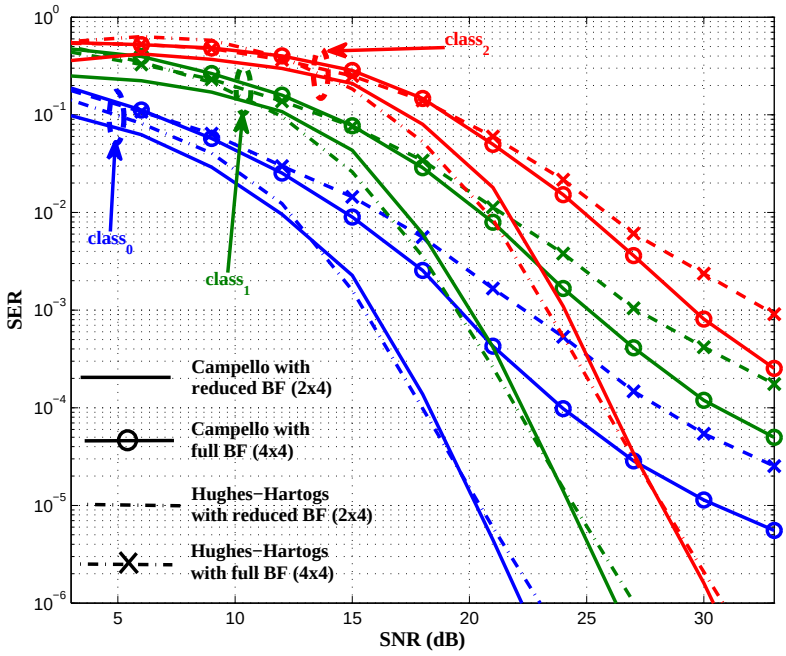

Figure 5.28: A comparison between the UEP Hughes-Hartogs and the UEP Campello bit-loading.

perform very similar in the case of a two-dimensional beamforming; Algorithm 5.5 succeeds in allocating slightly more power to the stronger subcarriers. This explains the small performance gain (< 0.8 dB) in case of 2-D beamforming at high SNR.

5.6 Summary for Adaptive Prioritized MIMO-OFDM

In this chapter, we presented four algorithms which realize UEP transmission using adaptive modulation. In the first two algorithms, we showed that the chosen margin separation between the data classes are achieved, even under partial CSI. Our modified adaptive V-BLAST algorithm succeeds in mitigating the inter-eigen interference by successive cancellation. For quantized/delayed CSI, with relatively low CSI errors, the V-BLAST ordering achieved the same order of the diagonalized channel. This enhances the performance, and reduces the sorting effort. However, for channel correlation feedback, the V-BLAST did not succeed to mitigate interference, as the channel order is not optimized. Thus, our robust sorting outperforms the V-BLAST in case of channel correlation feedback.

Finally, we propose another two algorithms that realize UEP bit-loading without subcarrier partitioning and presorting. This is achieved using multilevel (hierarchical and non-hierarchical) UEP-bit loading by modifying the Hughes-Hartogs-like and the Campello-like algorithms. We showed that Campello-like bit-loading (or rather an optimized water-filling approach bit-loading) outperforms the Hughes-Hartogs-like bit-loading in case of high CSI errors with prioritized transmission, as the first suppresses the weak eigenchannels.

Chapter 6

Prioritized Multiuser Transmission

Multiuser communication aims at sharing the resources amongst a number of users. Usually, these users require different levels of protection according to their applications and/or their classes of service. Strictly speaking, these users can be ranked according to their distinct channel conditions in order to realize different QoSs. The multiple access techniques introduced in Chapter 2, namely frequency division multiple access (FDMA) and spatial division multiple access (SDMA), are investigated here in order to realize multiuser transmission that manipulate prioritized transmissions. In the following, we discuss these multiplexing techniques and the steps required for constructing adaptive prioritized transmission.

I- Orthogonal frequency division multiple access (OFDMA)
OFDMA is selected due to its fine frequency granularity that exploits the multiuser diversity, thereby, enhancing the spectral efficiency. Moreover, it could simply realize different QoS requirements by adapting the transmission parameters to the different CSI of each user according to his required performance level. We referred to this in the previous chapters, i.e., in single-user communication, as UEP link adaptation or bit-loading. In that case, different performances are devoted to different parts of the transmitted data requiring different SER, by exploiting the different channel conditions across the subcarriers. This can similarly be transferred to multiuser OFDMA, assuming that each user requires different SER and his data are allocating to a portion of the available subcarriers. Additionally, applying multiple antenna arrays at each transceiver extends the adaptation freedom to the spatial domain as well. This could be simply realized by considering proper pre- and post-processing matrices as in Chapter 5. Since perfect CSI at the BS is a practically unrealistic assumption, we consider partial CSI that deviates from the instantaneous channel. This can roughly satisfy a given QoS profile exploiting multiuser diversity due to the channel randomness [108]. This increases the chance of exploiting the stronger subcarriers, thereby, making it more susceptible to harmful CSI errors.

Furthermore, we introduce a novel adaptation scheme that preserves the given performance margins between users, i.e., the QoS constraints. We extend Algorithm 5.2 in order to adapt the transmission for a number of prioritized users using the simple subcarrier sorting and partitioning method (proposed in Chapter 3). The MIMO channel matrices (for each user's subcarriers) are

decomposed into equivalent multiple parallel single links (eigenbeams) as in Chapter 5. Since OFDMA is assumed, any subcarrier (including all its eigenchannels) must be fully dedicated to a single user. To realize different QoS classes amongst the given users, the subcarriers of each user have to be sorted according to the total eigenchannels using one of the following proposed criteria: maximizing the channel capacity (full beamforming) or avoiding the inter-eigen interference (IEI) using a single beamformer.

Additionally, using the non-iterative subcarrier partitioning proposed in Algorithm 3.9, we succeed in devoting data with different priorities to multiple users who already require different average SER. This has been verified using the modified greedy methods, where we implemented a two-user transmission model with two prioritized data classes using Campello-like UEP bit-loading. This makes the overall performance equivalent to a single user with 4 prioritized classes [3].

II- Space division multiple access (SDMA)

As discussed in Chapter 2, SDMA exploits the available spatial channel dimensions in case of multiple antenna transmission. Thereby, in a multiuser environment, potentially high spectral efficiencies can be achieved. However, due to sharing the frequency and time resources, MUI becomes a crucial limiting factor that determines the system performance. Therefore, the pre- and post-filters have to be jointly optimized in order to limit the MUI. Several research works already consider this problem, [29, 31, 77].

We first consider the block-diagonalization (BD) scheme (discussed in Chapter 2), which avoids the MUI interference completely by allowing each user to transmit multiple data streams on the other users' null-spaces [28, 29]. This results in non-interfering (orthogonal or parallel) users. In this particular case, the total number of transmit antennas at the BS must be greater than or (at least) equal to the sum of all receive antennas at the users' MSs, i.e., providing sufficient null-space vectors [29]. As with single-user MIMO case, the CSI uncertainty can be a serious threat to keeping the users orthogonal (block-diagonalized). Nevertheless, we can keep the performance acceptable for the most important users by exploiting their stronger eigenchannels or automatically switching them to another multiple access scheme, e.g., FDMA. Here, the prioritized QoS constraints are fulfilled by modifying the sub-optimal multilevel bit-loading of Algorithm 5.5 in order to devote different constellation sizes to each user. Assuming a broadcast scenario, the SER steps between users are chosen to fulfill the arbitrary margin separations proposed in Chapter 4. Thus, the highest priority user is allowed first to consume the stronger subcarriers with a relatively low modulation order and a suitable symbol energy that fulfills his SER requirements. The next users are allowed to embed their data in the already used subcarriers (in a hierarchical fashion) or consume the unused ones based on the required SER and the given channel knowledge. This means that all users sharing the same subcarriers are receiving, physically, the same information symbol, i.e., multicast transmission[1], with different hierarchical code book. For BC with CSI uncertainties, one can simply implement an MMSE receiver at each user as with the single user case (as in Chapter 5). For comparison, the broadcast

[1] it is the delivery of a message to a group of destination receivers simultaneously in a single transmission [98]

scheme proposed in [109], which transmit the same information to every user, has been modified to accommodate hierarchical-multiuser modulation satisfying an MMSE criterion.

The second approach introduced here aims at minimizing the MUI under a fixed power constraint using a non-orthogonal SDMA [31]-[81]. In order to achieve a successful multiple access scheme, the MSE for all users has to be minimized simultaneously. This method reliefs the strict constraint on the number of antennas introduced by the BD method. For a downlink scenario, we implemented a beamforming scheme that exploits the duality between the uplink and the downlink to overcome the non-degraded feature of the MIMO BC [78]. The transmitter and the receiver filters are computed using the MSE duality [77] introduced in Chapter 2. Furthermore, different QoSs, among different users, are realized by jointly optimizing the linear transmit-receive filters to minimize the weighted sum MSE, i.e., using different weighting factors to realize users with different MSE. After realizing multiuser transmission with an MMSE, we opt for implementing a prioritized bit-loading to realize three different priority classes. The bit-loading is performed according to the achievable minimum sum MSE values for all user's subcarriers instead of their individual SNR [1].

The remainder of this chapter is organized as follows. Section 6.1 discusses the multiuser MIMO-OFDMA with simple subcarrier partitioning which was published in [4]. Section 6.2 discusses the prioritized SISO OFDMA using the non-iterative partitioning [3]. Section 6.3 presents the multiuser MIMO system using block diagonalization with prioritized user transmission, which realizes adaptive multilevel modulation [9]. Finally, Section 6.4 discusses an adaptive multiuser system with prioritized transmission using a non-orthogonal multiple access scheme [1].

6.1 Multiuser MIMO Multicarrier with Simple Partitioning

We extended Algorithm 5.2 to adapt the transmission for a number of prioritized users using the same subcarrier sorting and partitioning scheme proposed in Chapter 3. FDD is assumed with a separate CSI feedback channel, which leads to CSI errors. The pre- and post-processing matrices for each MIMO channel (for each user's subcarriers) are found using SVD or EVD in order to produce multiple parallel single links (eigenbeams). Imperfect CSI is a serious threat to preserving the orthogonality of the decomposed MIMO eigenchannels. However, the multiuser diversity increases the chance of exploiting the stronger subcarriers, only [4].

In this case, we assume OFDMA, where each subcarrier (including all its eigenchannels) is fully dedicated to a single user. Therefore, the subcarriers of each user have to be sorted in order to achieve either maximum channel capacity (using n-D beamformers) or IEI avoidance (using a single beamformer). Furthermore, we propose to maximize the capacity by sorting the subcarriers according to the product of their eigenvalues, i.e., $\prod_{s=0}^{R-1} \lambda_s$, similar to [4]. In the following, we describe the proposed MIMO-OFDMA channel model in Section 6.1.1, the implemented system model in Section 6.1.2, the optimum sorting mechanism is Section 6.1.3, and the proposed UEP bit-loading in Section 6.1.4. Finally, results are discussed in Section 6.1.5.

6.1.1 MIMO-OFDMA Channel Model

Herein, we consider a downlink transmission scenario, where the BS is equipped with N_T transmit antennas and N_u MSs, each with N_R receive antennas. This forms the MIMO channel matrices $\mathbf{H}_{k,u} \in \mathbb{C}^{N_R \times N_T}$, where u is the user index and k is the subcarrier index of the OFDMA frame assuming N subcarriers in total. We further assume a partial CSI with a quantized/outdated channel $\hat{\mathbf{H}}_{k,u}$, which deviates from the instantaneous channel $\mathbf{H}_{k,u}$ by the error $\mathbf{\Xi}_{k,u}$. As in Chapter 5, this error is defined as $\mathbf{\Xi}_{k,u} = \mathbf{H}_{k,u} - \hat{\mathbf{H}}_{k,u}$, where $\mathbf{\Xi} \in \mathbb{C}\mathcal{N}(0, \sigma^2_{\mathbf{\Xi}}\mathbf{I})$ [44]. Channel matrix entries are also modeled as independent Rayleigh fading blocks composed of 9 different paths (echoes) with an exponential power-delay profile. Moreover, one can assume the elements of $\mathbf{H}_k$ (in frequency domain) to be i.i.d. with ZMCSCG distribution, i.e., $\mathbf{H}_k \in \mathbb{C}\mathcal{N}(0, \sigma^2_{\tilde{\mathbf{H}}}\mathbf{I})$ [44]. This randomness ensures a better exploitation for the multiuser diversity [108].

6.1.2 System Model with Limited CSI Regime

Figure 6.1 depicts a multiuser-multiantenna system with different QoS levels receiving a combined OFDMA broadcast frame from a single BS through a MIMO downlink channel. The users' MSs are assumed to be randomly located around the BS, however, the impact of the large scale fading (path-loss and shadowing effect) is implicitly considered in the SNR calculated at the receiver front end. Further details like relative MSs distances and users synchronization issues are assumed to be ideally treated and out of the scope of this thesis.

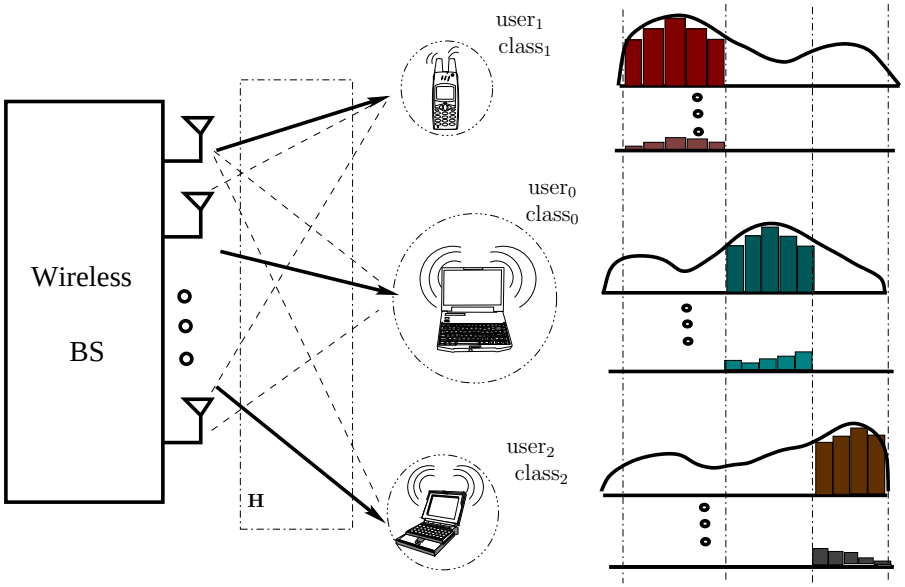

Figure 6.1: MIMO-OFDMA with different QoS, where user_0 has the highest QoS. Each user receives a downlink transmission from the BS and transmits a feedback signaling on the uplink

In OFDMA transmission, each user is entitled to transmit over a non-overlapping set of his stronger subcarriers. This ensures that the maximum SNRs are always utilized to guarantee maximum multiuser diversity exploitation[2]. Finally, for each subcarrier k, each user u transmits

[2]To avoid interference (due to delay spread), an appropriate cyclic-extension/guard-interval is assumed to be

back his quantized/delayed CSI $\hat{\mathbf{H}}_{k,u}$. In order to simplify our notations in the rest of this section, we omit the subscript $\{k, u\}$.

We decompose the MIMO channel into a number of parallel (non-interfering) single channels using EVD to decompose the Hermitian matrices $\hat{\mathbf{H}}^*\hat{\mathbf{H}}$ as follows

$$\hat{\mathbf{H}}^*\hat{\mathbf{H}} = \hat{\mathbf{V}}\hat{\mathbf{D}}\hat{\mathbf{V}}^*, \tag{6.1}$$

where $\hat{\mathbf{D}} = \text{diag}\{\lambda_1, \cdots, \lambda_R\}$; $R \leq \min\{N_R, N_T\}$, λ_s are the eigenvalues, $\hat{\mathbf{V}}$ is a matrix of R eigenvectors, and $s \in [1, R]$ is the spatial index. Bits and powers are allocated according to the eigenvalues λ_s. Hence, the total power is directed in the space according to the pre-processing (steering) matrix $\hat{\mathbf{F}} = \hat{\mathbf{V}}\mathbf{P}^{1/2}$, where $\hat{\mathbf{V}}$ is the eigenvectors matrix of $\hat{\mathbf{H}}^*\hat{\mathbf{H}}$ and $\mathbf{P}$ is the power loading matrix, i.e., a diagonal matrix with the allocated power values.

As in Chapter 5, a spatial equalizer is implemented to mitigate the possible IEI, however, with residual noise superposition. In here, we propose to use an MMSE equalizer where the received signal after equalization is given by

$$\begin{aligned} \mathbf{z} = \mathbf{W}\mathbf{y} &= \overbrace{(\hat{\mathbf{F}}^*\mathbf{H}^*\mathbf{H}\hat{\mathbf{F}}\mathbf{P}^{1/2} + \sigma_n^2\mathbf{I})^{-1}\hat{\mathbf{F}}^*\mathbf{H}^*}^{\mathbf{W}} \Big[\mathbf{H}\hat{\mathbf{F}}\mathbf{x} + \tilde{\mathbf{n}}\Big] \\ &= (\mathbf{\Psi}^*\mathbf{\Psi} + \sigma_n^2\mathbf{I})^{-1}\mathbf{\Psi}^*\mathbf{\Psi}\mathbf{x} + (\mathbf{\Psi}^*\mathbf{\Psi} + \sigma_n^2\mathbf{I})^{-1}\mathbf{\Psi}^*\tilde{\mathbf{n}}\,, \end{aligned} \tag{6.2}$$

where $\hat{\mathbf{F}}$ is the pre-processing matrix of the partial CSI, $\mathbf{H}$ is the instantaneous channel matrix, and $\tilde{\mathbf{n}}$ is the noise at the equalizer output. $\mathbf{\Psi} = \mathbf{H}\hat{\mathbf{V}}\mathbf{P}^{1/2}$ is the aggregated channel at the receiver input and $\mathbf{P}^{1/2}$ is the power loading and spectral shaping matrix.

6.1.3 UEP Adaptation Using Simple Subcarrier Partitioning

In OFDMA, any subcarrier, including all its eigenchannels, must be allocated to a single user. Therefore, the users' subcarriers have to be sorted properly in order to satisfy the QoS. In the following, we propose two different sorting schemes: one based on sum rate maximization and the other uses a single eigen-beamforming transmission.

6.1.3.1 Multiuser sorting achieving sum rate maximization

An optimal sorting may be easily derived from the capacity equation in [67] for Gaussian channels applying water-filling. User u achieves his channel capacity for the given N subcarriers, if the following sum rate (given by (2.45) and (2.49) in Chapter 2) is maximized:

$$\begin{aligned} \max\ C_u &= \max\ \frac{1}{N_u}\sum_{k=1}^{N_u}\sum_{s=1}^{S}\log_2(1 + \frac{p_{s,k}^u\lambda_{s,k}^u}{\sigma_n^2}) \\ &= \max\ \frac{1}{N_u}\sum_{k=1}^{N_u}\sum_{s=1}^{S}\left(\log_2(\frac{\mu_u}{\sigma_n^2}\lambda_{s,k}^u)\right)^+\,, \end{aligned} \tag{6.3}$$

added to each OFDMA frame to mitigate both inter-frame interference and inter-user interference [110].

where $(x)^+ \geq 0$, μ_u is the user μ_u water-level constant. This constant is computed to fulfill the total power constraint P_T, i.e., using (2.45), such that

$$\sum_{u=0}^{N_u-1}\sum_{s=0}^{R-1}\sum_{u=0}^{N_u-1} p_{s,k}^u \equiv \sum_{u=0}^{N_u-1}\sum_{s=0}^{R-1}\sum_{u=0}^{N_u-1} (\mu_u - \sigma_n^2/\lambda_{s,k}^u)^+ = P_T \ . \tag{6.4}$$

Accordingly, the maximum capacity given in (6.3) can be further simplified using the notation $\sum \log_2 x = \log_2 \prod x$, obtaining

$$\max_{\mathcal{M}_u} C_u \ = \ \max_{\mathcal{M}_u} \frac{1}{N_u}\sum_{k=1}^{N_u}\left(\log_2 \prod_{s=1}^{S}(\frac{\mu_u}{\sigma_n^2}\lambda_{s,k}^u)\right)^+ . \tag{6.5}$$

Due to the monotonically increasing behavior of the logarithmic function [56], the right hand side is easily maximized by maximizing the product $\prod \lambda_s$, i.e., maximizing the geometric-mean of λ_s. We refer to this method as *eigen-product sorting*.

6.1.3.2 Multiuser sorting based on 1-D beamforming

When the channel uncertainty increases, the stronger eigenchannels already produce a residual IEI to each other. Another possibility could be to sort the subcarriers according to their highest eigenchannel, only. Thus, the transmission power is completely directed (beamformed) towards the strongest eigenbeam. This method completely suppresses the undesired interferences from/to the weaker eigenvalues. Therefore, the error floor, which can be seen in case of residual interference, will not be there any more.

6.1.4 Multiuser UEP Bit-loading

Our proposed scheme is an extension to the Chow-like UEP bit-loading (Algorithm 5.2) to realize different users' QoSs assuming a margin separation Δ_γ between each two users. Hence, the different users' priorities are calculated (as in Chapter 3) using

$$\gamma_{u+1} = \gamma_u/\Delta_\gamma \quad u = 0..N_u - 1 \ . \tag{6.6}$$

Similar to (3.33) in Chapter 3, the quantized bit-rate $\hat{b}_{s,k}^u \in \mathbb{Z}$ is given by

$$\hat{b}_{s,k}^u = \left\lfloor b_{s,k}^u + \frac{1}{2}\right\rfloor_0^{b_{\max}} = \left\lfloor \log_2\left(1 + \frac{p_{s,k}^u \cdot \lambda_{s,k}^u}{\gamma_u \cdot \sigma_n^2}\right) + \frac{1}{2}\right\rfloor_0^{b_{\max}} \ , \tag{6.7}$$

where $b_{s,k}^u \in \mathbb{R}$, $\hat{b}_{s,k}^u \in \mathbb{Z}$ are the bit values a rounded to the nearest integer between 0 and $b_{\max}$ and $p_{s,k}^u$ is the power allocated to the s^{th} spatial index and the k^{th} subcarrier for user u. Each user should be provided with T_u bits, where the total target bit-rate is given by $B_T = \sum_{u=0}^{N_u-1} T_u$. Accordingly, the quantization error $\Delta b_{s,k}^u$ is given by

$$\Delta b_{s,k}^u = \hat{b}_{s,k}^u - b_{s,k}^u \ . \tag{6.8}$$

As with the original algorithm, the noise margin γ_m is iteratively approximated to satisfy the total required target sum rate B_T assuming $b^m_{s,k} \in \mathbb{R}$, following

$$\gamma_{m_{\text{new}}} = 2^{\frac{\sum_{s=0}^{S-1}\sum_{k=0}^{N-1}\log_2\left(\gamma_{m_{\text{old}}}+\mathcal{G}^m_{s,k}\right)-B_T}{N}} . \tag{6.9}$$

However, it is required to have integer bit values only. Therefore, γ_m has to be adapted iteratively to maintain B_T. Strictly speaking, the users individual data rates T_u have to be fulfilled, where $B_T = \sum_{u=0}^{N_u-1} T_u$. In the following we present modified version of Algorithm 5.2 in order to realize prioritized users.

Algorithm 6.1 QoS bit-loading based on the Chow-like algorithm for MIMO-OFDMA systems

Input: $\lambda^u_{s,k}/\sigma^2_n$ of the k^{th} subcarrier of the s^{th} spatial index for u^{th} user, total number of subcarriers N, total target bit-rate B_T, and bit-rate for every user T_u.

Output: the average $\mathcal{P}_u$ and bit allocation $b^u_{s,k}$.

Initialize: the subcarrier indices $\mathcal{M} \in \mathbb{Z}^{N\times R\times N_u}$, individual users' set $\mathcal{M}_u \in \mathbb{Z}^{2\times N_u}$, the subcarrier (sliding) index v, and the start index $\mathcal{I}$ with all zeros. $\tau_u = N \;\forall\; u = 0..N_u - 1$, target power P_T, target sum rate B_T, counter Cnt $= 0$, and $\gamma_{m_{\text{init}}} = \frac{\overline{\mathcal{G}}}{2^{B_T/NR}}$, where $\overline{\mathcal{G}} = \frac{\sum_{k=1}^{N}\sum_{s=1}^{R}\lambda^m_{s,k}}{NR\sigma^2_n}$ and m is the index of the middle class.

1: decompose the Hermitian channel $\mathbf{H}^{u,*}_k\mathbf{H}^u_k$ for every k and u using EVD to find the eigenvalues matrix $\mathbf{D}_k = \text{diag}\{\lambda_{1,k}, \lambda_{2,k}, ..., \lambda_{s,k}, ..., \lambda_{R,k}\},\ k = 0..N-1$

2: compute $\mathcal{G}^u_{s,k} = \lambda^u_{s,k}/\sigma^2_n$, also for every u, k, and s

3: sort the NR eigenchannels of each user in descending order according to $\prod_{s=0}^{R-1}\lambda^u_{s,k}$, in the u^{th} column of $\mathcal{M}$; map $\{k\} \multimap v$, where the spatial indices are already sorted $s = 0..R-1$

4: **repeat**

5: compute γ_m of the middle user m, i.e., assuming an odd number of users, using (3.36) and (3.37) (in Chapter 3)

6: compute user u individual γ_u using the relation between the noise margins (in dB scale), such that $\gamma_{u_{[dB]}} = \gamma_{m_{[dB]}} + (m-u)\cdot\Delta\gamma_{[dB]}$, where m is the middle user

7: **repeat**

8: calculate $\hat{b}^u_{s,v}, \forall\ s = 0..R-1$ and $v \in \mathcal{M}$, as in (6.7) using γ_u starting from $\mathcal{I}$

9: use the cumsum operator to accumulate $\hat{b}^u_{s,v}$, $v \in \mathcal{M}$ and $s = 0, ..R-1$

10: stop accumulating when T_u is fulfilled.

11: set τ_u to the location where the cumsum stops, i.e., $\sum_{v=\mathcal{I}}^{\tau_u}\left(\sum_{s=0}^{R-1}\hat{b}^u_{s,v}\right) = T_u$

12: update $\mathcal{M}_u(1) = \mathcal{I}$, $\mathcal{M}_u(2) = \tau_j$, $\mathcal{I} \Leftarrow \tau_u + 1$, and $u \Leftarrow u + 1$.

13: **until** $u = N_u$

14: γ_m is recalculated similar to Chapter 5, Algorithm 5.2

15: Cnt $\Leftarrow$ Cnt $+ 1$

16: **until** $\sum_{\{v,s\}\in\mathcal{M}} b^u_{s,v} \approx B_T$ or Cnt = MaxCnt

17: invert the mapping in Line 3, i.e., $\{k\} \multimap v$

18: the power is allocated and rescaled, to the total target power P_T, similar to Algorithm 5.2 from Line 21 to 22.

Power Allocation Scheme

To preserve a fixed SER for every user, the power on each subcarrier must be allocated considering the bit load values, the channel eigenbeams, and the required QoS (γ_u). Similar to (3.33), Chapter 3, the power loading value is given by

$$p_{s,k}^{u} = \gamma_u \frac{\sigma_{\mathrm{n}}^2}{\lambda_{s,k}^{u}} (2^{\hat{b}_{s,k}^{u}} - 1) \; . \tag{6.10}$$

The power mask will not stay perfectly constant, albeit fluctuating with a saw-tooth like shape, i.e, with discontinuities at bit-loading change or at the user boundaries (if the bit load value stays constant between these boundaries).

6.1.5 Analysis of MIMO-OFDMA Using UEP Bit-loading

To evaluate the performance of our UEP adaptive MIMO-OFDMA, we consider three users with 3 different priorities. Between each two users, a margin separation of $\Delta_\gamma = 3$ dB is preserved, i.e., a higher priority user outperforms the next user by 3 dB. The number of users receive antennas N_R and the number of the base station (BS) transmit antenna N_T are assumed to be 2 and 4, respectively[3]., while the BS deploys 4 transmit antennas, i.e., 2×4 MIMO channels. Thus, our OFDMA transmission can utilize two eigenbeams (at most) for $N = 512$ subcarriers.

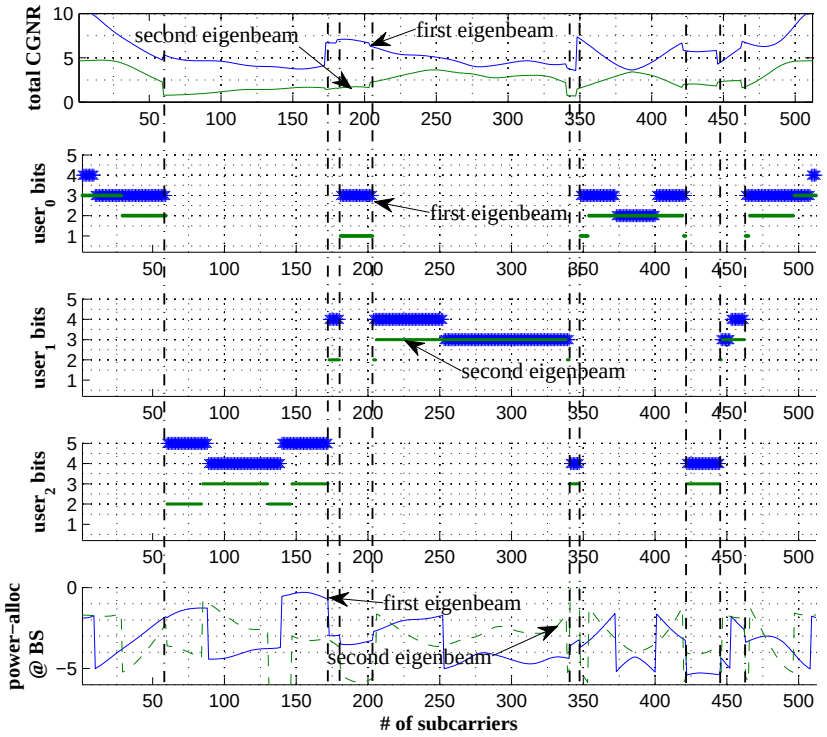

Figure 6.2: CGNR (in linear scale), bit loads, and normalized power allocation with $T_u = 1024$ bits and 512 subcarriers

[3]Two receive antenna is a reasonable assumption for a mobile terminal due to space limitations.

Figure 6.2 depicts the CGNR, the bit-loading, and the normalized power allocation for all users using the eigen-product sorting. As seen in the CGNR sub-figure, the first user already consumes the subcarriers with the strongest eigen-products (subcarrier ranges: 0-60, 178-205, and 465-511). The weakest eigen-products are devoted to the users with the lower QoS (e.g., the third user consumes the left-over subchannels with the weak eigen-products, i.e., 61-174, 345-349, and 425-450). Due to the fact that the bit-loading varies, the power curves are also varying by, almost, multiples of 3 dB.

6.1.6 MIMO-OFDMA Performance with Perfect CSI

We first assume perfect CSI conditions for multiple users with 3 dB margin separation between each two users. In Fig. 6.3, one can notice that the margin separation under perfect CSI is strictly preserved for both beamforming schemes. The optimum sorting, that utilizes the MIMO multiplexing gain, outperforms the 1-D eigen-beamforming by almost 3 dB. This is due to utilizing the full channel rank (double vs. single eigen-beamforming).

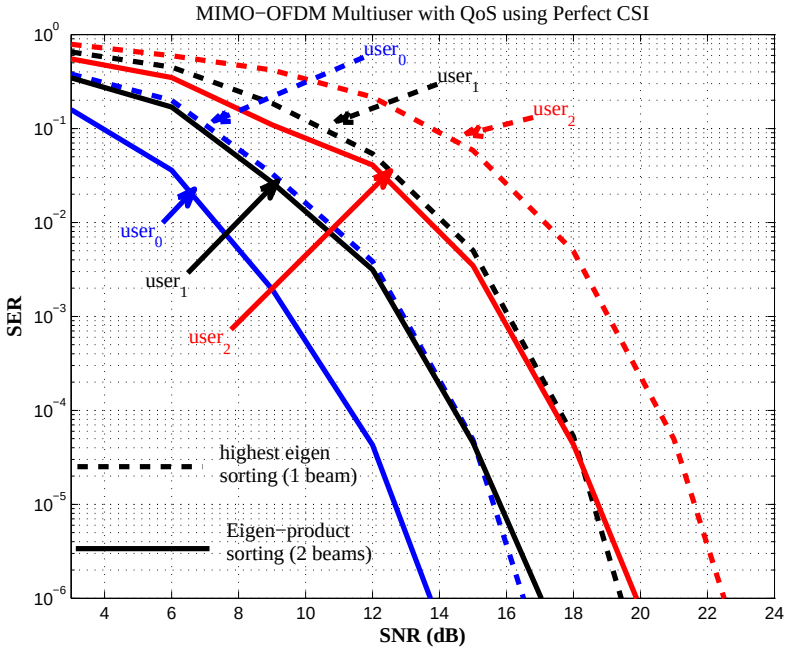

Figure 6.3: Multiuser MIMO-OFDM with different QoS and different sorting schemes

In Fig. 6.4, the performance of a multiuser 4×4 MIMO-OFDMA with 1024 bits/user for 3 users with 3 dB margin separations is compared to a single user case with 3 priority classes also allocating 1024 bits each. In both cases, we select only the highest 2 eigenbeams, i.e., 2-D beamforming. One can notice that the multiuser transmission (eigen-product) outperforms the single user by almost 1.5 dB at SER of 10^{-6}. This is due to the exploitation of the multiuser diversity. From Fig. 6.5, one can notice that increasing the number of antennas enhances the system. Thus, the 4×4 scenario with selection of the two highest eigenbeams outperforms the 4×2 using the same number of eigenbeams and both outperform the 2×2 case.

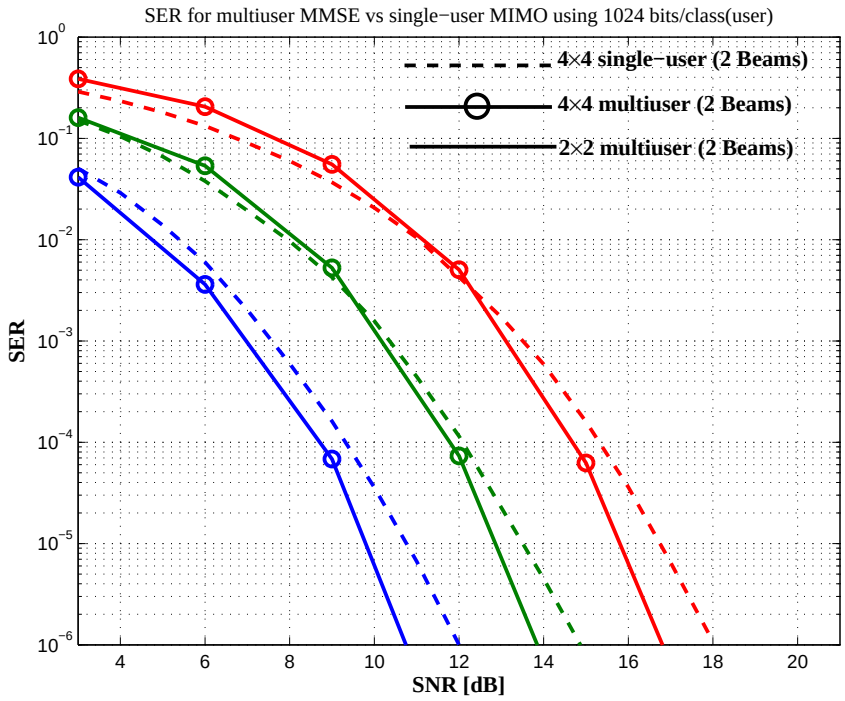

Figure 6.4: Multiuser MIMO-OFDMA vs single user with the same sum rate 3072 bits/OFDM frame

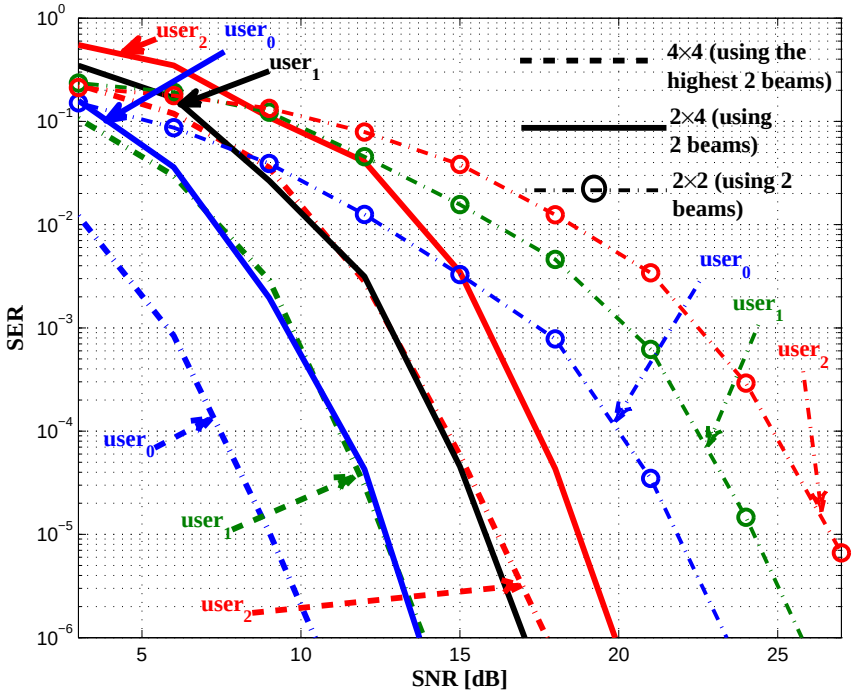

Figure 6.5: MIMO-OFDMA with different numbers of antennas and a sum rate of 3072 bits/OFDM-frame

6.1.7 MIMO-OFDMA Performance with Imperfect CSI

Here, we consider an erroneous feedback and a quantization which delivers a non-negligible quantization error. The CSI errors are assumed to be Gaussian distributed with a variance equal to 25% of that of the original channel. In Fig. 6.6, the 2nd user's curves are removed to

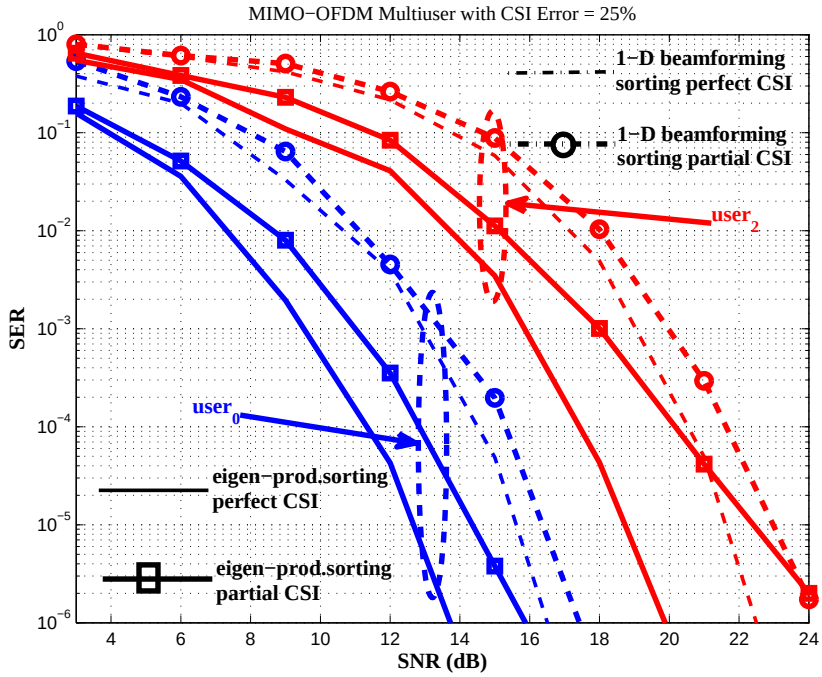

Figure 6.6: Different CSI conditions for the proposed sorting schemes

not overload the figure. One can observe that the 3 dB margin separation (or rather the 6 dB between the first and the third user) is becoming much wider with this erroneous CSI (curves with squares). Even worse, the SER curves are deteriorating at high SNRs. This is certainly due to the IEI results from the imperfect channel diagonalization. However, the 1-D beamforming does not suffer from this disadvantage. The performance of this scheme outperforms the eigen-product sorting at high SNR. Moreover, no error floor can be seen in these curves and the margin separations are better preserved. This makes the latter sorting scheme very suitable for adaptive MIMO-OFDMA with CSI errors and a restricted QoS constraint. Additionally, the sorting in case of 1-D beamforming is also faster than the optimum one. The only disadvantage of this scheme could be figured out at the lower SNRs, where the optimum sorting outperforms the 1-D beamforming by almost 2.2 dB at SER= 10^{-5}.

6.2 UEP Adaptation Using Non-iterative Partitioning

Using the partitioning scheme proposed in Chapter 3, Section 3.2.4, we implemented a two-user case sharing 2048 subcarriers using a SISO OFDMA transmission with Rayleigh channel fading. Since the users are assumed to share the frequency domain, each subcarrier is dedicated to

a single user at a time. We assume that each user has two classes of service with a margin separation between these two classes of 3 dB. Furthermore, we assume also that the margin separation between the least priority class of the first user and the highest priority class of second user equals 3 dB. Thus, for this two-user scenario, we get an equivalent single user case with four classes of service and 3 dB separation between each two classes.

Algorithm 3.9 in Chapter 3 is used to allocate these subcarriers assuming an equivalent single user with 4 data classes and the same total sum rate, i.e., $B_T = \sum_{j=0}^{N_g-1} \sum_{u=0}^{N_u-1} T_u^j$. Since the number of classes are even, one has to interpolate 3 extra classes to compute the equivalent number of bits of these four classes. According to Appendix B, Example 2, the equivalent sum rate of the first and the second classes of the first and the second user are $B_T - 3/2N$, $B_T - 1/2N$, $B_T + 1/2N$, and $B_T + 3/2N$, respectively.

Following the partitioning and sorting scheme proposed in Chapter 3 (demonstrated in Fig. 3.15), the highest priority user is allowed to allocate his two classes to his highest channel gains. The second user sorts the leftover subcarrier indices (of his own channel) and allocates his classes to them as in Fig. 3.15, Chapter 3.

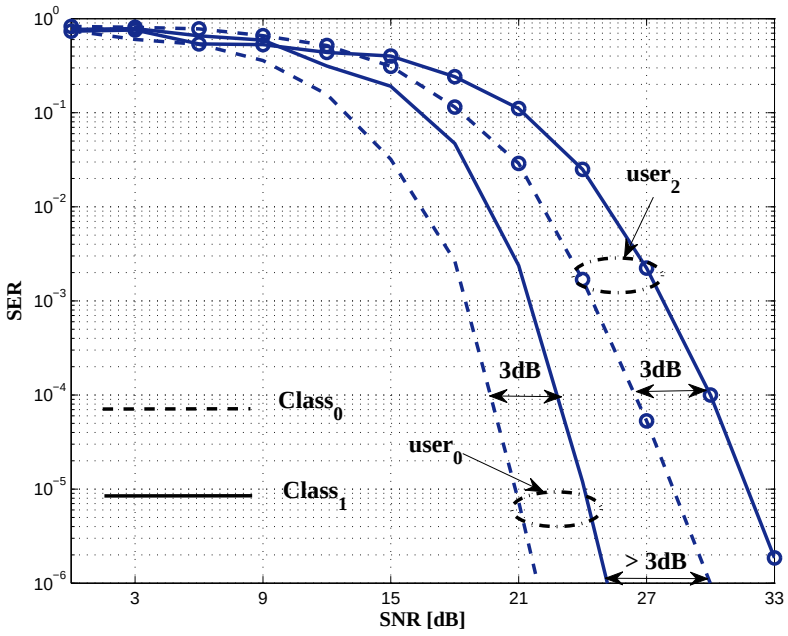

Figure 6.7: Adaptive OFDMA with two users with different QoS, each of which has two classes of protection levels with 1536 bits each, i.e., 6144 bits in total

Figure 6.7 shows the performance of our two-user example, where the 3 dB margin separation between the user's data classes is preserved. However, the margin separation between the two users (between the least priority class of the first user and the highest priority class of the second user) varies from low to high SNR. At low SNR, the margin separation is slightly less than 3 dB. This is due to multiuser diversity, where opportunistically switching to another channel increases the chance of having good-SNR subcarriers. However, at higher SNR, the users order is kept safe, while the 3 dB becomes slightly wider ($\sim$ 3.8 dB at SER= 10^{-6}).

6.3 Adaptive Multiuser MIMO Using Block Diagonalization

Block diagonalization (BD) is a linear precoding technique for a multiuser MIMO channel considering a BC scenario only. In this scheme, multiple data streams are transmitted to multiple users' receivers with no multiuser interference (MUI), i.e., orthogonal multiple access. Though the complexity is very low compared to non-linear MUI cancellation schemes, this scheme requires a very accurate channel knowledge at the BS. We consider two scenarios, first, the CSI is perfectly known at both the BS and the MS sets. In the second scenario, we consider a limited feedback regime, e.g., outdated CSI with a fixed delay at the transmitter side. However, the user's receiver knows the channel perfectly, i.e., for perfect linear equalization.

Here, we mainly opt for realizing multiuser transmission with different QoS. For this reason, we extended the UEP bit-loading algorithm in Chapter 5, where multiple users are treated, again, similar to the data with different priorities. In addition to our diagonal SDMA scheme, we adopted the multiuser multiple access using hierarchical modulation considering a modified version of Algorithm 5.5. In this case, users are allowed to be multiplexed using the BD plus hierarchical modulation, i.e., the same symbol transmitted to different users, when the users' subcarriers are enjoying high CGNR. However, our scheme automatically switches to OFDMA transmission, as with Section 6.1, when the users' subcarriers are exposed to deep fades. In the following, we discuss our channel model, system model, and the null-space (or namely BD) constraint (sections 6.3.1 and 6.3.2). The adaptive transmission using BD is discussed in Section 6.3.4 which is compared to the vector broadcasting scheme proposed in [109] (Section 6.3.3) in the results and analysis Section 6.3.5.

6.3.1 Block Diagonalized Channel Model

We consider an $(N_u N_R) \times N_T$ MIMO BC matrix $\mathbf{H}_{k,u}$, where N_R is the number of the receive antennas at each user terminal, N_u is the number of users, N_T is the number of the transmit antennas, k is the subcarrier index, and u is the user index. The total number of subcarriers is N. We assume a partial CSI with the delayed channel version $\hat{\mathbf{H}}_{k,u}$. The error matrix can be defined as $\mathbf{\Xi}_{k,u} = \mathbf{H}_{k,u} - \hat{\mathbf{H}}_{k,u}$, where $\mathbf{\Xi} \in \mathbb{C}\mathcal{N}(0, \sigma^2_{\mathbf{\Xi}}\mathbf{I})$ [8]. The channel matrix entries are uncorrelated zero mean circularly symmetric complex Gaussian (ZMCSCG) values and modeled as independent Rayleigh fading blocks with an exponentially decaying power profile.

6.3.2 System Model and Null-space Constraint

Assuming OFDM transmission, the received vector at user u^{th} and subcarrier k^{th} is given by

$$\mathbf{Y}_{k,u} = \mathbf{H}_{k,u}\mathbf{F}_{k,u}\mathbf{X}_{k,u} + \overbrace{\mathbf{H}_{k,u}\sum_{i=0,i\neq u}^{N_u-1}\mathbf{F}_{k,i}\mathbf{X}_{k,i}}^{\text{MUI}} + \mathbf{n}_{k,u}\ , \tag{6.11}$$

where $\mathbf{F}_{k,u}$ is the pre-processing matrix at the transmitter side, $\mathbf{X}_{k,u}$ is the transmitted vector, and $\mathbf{n}_{k,u}$ is a zero mean additive white Gaussian noise (AWGN) with a variance σ_n^2. To simplify

our notations, we henceforth omit the subcarrier index k throughout this section.

To approach the sum capacity of the BC with multiusers MIMO transmission, the MUI has to be mitigated. ZF can certainly mitigate the interference, despite being not optimum. However, as proposed in Chapter 2, Section 2.3.2, block diagonalization completely suppresses the MUI by projecting each user onto the null-space of the others, which succeeds in approaching the dirty-paper code BC capacity region. Projecting the u^{th} user onto the null-space of the others mean that his precoding matrix $\mathbf{F}_i$ spans the null spaces (zero eigenvalues) of the other users matrix, i.e., $\mathbf{H}_{i\neq u}\mathbf{F}_u = \mathbf{0}$. Similar to Chapter 2, (2.54), $\mathbf{F}_u \in \mathbb{C}^{(N_T \times M_u)}$ spans the M_u null spaces (eigenvectors corresponds to the zero eigenvalues, where $M_u \leq N_R$ as in Chapter 2) of the matrix formed by concatenating all users's channel matrix, excluding our u user as

$$\mathbf{H}_u^{\text{null}} = \left[\mathbf{H}_{i=0}^T \cdots \mathbf{H}_{i\neq u}^T \cdots \mathbf{H}_{i=N_u-1}^T\right]^T \ \forall\ u \neq i\ , \tag{6.12}$$

where $M_u \leq N_R$. The drawback of this null-space approach is the strict limitation on the number of antennas, where the total number of receive antennas ($N_u N_R$) has to be less than or equal to the number of transmit antennas N_T.

Accordingly, the optimal bit and power loads are computed based on the eigenvalues resulting from a decomposition of the new resulting channel matrix (as in (2.57))

$$\mathbf{H}_u^\star = \mathbf{H}_u\mathbf{F}_u = \mathbf{H}_u\mathbf{U}_{\mathbf{T}_u}\mathbf{Q}_{\mathbf{T}_u}\ , \tag{6.13}$$

where $\mathbf{U}_{\mathbf{T}_u}$ is the orthonormal basis for the null-space of $\mathbf{H}_u^{\text{null}}$ and $\mathbf{Q}_u$ is the spectral shaping (diagonal) matrix addressing the spatial substreams $s = 0..M_u - 1$. Henceforth, $\mathbf{H}_u^\star$ can be treated as a non-interfering single-user MIMO channel. Since the system is reduced to the single user case, the authors in [29] suggested to adapt the spectral shaping $q_{u,s}$ according to MMSE criterion assuming a unity power on each subcarrier. This minimizes the inter-eigen interference for each user, where $q_{u,s}$ is found (similar to multiuser water-filling in Appendix D) to be

$$q_{u,s}^2 = \left[\frac{1}{\sqrt{\mu}}\frac{\sigma_n}{\lambda_{u,s}} - \frac{\sigma_n^2}{\lambda_{u,s}^2}\right]^+\ ,\ \forall\ s = 0..M_u - 1\ , \tag{6.14}$$

where $[x]^+$ denotes that $x \geq 0$, μ is a Lagrangian multiplier that can be found iteratively or using the closed form given in Appendix D such that $\sum_{s=0}^{M_u-1} q_{u,s}^2 = 1$, and λ_{us}^2 is the eigenvalues of $\mathbf{F}_u^*\mathbf{H}_u^*\mathbf{H}_u\mathbf{F}_u$.

Hence, the eigenvalue decomposition of $\mathbf{H}_u^{\star,*}\mathbf{H}_u^\star$ results in the beamforming vectors $\mathbf{V}_u$ and the channel eigenvalues $\lambda_{s,u}^2$. In case of CSI delays, $\hat{\mathbf{H}}_u$ is introduced as the erroneous channel matrix that is deviated from the instant channel values by $\mathbf{\Xi}_u$, i.e., $\mathbf{H}_u = \hat{\mathbf{H}}_u + \mathbf{\Xi}_u$. Accordingly, the pre-processing and the null-space matrices are the erroneous ones $\hat{\mathbf{V}}_u$ and $\hat{\mathbf{F}}_u$, respectively. Similar to (2.57), the received symbol is given by

$$\mathbf{y}_u \ = \ \hat{\mathbf{H}}_u\hat{\mathbf{U}}_{\mathbf{T}_u}\hat{\mathbf{Q}}_{\mathbf{T}_u}\hat{\mathbf{V}}_u\hat{\mathbf{P}}_u\mathbf{x}_u + \overbrace{\mathbf{\Xi}_u\sum_{i=0,i\neq u}^{N_u-1}\hat{\mathbf{U}}_{\mathbf{T}_i}\hat{\mathbf{Q}}_{\mathbf{T}_i}\hat{\mathbf{V}}_i\hat{\mathbf{P}}_i\mathbf{x}_i}^{\text{residual MUI}} + \mathbf{n}_u\ . \tag{6.15}$$

where $\mathbf{P}_u^{1/2}$ is a diagonal matrix containing the power allocations based on $\lambda_{s,u}^2$. By assuming hierarchical modulation alphabets for each user, the total transmitted symbol $\mathbf{X}$ and the power

allocation matrix $\mathbf{P}$ are the same for every user (as the BS transmit to each user, physically, the same hierarchical symbol). Now, (6.15) can be rewritten as follows

$$\begin{aligned}\mathbf{Y}_u &= \overbrace{\left(\hat{\mathbf{H}}_u\hat{\mathbf{F}}_u\hat{\mathbf{V}}_u + \sum_{i=0,i\neq u}^{N_u-1}\boldsymbol{\Xi}_u\hat{\mathbf{F}}_i\hat{\mathbf{V}}_i\right)}^{\text{equivalent channel } \mathbf{H}_{\text{eq}}}\hat{\mathbf{P}}_u^{1/2}\mathbf{X}_u + \mathbf{n}_u \\ &= \mathbf{H}_{\text{eq}}\mathbf{P}^{1/2}\mathbf{X}_u + \mathbf{n}_u\ . \end{aligned} \tag{6.16}$$

This reduces our multiuser system with low CSI errors to a simple single user MIMO system with a full (but diagonally dominant) channel matrix that can be decoded using an MMSE receiver. However, for severe channel uncertainties, the matrix $\mathbf{H}_{\text{eq}}$ is not a diagonal-dominant. Thus, MMSE is not the optimal receiver any more. Successive interference cancellation or space-time block codes can be an alternative in this case. However, this is beyond the scope of this thesis.

6.3.3 Vector Broadcasting Using MMSE

Here, we modify the vector broadcast (VB) multiuser transmission proposed in [109] to compare it to our multilevel block diagonalized multiuser MIMO system. When the channel matrix is diagonalizable, as in the case of OFDM that employs a cyclic prefix, the optimization reduces to a simple MMSE water-filling-like solution (similar to (6.14) which is given in Appendix D). For the case of a circulant[4] channel matrix $\mathbf{H}^{N\times N}$ that is diagonalized using the discrete Fourier transform (DFT) and the inverse discrete Fourier transform (IDFT) matrices at the receiver and the transmitter, respectively, the problem is described as follows

$$\begin{aligned}\underset{q_k}{\text{minimize}} \quad & \sum_{k=0}^{N-1}\frac{\sigma_n^2}{q_k\sum_{i=0}^{N_u-1}\frac{\lambda_{i,k}^2}{N_u-1}+\sigma_n^2} \\ \text{subject to} \quad & \sum_{k=0}^{N-1}q_k \le P_T\ ; \quad q_k \ge 0\ , \end{aligned} \tag{6.17}$$

where $\lambda_{u,k}$ is the channel coefficient, and q_k is the power spectral shaping across the given subcarriers. Solving (6.17) using KKT conditions, similar to Appendix D, we obtain[5]

$$q_k^2 = \left[\frac{1}{\sqrt{\mu}}\frac{\sigma_n}{\sqrt{\sum_{i=0}^{N_u-1}\lambda_{i,k}^2/N_u}} - \frac{\sigma_n^2}{\sum_{i=0}^{N_u-1}\lambda_{i,k}^2/N_u}\right]^+\ ,\ k=0..N-1\ , \tag{6.18}$$

where $[\ .\ ]^+$ denotes a positive or zero value, μ is the Lagrangian multiplier that can be found iteratively such that $\sum_{k=0}^{N-1}q_k = P_T$, where q_k^2 is the power of the k^{th} subcarrier. Removing the individual user power constraint is only convenient in BC scenarios. Thus the solution becomes similar to the one in [111].

In the original VB design, the authors in [109] considered a single transmit antenna and multiple users, each with a single receive antenna. However, in our deployment, we accommodate the transmitter with N_T antennas sending the same information symbol (multicast) with a total transmit power P_T, i.e., a MISO channel with transmit diversity. Furthermore, each information symbol is encoded in a hierarchical fashion, allowing each user to receive different information from the same symbol.

[4] See Chapter 2 for more details about diagonalizing the multicarrier transmission.

[5] Our power allocation seems to have a unit-less as we target a normalized power, i.e., set to unity.

6.3.4 Adaptive Prioritized Multiuser Multilevel Modulation

Based on the multilevel adaptive modulation Algorithm 4.2, Chapter 4, we propose an adaptive scheme that realizes prioritized user transmission using multilevel (hierarchical and non-hierarchical) modulation assuming a BC scenario. We realize fixed margin separations between the different users under different channel conditions and different user target data rates. As with Chapter 4, the highest priority user is allowed to consume the good-CGNR subcarriers first. Thereafter, the bits of less important users are allowed to be allocated to either already used subcarriers in a hierarchical fashion if the quantized CGNR and the remaining power are sufficient to accommodate more bits. If not, free subcarriers can instead be used based on the margin separation $\Delta\gamma$ using homogeneous constellations. Assuming a margin-adaptive bit-loading with the following definition:

$$\begin{aligned} \underset{p_k}{\text{minimize}} \quad & P_\sigma = \sum_{k=0}^{N-1} \sum_{u=0}^{N_u-1} \sum_{s=0}^{M_u-1} p_{s,k}^u \\ \text{subject to} \quad & \sum_{k=0}^{N-1} \sum_{u=0}^{N_u-1} \sum_{s=0}^{M_u-1} \log_2 \left(1 + \frac{p_{s,k}^u \mathcal{G}_{k,s}^u}{\Gamma}\right) = B_T \;\text{ and }\; P_\sigma \leq P_T \,, \end{aligned} \tag{6.19}$$

where $p_{s,k}^u$ is the power allocated to the k^{th} subcarrier, the s^{th} stream, and the i^{th} user, P_T is the given target power, P_σ is the accumulated power, and the "gap" approximation is, as in Chapter 3, given by $\Gamma = \frac{2}{3}\left[\text{erfc}^{-1}\left(\frac{\mathcal{P}}{2}\right)\right]^2$. Thus, the maximum system margin is defined as

$$\gamma_{\max} = \frac{P_T}{P_\sigma} \,. \tag{6.20}$$

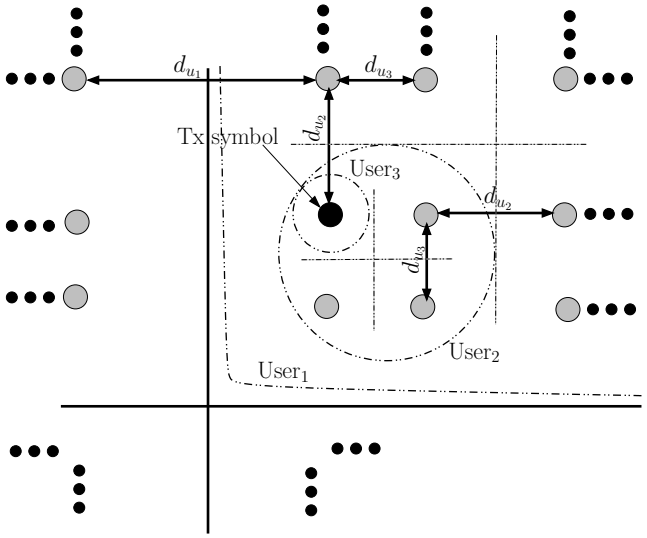

Figure 6.8: Hierarchical modulation 4/16/64-HQAM: the decision boundaries of user$_0$ is a 4-QAM embedded in the 16-QAM of user$_1$; user$_1$ decision boundaries is a 4-QAM embedded in the 64-QAM of user$_2$, where user$_2$ has to detect the smallest 4-QAM hierarchical level.

6.3.4.1 Hierarchical multilevel modulation

Using hierarchical modulation, the symbols of the different users with different priorities can be embedded into each other creating different Euclidean distances d_i (as in Chapter 4). The relative margin separations between users are adjusted using the ratios of their constellation distances ($\frac{d_{u_i}}{d_{u_{i-1}}}$, where u_i and u_{i-1} are two different users). In Fig. 6.8, the distances between hierarchical users d_{u_i} are selected based on γ_i, which may, e.g., be set to 3 dB, i.e., $\frac{d_{u_i}}{d_{u_{i-1}}} = \sqrt{2}$. In this chapter as well, we use the same hierarchical construction as in Chapter 4.

Our hierarchical modulation scheme automatically allows for different hierarchical levels based on the CGNR of each user, where the maximum number of hierarchy levels is limited by the number of users N_u. Even more, homogeneous constellations (non-hierarchical modulation) are also allowed on some subcarriers if their SNRs (for a certain user) are far better than the equivalent subcarriers of other users. This is automatically decided based on the prioritized adaptive algorithm described subsequently.

6.3.4.2 Adaptive algorithm for prioritized QoS bit-loading

Based on Algorithm 4.2, we propose a multiuser computationally efficient bit-loading algorithm that allocates bits and powers according to the quantized $\mathcal{G}^u_{k,s}$. A total target sum rate of B_T is required to be fulfilled subject to the total power constraint P_T. According to Chapter 4, the discrete bit allocation b_k is given by

$$b^u_{k,s} = \left\lfloor \lfloor \log_2 \mathcal{G}^u_{k,s} \rfloor + i^u_{B_{\text{opt}}} \right\rceil_0^{b_{\max}} , \tag{6.21}$$

where $i^u_{B_{\text{opt}}} \in \mathbb{Z}$ is an arbitrary constraint adjusted such that $\sum_{s=1}^{M_u} \sum_{k=1}^{N} b^u_{k,s} \leq B_T$, i.e., similar to (3.63). The floor operator allows different subcarriers, with different $\mathcal{G}^u_{k,s}$, to take the same bit value b_μ, i.e., there will be groups of identically loaded subcarriers due to the quantization process. Hence, let κ be the maximum number of the subcarrier groups allocated to the same $\bar{b}_\mu \; \forall \; \mu \in [0, \kappa - 1]$. Let a positive quantized CGNR be given by

$$\beta^u_{k,s} = \lfloor \log_2 \mathcal{G}^u_{k,s} - \log_2 \mathcal{G}^u_{\min} \rfloor , \tag{6.22}$$

where $\mathcal{G}^u_{\min}$ is minimum CGNR for user u. A positive quantization error Δ_k on each subcarrier is calculated, using (6.22) as

$$\Delta_k = \{\log_2 \mathcal{G}^u_{k,s} - \log_2 \mathcal{G}^u_{\min}\} - \beta^u_{k,s} . \tag{6.23}$$

Based on the linear programming proposed in Chapter 3, Section 3.2.6, and the relaxation in (3.63), an estimated value for i_B is calculated such that the users' individual target rates are achieved. Following, the same footprints of Algorithm 4.2, however, using N_u prioritized users with target rates T_u instead of the N_g data classes used in the original algorithm.

6.3.5 Analysis of UEP Bit-loading using Block Diagonalization

To evaluate the latter adaptation scheme, we consider three users with 3 different priorities. A fixed margin separation between these users (3 dB) is considered. This is easily guaranteed by

defining the hierarchical modulation priority ratio to be $\frac{d_{u_i}}{d_{u_{i-1}}} = \sqrt{2}$ at those subcarriers where hierarchical modulation is applied. However, when hierarchical modulation is not implemented, our bit-loading algorithm takes care of the 3 dB separations. In our simulations, we assumed that the total number of subcarriers N is 512. Additionally, the homogeneously modulated subcarriers are allowed to allocate quadrature amplitude modulation (QAM) with a constellation size of, at maximum, 8 bits. The hierarchically modulated ones are allowed to have a maximum of 6 bits on each layer. As can be seen from Fig 6.9, assuming 1024 bits/user, the margin

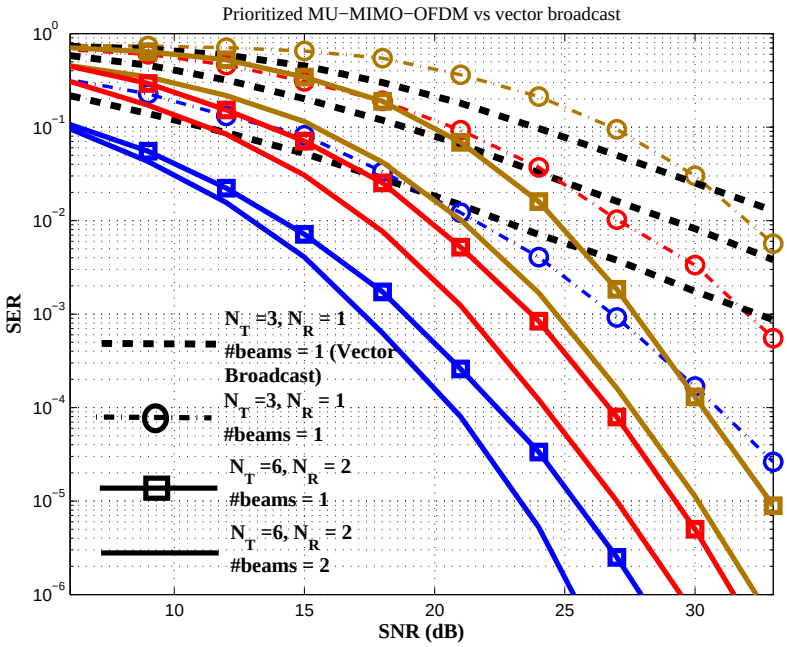

Figure 6.9: Adaptive BD vs VB with different number of antenna setup using 1024 bits/user.

separations in case of perfect CSI are preserved for the single eigen-beamforming as well as for the full eigen-beamforming. From the same figure, the vector broadcast (VB) design (the dashed black curves) seems to be an upper bound to our scheme. Nevertheless, when the same number of antennas are used with BD and prioritized adaptive modulation, the VB outperforms it at low SNR. However, this gain becomes even a significant loss at high SNR, i.e., likewise any comparison between an adaptive and a non-adaptive systems. Figure 6.10 depicts the full eigen-beamforming performance under CSI error (σ_{Ξ}^2) of 0.25 with (and without) spectral shaping $\mathbf{\Phi}$. The one with the spectral shaping outperforms the other by almost 7 dBs, since the spectral shaping proposed in (6.14) suppresses the weaker channels. In this case, they are not allocated during the bit-loading process. As could be also seen in this figure, the single eigen-beamforming already outperforms the full eigen-beamforming, even with the spectral shaping, in case of CSI errors. This shows the drawback (the sub-optimality) of (6.14). Finally, Fig. 6.11 depicts the performance of the reduced target bit-rate (512 bits/user). One can notice that the performance of the full/single beamforming is dramatically improved. However, the single beamforming still performs the best amongest the other setups.

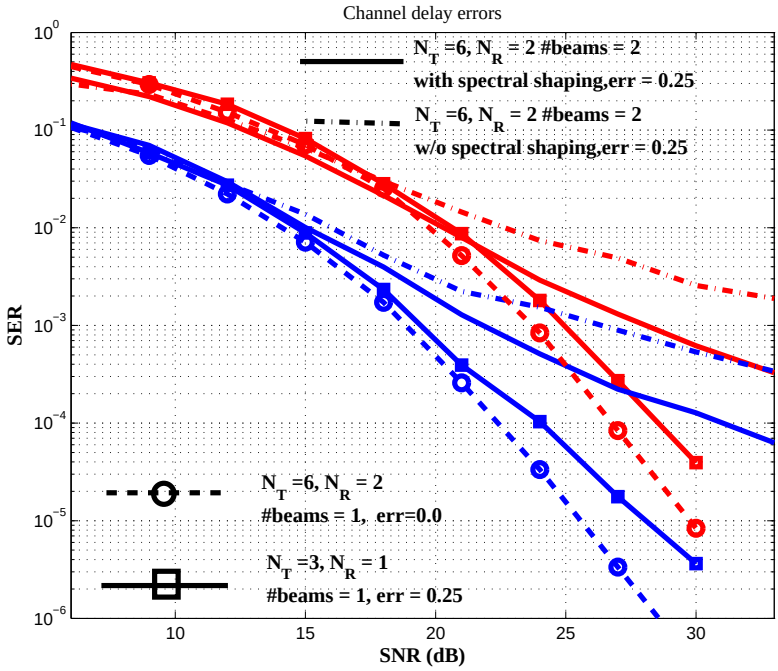

Figure 6.10: Block-diagonalization using with CSI errors with/without spectral shaping and different beamforming modes.

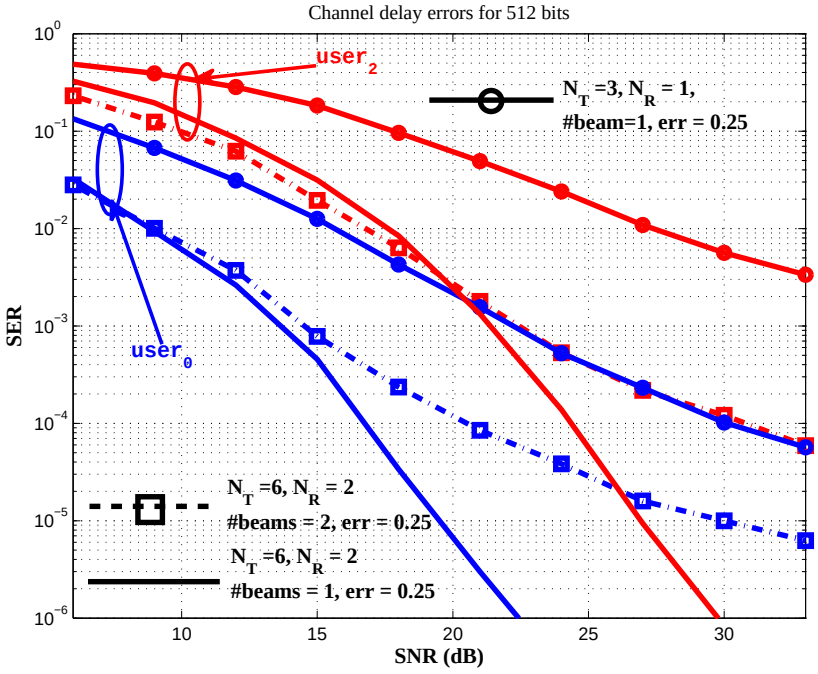

Figure 6.11: The performance under reduced bit-rate (512 bits/user).

6.4 Non-diagonal Multiuser MIMO Using the MMSE Criterion

In this section, a double-prioritized transmission is realized in a non-orthogonal multiuser MIMO-OFDM. The first prioritized transmission realizes different QoSs among different users via optimizing their transceiver linear filters $\mathbf{F}$ and $\mathbf{W}$ using the minimum weighted sum-MSE with different weighting factors. These factors are selected according to the required QoSs by solving a dual MAC scenario instead of the required BC. The second priority approach succeeds in implementing UEP bit-loading that realizes three prioritized classes. In this case, bits and power values are allocated according to the achievable MMSE. The remainder of this chapter is organized as follows. Section 6.4.1 describes the Sum-MSE optimization approach. Section 6.4.2 discusses the constraint gradient algorithm, which obtains the optimum transceiver filters while achieving a minimum MSE. The dual MAC channel is converted back to the required BC channel in Section 6.4.2. In Section 6.4.3, we propose the modifications required for realizing UEP bit-loading using the same steps of Algorithm 6.1. Finally, we present our results in Section 6.4.4, where some of these results have been published in [1].

6.4.1 Formulation of the Sum-MSE

Since our approach uses the MAC-BC duality, one can solve the dual (virtual) MAC scenario to determine the transmit and the receive filters. Thereafter, these filters are linearly mapped to the original scenario [79]. For a dual MAC, the transmit and the receive antennas are interchanged, i.e., the mobile terminals act (virtually) as the transmitters, where each of the N_u mobile terminals is loaded with N_R (virtual transmit) antennas, while the base-station is deployed with N_T (virtual receive) antennas. This is simply done by considering the original channel matrix to be $\mathbf{H}_u^*$, while the virtual MAC remains $\mathbf{H}_u$. Hence, the overall equivalent (dual) uplink received signal at the u^{th} user, after passing through the receiver post-processing $\mathbf{W} \in \mathbb{C}^{N_T \times N_R}$, is given by

$$\mathbf{r} = \mathbf{W} \sum_{u=0}^{N_u-1} \mathbf{H}_u \mathbf{F}_u \mathbf{x}_u + \mathbf{W}\mathbf{n} \, , \tag{6.24}$$

where $\mathbf{W} = [\mathbf{W}_0^{\mathrm{T}} ... \mathbf{W}_u ... \mathbf{W}_{N_u-1}^{\mathrm{T}}]^{\mathrm{T}}$ and $\mathbf{W}_u$ is the dual individual post-processing for each user. $\mathbf{F}_u \in \mathbb{C}^{N_R \times N_R}$ is the user's dual pre-coding matrix, such that $\mathrm{Tr}(\mathbf{F}_u^* \mathbf{F}_u) \leq P_T$, and $\mathbf{n} \in \mathbb{C}^{N_T \times 1}$ is the zero mean Gaussian noise vector with a variance σ_n^2.

In order to find the minimum sum-MSE, the following optimization problem must be solved

$$\begin{aligned} \underset{\mathbf{F},\mathbf{W}}{\text{minimize}} \quad & \textstyle\sum_{u=0}^{N_u-1} E_u^{\mathrm{UL}} \\ \text{subject to} \quad & \textstyle\sum_{u=0}^{N_u-1} \mathrm{Tr}\left(\mathbf{F}_u^* \mathbf{F}_u\right) \leq P_T \, , \end{aligned} \tag{6.25}$$

where E_u denotes the mean-squared error of the u^{th} user's symbols. Thus, we obtain the dual uplink MSE $E_u^{\mathrm{UL}} = E[||\mathbf{r}_u - \mathbf{x}_u||_2^2]$ of user u, as given in Appendix D in (D.9), to be

$$E_u^{\mathrm{UL}} = \mathrm{Tr}\left[\mathbf{I}_{N_{R_u}} - \mathbf{W}_u \mathbf{H}_u \mathbf{F}_u - \mathbf{F}_u^* \mathbf{H}_u^* \mathbf{W}_u^*\right] + \mathrm{Tr}\left[\mathbf{W}_u \left(\sum_{i=0}^{N_u-1} \mathbf{H}_i \mathbf{F}_i \mathbf{F}_i^* \mathbf{H}_i^*\right) \mathbf{W}_u^* + \sigma_n^2 \mathbf{W}_u \mathbf{W}_u^*\right] \, , \tag{6.26}$$

while the sum-MSE is given as

$$\begin{aligned} E^{\mathrm{UL}} = \sum_{u=0}^{N_u-1} E_u^{\mathrm{UL}} &= \sum_{u=0}^{N_u-1} N_{R_u} - \sum_{u=0}^{N_u-1} \mathrm{Tr}\left[\mathbf{W}_u\mathbf{H}_u\mathbf{F}_u + \mathbf{F}_u^*\mathbf{H}_u^*\mathbf{W}_u^*\right] \\ &+ \sum_{u=0}^{N_u-1} \mathrm{Tr}\left[\mathbf{W}_u\left(\sum_{i=0}^{N_u-1}\mathbf{H}_i\mathbf{F}_i\mathbf{F}_i^*\mathbf{H}_i^*\right)\mathbf{W}_u^* + \sigma_n^2\mathbf{W}_u\mathbf{W}_u^*\right] \\ &= \sum_{u=0}^{N_u-1} N_{R_u} - \mathrm{Tr}\left[\mathbf{WHF} + \mathbf{F}^*\mathbf{H}^*\mathbf{W}^*\right] \\ &+ \mathrm{Tr}\left[\mathbf{WHFF}^*\mathbf{H}^*\mathbf{W}^* + \sigma_n^2\mathbf{WW}^*\right] , \end{aligned} \tag{6.27}$$

where $\mathbf{H} = [\mathbf{H}_1, ..., \mathbf{H}_{N_u}] \in \mathbb{C}^{N_T \times \sum_{i=0}^{N_u-1} N_R}$. $\mathbf{F} \in \mathbb{C}^{\sum_{u=0}^{N_u} M_u \times \sum_{u=0}^{N_u-1} M_u}$ is a block-diagonal matrix holds on each of the diagonal blocks the u user $\mathbf{F}_u,\ u = 0..N_u - 1$.

In order to convert the dual uplink into the original downlink, the following positive conversion factor $\alpha \in \mathbb{R}_+$ is needed to model the near-far power scaling effect[6]. In [79], the transmit-receiver filters used in the downlink are assumed to be

$$\mathbf{F}^{\mathrm{DL}} = \alpha\mathbf{W}^* \quad \text{and} \quad \mathbf{W}^{\mathrm{DL}} = 1/\alpha\mathbf{F}^* . \tag{6.28}$$

Accordingly, the equivalent downlink sum-MSE can be found by replacing $\mathbf{H} \Rightarrow \mathbf{H}^*$ and substituting with $\mathbf{F}^{\mathrm{DL}}$ and $\mathbf{W}^{\mathrm{DL}}$. Now, using (6.28) in (6.27) we get

$$\begin{aligned} E^{\mathrm{DL}} = \sum_{u=0}^{N_u-1} E_u^{\mathrm{DL}} &= \sum_{u=0}^{N_u-1} M_u - \mathrm{Tr}\left[\mathbf{F}^*\mathbf{H}^*\mathbf{W}^* + \mathbf{WHF}\right] + \mathrm{Tr}\left[\mathbf{F}^*\mathbf{H}^*\mathbf{W}^*\mathbf{WHF}\right] \\ &+ \frac{1}{\alpha^2}\sigma_n^2\mathrm{Tr}\left[\mathbf{F}^*\mathbf{F}\right] . \end{aligned} \tag{6.29}$$

Since the MSE of the downlink and its dual uplink are equal, one can directly equate (6.27) into (6.29) to find α as

$$\alpha^2 = \frac{\mathrm{Tr}\left[\mathbf{F}^*\mathbf{F}\right]}{\mathrm{Tr}\left[\mathbf{W}^*\mathbf{W}\right]} = \frac{P_T}{||\mathbf{W}||_F^2} = \frac{P_T}{\sum_{u=0}^{N_u-1}||\mathbf{W}_u||_F^2} , \tag{6.30}$$

i.e., assuming that the dual uplink has the same power as the downlink.

As in [77, 79], the receive filter is assumed to be an MMSE equalizer that minimizes the MSE of each user individually, where the dual-uplink post-processing matrix $\mathbf{W}_u$ is given by

$$\begin{aligned} \mathbf{W}_u &= \mathbf{F}_u^*\mathbf{H}_u^*\mathbf{T}^{-1} \\ &= \mathbf{F}_u^*\mathbf{H}_u^*\left[\sigma_n^2\mathbf{I}_{N_R} + \sum_{u=0}^{N_u-1}\mathbf{H}_u\mathbf{F}_u\mathbf{F}_u^*\mathbf{H}_u^*\right]^{-1} . \end{aligned} \tag{6.31}$$

After substituting the previous equation into (6.26), with further linear operations as in Appendix D, (D.12), one can simplify E_u^{UL} as

$$E_u^{\mathrm{UL}} = M_u - \mathrm{Tr}\left[\mathbf{F}_u^*\mathbf{H}_u^*\left[\sum_{u=0}^{N_u-1}\mathbf{H}_u\mathbf{F}_u\mathbf{F}_u^*\mathbf{H}_u^* + \sigma_n^2\mathbf{I}\right]^{-1}\mathbf{H}_u\mathbf{F}_u\right] , \tag{6.32}$$

[6] In Chapter 2, Section 2.3.2.2, a similar factor is used to model the dirty-paper code (DPC) MAC-BC duality.

where M_u is the number of streams used by the u^{th} user. Following the linear manipulations in (D.13), Appendix D, we get the dual uplink optimization problem in (6.25) to be

$$\begin{aligned} \underset{\mathbf{F}_1,\ldots,\mathbf{F}_{N_u}}{\text{minimize}} \quad & \sigma_n^2 \text{Tr}\left(\left[\sum_{u=0}^{N_u-1} \mathbf{H}_u\mathbf{F}_u\mathbf{F}_u^*\mathbf{H}_u^* + \sigma_n^2\mathbf{I}\right]^{-1}\right) \\ \text{subject to} \quad & \text{Tr}\left(\mathbf{F}\mathbf{F}^*\right) \leq P_T \ . \end{aligned} \tag{6.33}$$

This is convex in every product of $\mathbf{F}_u\mathbf{F}_u^*$ as far as $\text{Tr}[(.)^{-1}]$ is a convex function, which is valid for any positive semidefinite arguments, i.e., $\mathbf{F}\mathbf{F}^*$ is strictly positive semidefinite [76]-[81]. In [77]-[81], (6.33) is reformulated to a semidefinite programing (SDP) problem [56], which can be solved efficiently by means of standard optimization tools, e.g., SeDuMi [112] and YALMIP [113]. This method guarantees achieving the global minimum MSE, however, with considerably high complexity. This will be discussed briefly in Appendix E.

Another method, which relies on the Lagrangian iterative method, is proposed in [76, 78, 79, 80]. In this case, only local minima are guaranteed, however, with fewer iterations. The following section shows how to fulfill the KKT conditions of the Lagrangian problem corresponds to (6.25). The MMSE in this case is achieved using the iterative scaled gradient projection methods [78, 114] for different QoS, i.e., using the weighted sum-MSE proposed in Chapter 2.

6.4.2 Prioritized Multiuser Transmission Using Weighted Sum-MSE

The optimum resource allocation based on the weighted sum-MSE in (6.25) aims at minimizing the sum-MSE multiplied by a weighting vector $\mathbf{w} = [w_1, .., w_{N_u}]^{\text{T}}$, where $\mathbf{1}\cdot\mathbf{w} = 1$. For each user u, w_u can be arbitrarily chosen in order to realize certain QoS constraint [81]. In general, achieving this minimum sum-MSE results in switching off users with weaker channel gains and, instead, concentrate the power only on the users with the better channel conditions. This can easily maintain a QoS-based transmission among users.

After proving the convexity of (6.32), we can now satisfy our goal of delivering different QoSs among users, i.e., different E_u^{UL} for each user. Thus, we need to minimize the following optimization problem

$$\begin{aligned} \underset{\mathbf{F},\mathbf{W}}{\text{minimize}} \quad & \textstyle\sum_{u=0}^{N_u-1} w_u E_u^{\text{UL}} \\ \text{subject to} \quad & \textstyle\sum_{u=0}^{N_u-1} \text{Tr}\left(\mathbf{F}^*\mathbf{F}\right) \leq P_T \ , \end{aligned} \tag{6.34}$$

where E_u denotes the mean-squared error of user u symbols and w_u are positive weighting factors required to adapt the individual QoS of each user. Similar to [78] and [80], the Lagrangian function of (6.34) given E_u^{UL} in (6.32), is given by

$$\mathcal{L}_\mu^E = \sum_{u=1}^{N_u} w_u N_{R_u} - \sum_{u=1}^{N_u} w_u \text{Tr}\left[\mathbf{F}_u^*\mathbf{H}_u^*\mathbf{T}^{-1}\mathbf{H}_u\mathbf{F}_u\right] - \mu\left(\sum_{u=0}^{N_u-1} \text{Tr}\left(\mathbf{F}_u^*\mathbf{F}_u\right) - P_T\right) \ , \tag{6.35}$$

where $\mathbf{T} = \left[\sum_{u=0}^{N_u-1} \mathbf{H}_u\mathbf{F}_u\mathbf{F}_u^*\mathbf{H}_u^* + \sigma_n^2\mathbf{I}\right]$[7] and the minimum MSE is computed by evaluating $\frac{\partial L_E}{\partial \mathbf{F}_u^*}$ and setting it to zero. According to Appendix D (from (D.14) to (D.20)), we get that the

[7] If the downlink is considered instead of its dual uplink, one has to compute N_u inverses of $\mathbf{T}_u = \left[\mathbf{H}_u^*\mathbf{F}^{\text{DL}}\mathbf{F}^{*,\text{DL}}\mathbf{H}_u + \sigma_n^2\mathbf{I}\right]$ which is more complex than our dual approach that computes one inverse only.

solution of this Lagrangian problem is given by

$$\frac{\partial \mathcal{L}_{\mu}^{E}}{\partial \mathbf{F}_{u}^{*}} = \mu \mathbf{F}_{u} - \mathbf{H}_{u}^{*}\mathbf{T}^{-1}\left(w_{i}\mathbf{T} - \mathbf{S}\right)\mathbf{T}^{-1}\mathbf{H}_{u}\mathbf{F}_{u} = \mathbf{0}\,, \tag{6.36}$$

where $\mathbf{S} = \sum_{u=1}^{N_u} w_u \mathbf{H}_u \mathbf{F}_u \mathbf{F}_u^* \mathbf{H}_u^*$. This means

$$\mu \mathbf{F}_{u}^{\text{new}} = \mathbf{H}_{u}^{*}\mathbf{T}^{-1}\left(w_{i}\mathbf{T} - \mathbf{S}\right)\mathbf{T}^{-1}\mathbf{H}_{u}\mathbf{F}_{u}\,. \tag{6.37}$$

The authors in [78] and [79] found that the weighting factors follow almost the same linear system of equations as the conversion factor α_u in (6.30) if the individual MSE need to be preserved. This can easily be seen if we multiply (6.37) for each user u with $\mathbf{F}_u^*$ from the left and take the trace for each $u = 1..N_u$. Therefore, one can compute α_u knowing the sum-MSE α and the weighting factor w_u as follows

$$\alpha_u = \alpha\sqrt{w_u}\,, \tag{6.38}$$

where

$$\frac{\alpha_1}{w_1} = \frac{\alpha_2}{w_2} = ... = \frac{\alpha_u}{w_u} = ... = \frac{\alpha_{N_u}}{w_{N_u}}\,. \tag{6.39}$$

In order to solve the constraint optimization problems in (6.25), the authors in [79] proposed to solve a standard unconstrained gradient algorithm which is modified in order to accommodate the power constraint as follows ([78] and[114])

$$\mathbf{F}^{(t+1)} = \left[\mathbf{F}^{(t)} - \frac{1}{d}\mathbf{M}^{-1}\nabla E\left(\mathbf{F}^{(\mathbf{t})}\right)\right]^{\perp}\,, \tag{6.40}$$

where E is the total error given in (6.32), $\frac{1}{d}$ is the step size, ∇ corresponds to the matrix-valued Nabla operator (Jacobian matrix) [114, Chapter 3], and the notation $[x]^{\perp}$ denotes the orthogonal projection (with respect to the Euclidean norm) of a vector x onto its convex set, say, X. In particular, $[x]^{\perp}$ is defined as in [114, Chapter 3] by $[x]^{\perp} = \arg\min_{z\in X} ||z - x||_2$. $\mathbf{M}$ represents a preconditioning positive definite diagonal matrix, which is chosen (according to [114, Section 3.2]) to be

$$\mathbf{M}^{-1}(t) = \sqrt{\frac{P_T}{\sum_{u=0}^{N_u-1}\nabla E\left(\mathbf{F}_i^{(t)}\right)}}\,\mathbf{I}\,, \tag{6.41}$$

where P_T is the accommodated power constraint. The denominator in this equation has a very small value at high SNR, i.e., becomes independent of the SNR[8]. Due to this reason, this scheme always guarantees similar power allocation across different streams at high SNR. Thus, $\nabla E_u\left(\mathbf{F}^{(t)}\right)$ is defined as in Appendix D (also from (D.15) to (D.20))[9] to be

$$\begin{aligned}\nabla E_u\left(\mathbf{F}_u^{(t)}\right) &= \frac{\partial E_u(\mathbf{F_u}^{(t)})}{\partial \mathbf{F}_u^{*(t)}} \\ &= -\mathbf{H}_u^*\mathbf{T}^{-1}\left(w_i\mathbf{T} - S\right)\mathbf{T}^{-1}\mathbf{H}_u\mathbf{F}_u\,.\end{aligned} \tag{6.42}$$

[8]From (6.33), the denominator is function of the noise variance; when the noise go to zero, $\mathbf{M^{-1}}$ becomes ∞ and now (6.40) has a zero multiplied by ∞.

[9]This is similar to the Lagrangian method in [80], however, using an iterative method to solve an original MAC scenario with equal weights as in Appendix D (D.22).

Now, we substitute (6.42) into (6.41), then into (6.40) to achieve an accurate $\mathbf{F}_u$. Then $\mathbf{T}$ is calculated using (6.31). Finally, $\mathbf{W}_u$ is computed using (6.31); further iterations are required for enhancing the results. In the following, we summarize the steps needed to implement the gradient projection method[10] for the dual MAC.

Algorithm 6.2 Multiuser MIMO weighted sum-MSE using scaled gradient projection method

Initialize: $\mathbf{F}_u^{(0)} \Leftarrow \sqrt{\frac{P_T}{N_R}}\mathbf{I}_{N_R}\ \forall\ k\ ,\ d \Leftarrow 2\ ,\ t \Leftarrow 0$, and the maximum loop counter is MaxCnt.
Output: $\mathbf{F}_{\mathbf{u}}^{\mathrm{DL}}$ and $\mathbf{W}_{\mathbf{u}}^{\mathrm{DL}}$
Require: minimize the MSE and $\forall\ k$ and jointly allocate each user's streams.
Ensure: $\sum_{i=0}^{N_u-1}\mathrm{Tr}\left(\mathbf{F}_i^*\mathbf{F}_i\right) = P_T$

repeat
  $t \Leftarrow t+1$
  $\mathbf{T}^{(t)} \Leftarrow \sigma_n^2\mathbf{I}_{N_T} + \sum_{u=0}^{N_u-1}\mathbf{H}_u\mathbf{F}_u^{(t-1)}\mathbf{F}_u^{*,(t-1)}\mathbf{H}_u^*$
  $\mathbf{S}^{(t)} \Leftarrow \sum_{u=0}^{N_u-1} w_u\mathbf{H}_u\mathbf{F}_u^{(t-1)}\mathbf{F}_u^{*,(t-1)}\mathbf{H}_u^*$
  for $u = 1$ to N_u **do**
    gradient: $\nabla E_u\left(\mathbf{F}_u^{(t)}\right) \Leftarrow -\mathbf{H}_u^{*,(t)}\mathbf{T}^{-1,(t)}\left(w_i\mathbf{T}^{(t)} - S^{(t)}\right)\mathbf{T}^{-1,(t)}\mathbf{H}_u^{(t)}\mathbf{F}_u^{(t)}$
    scaled: $\mathbf{F}_u^{(t)} \Leftarrow \mathbf{F}_u^{(t-1)} - \frac{1}{d}\sqrt{P_T/\left(\sum_{u=0}^{N_u-1}\nabla E_u\left(\mathbf{F}_u^{(t)}\right)\right)}\nabla E_u\left(\mathbf{F}_u^{(t)}\right)$
    projection: $\mathbf{F}_u^{(t)} \Leftarrow \mathbf{F}_u^{(t)}\sqrt{P_T/\left(\sum_{u=0}^{N_u-1}\nabla E_u\left(\mathbf{F}_u^{(t)}\right)\right)}$ (projecting to the power constraint)
    if the sum-MSE $E^{(t)} >$ the sum-MSE $E^{(t-1)}$ **then**
      increment step size inverse: $d \Leftarrow d+1$
      reduce time by one (stay in the loop): $t \Leftarrow t-1$
    end if
  end for
until achieving the desired accuracy ϵ, i.e., $E^{(t)} - E^{(t-1)} < \epsilon$, or $t =$MaxCnt
perform uplink/downlink conversion using the following steps

Uplink/downlink conversion: after the transceiver filters are computed for the dual problem, we need to be convert them the original BC filters, i.e., $\mathbf{F}_u^{\mathrm{DL}}$ and $\mathbf{W}_u^{\mathrm{DL}}$. This conversion is performed based on the following steps:

1. compute the scaling factor α_0 (defined in (6.30)) of the first user ($u = 0$), i.e., assuming that all users have the same weighting w_u and that MMSE is given by (6.33) [79, Algorithm 1], as follows

$$\alpha_0 = \sqrt{\frac{P_T}{\mathrm{Tr}\left(\sum_{u=0}^{N_u-1} w_u\mathbf{F}_u^*\mathbf{H}_u^*\mathbf{T}^{-2}\mathbf{H}_u\mathbf{F}_u\right)}}\ , \tag{6.43}$$

   where α is the factor used to model the near-far effect in the dual MAC assuming $w_1 = w_2 = ... = w_{N_u} = 1/N_u$,

[10] The convergence of this algorithm is discussed in [114, Chapter 3].

2. compute the exact scaling factor for all users using their actual MSE weighting values, such that $\alpha_u = \alpha_0 \sqrt{w_u}$,

3. find the downlink transceiver filters using the relation in (6.28)

$$\begin{aligned} \mathbf{F}^{\mathrm{DL}} &= [\alpha_u \mathbf{W}_1 ... \alpha_u \mathbf{W}_{N_u}]^{\mathrm{T}} = [\alpha_u \mathbf{T}^{-\mathbf{1}} \mathbf{H}_1 \mathbf{F}_1 ... \alpha_u \mathbf{T}^{-\mathbf{1}} \mathbf{H}_{N_u} \mathbf{F}_{N_u}]^{\mathrm{T}} \; ; \\ \mathbf{W}_u^{\mathrm{DL}} &= \frac{1}{\alpha_u} \mathbf{F}_u^* \; . \end{aligned} \tag{6.44}$$

6.4.3 Throughput Maximization of a Non-diagonal SDMA

6.4.3.1 Per-user sum rate

The previous MSE minimization does not guarantee independence (diagonalization) across users, which is the tool utilized throughout this thesis to realize adaptive and prioritized transmission. Furthermore, the individual user's streams are not jointly optimized and, hence, cannot be used directly by any of our previously proposed adaptive algorithms. Thus, it is required to minimize the MSE of each stream separately. However, the question here will be: can we make these streams independent? On the one hand, this is a very complex optimization approach. On the other hand, if even complexity is not an issue, it will not be an optimum solution from the capacity point of view. The reason for sub-optimality is the non-convexity of (6.25) in $\{\mathbf{F}_u^s, \mathbf{W}_u^s\}$ (per-stream s) [31], which always results in local minima[11]. Therefore, it is required to imitate, e.g., the block-diagonalization. This virtual diagonalization can only be achieved if the SINR is used in the sum rate formula (instead of the CGNR used in the previous chapters) [31] such that

$$R_u^i = \log_2 \left(1 + \mathrm{SINR}_u\right) \quad \forall \; i \in \{0..N_u - 1\} \; , \tag{6.45}$$

To use the proposed weighted sum-MSE duality, one has to exploit the relation between the SINR and the MMSE. This relation is found, similar to the linear MMSE equalizer derivation given in [15, Chapter 10] or the bijective mapping [79], to be

$$\mathrm{MMSE}_u = \frac{1}{1 + \mathrm{SINR}_u} \; , \tag{6.46}$$

where MMSE_u is the summation of all individual MMSE for the data streams used by user u. Hence, the per-user sum rate given as

$$R_u = -\log_2 \left(\mathrm{MMSE}_u\right) \; . \tag{6.47}$$

This can still give a good estimate for the overall data rate for the u^{th} user's streams without the need for optimizing each stream separately [78]. However, different streams are allocated equally, i.e., using the same power and number of bits.

[11] As it is impossible to merge the individual inverses of $\mathbf{T}$ as we did for achieving (D.13) in Appendix D.

6.4.3.2 UEP bit-loading

Similar to Algorithm 6.1, the $\text{MMSE}_{u,k}$ for each user u and for every subcarrier k are sorted in descending order (from low to high). According to the intuitive sorting scheme, the bits of the first class are allocated to the stronger subcarriers (with the lowest MMSE). Using the formulas (6.47) and (6.7) in Section 6.1.4, the average number of bits allocated to all streams, i.e., bits/user, is given by

$$\hat{b}_{u,k}^{j} \approx \left\lfloor -\log_2\left(\text{MMSE}_{u,k}\gamma_{u,j}\right) + \frac{1}{2} \right\rfloor_0^{b_{\max}}, \tag{6.48}$$

where the u^{th} user's noise margin $\gamma_{u,j}$ is adapted iteratively in order to fulfill the required sum rate, according to Algorithm 6.1, and to preserve the margin separation between the user's different data classes[12]. Since we do not have the per-stream individual MSE information, we are only able to allocate all streams equally. Accordingly, the individual target rate for each stream (of the M_u streams) is T_u/M_u bits, where the target rate for each user is T_u and the target rate of the u^{th} user's j^{th} class is $T_j^u = T_u/N_g = B_T/N_u/N_g$, i.e., assuming that the target rate for all users are equal and the target rate for their classes are also equal. Thus, to allocate each stream (of the given M_u streams) equally, we allocate only $1/M_u$ of the required rate (either per-user or per-class). Thus, $T_j^{u,s} = T_j^u/M_u$ and $T_u^s = T_u/M_u$ [14]. Finally, the

Algorithm 6.3 UEP bit-loading based on the Chow-like algorithm

Ensure: number of subcarrier N, $\mathcal{M} \in \mathbb{Z}^{N\times N_u}$, running indices v, start index $\mathcal{I} = 0$, $\tau_u = N$,l $u = 0..N_u - 1$, middle class $m = \lfloor N_u/2 \rfloor + \frac{1}{2}$ target power P_T, target sum rate B_T, counter Cnt $= 0$, margin separation $\Delta_\gamma = 3$ dB, number of data classes N_g, the class index $j = 0$, and the initial noise margin $\gamma_m = \frac{\overline{\text{MMSE}_u}}{2^{B_T/N}}$, where $\overline{\text{MMSE}}_{u,k} = \frac{\sum_{k=0}^{N-1}\text{MMSE}_{u,k}}{N}$

1: sort the subcarrier according to their MMSE in ascending order in $\mathcal{M}$
2: **repeat**
3: **repeat**
4: compute γ_m (similar to Algorithm 3.7) $\gamma_m^{\text{new}} = 2^{\frac{\sum_{k=0}^{N-1}\log_2\left(\gamma_m^{\text{old}}+\text{MSER}_{u,k}^{-1}-1\right)-B_T}{N}}$
5: compute user u individual γ_u (in dB scale), such that $\gamma_{u_{[dB]}} = \gamma_{m_{[dB]}} + (m-u)\cdot\Delta\gamma_{[dB]}$
6: **repeat**
7: calculate $\hat{b}_{u,v}$ and $v \in \mathcal{M}$, as in (6.48) using γ_u starting from $\mathcal{I}$
8: accumulate $\hat{b}_{u,v}$, $v \in \mathcal{M}$ using cumsum as in Algorithm 3.5 in Chapter 3
9: set τ_u to the location where $\sum_{v=\mathcal{I}}^{\tau_u}\hat{b}_{s,v}^u = T_j^u = B_T/N_g/N_u/M_u$, assuming the same target rate for each user and each class of his classes
10: update $\mathcal{I} \Leftarrow \tau_u + 1$ and $j \Leftarrow j + 1$
11: **until** $j = N_g$
12: Cnt $\Leftarrow$ Cnt $+ 1$
13: **until** $\sum_{\{v\}\in\mathcal{M}} b_{u,v} \approx B_T/N_u/M_u$ or Cnt $=$ MaxCnt
14: $u \Leftarrow u + 1$
15: **until** $u = N_u$

[12] In our simulation, we consider a 3 dB margin separation between each two classes for a given user.

overall target rate $B_T = \sum_{u=0}^{N_u-1} T_u$. In the previous algorithm (Algorithm 6.3 which is based on Algorithm 6.1), we perform the bit-loading considering the user MMSE_u (as in (6.48)) and the arbitrary noise margin γ_u, j, i.e., for user u and his individual j data classes. In this algorithm, the first stream for each user is allocated, as in Algorithm 6.3, using T_u/M_u bits. Thereafter, the computed bit loads are copied to the user's $M_u - 1$ remaining streams.

6.4.3.3 Power allocation

The power allocated via the gradient projection method, proposed in the previous section, is a sub-optimal method due to allocating similar power values across subcarriers with high-SNR [76]. However, we can still reshape the spectral using the power allocation performed by Algorithm 6.1, i.e., based on the bit load values on each subcarrier and the user's margin $\gamma_{u,j}$. Accordingly, no-power is allocated to the users' weaker subcarriers, i.e., with low MMSE. Therefore, the number of users sharing the same subcarriers is reduced, i.e., reduces the MUI on these subcarriers.

6.4.4 Analysis of the Non-diagonal Multiuser with UEP Bit-loading

Figure 6.12 depicts the performance of the non-adaptive prioritized weighted sum-MSE. In this case, $w_0 > w_1 > w_2$, i.e., user_0 has the highest priority and user_2 has the least one. These results have been generated using 2 bits/symbol/stream, i.e., 4 bits/user[13]. One can notice that the

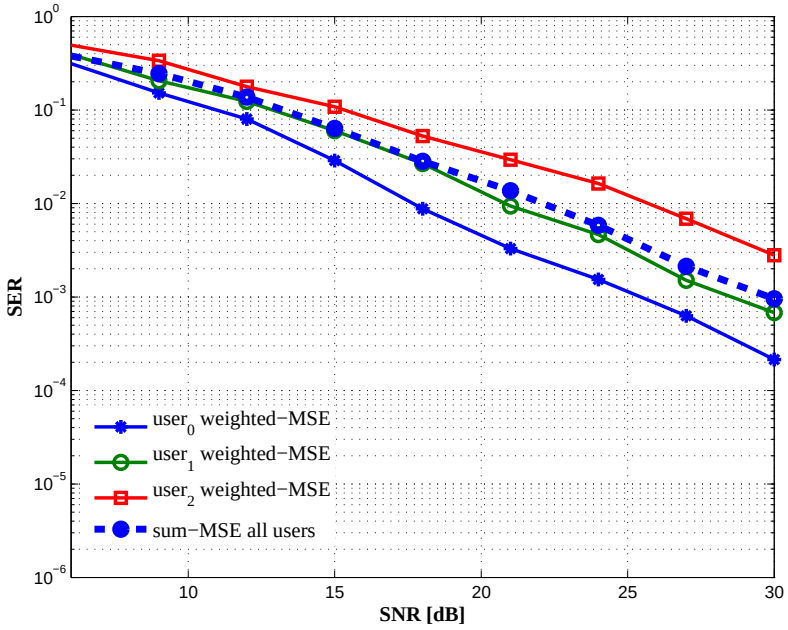

Figure 6.12: Non-adaptive sum-MSE vs weighted MSE with 4 bits/user

[13]In this case we assume an OFDM transmission with 1024 subcarrier an 4 bits/subcarrier/user, i.e., in total 12 bits/subcarrier.

non-weighted sum-MSE minimization (thick dashed-line) performs similar to the middle user, assuming the same number of bits/symbol, i.e., an average of the highest and the lowest priority user.

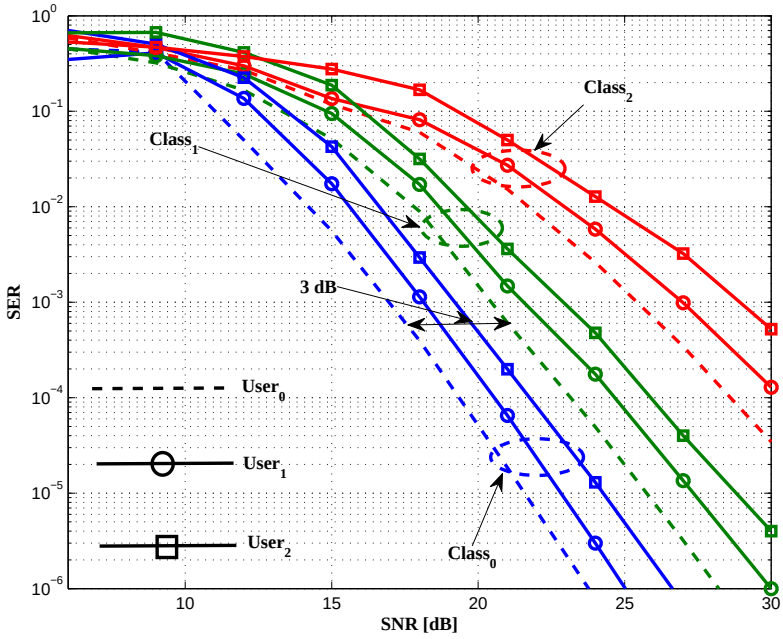

Figure 6.13: SER for 3 users with 3 data priority classes (using UEP) with 1365 bits/class

In Fig. 6.13 (using 4096 bits/user with 1024 subcarrier, i.e., 4 bits/subcarrier in average), the performance of three users with weighted sum-MSE are depicted using UEP bit-loading with 3 priority classes and a margin separation between the users' different data classes equal $\Delta_\gamma = 3$ dB. Thus, one can notice that we achieved a double prioritized transmission. This is performed using the weighted sum-MSE Algorithm 6.4.2 to realize different users with different QoS. Moreover, the UEP bit-loading Algorithm 6.1 is used to realize the users' different data classes with different priorities. We succeed to preserve (almost) equal separations between classes (more than the required 3 dB; rather 4 dB) and the users (~ 1 dB).

The separations between users can be further adapted using different weighting factors w_u. However, this is still a suboptimal procedure, as the bit-loading is performed after these weighting values are computed. Thus, when the number of users changes, i.e., by allocating zero-power to some users, their feasible MMSE points change and, therefore, it changes the separation between them. As a solution, Algorithm 6.4.2 can be repeated once again, at least, for subcarriers where one or more users are transmitting no-power.

Figure 6.14 depicts the same results as in Fig. 6.13, however, compared to the non-adaptive scheme. One can easily notice a performance gain of 12 dB (between the first user's highest protected class and the same user using non-adaptive modulation). However, at very low-SNR subcarriers, the non-adaptive scheme outperforms the adaptive one due to overloading the high-SNR subcarriers. In Fig. 6.15, the UEP bit-loading (using a non-weighted sum-MSE)

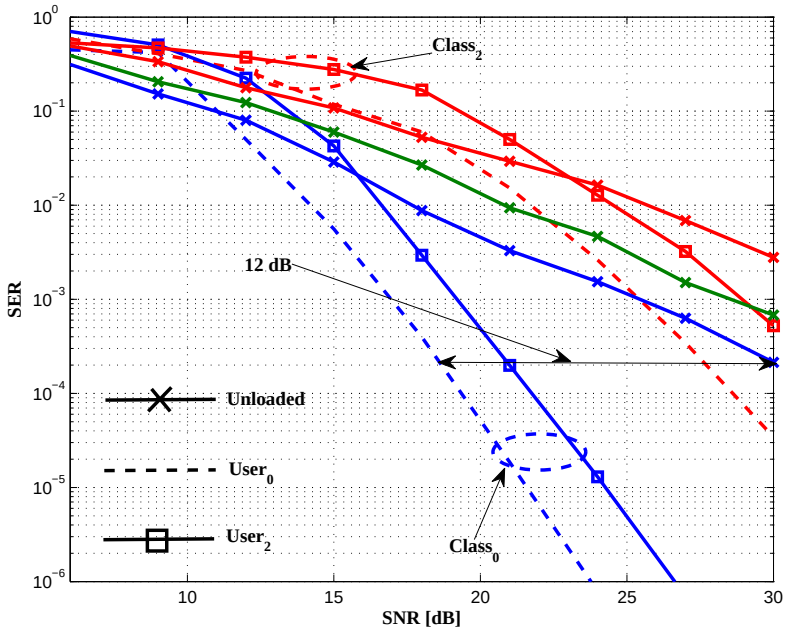

Figure 6.14: SER for adaptive and non-adaptive modulation

is delivering an average performance between the highest and the least protected users with weighted sum-MSE.

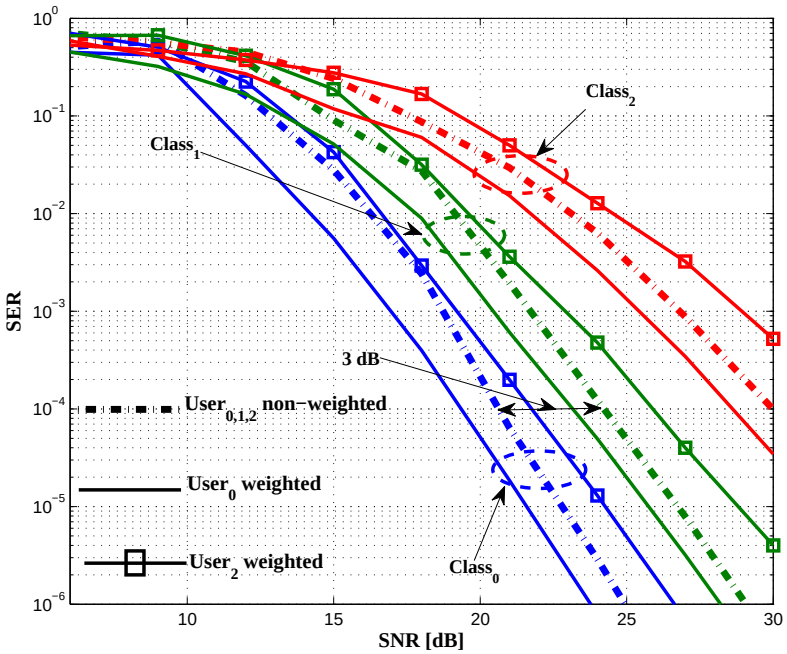

Figure 6.15: Sum-MSE vs weighted sum-MSE using 4 bits/user with 1024 subcarriers

For comparison, we consider a 2×6 MIMO-OFDMA transmission, similar to the one discussed in Section 6.1, using 1024 bits/user and 512 subcarriers. This case is compared to the dual

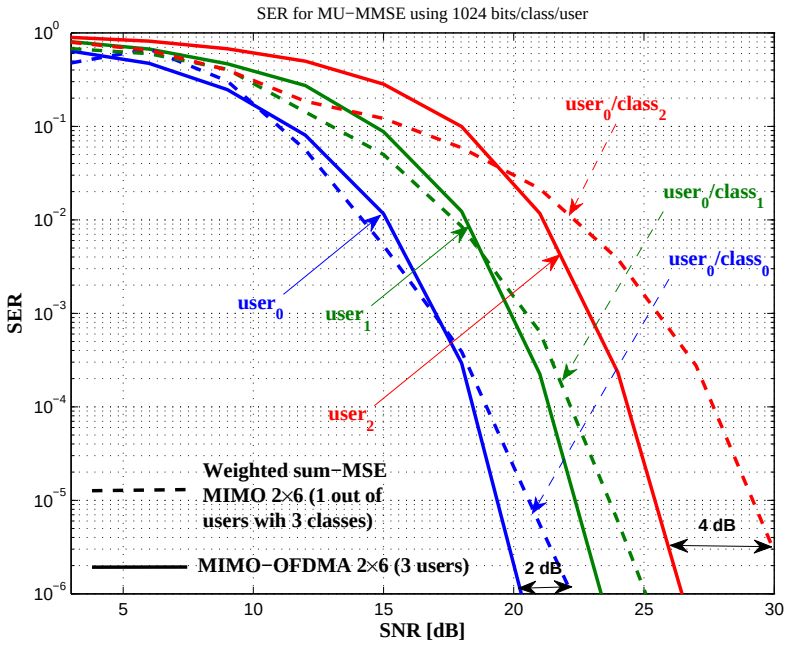

Figure 6.16: Sum-MSE vs weighted MSE using 1024 bits/user with 512 subcarriers

weighted sum-MSE scheme also using 1024 bits/user and 512 subcarriers, however, with extra three classes for each user using 3 classes, i.e., the same number of bits/class. In Fig. 6.16, the MIMO-OFDMA transmission outperforms the non-diagonal multiuser (for his first class) by almost ~ 2 dB. This is because the MIMO-OFDMA utilizes the individual streams, where the bit-loading algorithm allocates fewer, or even zero, bits at the weaker eigenchannels. This is even clearer in the results of the first user's least priority class and the last user using MIMO-OFDMA. In this case, the non-diagonal transmission already consumes the subcarriers with the weakest MMSE, making it almost 4 dB worse than the MIMO-OFDMA least priority user.

However, at low SNR, the non-diagonal MMSE performs better than the OFDMA. This certainly means that our results can be further improved if we consider optimizing the individual streams of each subcarrier, which is out of the scope of this thesis. Another solution could be to switch between both multiple access scheme based on the current SNR, i.e., at low SNR use SDMA and at high SNR use OFDMA.

Chapter 7

Summary and Outlook

7.1 Summary and Conclusions

This thesis was motivated by the need of understanding and investigating the advantages and the limitations of prioritized transmission. Several approaches had been proposed to obtain unequal error protection utilizing the diagonalized transmission systems using uncoded adaptive techniques. Consequently, adaptive OFDM and diagonalized SVD MIMO have been implemented for both single-user and multiuser scenarios utilizing non-interfering sub-channels in frequency and space. In order to realize unequal error protection (UEP), we implemented several adaptation methods by modifying, extending, and optimizing the preexisting adaptive modulation algorithms in order to devote different data segments to different error protection levels.

In our results, we chose to fulfill a given UEP profile that allowed different SNR operating points for different data classes or users. Exploiting the UEP capabilities using only adaptive modulation reduces the extra complexity, which would otherwise be needed for UEP coding. Moreover, our developed algorithms are found to be more precise than the UEP channel coding approaches in preserving the given margin separations. The major contributions of this thesis can be summarized as follows:

- Assuming a single-user model with SISO-OFDM(DMT) transmission, we described a set of UEP bit-loading schemes that allowed for arbitrary margin separations among different bit streams of different priorities using a simple subcarrier partitioning scheme, i.e., Chow-like and Fischer-like UEP bit-loading. They further allowed to devote an arbitrary number of bits to these classes. We implemented these schemes assuming different transmission media. First, we assumed a VDSL-like environment with stationary and non-stationary noise. Our proposed robust-sorting scheme ensured that the high-priority class is still well protected even under non-stationary noise conditions. This resulted in somewhat worse performance under stationary conditions although the performance under non-stationary conditions was encouraging for further investigations in different media and under different

non-stationary noise. Second, we explored the performances of these techniques under wireless Rayleigh fading channels using OFDM.

We also succeeded in implementing the same prioritized adaptation modifying the greedy algorithm (by Hughes-Hartogs) and the semi-greedy (by Campello), based on our proposed simple subcarriers partitioning. Thus, the computationally efficient Campello-like UEP bit-loading can be thought of as a practical solution for wireless systems with limited (quantized) channel feedback. This has become even more feasible after our proposed non-integer relaxation.

- We implemented the same UEP adaptive modulation for MIMO-OFDM as a two-dimensional channel adaptation by allocating arbitrary numbers of bits with different priorities to eigenchannels. We also allowed for arbitrary margin definitions according to the same UEP profile considering 3-dB separations between classes as an example. The reduced order beamforming enhanced the performance compared to full length beamforming in case of channel state information errors and high antenna correlation. This was achieved by suppressing of the weaker eigenchannels, which were more susceptible to inter-eigen interference.

  When robust subcarrier sorting was used for imperfect channel state information, the weaker eigenchannels were also suppressed. The size of the eigen-beamforming automatically shrinks as the high priority data is allocated to the weaker eigenchannels. This is also capable of protecting the system against channel state information variations on the weaker eigenchannels.

  In order to mitigate the inter-eigen interference, we adopted V-BLAST to our design to act as a successive interference cancellation controlling our adaptive (precoded) scheme. The adaptive V-BLAST MIMO succeeded in outperforming the traditional precoded adaptive MIMO systems. Moreover, it fulfilled the proposed UEP profile better preserving the margin separations.

- As a follow-up investigation of imperfect channel state information, we considered using the channel covariance feedback. This was achieved by allocating an arbitrary number of bits with different noise margins to different eigenbeams over a number of subcarriers. In this case, we observed that the margin separations were not strictly preserved as in perfect channel state information. Nevertheless, the order of the classes was kept the same with sufficient margin separations.

  Furthermore, the robust bit-loading outperformed the intuitive method by exploiting its implicit diversity-multiplexing trade-off. Consequently, it reduces the inter-eigen interference, and approached an optimum performance in the case of a single eigenbeam channel. This also outperformed the adaptive V-BLAST using covariance feedback, where the latter did not succeed in preserving the 3 dB separations.

- Our multilevel modulation succeeded in eliminating the subcarrier partitioning by embedding different layers within each other in a hierarchical fashion. This was very useful for

realizing UEP by means of a greedy bit-loading algorithm. Thus, we modified the Hughes-Hartogs algorithm to realize UEP adaptive multilevel modulation allowing for arbitrary margin separations. Due to its capabilities of reducing the computational complexity, the bit-loading algorithm by Campello was likewise modified to realize UEP. The results of the MIMO-OFDM with a limited feedback showed that the 2-D beamforming outperforms the full eigen-beamforming.

- Utilizing a simple subcarrier grouping, as with the proposed Fischer-like UEP bit-loading, a two-users model with different QoS has been implemented using SISO-OFDMA. The OFDMA transmission has been considered to maintain the user orthogonality. We were able to realize a modern prioritized wireless multiuser systems with multiple QoSs, using only adaptive modulation.

  Furthermore, we modified the Chow-like UEP bit-loading for multiuser MIMO-OFDMA to realize different users with different QoSs. We presented two different sorting schemes, the eigen-product, which maximizes the sum rate by sorting the subcarrier based on the product of their eigenvalues, and the rank-1 sorting, which sorts the subcarriers according to the maximum eigenbeam. Both schemes succeeded in preserving the margin separation strictly, i.e., in perfect channel state information conditions, where the eigen-product outperformed the other method by 3 dB. However, considering a limited feedback regime with self-interference due to channel state information errors, the eigen-product sorting scheme started to have a wider separation. Moreover, an error floor started to appear at high SNRs. In contrast to this, the rank-1 sorting preserved the margin more strictly in such noisy channel state information without any noticeable error floor.

- We extended our multiuser transmission to consider the orthogonal block-diagonalized space-division multiple access (SDMA) to eliminate multiuser interference. We succeeded in preserving our given QoS constraint under perfect channel conditions using UEP adaptive multilevel modulation. For imperfect channel state information, the margin separations became wider, where the overall performance deteriorated due to smearing the other users' noise as a results of using zero-forcing (ZF) or minimum mean-square error (MMSE) receivers. The proposed adaptive scheme outperformed the vector broadcast (non-adaptive) transmission scheme, i.e., assuming the same data-rates and channel conditions.

- Finally, we succeeded in providing a double-prioritized adaptive UEP transmission using a non-orthogonal SDMA transmission. Thus, a weighted MMSE, utilizing the MAC-BC duality, succeeded to realize different QoSs. Additionaly, a UEP bit-loading, i.e., based on the modified Chow-like algorithm, allowed for distinct margin separations for each user's different data classes. Our adaptive multiuser MIMO-OFDM SDMA outperformed the non-adaptive case by almost 12 dB. That was due to utilizing the stronger subcarriers and limiting the number of users on the weaker ones, i.e., with the high mean-square error.

7.2 Future Work

This thesis has focused on realizing UEP in diagonalized and non-diagonalized transmission. However, there are still more issues to be studied separately or as an extension to our work. In the following, we sketch these topics that would be interesting to study in the future.

1. It is important to investigate more the non-orthogonal SDMA and combine it with a per-user/per-stream adaptation using practical UEP profiles. Strictly speaking, the investigation of SINR duality [31] may lead to better switching between multiplexing schemes by studying the SINR switching thresholds according to the feasible SINR range and the given QoS for either users or their data.

2. It is also important to study more the channel state information uncertainty and to investigate the suitability of delivering a closed form expression to simplify the calculations needed for realizing a robust transmission that utilizes the different QoS between users.

3. It is interesting to study the combination of different coding schemes, while preserving the UEP profile. Especially, the co-design of adaptive modulation and LDPC codes looks promising. It is known well that irregular LDPC codes have a better performance. However, the irregularities do not need to come from the code itself, but can also partly come from the channel, i.e., from different SNRs. Thus, with our UEP bit allocation methods, we can easily modify the channel properties, which will in the end simplify the LDPC design.

4. Our proposed schemes can be used for security applications, since one could design a UEP profile that is reliably decodable within a certain environment, e.g., inside a room or a building or even between separated robots and wireless sensors, however, there would be almost nothing useful received outside these regions. With our UEP methods, we would be able to generate many levels of security and reliable communication that suit many modern networking applications.

Appendix A

Binary Search

The iterative process to find the exact τ_j in the set $\mathcal{M}$ to fulfill the individual target rates T_j by performing binary search as follows

Algorithm A.1 Binary search

Initialize: $\tau_j = N$, starting index $\mathcal{I} = 0$, and $\mathcal{M} = \text{sort}(\mathcal{G}_k)$, $j = 0..N_g - 1$

Input: number of sub carriers N

Output: τ_j and $\mathcal{M}_j$

reset the class counter j to zero
repeat
  repeat
    find the number of bits in the set $\mathcal{M}_j = \mathcal{M}(\mathcal{I} : \tau_j)$: $\sum_{k\in\mathcal{M}_j} \hat{b}_k^j$
    if $\sum_{k\in\mathcal{M}} \hat{b}_k^j > T_j$ **then**
      divide the set $\mathcal{M}$ to half and move the threshold τ_j to this index
    else if $\sum_{k\in\mathcal{M}} \hat{b}_k^j < T_j$ **then**
      divide the next $N_g - 1 - j$ classes into half and move the threshold τ_j to this index
    end if
  until $\sum_{k\in\mathcal{M}} \hat{b}_k^j = T_j$
  $\mathcal{M}_j = [\mathcal{M}(\mathcal{I}), \mathcal{M}(\mathcal{I}+1), ..., \mathcal{M}(\tau_j)]$
  update the starting index: $\mathcal{I} = \tau_j + 1$
  the remaining subcarriers are divided equally, such that , $\tau_{j+1} = \tau_j + \frac{N-\tau_j}{2}$
  Increment j: $j \Leftarrow j + 1$
until $j = N_g$

Notes

The number of bits in the last class, i.e., $\mathcal{M}_{N_g-1}$, is allowed to slightly vary (than T_{N_g-1}) such that B_T is fulfilled.

Appendix B

Equivalent Sum Rate Calculations

.

Example 1: Assuming an odd number of classes (e.g., 3) with individual target rates T_j ($B_T = \sum_{j=0}^{2} T_j$) and 3 dB margin separations, i.e., linear $\Delta_\gamma = 2$ such that $\gamma_j = 2\gamma_{j+1}$. Therefore, the approximated sum rate after omitting the one in the Shannon capacity formula is given as

$$\begin{aligned} B_T &= T_0 + T_1 + T_2 \\ &= \sum_{k=0}^{\tau_0-1} \log_2 \frac{\mathcal{G}_k}{\gamma_0} + \sum_{k=\tau_0+1}^{\tau_1} \log_2 \frac{\mathcal{G}_k}{\gamma_0/2} + \sum_{k=\tau_1+1}^{N-1} \log_2 \frac{\mathcal{G}_k}{\gamma_0/4} \\ &= \sum_{k=0}^{N-1} \log_2 \frac{\mathcal{G}_k}{\gamma_0} + \sum_{k=\tau_0+1}^{\tau_1} \log_2 2 + \sum_{k=\tau_1+1}^{N-1} \log_2 4 \\ &= B_{T_0} + L_{\mathcal{M}_1} + 2\, L_{\mathcal{M}_2}\,. \end{aligned} \tag{B.1}$$

Now, assuming that the subcarriers (on average) are equally divided over the given classes, i.e., $L_{\mathcal{M}_0} = L_{\mathcal{M}_1} = ... = L_{\mathcal{M}_{N_g-1}}$, thus, $L_{\mathcal{M}_1} + 2\, L_{\mathcal{M}_2} \approx N$. Hence,

$$B_T \approx B_{T_0} + N\,. \tag{B.2}$$

Following the same approximation in Eqn. (B.1) and starting with γ_1 (middle class), we find that, $B_T \approx B_{T_1}$. Similarly, when we start with γ_2 we obtain $B_T \approx B_{T_2} - N$.

For even number of classes, an extra interpolation, one hypothetical class between each two, is need to convert it into odd. This make it similar to the previous computation.

Example 2: For 4 levels with 3 dB separation, one has to interpolate 3 extra levels, i.e., a level between each two. The separation between the resultant level is only 1.5 dB, i.e., linear $\Delta_\gamma = \sqrt{2}$. Similar to the previous calculations, the equivalent rates of the four original classes are $B_{T_0} \approx B_T - 3/2N$, $B_{T_1} \approx B_T - 1/2N$, $B_{T_2} \approx B_T + 1/2N$, and $B_{T_3} \approx B_T + 3/2N$.

Appendix C

Hierarchical Modulation Power Allocation

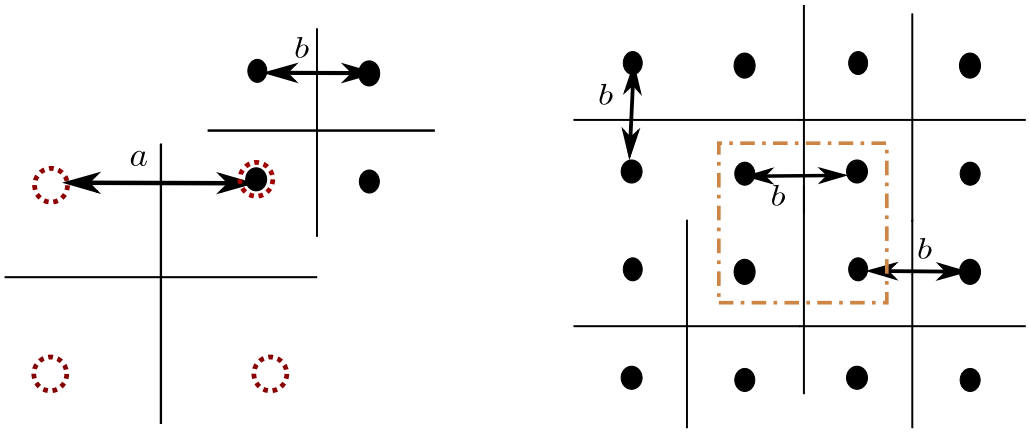

Figure C.1: Hierarchical (4/16-QAM) and non-hierarchical (16-QAM) square constellation

From the previous figure, we can easily calculate the average power of the 4-QAM, with a minimum Euclidean distance of a, as follows:

$$E_{\text{QAM}}^{\text{av}} = \frac{a^2}{2} \,, \tag{C.1}$$

and the average power after allocating 2 more bits to the second level, i.e., with a minimum Euclidean distance b using hierarchical-QAM (HQAM), by extending the previous formula as

$$E_{\text{HQAM}}^{\text{av}} = \frac{1}{4}\left(2a^2 + 4b^2 + 4ab\right) = \frac{a^2}{2} + b^2 + ab \,. \tag{C.2}$$

Thus, the incremental power needed for allocating the extra 2 bits, i.e., to the second level, is

$$\Delta_{E_{\text{HQAM}}^{ab}} = \frac{a^2}{2} + b^2 + ab - \frac{a^2}{2} = ab + b^2 \,. \tag{C.3}$$

Let us assume a homogenous modulation, as depicted in Fig. C.1 (on the right hand side), with a 4-QAM, i.e., the small dashed square in the middle. The average power is given by

$$E_{\text{QAM}}^{\text{av}} = \frac{b^2}{2} \,. \tag{C.4}$$

However, the average power needed for adding another 2 more bits, i.e., with the same a minimum Euclidean distance b, to change it into a 16-QAM, is given by

$$E_{\text{QAM}}^{\text{av}} = \frac{b^2}{2} + 2b^2 \ . \tag{C.5}$$

Thus, the incremental power needed for adding these 2 bits is given by

$$\Delta_{E_{\text{QAM}}^{b}} = 2b^2 \ . \tag{C.6}$$

Assuming that $a > b$ (as we proposed in Chapter 4), therefore

$$ab + b^2 > b^2 + b^2 \ , \tag{C.7}$$

which means that

$$\Delta_{E_{\text{QAM}}^{b}} < \Delta_{E_{\text{HQAM}}^{ab}} \ , \tag{C.8}$$

for the same number of bits per-symbol, i.e., 4 bits in both cases. This also means that the incremental power of the homogenous modulation can be considered as a lower bound to the incremental power in case of hierarchical modulation with quadratic constellations, i.e., when both extensions preserve the same distance b.

For a single bit addition, starting from a quadratic constellation, the final constellation does not have a square form anymore. Thus, in the following we show that the previous observation is also valid for non-quadratic cases as well. Now, let us depict the 2/4-HQAM, where it looks like a PAM with 45° phase shift.

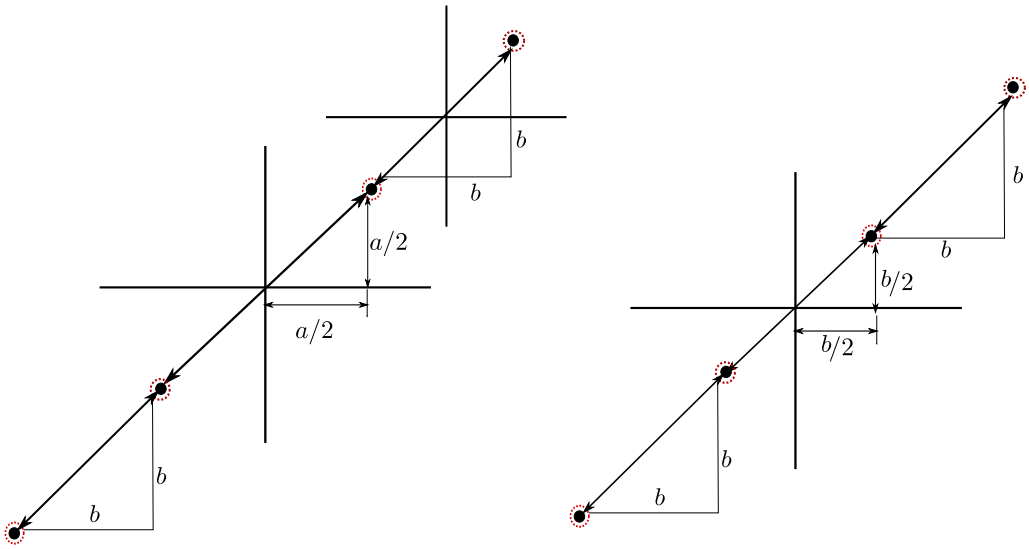

Figure C.2: Hierarchical (4/16-QAM) and non-hierarchical (16-QAM) non-square constellation

For the special case depicted in Fig. C.2, the average power is identical to the previous quadratic case, i.e., (C.1)-(C.7) apply to this case. Hereto, $\Delta_{E_{\text{QAM}}^{b}} < \Delta_{E_{\text{HQAM}}^{ab}}$, which also means that the incremental power for the homogenous constellation in order to address an extra bit with a minimum distance b, e.g., achieving a 4-PAM-like in this case, is a lower bound to the increment in power needed for an equivalent hierarchical constellation, e.g., the left hand-side constellation in Fig. C.2.

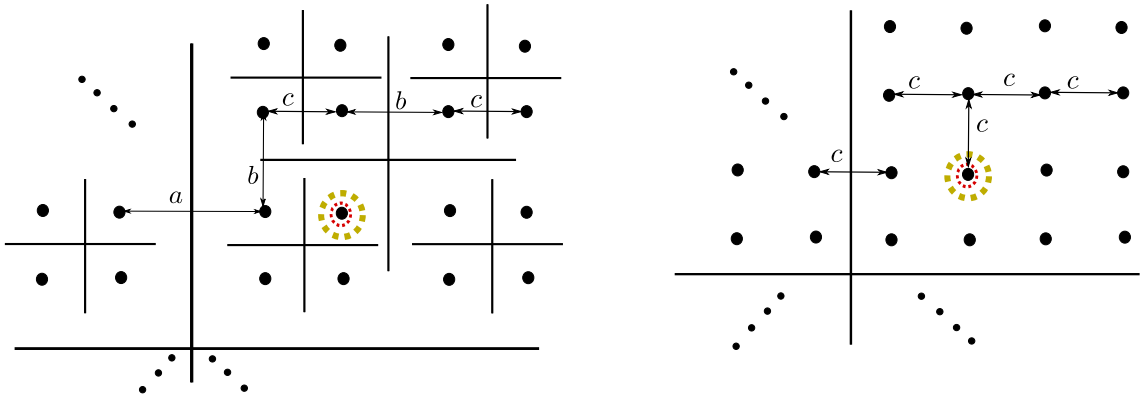

Figure C.3: Hierarchical (4/16-QAM) and non-hierarchical (16-QAM) non-square constellation

Similarly, we can extend the previous results to a third hierarchical class with a minimum Euclidean distance c. In Fig. C.3, we depict (on the left hand-side) a 3-layer hierarchical constellation with 3 different separations, i.e., a, b, and c. On the right hand-side of the same figure, a 64-QAM using a minimum distance equal to c, is depicted. From (C.2) and (C.5) we know the average power of the hierarchical modulation 4/16-QAM (two bits less than what is depicted in Fig. C.3) and the 16-QAM homogenous modulation. Thus, for HQAM, the incremental power needed, for allocating another 2 more, to the power calculated in (C.2) will lead to an average power equal to

$$\begin{aligned} E^{\text{av}} \cdot 16 &= 2a^2 + 4ac + 4c^2 \\ &+ \left(2a^2 + 8ac + 14c^2 + 4b^2 + 14cb + 4ab\right) \cdot 2 \\ &+ 2a^2 + 12ac + 20c^2 + 8b^2 + 24cb + 8ab \\ &= 8a^2 + 32ac + 48c^2 + 16b^2 + 48cb + 16ab \,. \end{aligned} \tag{C.9}$$

Finally, the average energy is given by

$$E^{\text{av}} = a^2/2 + ab + b^2 + 48c^2 + 32ac + 48cb \,, \tag{C.10}$$

and the incremental power to add these two extra bits is found by subtracting (C.2) from (C.10)

$$\Delta_{E^{abc}_{\text{HQAM}}} = E^{\text{av}} - a^2/2 + ab + b^2 = 48c^2 + 32ac + 48cb \,. \tag{C.11}$$

Similarly, we can find the average power of the non-hierarchical modulation (Fig. C.3, right hand-side) by substituting with $a = b = c$. Hence, we get

$$E^{\text{av}} = c^2/2 + 2c^2 + 48c^2 + 32c^2 + 48c^2 \,, \tag{C.12}$$

and the incremental power to extend the 16-QAM to 64-QAM is given by

$$\Delta_{E^{c}_{\text{QAM}}} = E^{\text{av}} - c^2/2 + 2c^2 = 48c^2 + 32c^2 + 48c^2 \,. \tag{C.13}$$

Assuming that $a > b > c$, the incremental power of the homogenous modulation can also be considered as a lower bound to the incremental power in the equivalent hierarchical case, i.e, with extension by c.

Finally, the incremental power factor can be exactly computed using the ratios between the hierarchical distances, e.g., for a 3 dB separations, $a = \sqrt{2} \cdot b = 2 \cdot c$. In this case, for 3 levels with $a, a/\sqrt{2}$, and $a/2$, we get

$$\Delta_{E^c_{\text{QAM}}} = a^2/4(128) = 32a^2 \ , \tag{C.14}$$

and

$$\Delta_{E^{abc}_{\text{HQAM}}} = 48a^2/4 + 32a^2/2 + 48a^2/(2\sqrt{(2)}) \approx 45a^2 \ . \tag{C.15}$$

Therefore,

$$\Delta_{E^{abc}_{\text{HQAM}}} = 45/32\Delta_{E^c_{\text{QAM}}} \ . \tag{C.16}$$

One can compute this relations for any hierarchical configuration, where the incremental power of either 1 or 2 bits is related to the non-hierarchical one, i.e., using the equivalent distance of this new bits, as follows

$$\Delta_{E_{\text{HQAM}}} = \beta\Delta_{E_{\text{QAM}}} \ , \tag{C.17}$$

where $\beta \geq 1$.

Appendix D

Multiuser Water-filling Using the MMSE Criterion

The pre-processing matrix $\mathbf{F} = \mathbf{U}_{\mathbf{F}}\mathbf{\Phi}_{\mathbf{F}}$ (defined in Chapter 2) of the BD scheme ensures both orthogonality and power optimization. The post-processing matrix $\mathbf{W}_u$ (for the dual uplink) is assumed to be an MMSE spatial equalizer, such that

$$\mathbf{W}_u = \mathbf{F}_u^*\mathbf{H}_u^* \left[\sigma_n^2\mathbf{I}_{N_R} + \sum_{i=0}^{N_u-1} \mathbf{F}_i\mathbf{H}_i\mathbf{F}_i^*\mathbf{H}_i^*\right]^{-1} = \mathbf{F}_u^*\mathbf{H}_u^*\mathbf{T}^{-1} \, . \tag{D.1}$$

Thus, the equalized received vector $\mathbf{r}_u$ of the u^{th} user is given by

$$\hat{\mathbf{x}}_u \;\; = \;\; \mathbf{W}_u \sum_{i=0}^{N_u-1} \mathbf{H}_i\mathbf{F}_i\mathbf{x}_i + \mathbf{W}_u\mathbf{n}_u \, . \tag{D.2}$$

where the vector $\mathbf{x}$ contains the symbols of all users and $\mathbf{W}_u$ is given by (D.1). To obtain the optimal $\mathbf{F}_u$ and $\mathbf{W}_u$, we use the joint transmit-receive optimization, proposed in Chapter 6. Therefore, it is required to minimize the following sum-MSE on $\mathbf{R}_u = \mathbf{F}\mathbf{F}^*$

$$\begin{array}{ll} \underset{\mathbf{R}_u}{\text{minimize}} & \text{Tr}\left(E\left[||\hat{\mathbf{x}}_u - \mathbf{x}_u||^2\right]\right) \\ \text{subject to} & \text{Tr}\left(\mathbf{R}_u\right) = \text{Tr}\left(\mathbf{F}_u\mathbf{F}_u^*\right) = \text{Tr}\left(\mathbf{F}_u^*\mathbf{F}_u\right) = P_m \, . \end{array} \tag{D.3}$$

To solve (D.3) considering an MMSE receiver, we need to study the dual uplink channel as stated in Chapter 2, where the error covariance matrix is given by

$$\begin{aligned} \mathbf{R}_E^u &= E\left(\left(\hat{\mathbf{x}}_u - \mathbf{x}_u\right)\left(\hat{\mathbf{x}}_u - \mathbf{x}_u\right)^*\right) = E\left(\hat{\mathbf{x}}_u\hat{\mathbf{x}}_u^*\right) + E\left(\mathbf{x}_u\mathbf{x}_u^*\right) - E\left(\hat{\mathbf{x}}_u\mathbf{x}_u^*\right) - E\left(\mathbf{x}_u\hat{\mathbf{x}}_u^*\right) \\ &= E\left(\left(\mathbf{W}_u\sum_{i=0}^{N_u-1}\mathbf{H}_i\mathbf{F}_i\mathbf{x}_i + \mathbf{W}_u\mathbf{n}_u\right)\left(\sum_{i=0}^{N_u-1}\mathbf{x}_i^*\mathbf{F}_i^*\mathbf{H}_i^*\mathbf{W}_u^* + \mathbf{n}_u^*\mathbf{W}_u^*\right)\right) + E\left(\mathbf{x}_u\mathbf{x}_u^*\right) \\ &- E\left(\left(\mathbf{W}_u\sum_{i=0}^{N_u-1}\mathbf{H}_i\mathbf{F}_i\mathbf{x}_i + \mathbf{W}_u\mathbf{n}_u\right)\mathbf{x}_u^*\right) - E\left(\mathbf{x}_u\left(\sum_{i=0}^{N_u-1}\mathbf{x}_i^*\mathbf{F}_i^*\mathbf{H}_i^*\mathbf{W}_u^* + \mathbf{n}_u^*\mathbf{W}_u^*\right)\right) \, , \end{aligned} \tag{D.4}$$

where there is no correlation between the noise and the input or the output data $\mathbf{x}_u$ and $\hat{\mathbf{x}}_u$, we obtain

$$\begin{aligned}\mathbf{R}_E^u &= E\left(\mathbf{W}_u \sum_{i=0}^{N_u-1} \mathbf{H}_i\mathbf{F}_i\mathbf{x}_i \sum_{j=1}^{N_u} \mathbf{x}_j^*\mathbf{F}_j^*\mathbf{H}_j^*\mathbf{W}_u^*\right) + \mathbf{W}_u E\left(\mathbf{n}_u\mathbf{n}_u^*\right)\mathbf{W}_u^* + E\left(\mathbf{x}_u\mathbf{x}_u^*\right) \\ &- E\left(\mathbf{W}_u \sum_{i=0}^{N_u-1} \mathbf{H}_i\mathbf{F}_i\mathbf{x}_i\mathbf{x}_u^*\right) - E\left(\mathbf{x}_u \sum_{i=0}^{N_u-1} \mathbf{x}_i^*\mathbf{F}_i^*\mathbf{H}_i^*\mathbf{W}_u^*\right) . \end{aligned} \tag{D.5}$$

Assuming an identity input covariance matrix $\mathbf{I}$ and a noise covariance matrix $\sigma_n^2\mathbf{I}$, we get

$$\begin{aligned}\mathbf{R}_E^u &= \mathbf{W}_u \sum_{i=0}^{N_u-1} \mathbf{H}_i\mathbf{F}_i E\left(\mathbf{x}_i\mathbf{x}_i^*\right)\mathbf{F}_i^*\mathbf{H}_i^*\mathbf{W}_u^* + \mathbf{W}_u E\left(\mathbf{n}_u\mathbf{n}_u^*\right)\mathbf{W}_u^* + E\left(\mathbf{x}_u\mathbf{x}_u^*\right) \\ &- \mathbf{W}_u\mathbf{H}_u\mathbf{F}_u E\left(\mathbf{x}_{i=u}\mathbf{x}_u^*\right) - E\left(\mathbf{x}_u\mathbf{x}_{i=u}^*\right)\mathbf{F}_u^*\mathbf{H}_u^*\mathbf{W}_u^* . \end{aligned} \tag{D.6}$$

Finally, we get

$$\mathbf{R}_E^u = \mathbf{W}_u \sum_{i=0}^{N_u-1} \mathbf{H}_i\mathbf{F}_i\mathbf{F}_i^*\mathbf{H}_i^*\mathbf{W}_u^* + \sigma_n^2\mathbf{W}_u\mathbf{W}_u^* + \mathbf{I} - \mathbf{W}_u\mathbf{H}_u\mathbf{F}_u - \mathbf{F}_u^*\mathbf{H}_u^*\mathbf{W}_u^* , \tag{D.7}$$

After substituting with $\mathbf{W}_{=}\mathbf{F}_u^*\mathbf{H}_u^*\mathbf{T}^{-1}$ (given by (D.1)) in (D.7), we find that

$$\begin{aligned}\mathbf{R}_E^u &= \mathbf{I} + \mathbf{F}_u^*\mathbf{H}_u^*\mathbf{T}^{-1} \sum_{i=0}^{N_u-1} \mathbf{H}_i\mathbf{F}_i\mathbf{F}_i^*\mathbf{H}_i^*\mathbf{T}^{*^{-1}}\mathbf{H}_u\mathbf{F}_u + \sigma_n^2\mathbf{F}_u^*\mathbf{H}_u^*\mathbf{T}^{-1}\mathbf{T}^{*^{-1}}\mathbf{H}_u\mathbf{F}_u \\ &- \mathbf{F}_u^*\mathbf{H}_u^*\mathbf{T}^{-1}\mathbf{H}_u\mathbf{F}_u - \mathbf{F}_u^*\mathbf{H}_u^*\mathbf{T}^{*^{-1}}\mathbf{H}_u\mathbf{F}_u , \end{aligned} \tag{D.8}$$

The MSE is found by applying the trace operator to the error covariance matrix, i.e., $\mathrm{Tr}\left(\mathbf{R}_E^u\right)$. Therefore, the MSE is given by

$$\begin{aligned}E_u^{\mathrm{UL}} = \mathrm{Tr}\left(\mathbf{R}_E^u\right) &= \mathrm{Tr}\left(\mathbf{I} + \mathbf{F}_u^*\mathbf{H}_u^*\mathbf{T}^{-1} \sum_{i=0}^{N_u-1} \mathbf{H}_i\mathbf{F}_i\mathbf{F}_i^*\mathbf{H}_i^*\mathbf{T}^{*^{-1}}\mathbf{H}_u\mathbf{F}_u + \sigma_n^2\mathbf{F}_u^*\mathbf{H}_u^*\mathbf{T}^{-1}\mathbf{T}^{*^{-1}}\mathbf{H}_u\mathbf{F}_u\right) \\ &- \mathrm{Tr}\left(\mathbf{F}_u^*\mathbf{H}_u^*\mathbf{T}^{-1}\mathbf{T}^*\mathbf{T}^{*^{-1}}\mathbf{H}_u\mathbf{F}_u + \mathbf{F}_u^*\mathbf{H}_u^*\mathbf{T}^{-1}\mathbf{T}\mathbf{T}^{*^{-1}}\mathbf{H}_u\mathbf{F}_u\right) \\ &= \mathrm{Tr}\left(\mathbf{I} + \mathbf{F}_u^*\mathbf{H}_u^*\mathbf{T}^{-1}\left(\left[\sum_{i=0}^{N_u-1} \mathbf{H}_i\mathbf{F}_i\mathbf{F}_i^*\mathbf{H}_i^* + \sigma_n^2\mathbf{I}\right] - \mathbf{T} - \mathbf{T}^*\right)\mathbf{T}^{*^{-1}}\mathbf{H}_u\mathbf{F}_u\right) \\ &= \mathrm{Tr}\left(\mathbf{I} + \mathbf{F}_u^*\mathbf{H}_u^*\mathbf{T}^{-1}\left(-\mathbf{T}^*\right)\mathbf{T}^{*^{-1}}\mathbf{H}_u\mathbf{F}_u\right) \\ &= \mathrm{Tr}\left(\mathbf{I} - \mathbf{F}_u^*\mathbf{H}_u^*\mathbf{T}^{-1}\mathbf{H}_u\mathbf{F}_u\right) . \end{aligned} \tag{D.9}$$

Finally, the user u MSE is given by

$$E_u^{\mathrm{UL}} = \mathrm{Tr}\left(\mathbf{I} - \mathbf{F}_u^*\mathbf{H}_u^*\left[\sigma_n^2\mathbf{I}_{N_R} + \sum_{i=0}^{N_u-1} \mathbf{F}_i\mathbf{H}_i\mathbf{F}_i^*\mathbf{H}_i^*\right]^{-1}\mathbf{H}_u\mathbf{F}_u\right) , \tag{D.10}$$

where the sum-MSE for the dual uplink channel is given by

$$\begin{aligned}E^{\mathrm{UL}} &= \sum_{i=0}^{N_u-1} E_i^{\mathrm{UL}} \\ &= \sum_{u=0}^{N_u-1} \mathrm{Tr}\left(\mathbf{I} - \mathbf{F}_u^*\mathbf{H}_u^*\left[\sigma_n^2\mathbf{I}_{N_R} + \sum_{i=0}^{N_u-1} \mathbf{F}_i\mathbf{H}_i\mathbf{F}_i^*\mathbf{H}_i^*\right]^{-1}\mathbf{H}_u\mathbf{F}_u\right) . \end{aligned} \tag{D.11}$$

Since the trace operator is invariant under cyclic permutations (as in Appendix G, Lemma G.1.4), one can rewrite (D.11) as

$$\begin{aligned}\mathrm{MSE}^{\mathrm{UL}} &= \sum_{u=0}^{N_u-1} M_u - \sum_{u=0}^{N_u-1} \mathrm{Tr}\left(\left[\sigma_n^2\mathbf{I}_{N_R} + \sum_{i=0}^{N_u-1}\mathbf{F}_i\mathbf{H}_i\mathbf{F}_i^*\mathbf{H}_i^*\right]^{-1}\mathbf{H}_u\mathbf{F}_u\mathbf{F}_u^*\mathbf{H}_u^*\right)\\ &= \sum_{u=0}^{N_u-1} M_u - \sum_{u=0}^{N_u-1} \mathrm{Tr}\left(\left[\sum_{u=0}^{N_u-1}\mathbf{H}_u\mathbf{R}_u\mathbf{H}_u^* + \sigma_n^2\mathbf{I}\right]^{-1}\mathbf{H}_u\mathbf{R}_u\mathbf{H}_u^*\right)\ , \end{aligned} \tag{D.12}$$

where $\mathbf{R}_u = \mathbf{F}\mathbf{F}^*$. Knowing that the trace of a (square or Hermitian) matrix is equivalent to the sum of the eigenvalues (Lemma G.1.10 and G.1.11), one can simplify (D.12) to be

$$\begin{aligned}\mathrm{MSE}^{\mathrm{UL}} &\equiv \sum_{u=0}^{N_u-1} M_u - \sum_{z=0}^{N_T-1}\frac{\lambda_z^2\rho_z^2}{\lambda_z^2\rho_z^2+\sigma_n^2}\\ &= \sum_{u=0}^{N_u-1} M_u - \sum_{z=0}^{N_T-1}\frac{(\lambda_z^2\rho_z^2+\sigma_n^2)-\sigma_n^2}{\lambda_z^2\rho_z^2+\sigma_n^2}\\ &= \sum_{u=0}^{N_u-1} M_u - \sum_{z=0}^{N_T-1}\frac{(\lambda_z^2\rho_z^2+\sigma_n^2)-\sigma_n^2}{\lambda_z^2\rho_z^2+\sigma_n^2}\\ &= \sum_{u=0}^{N_u-1} M_u - N_T + \sum_{z=0}^{N_T-1}\frac{\sigma_n^2}{\lambda_z^2\rho_z^2+\sigma_n^2}\\ &\equiv \sum_{u=0}^{N_u-1} M_u - N_T + \sigma_n^2\mathrm{Tr}\left(\left[\sum_{u=0}^{N_u-1}\mathbf{H}_u\mathbf{R}_u\mathbf{H}_u^* + \sigma_n^2\mathbf{I}\right]^{-1}\right)\ , \end{aligned} \tag{D.13}$$

where λ_z^2 and ρ_z^2 are the eigenvalues of $\mathbf{H}\mathbf{H}^*$ and $\mathbf{R}$, respectively. In order to minimize the sum-MSE in (D.13), it is sufficient to minimize the last term on the right-hand side. Therefore, (D.3) can be simplified as

$$\begin{aligned}\text{minimize}_{\ \mathbf{R}_u} \quad & \sigma_n^2\mathrm{Tr}\left(\left[\sum_{u=0}^{N_u-1}\mathbf{H}_u\mathbf{R}_u\mathbf{H}_u^* + \sigma_n^2\mathbf{I}\right]^{-1}\right)\\ \text{subject to} \quad & \mathrm{Tr}\left(\mathbf{R}_u\right) = P_m \quad 0 \le u < N_u\ . \end{aligned} \tag{D.14}$$

D.1 Proof of the Gradient Expression and KKT Conditions

Next, the gradient for a weighted sum-MSE optimization is computed, where the MSE is given as (D.9) and (D.12)

$$\sum_{u=0}^{N_u-1} E_u^{UL} = f\left(\mathbf{F}_1,...,\mathbf{F}_{N_u}\right) = \sum_{u=0}^{N_u-1}\mathrm{Tr}\left(\mathbf{I} - w_u\mathbf{F}_u^*\mathbf{H}_u^*\mathbf{T}^{-1}\mathbf{H}_u\mathbf{F}_u\right)\ . \tag{D.15}$$

The minimum MSE is computed by evaluating $\frac{\partial f}{\partial \mathbf{F}_u^*}$ and equating it to zero. Thus, as in [115] [116], we define $\nabla_{\mathbf{F}_u^*}\mathbf{f} = \frac{\partial f}{\partial \mathbf{F}_u^*}$ as the complex gradient operator. This gradient is a matrix with the $[n,m]^{\text{th}}$ element defined as:

$$[\nabla_{\mathbf{F}_u} f]_{n,m} = \nabla_{[\mathbf{F}_u]_{n,m}} f = \frac{\partial f}{\partial [\mathbf{F}_u^*]_{n,m}}\ ,$$

only if f is dependent on u, i.e., no more elements to differentiate. However, if f_i dependent on i, where $i = 1..N_u$, we need to differentiate element wise (as in (G.14) and (G.15)). From the KKT conditions, a local optimum must be satisfied for all u: $\nabla_{\mathbf{F}_u^*}\left(\sum_{i=0}^{N_u-1} E_i^{UL}\right) = 0$ [115]. Accordingly, the gradient of E_u and E_i, $i = 1..N_u$ with respect to the transmit filter $\mathbf{F}_u^*$ is computed. Thus, (G.15) and the chain and product rules in Appendix G, we get

$$\nabla_{\mathbf{F}_u^*} E_u = \frac{\partial E_u}{\partial \mathbf{F}_u^*} = \mathbf{H}_u^* \mathbf{T}^{-1} \mathbf{H}_u \mathbf{F}_u \ , \tag{D.16}$$

where $\mathbf{T}$ is assumed to be independent of $\mathbf{F}_u$ to perform the product-rule. Afterward, we compute $\frac{\partial E_i}{\partial \mathbf{T}} \frac{\mathbf{T}}{\partial \mathbf{F}_u^*}, i = 1..N_u$ using the chain-rule (similar to the proof in [115]) as follows

$$\begin{aligned}
\nabla_{[\mathbf{F}_u^*]_{nm}} E_i(\mathbf{T}(\mathbf{F}_u^*)) &= \frac{\partial E_u}{\partial \mathbf{T}} \frac{\mathbf{T}}{\partial \mathbf{F}_u^*} = \mathrm{Tr}\left(\mathbf{F}_i^* \mathbf{H}_i^* \left(-\mathbf{T}^{-1} \frac{\partial \mathbf{T}}{\partial [\mathbf{F}_u^*]} \mathbf{T}^{-1}\right) \mathbf{H}_i \mathbf{F}_i\right) \\
&= -\mathrm{Tr}\left(\mathbf{F}_i^* \mathbf{H}_i^* \left(-\mathbf{T}^{-1} \mathbf{H}_u \mathbf{F}_u \mathbf{e}_m \mathbf{e}_n^* \mathbf{H}_u^* \mathbf{T}^{-1}\right) \mathbf{H}_i \mathbf{F}_i\right) \\
&= -\mathbf{e}_n^* \mathbf{H}_u^* \mathbf{T}^{-1} \mathbf{H}_i \mathbf{F}_i \mathbf{F}_i^* \mathbf{H}_i^* \mathbf{T}^{-1} \mathbf{H}_u \mathbf{F}_u \mathbf{e}_m \ ,
\end{aligned} \tag{D.17}$$

where the cyclic rotation (Lemma G.1.4) has been used in the last step. Furthermore, $\mathbf{e}_i$ is the i^{th} column of $\mathbf{I}$ (see Appendix G, (G.1.8)). Now, we obtain

$$-\nabla_{\mathbf{F}_u^*} E_i = -\mathbf{H}_u^* \mathbf{T}^{-1} \mathbf{H}_i \mathbf{F}_i \mathbf{F}_i^* \mathbf{H}_i^* \mathbf{T}^{-1} \mathbf{H}_u \mathbf{F}_u \ , \tag{D.18}$$

and, finally, the total weighted sum-MSE is given as

$$\begin{aligned}
\nabla_{\mathbf{F}_u^*} f &= w_u \nabla_{\mathbf{F}_u^*} E_u + \sum_{i=0}^{N_u-1} w_i \nabla_{\mathbf{F}_u^*} E_i \\
&= w_u \mathbf{H}_u^* \mathbf{T}^{-1} \mathbf{H}_u \mathbf{F}_u - \sum_{i=0}^{N_u-1} w_i \mathbf{H}_u^* \mathbf{T}^{-1} \mathbf{H}_i \mathbf{F}_i \mathbf{F}_i^* \mathbf{H}_i^* \mathbf{T}^{-1} \mathbf{H}_u \mathbf{F}_u \\
&= w_u \mathbf{H}_u^* \mathbf{T}^{-1} \mathbf{T} \mathbf{T}^{-1} \mathbf{H}_u \mathbf{F}_u - \mathbf{H}_u^* \mathbf{T}^{-1} \left(\sum_{i=0}^{N_u-1} w_i \mathbf{H}_i \mathbf{F}_i \mathbf{F}_i^* \mathbf{H}_i^*\right) \mathbf{T}^{-1} \mathbf{H}_u \mathbf{F}_u \ ,
\end{aligned} \tag{D.19}$$

by taking $\mathbf{H}_u^* \mathbf{T}^{-1}$ and $\mathbf{T}^{-1} \mathbf{H}_u \mathbf{F}_u$ as common factors from both sides, we obtain

$$\frac{\partial f}{\partial \mathbf{F}_u^*} = -\mathbf{H}_u^* \mathbf{T}^{-1} \left(w_u \mathbf{T} - \sum_{i=0}^{N_u-1} w_i \mathbf{H}_i \mathbf{F}_i \mathbf{F}_i^* \mathbf{H}_i^*\right) \mathbf{T}^{-1} \mathbf{H}_u \mathbf{F}_u \ , \tag{D.20}$$

which is the same result as in [78, 79]. Let $\mathbf{S} = \sum_{i=0}^{N_u-1} w_i \mathbf{H}_i \mathbf{F}_i \mathbf{F}_i^* \mathbf{H}_i^*$, we finally put $\frac{\partial f}{\partial \mathbf{F}_u^*}$ in the following form

$$\frac{\partial f}{\partial \mathbf{F}_u^*} = -\mathbf{H}_u^* \mathbf{T}^{-1} \left(w_u \mathbf{T} - \mathbf{S}\right) \mathbf{T}^{-1} \mathbf{H}_u \mathbf{F}_u \ . \tag{D.21}$$

In case of equal weights or sum-MSE, i.e., $w_1 = w_2 = ... = w_{N_u}$, however, using the MMSE derived in (D.14), we get the following

$$\frac{\partial f}{\partial \mathbf{F}_u^*} = -\sigma_n^2 \mathbf{H}_u^* \mathbf{T}^{-2} \mathbf{H}_u \mathbf{F}_u \tag{D.22}$$

where σ_n^2 is also the constant noise variance seen in (D.14), which appears here, since $\mathbf{T} - \mathbf{S} = \sigma_n^2 \mathbf{I}$.

Finally, the same proof (from (D.15) to (D.20)) can be conducted for the Lagrangian function, i.e., assuming weighted sum-MSE, associated with the same minimization problem. Therefore, given the Lagrangian function in Chapter 6, Section 6.4, as

$$\mathcal{L}_{\mu}^{f} = f\left(\mathbf{F}_1, ..., \mathbf{F}_{N_u}\right) = \sum_{u=0}^{N_u-1} w_u N_{R_u} - \sum_{u=0}^{N_u-1} w_u \mathrm{Tr}\left[\mathbf{F}_u^{*}\mathbf{H}_u^{*}\mathbf{T}^{-1}\mathbf{H}_u\mathbf{F}_u\right] - \mu\left(\sum_{u=0}^{N_u-1}\mathrm{Tr}\left(\mathbf{F}_u^{*}\mathbf{F}_u\right) - P_m\right) , \tag{D.23}$$

we get the following result

$$\frac{\partial \mathcal{L}_{\mu}^{f}}{\partial \mathbf{F}_u^{*}} = \mu\mathbf{F}_u - \mathbf{H}_u^{*}\mathbf{T}^{-1}\left(w_i\mathbf{T} - \mathbf{S}\right)\mathbf{T}^{-1}\mathbf{H}_u\mathbf{F}_u = \mathbf{0} . \tag{D.24}$$

D.2 Solving KKT Conditions for BD Downlink

Knowing that the users matrix is $\mathbf{H}_u$, while $\mathbf{H}$ is the vertical concatenation of the users channel matrices and $\mathbf{F}$ is the overall transmit filter at the BS, such that

$$\mathbf{H} = \left[\mathbf{H}_1^{T}\mathbf{H}_2^{T}...\mathbf{H}_{N_u}^{T}\right]^{T}$$

and

$$\mathbf{F} = \left[\mathbf{F}_1\mathbf{F}_2...\mathbf{F}_{N_u}\right] .$$

Similar to (D.14), the following is the MSE optimization problem for the downlink channel

$$\begin{aligned} \text{minimize }_{\mathbf{F}_u} \quad & \sigma_n^2\mathrm{Tr}\left(\left[\mathbf{H}\mathbf{F}\mathbf{F}^{*}\mathbf{H}^{*} + \sigma_n^2\mathbf{I}\right]^{-1}\right) \\ \text{subject to} \quad & \mathrm{Tr}\left(\mathbf{R}_u\right) = P_m \quad 0 \le u < N_u . \end{aligned} \tag{D.25}$$

One can write its Lagrangian optimization problem as

$$\begin{aligned} \mathcal{L}_{\mu}\left(\mu_u, \mathbf{F}_u\right) &= \sigma_n^2\mathrm{Tr}\left(\left[\mathbf{H}\mathbf{F}\mathbf{F}^{*}\mathbf{H}^{*} + \sigma_n^2\mathbf{I}\right]^{-1}\right) + \mu_u\left[\mathrm{Tr}\left(\mathbf{R}_u\right) - P_m\right] \\ &\equiv \sum_{z=0}^{N_T-1}\frac{\sigma_n^2}{\lambda_z^2\rho_z^2 + \sigma_n^2} + \mu_u\left[\sum_{z=0}^{N_T-1}\rho_z^2 - P_m\right] , \end{aligned} \tag{D.26}$$

where μ_u is the Lagrangian multiplier, which has to be selected to satisfy the power constraint of all users P_m and ρ_z^2 are the eigenvalues of $\mathbf{F}^{*}\mathbf{F}$ which will be used for power allocation using a diagonal matrix $\mathbf{P}_{\mathbf{F}} = \mathrm{diag}\left(\rho_1^2, \rho_2^2, ..., \rho_{N_u}^2\right)$. The following KKT conditions are necessary and sufficient for optimality: $\mathbf{F}_u$ is optimal if and only if there is a μ_u that together with $\mathbf{F}_u$ satisfies

$$\nabla_{\mathbf{P}}\mathcal{L}_{\mu}\left(\mu_u, \mathbf{F}_u\right) = 0 , \tag{D.27}$$

also equivalent to [80]

$$\nabla_{\mathbf{P}}\mathcal{L}_{\mu}\left(\mu_u, \mathbf{R}_u\right) = 0 , \tag{D.28}$$

or can be simply written as

$$\nabla_{\mathbf{P}}\mathcal{L}_{\mu}\left(\mu_u, \rho_u^2\right) = 0 , \tag{D.29}$$

where

$$\mu_u \ge 0 , \quad \sum_{z=0}^{N_T-1}\rho_z^2 - P_m \le 0 . \tag{D.30}$$

By differentiating (D.26) with respect to ρ_z^2, i.e., power values, and equating it to zero we get

$$\mu_u = \frac{\lambda_z^2 \sigma_n^2}{\left(\lambda_z^2 \rho_z^2 + \sigma_n^2\right)^2} \,, \tag{D.31}$$

or

$$\sqrt{\frac{1}{\mu_u}} \sqrt{\lambda_z^2 \sigma_n^2} = \lambda_z^2 \rho_z^2 + \sigma_n^2 \,. \tag{D.32}$$

Finally, we find the power allocation to be (also similar to [117])

$$\rho_{u,s}^2 = \left[\frac{1}{\sqrt{\mu}} \frac{\sigma_n}{\lambda_{u,s}} - \frac{\sigma_n^2}{\lambda_{u,s}^2} \right]^+ \,, \tag{D.33}$$

where σ_n^2 is the noise variance, $\lambda_{u,s}^2$ is the channel eigenvalue, $1/\sqrt{\mu}$ is the multiuser water-level, and $[x]^+ \geq 0$, which can be relaxed if $\frac{\sigma_n}{\sqrt{\mu_u}} \lambda_{u,s}^{-1} \geq \sigma_n^2 \lambda_{u,s}^{-2}$. Since we assume an identity input covariance matrix, the power allocation in this process is unit-less and acts only as power factors, which scale the overall power constraint.

D.3 Computation of the Lagrange Multiplier

We need to obtain $\sqrt{\mu_u} > 0$ that satisfies the power constraint

$$\mathrm{Tr}\left(\mathbf{P}_u^* \mathbf{P}_u\right) = P_m \,. \tag{D.34}$$

After relaxing the positivity condition in (D.33), one can rewrite it as

$$\sum_{u=0}^{N_u-1} \sum_{z=1}^{M_u} \left(\frac{\sigma_n}{\sqrt{\mu_u}} \left(\lambda_{u,z}\right)^{-1} - \sigma_n^2 \left(\lambda_{u,z}\right)^{-2} \right) = P_m \,. \tag{D.35}$$

Thus,

$$\sigma \mu_u^{-1/2} \sum_{u=0}^{N_u-1} \sum_{z=1}^{M_u} \left(\lambda_{u,z}\right)^{-1} - \sigma^2 \sum_{u=0}^{N_u-1} \sum_{z=1}^{M_u} \left(\lambda_{u,z}\right)^{-2} - P_m = 0 \,. \tag{D.36}$$

Since we only use normalized power, we select $P_m = 1$. This makes our MU water-filling equation results unit-less. Therefore, the Lagrangian multiplier is found using (D.36) to be

$$\mu_u^{1/2} = \frac{\sigma_n \sum_{j=1} \left(\lambda_j\right)^{-1}}{1 + \sigma_n^2 \sum_{j=1} \left(\lambda_j\right)^{-2}} \,. \tag{D.37}$$

Appendix E

MMSE Using Convex Optimization Tools

As seen in Appendix D, to minimize the sum-MSE in (D.13), it is sufficient to minimize (D.3), which can be stated in detail as

$$\begin{aligned} \text{minimize}_{\,\mathbf{R}_u,\mathbf{\Phi}} \quad & \sigma_n^2 \mathrm{Tr}\left(\mathbf{\Phi}\right) \\ \text{subject to} \quad & \mathbf{\Phi} \succeq \left(\sum_{u=0}^{N_u-1} \mathbf{H}_u \mathbf{R}_u \mathbf{H}_u^* + \sigma_n^2 \mathbf{I}\right)^{-1} \\ & \mathrm{Tr}\left(\mathbf{R}_u\right) = P_m \qquad\qquad 0 \leq u \leq N_u \\ & \mathbf{R}_u \succeq 0\,. \quad \text{(positive semidefinit)} \end{aligned} \tag{E.1}$$

Using the Schur complement defined in Appendix G, Proposition G.1.17, the first constraint in (E.1), i.e., $\mathbf{\Phi} \succeq \left(\sum_{u=0}^{N_u-1} \mathbf{H}_u \mathbf{R}_u \mathbf{H}_u^* + \sigma_n^2 \mathbf{I}\right)^{-1}$, can be written as the following linear matrix inequality

$$\mathbf{0} = \mathbf{C} - \mathbf{I}^* \left(\sum_{u=0}^{N_u-1} \mathbf{H}_u \mathbf{R}_u \mathbf{H}_u^* + \sigma_n^2 \mathbf{I}\right)^{-1} \mathbf{I}\,. \tag{E.2}$$

Hence, using (G.31), one can rewrite the previous linear matrix inequality as

$$\begin{bmatrix} \mathbf{\Phi} & \mathbf{I} \\ \mathbf{I} & \sum_{u=0}^{N_u-1} \mathbf{H}_u \mathbf{R}_u \mathbf{H}_u^* + \sigma_n^2 \mathbf{I} \end{bmatrix} \succeq \mathbf{0}\,. \tag{E.3}$$

Finally, (E.1) can be written as

$$\begin{aligned} \text{minimize}_{\,\mathbf{R}_u,\mathbf{\Phi}} \quad & \sigma_n^2 \mathrm{Tr}\left(\mathbf{\Phi}\right) \\ \text{subject to} \quad & \begin{bmatrix} \mathbf{\Phi} & \mathbf{I} \\ \mathbf{I} & \sum_{u=0}^{N_u-1} \mathbf{H}_u \mathbf{R}_u \mathbf{H}_u^* + \sigma_n^2 \mathbf{I} \end{bmatrix} \succeq \mathbf{0} \\ & \mathrm{Tr}\left(\mathbf{R}_u\right) = P_m \qquad\qquad 0 \leq u \leq N_u \\ & \mathbf{R}_u \succeq 0\,, \end{aligned} \tag{E.4}$$

which can be solved using a number of general purpose optimization tools. In the following section, we are going to give a MATLAB example of the previous optimization problem using YALMIP [113], which internally uses the SeDuMi [112] solver.

E.1 YALMIP Solver

YALMIP is a very high-level MATLAB script language. Herewith, (E.4) is programmed straightforward as follows:

1. Initialize the number of antennas at the receiver to Nr=2, the number of antennas at the transmitter to Nt=6, and the number of users to Nu=3.

2. Define the SDP class "spdvar" for the Hermitian pre-processing matrix R_u at the MSs of the 3 users, i.e., R1, R2, and R3, such that

```
R1 = sdpvar(Nr,Nr,'hermitian','complex');
R2 = sdpvar(Nr,Nr,'hermitian','complex');
R3 = sdpvar(Nr,Nr,'hermitian','complex');
Phi = sdpvar(Nt,Nt,'hermitian','complex'); % constraint variables
```

3. the core optimization steps, where "F" collects the required constraints, "set" defines these constraints, "solvesdp" minimize the objective $\mathrm{Tr}\left(\sigma_n^2 \mathbf{T}^{-1}\right)$, and W= $\mathbf{T}^{-1}$

```
F = set((trace(R1)+trace(R2)+trace(R3))≤1); % power constraint
F = F + set([Phi eye(Nt); ... % linear matrix inequality constraint
            eye(Nt) (H1*R1*H1'+H2*R2*H2'+ H3*R3*H3'+ N)]≥0);
F = F + set(R1 ≥ 0)+set(R2 ≥ 0)+set(R3 ≥ 0); % semidefinit constraint
solvesdp(F,trace((W*N))); % where N is the noise variance
```

4. extract the required double format of the pre-processing Hermitian matrices Rud from the "spdvar" class Ru, where $u = 1, 2, 3$

```
R1d = (double(R1)); % retrieve the double format of the Ru sdpvar matrices
R2d = (double(R2)); % by converting into double using double(.)
R3d = (double(R3));
```

Appendix F

Symbol-Error Ratio Calculations

As in [15], the symbol-error rate equation of $\sqrt{M}$-ary pulse amplitude modulation (PAM) is

$$\mathcal{P}_{e,\sqrt{M}} = \left(1 - \frac{1}{\sqrt{M_k}}\right) \operatorname{erfc}\left(\sqrt{\frac{3}{2(M_k-1)} p_k \mathcal{G}_k}\right) , \tag{F.1}$$

where $M = 2^{\hat{b}_k}$. p_k and $\mathcal{G}_k$ are the k^{th} subcarrier power value and the CGNR, respectively. Then, for M-ary QAM

$$\mathcal{P}_{e,M} = 1 - \left(1 - \mathcal{P}_{e,\sqrt{M}}\right)^2 = 1 - \left[1 - 2\,\mathcal{P}_{e,\sqrt{M}} + \mathcal{P}^2_{e,\sqrt{M}}\right] = 2\,\mathcal{P}_{e,\sqrt{M}} - \mathcal{P}^2_{e,\sqrt{M}} . \tag{F.2}$$

Now, substitute (F.1) into (F.2) we get the QAM SER, which can be written as

$$\mathcal{P}_{e,M} = 2\left(1 - \frac{1}{\sqrt{M_k}}\right) \operatorname{erfc}\left(\sqrt{\frac{3/2}{(M_k-1)} p_k \mathcal{G}_k}\right) - \left[\left(1 - \frac{1}{\sqrt{M_k}}\right) \operatorname{erfc}\left(\sqrt{\frac{3/2\; p_k \mathcal{G}_k}{(M-1)}}\right)\right]^2 , \tag{F.3}$$

were $p_k\mathcal{G}_k$ is the SNR at the k^{th} subcarrier. At high SNR, the squared term can be neglected. Thus, we can consider an approximated version of (F.3), which is given by

$$\mathcal{P}_{e,M} \approx 2\left(1 - \frac{1}{\sqrt{M_k}}\right) \operatorname{erfc}\left(\sqrt{\frac{3/2}{(M_k-1)} p_k \mathcal{G}_k}\right) , \tag{F.4}$$

which is equivalent to twice the SER of the $\sqrt{M}$-ary PAM.

F.1 Relation between the Noise Margin and the SER

From the bit rate formula in (3.33), we obtain

$$p_k \mathcal{G}_k = \gamma \cdot \left(2^{\hat{b}_k} - 1\right) = \gamma \cdot (M_k - 1) , \tag{F.5}$$

where the noise margin is given as

$$\gamma = \frac{p_k \mathcal{G}_k}{(M_k - 1)} , \tag{F.6}$$

Finally, using (F.6), one can write (F.4) as a function of the noise margin γ as follows

$$\mathcal{P}_{e,M} = 2\left(1 - \frac{1}{\sqrt{M_k}}\right) \operatorname{erfc}\left(\sqrt{\frac{3\gamma_j}{2}}\right) . \tag{F.7}$$

F.2 SER in Rayleigh Fading Channels

Equations (F.3) and (F.4) are valid for AWGN channels only. However, for a Rayleigh fading channels, with the coefficient γ in a frequency non-selected slow fading, the instantaneous SNR is given by

$$\mathrm{SNR}_{\hat{b}} = \lambda^2 p_k / \sigma_n^2 \,, \tag{F.8}$$

where λ has a Rayleigh probability distribution and λ^2 is a chi-square distribution, which can be considered as a fixed channel coefficient during the signal interval [15]. Thus, the error probability is given by

$$\mathcal{P}_{e,\hat{b}} = \int_0^\infty \mathcal{P}_e(\mathrm{SNR}_{\hat{b}}) p(\mathrm{SNR}_{\hat{b}}) d(\mathrm{SNR}_{\hat{b}}) \,, \tag{F.9}$$

where $p(\mathrm{SNR}_{\hat{b}})$ is the probability density function of $\mathrm{SNR}_{\hat{b}}$ (also chi-square) using $\hat{b}$ bits. It is shown in [15] that the SER in this case is the integration over the whole SNR range, i.e., from 0 to ∞ using the distribution of the SNR, such that,

$$p(\mathrm{SNR}_{\hat{b}}) = \frac{1}{\overline{\mathrm{SNR}}_{\hat{b}}} e^{-\mathrm{SNR}_{\hat{b}}/\overline{\mathrm{SNR}}_{\hat{b}}} \,, \tag{F.10}$$

where $\overline{\mathrm{SNR}}_{\hat{b}}$ is the average SNR.

F.3 Suitability of SINR and MMSE for SER Calculation

As in [70], the SER can also be written as a function of the SINR or MMSE, such that

$$\mathcal{P}_e^i = f\left(\mathrm{SINR}_i\right) = f\left(\frac{1}{\mathrm{MMSE}_i} - \nu\right) \,, \tag{F.11}$$

where $\nu = 1$ for MMSE and $\nu = 0$ for ZF equalizer. However, $\mathcal{P}_e^i(\mathrm{MMSE}_i)$ is valid if, and only if, (F.11) is a convex increasing (in MMSE) function and $f(\mathrm{SINR}_i)$ is a convex decreasing function (in SINR).

SER using SINR: To prove that the SER is decreasing and convex in SINR, it suffices to show that the first and the second derivative of erfc $\sqrt{2\beta x}$ are negative and positive, respectively. Thus, as in [70], we get

$$\begin{aligned}
\frac{d}{dx}\mathrm{erfc}\left(\sqrt{2\beta x}\right) &= -\sqrt{\frac{\beta}{8\pi}} e^{-\beta x/2} x^{-1/2} < 0 \qquad && 0 < x < \infty \\
\frac{d^2}{dx^2}\mathrm{erfc}\left(\sqrt{2\beta x}\right) &= \frac{1}{2}\sqrt{\frac{\beta}{8\pi}} e^{-\beta x/2} x^{-1/2}\left(\frac{1}{x} + \beta\right) > 0 \qquad && 0 < x < \infty \,.
\end{aligned} \tag{F.12}$$

SER using MMSE Knowing from [15] the relation between SINR and MMSE to be

$$\mathrm{SINR}_i = \frac{1}{\mathrm{MMSE}_i} - \nu \,, \tag{F.13}$$

the SER as a function of the MMSE is given by

$$\mathcal{P}_e^i(\text{MMSE}_i) = \text{erfc}\left(\sqrt{2\beta\left(x^{-1}-\nu\right)}\right) . \tag{F.14}$$

Finally, to show the convexity and the increasing characteristic of $\mathcal{P}_e^i(\text{MMSE}_i)$, we show that the first and the second derivative are both positive. Similar to [70], we get

$$\begin{aligned}
\frac{d}{dx}\text{erfc}\left(\sqrt{2\beta(x^{-1}-\nu)}\right) &= -\sqrt{\frac{\beta}{8\pi}}\frac{e^{-\beta(x^{-1}-\nu)/2}}{(x^3-\nu x^4)^{-1/2}} \geq 0 \qquad 0<x<1 \\
\frac{d^2}{dx^2}\text{erfc}\left(\sqrt{2\beta(x^{-1}-\nu)}\right) &= -\sqrt{\frac{\beta}{8\pi}}\frac{e^{-\beta(x^{-1}-\nu)/2}}{(x^3-\nu x^4)^{-1/2}}\left(\frac{\beta}{x^2}-\frac{3-\nu 4x}{x-\nu x^2}\right) \geq 0 \\
& \qquad\qquad 0<x<\infty . \qquad \text{(F.15)}
\end{aligned}$$

✍ Note: ν is set to "1" for MMSE and "0" for ZF receivers [15].

F.4 SER for MIMO using ZF and MMSE

Knowing that the Wiener filter is given by (see Appendix D)

$$\begin{aligned}
\mathbf{W} &= \left(\mathbf{HFF}^*\mathbf{H}^* + \nu\mathbf{I}\right)^{-1}\mathbf{HF} \\
&= \mathbf{HF}\left(\nu\mathbf{I} + \mathbf{F}^*\mathbf{H}^*\mathbf{HF}\right)^{-1} ,
\end{aligned} \tag{F.16}$$

where $\mu = 0$ for ZF and $\mu = 1$ for MMSE. As in Appendix D, the MSE is given by

$$\begin{aligned}
\mathbf{E} &= \mathbf{I} - \mathbf{F}^*\mathbf{H}^*\left(\mathbf{HFF}^*\mathbf{H}^* + \nu\mathbf{I}\right)^{-1}\mathbf{HF} \\
&= \left(\nu\mathbf{I} + \mathbf{F}^*\mathbf{H}^*\mathbf{HF}\right)^{-1} ,
\end{aligned} \tag{F.17}$$

where the second expression follows from the matrix inversion Lemma G.1.12 [70]. According to Section F.4, it is clear that maximizing the SINR (or minimizing the MSE) minimizes the SER as well. The SINR (per-stream i or vector i) is given by (using (D.25))

$$\text{SINR}_i = \frac{|\,\mathbf{w}_i^*\mathbf{H}\mathbf{f}_i\,|^2}{\mathbf{w}_i^*\mathbf{R}_{n,i}\mathbf{w}_i} , \tag{F.18}$$

where $\mathbf{R}_n$ is the interference plus the noise covariance matrix. One can be conducted from (D.25) to have the Gaussian noise plus the color noise superposition at high CGNR, i.e., very low σ_n^2 with high channel gain and interference dominant, as follows

$$\begin{aligned}
\widetilde{\mathbf{n}}_i &= \left(\mathbf{F}^*\mathbf{H}^*\mathbf{HF} + \sigma_n^2\mathbf{I}\right)^{-1}\mathbf{F}^*\mathbf{H}^*\mathbf{n} \\
&\approx \left(\mathbf{F}^*\mathbf{H}^*\mathbf{HF}\right)^{-1}\mathbf{F}^*\mathbf{H}^*\mathbf{n} \\
&= \left(\hat{\mathbf{V}}^*\left(\hat{\mathbf{H}}+\boldsymbol{\Xi}\right)^*\left(\hat{\mathbf{H}}+\boldsymbol{\Xi}\right)\hat{\mathbf{V}}\right)^{-1}\hat{\mathbf{V}}^*\left(\hat{\mathbf{H}}+\boldsymbol{\Xi}\right)^*\mathbf{n} ,
\end{aligned} \tag{F.19}$$

for a full and invertible matrix $\left(\hat{\mathbf{H}}+\boldsymbol{\Xi}\right)\hat{\mathbf{V}}$, the previous is a pseudo-inverse, which results in (assuming square matrices and using Lemma G.1.14)

$$\begin{aligned}\tilde{\mathbf{n}}_c &\equiv \left(\hat{\mathbf{H}}+\boldsymbol{\Xi}\right)\hat{\mathbf{V}}\left(\left(\hat{\mathbf{H}}+\boldsymbol{\Xi}\right)\hat{\mathbf{V}}\hat{\mathbf{V}}^*\left(\hat{\mathbf{H}}+\boldsymbol{\Xi}\right)^*\right)^{-1}\mathbf{n}\\ &= \left(\hat{\mathbf{V}}^*\left(\hat{\mathbf{V}}\hat{\mathbf{D}}\hat{\mathbf{U}}^*+\boldsymbol{\Xi}^*\right)\right)^{-1}\mathbf{n}\\ &= \left(\hat{\mathbf{D}}\hat{\mathbf{U}}^*+\hat{\mathbf{V}}^*\boldsymbol{\Xi}^*\hat{\mathbf{U}}\hat{\mathbf{U}}^*\right)^{-1}\mathbf{n}\\ &= \left(\hat{\mathbf{D}}-\tilde{\boldsymbol{\Xi}}\right)^{-1}\hat{\mathbf{U}}\mathbf{n}\,, \end{aligned} \tag{F.20}$$

where $\tilde{\mathbf{n}}=\hat{\mathbf{U}}\mathbf{n}$ and $\tilde{\boldsymbol{\Xi}}=-\hat{\mathbf{V}}^*\boldsymbol{\Xi}^*\hat{\mathbf{U}}$, which have the same distribution as $\mathbf{n}$ and $\boldsymbol{\Xi}$, respectively. Now, using inversion Lemma G.1.14 and matrix Taylor expansion in Proposition G.1.13, we can rewrite (F.20) as

$$\begin{aligned}\tilde{\mathbf{n}}_c &= \left(\mathbf{I}-\tilde{\boldsymbol{\Xi}}\hat{\mathbf{D}}^{-1}\right)^{-1}\hat{\mathbf{D}}^{-1}\tilde{\mathbf{n}}=\hat{\mathbf{D}}^{-1}\left(\mathbf{I}-\hat{\mathbf{D}}^{-1}\tilde{\boldsymbol{\Xi}}\right)^{-1}\tilde{\mathbf{n}}\\ &= \hat{\mathbf{D}}^{-1}\left(\mathbf{I}+\hat{\mathbf{D}}^{-1}\tilde{\boldsymbol{\Xi}}+\left(\hat{\mathbf{D}}^{-1}\tilde{\boldsymbol{\Xi}}\right)^2+\left(\hat{\mathbf{D}}^{-1}\tilde{\boldsymbol{\Xi}}\right)^3+\cdots\right)\tilde{\mathbf{n}}\,. \end{aligned} \tag{F.21}$$

This represents mainly a noise ($\tilde{\mathbf{n}}$) plus a main crosstalk ($\hat{\mathbf{D}}^{-1}\tilde{\boldsymbol{\Xi}}$) plus smaller ones $\left(\hat{\mathbf{D}}^{-1}\tilde{\boldsymbol{\Xi}}\right)^n$. Knowing that the variance of the error matrix $\boldsymbol{\Xi}$ is relatively small, one can approximate the previous equation by neglecting the squared terms. Finally, (F.20) as

$$\begin{aligned}\tilde{\mathbf{n}}_c &\approx \hat{\mathbf{D}}^{-1}\left(\mathbf{I}+\hat{\mathbf{D}}^{-1}\tilde{\boldsymbol{\Xi}}\right)\tilde{\mathbf{n}}\\ &= \hat{\mathbf{D}}^{-1}\left(\tilde{\mathbf{n}}+\hat{\mathbf{D}}^{-1}\tilde{\boldsymbol{\Xi}}\tilde{\mathbf{n}}\right)\,, \end{aligned} \tag{F.22}$$

where $\hat{\mathbf{D}}^{-1}$ is a diagonal matrix (which has, without loss of generality, an identity covariance matrix) that represents a scaling of the noise by the channel gains. Thus, $\tilde{\mathbf{n}}$ is also denoted as noise-to-channel gains. Now, let us find the noise covariance matrix, i.e., covariance matrix of $\hat{\mathbf{D}}\tilde{\mathbf{n}}_c$

$$\begin{aligned}\mathbb{E}\left(\hat{\mathbf{D}}\tilde{\mathbf{n}}_c\tilde{\mathbf{n}}_c^*\hat{\mathbf{D}}\right) &= \mathbb{E}\left(\left(\tilde{\mathbf{n}}+\hat{\mathbf{D}}^{-1}\tilde{\boldsymbol{\Xi}}\tilde{\mathbf{n}}\right)\left(\tilde{\mathbf{n}}+\hat{\mathbf{D}}^{-1}\tilde{\boldsymbol{\Xi}}\tilde{\mathbf{n}}\right)^*\right)\\ &= \mathbb{E}\left(\tilde{\mathbf{n}}\tilde{\mathbf{n}}^*\right)+\mathbb{E}\left(\tilde{\mathbf{n}}\tilde{\mathbf{n}}^*\right)\mathbb{E}\left(\tilde{\boldsymbol{\Xi}}\tilde{\boldsymbol{\Xi}}^*\right)\\ &= \sigma_n^2\mathbf{I}+\sigma_n^2\sigma_{\tilde{\boldsymbol{\Xi}}}^2\mathbf{I}=\sigma_n^2\left(\sigma_{\tilde{\boldsymbol{\Xi}}}^2\mathbf{I}+\mathbf{I}\right)\,, \end{aligned} \tag{F.23}$$

after assuming that $\hat{\mathbf{D}}=\mathbf{I}$. Another method to find the noise covariance matrix is similar to the one in [70]. Thus, knowing the noise covariance matrix

$$
\begin{aligned}
\mathbf{R}_{n,i} &= \sigma_n^2\mathbb{E}\left(\sum_{j\neq i}\mathbf{f}_j^*\mathbf{H}^*\mathbf{H}\mathbf{f}_j\right)+\sigma_n^2\mathbf{I}\\
&= \sigma_n^2\mathbb{E}\left(\sum_{j\neq i}\mathbf{f}_j^*\left(\hat{\mathbf{H}}^*+\boldsymbol{\Xi}^*\right)\left(\hat{\mathbf{H}}+\boldsymbol{\Xi}\right)\mathbf{f}_j\right)+\sigma_n^2\mathbf{I}\\
&= \sigma_n^2\mathbb{E}\left(\sum_{j\neq i}\left(\mathbf{f}_j^*\hat{\mathbf{H}}^*+\mathbf{f}_\mathbf{j}^*\boldsymbol{\Xi}^*\right)\left(\hat{\mathbf{H}}\mathbf{f}_\mathbf{j}+\boldsymbol{\Xi}\mathbf{f}_\mathbf{j}\right)\right)+\sigma_n^2\mathbf{I}\\
&= \sigma_n^2\mathbb{E}\left(\sum_{j\neq i}\left(\mathbf{f}_j^*\hat{\mathbf{H}}^*\hat{\mathbf{H}}\mathbf{f}_j+\mathbf{f}_j^*\boldsymbol{\Xi}^*\boldsymbol{\Xi}\mathbf{f}_j+\mathbf{f}_j^*\boldsymbol{\Xi}^*\hat{\mathbf{H}}\mathbf{f}_j+\mathbf{f}_j^*\hat{\mathbf{H}}^*\boldsymbol{\Xi}\mathbf{f}_j\right)\right)+\sigma_n^2\mathbf{I}\\
&= \sigma_n^2\mathbb{E}\left(\sum_{j\neq i}\left(\mathbf{0}+\mathbf{f}_j^*\boldsymbol{\Xi}^*\boldsymbol{\Xi}\mathbf{f}_j+\mathbf{f}_j^*\boldsymbol{\Xi}^*\hat{\mathbf{H}}\mathbf{f}_j+\mathbf{f}_j^*\hat{\mathbf{H}}^*\boldsymbol{\Xi}\mathbf{f}_j\right)\right)+\sigma_n^2\mathbf{I}\\
&= \sigma_n^2\sum_{j\neq i}(\mathbf{0})+\sum_{j\neq i}\mathbf{f}_j^*\underbrace{\mathbb{E}\left(\boldsymbol{\Xi}^*\boldsymbol{\Xi}\right)}_{\sigma_{\boldsymbol{\Xi}}^2}\mathbf{f}_j+\sum_{j\neq i}\mathbb{E}\left(\mathbf{f}_j^*\boldsymbol{\Xi}^*\hat{\mathbf{H}}\mathbf{f}_j\right)+\sum_{j\neq i}\mathbb{E}\left(\mathbf{f}_j^*\hat{\mathbf{H}}^*\boldsymbol{\Xi}\mathbf{f}_j\right)+\sigma_n^2\mathbf{I}\\
&= \sigma_n^2\sigma_{\boldsymbol{\Xi}}^2\mathbf{I}+\sigma_n^2\mathbf{I}=\sigma_n^2\left(\sigma_{\boldsymbol{\Xi}}^2\mathbf{I}+\mathbf{I}\right), \qquad \text{(F.24)}
\end{aligned}
$$

where $\sigma_n^2\mathbf{I}$ is the white noise covariance matrix and $\sum_{j\neq i}\mathbf{f}_j^*\mathbf{H}^*\mathbf{H}\mathbf{f}_j$ is the off-diagonal inter-stream(eigen) interference. Thus, the SINR can be rewritten as

$$
\mathrm{SINR}_i=\frac{\mathbf{w}_i^*\mathbf{f}_i^*\mathbf{H}^*\mathbf{H}\mathbf{f}_i\mathbf{w}_i}{\mathbf{w}_i^*\mathbf{R}_{n,i}\mathbf{w}_i}, \qquad \text{(F.25)}
$$

which can be maximized using the generalized matrix pair $(\mathbf{f}_i^*\mathbf{H}^*\mathbf{H}\mathbf{f}_i,\mathbf{R}_n)$ [31]. Consequently, the MSE in (F.26) is given by

$$
\mathbf{E} = \left(\nu\mathbf{I}+\mathbf{F}^*\mathbf{H}^*\mathbf{R}_n^{-1}\mathbf{H}\mathbf{F}\right)^{-1}. \qquad \text{(F.26)}
$$

Since the interference and the noise are coming from white Gaussian sources, and the power matrix $\mathbf{F}$ is assumed to be scaled to the SNR, we can conduct the following interference-plus-noise covariance matrix (from the channel uncertainty in Chapter 2 assuming the input to have an input covariance matrix equals to $\mathbf{I}$)

$$
\mathbf{R}_n = \mathbf{I}+\sigma_{\boldsymbol{\Xi}}^2\mathbf{I}=\mathbf{I}+\mathbf{Q}_{\boldsymbol{\Xi}}, \qquad \text{(F.27)}
$$

where $\mathbf{Q}_{\boldsymbol{\Xi}}$ is a general interference covariance matrix. Hence, the MSE (for white Gaussian noise and interference) is given by

$$
\mathbf{E} = \left(\nu\mathbf{I}+1/\sigma_n^2\mathbf{F}^*\mathbf{H}^*\left(\mathbf{I}+\mathbf{Q}_{\boldsymbol{\Xi}}\right)^{-1}\mathbf{H}\mathbf{F}\right)^{-1}. \qquad \text{(F.28)}
$$

This result is valid also when the channel is feedback to the transmitter using a noisy channel, which delivers a white Gaussian noise of a variance $\sigma_{\boldsymbol{\Xi}}^2$. This is also valid if the channel variance is scaled by $(1+\sigma_{\boldsymbol{\Xi}}^2)$.

In the previous cases, the MSE is given as in (F.28) or (F.26), where the SINR for the zero forcing on stream i is given for ZF as

$$
\mathrm{SINR}_i = \frac{1}{\mathrm{MSE}_i}-1=\frac{\left(\mathbf{f}_i^*\mathbf{H}^*\mathbf{H}\mathbf{f}_i\right)}{\sigma_n^2\left(1+\sigma_{\boldsymbol{\Xi}}^2\right)}-1, \qquad \text{(F.29)}
$$

or

$$1 + \mathrm{SINR}_i = \frac{(\mathbf{f}_i^* \mathbf{H}^* \mathbf{H} \mathbf{f}_i)}{\sigma_n^2 \left(1 + \sigma_{\mathbf{\Xi}}^2\right)} , \tag{F.30}$$

which can be used directly in the capacity formula, if the channel error is assumed to be Gaussian. For diagonal systems, i.e., perfect CSI with $\sigma_{\mathbf{\Xi}}^2 = 0$, the SINR is given by

$$1 + \mathrm{SINR}_i = \frac{1}{(\sigma_n^2 \mathbf{w}_i^* \mathbf{w}_i)} . \tag{F.31}$$

For MMSE receivers, i.e., $\nu = 1$, we get the following

$$1 + \mathrm{SINR}_i \quad = \quad \frac{1}{\mathrm{MSE}_i} = \left(1 + \frac{\mathbf{f}_i^* \mathbf{H}^* \mathbf{H} \mathbf{f}_i}{\sigma_n^2 \left(1 + \sigma_{\mathbf{\Xi}}^2\right)}\right) . \tag{F.32}$$

The authors in [24] proved a similar results when the feedback is perfect and the CSI is estimated with error of the same variance $\sigma_{\mathbf{\Xi}}^2$, such that

$$\mathbf{E} \quad = \quad \left(\nu \mathbf{I} + \mathbf{F}^* \mathbf{H}^* \left(\sigma_n^2 \mathbf{I} + \mathbf{Q}_{\mathbf{\Xi}} \mathbb{E}\left(\mathbf{x}\mathbf{x}^*\right)\right)^{-1} \mathbf{H}\mathbf{F}\right)^{-1} , \tag{F.33}$$

where $\mathbb{E}\left(\mathbf{x}\mathbf{x}^*\right)$ is the input $\mathbf{x}$ covariance matrix. The main different between (F.28) and (F.33) is the error floor seen at very low noise, i.e., very high CGNR.

Appendix G

Linear Algebra Notes

G.1 Some Useful Notes on Linear Algebra

Most of the following lemmas and propositions are taken from [118] and [119].

Proposition G.1.1 (Singular Value Decomposition (SVD))
For any general complex matrix $\mathbf{A} \in \mathbb{C}^{m \times n}$, can decompose it as

$$\mathbf{A} = \mathbf{U}\mathbf{D}\mathbf{V}^* \,, \tag{G.1}$$

where $\mathbf{U} \in \mathbb{C}^{m \times m}$ and $\mathbf{V} \in \mathbb{C}^{n \times n}$ are unitary square matrices, such that $\mathbf{U}^*\mathbf{U} = \mathbf{I}_m$ and $\mathbf{V}^*\mathbf{V} = \mathbf{I}_n$. $\mathbf{D} \in \mathbb{R}^{m \times n}$ is a non-negative main diagonal matrix; the rank of $\mathbf{D}$ is the same as the rank of the original matrix $\mathbf{A}$.

Proposition G.1.2 (Eigenvalue Decomposition (EVD))
Any general square positive definite or at least Hermitian matrix, $\mathbf{A}^*\mathbf{A} \in \mathbb{C}^{n \times n}$, can be decompose as

$$\mathbf{A}^*\mathbf{A} = \mathbf{V}\mathbf{D}\mathbf{V}^* \,, \tag{G.2}$$

where $\mathbf{V} \in \mathbb{C}^{n \times n}$ is a unitary square matrix containing the eigenvectors of $\mathbf{A}^*\mathbf{A}$ along its columns. $\mathbf{D} \in \mathbb{R}^{n \times n}$ is a square non-negative main diagonal matrix; the rank of $\mathbf{D}$ is the same as the rank of the original matrix $\mathbf{A}$. This diagonal matrix contains the eigenvalues on its main diagonal.

Proposition G.1.3 (Trace of matrices)
The trace of a square matrix $\mathbf{A} \in \mathbb{C}^{n \times n}$, i.e., complex matrix, is given by

$$\mathrm{Tr}\left(\mathbf{A}\right) = \sum_{i=1}^{n} a_{i,i} \,, \tag{G.3}$$

which in general can be complex as well.

Lemma G.1.4 (Matrix trace properties - cyclic rotation)

$$\mathrm{Tr}\left(\mathbf{ABC}\right) = \mathrm{Tr}\left(\mathbf{CAB}\right) = \mathrm{Tr}\left(\mathbf{BCA}\right) \,, \tag{G.4}$$

but

$$\mathrm{Tr}\left(\mathbf{ABC}\right) \neq \mathrm{Tr}\left(\mathbf{ACB}\right) \,. \tag{G.5}$$

Lemma G.1.5 (Trace properties with invertible matrices)
If $\mathbf{A} \in \mathbb{C}^{n\times n}$ and $\mathbf{B} \in \mathbb{C}^{n\times n}$ is invertible, the following applies

$$\mathrm{Tr}\left(\mathbf{A}\right) = \mathrm{Tr}\left(\mathbf{A}\mathbf{B}^{-1}\mathbf{B}\right) = \mathrm{Tr}\left(\mathbf{B}\mathbf{A}\mathbf{B}^{-1}\right) \ . \tag{G.6}$$

Lemma G.1.6 (Trace properties for Hermitian matrices)
The trace is a linear operator, such that

$$\mathrm{Tr}\left(\mathbf{A}\mathbf{B}\right) = \mathrm{Tr}\left(\mathbf{B}^*\mathbf{A}^*\right) \ . \tag{G.7}$$

Lemma G.1.7 (Linearity of matrix trace)
The trace is a linear operator as it holds

$$\mathrm{Tr}\left(\mathbf{A}+\mathbf{B}\right) = \mathrm{Tr}\left(\mathbf{A}\right) + \mathrm{Tr}\left(\mathbf{B}\right) \ , \tag{G.8}$$

$$\mathrm{Tr}\left(c\mathbf{A}\right) = c\mathrm{Tr}\left(\mathbf{A}\right) \ . \tag{G.9}$$

Proposition G.1.8 (Derivative of matrix traces – element-wise)

$$\frac{\partial \mathbf{X}}{\partial x_{ij}} = \mathbf{e}_i\mathbf{e}_j^T \ , \tag{G.10}$$

where $\mathbf{e}_i$ is the i^{th} column of $\mathbf{I}$. Note that $\mathbf{e}_i\mathbf{e}_j^T$ is a matrix containing a 1 in position i,j and zeros elsewhere.

Proposition G.1.9 (Derivative of matrix traces)
The trace is a linear operator, hence, its derivative is given by

$$\partial\mathrm{Tr}\left(\mathbf{A}\right) = \mathrm{Tr}\left(\partial\mathbf{A}\right) \ . \tag{G.11}$$

Similarly, due to linearity, the following properties hold

$$\frac{\partial\ \mathrm{Tr}(\mathbf{A}\mathbf{X}\mathbf{B})}{\partial\ \mathbf{X}} = \frac{\partial\ \mathrm{Tr}(\mathbf{B}^*\mathbf{X}^*\mathbf{A}^*)}{\partial\ \mathbf{X}} = \mathbf{A}^*\mathbf{B}^* \ , \tag{G.12}$$

and

$$\frac{\partial\ \mathrm{Tr}(\mathbf{A}\mathbf{X}\mathbf{B}\mathbf{X}^*\mathbf{C})}{\partial\ \mathbf{X}} = \mathbf{B}\mathbf{X}^*\mathbf{C}\mathbf{A} + \mathbf{B}^*\mathbf{X}^*\mathbf{A}^*\mathbf{C}^* \ . \tag{G.13}$$

Now, let us assume $\mathbf{B}$ and $\mathbf{C}$ to be Hermitian symmetric, then

$$\frac{\partial\ \left(\mathrm{Tr}\left(\mathbf{A}\mathbf{X}^{-1}\mathbf{B}\right)\right)}{\partial\ \mathbf{X}} = -(\mathbf{X}^{-1}\mathbf{B}\mathbf{A}\mathbf{X}^{-1})^T \ . \tag{G.14}$$

Proof

$$\begin{aligned}
\frac{\partial\left(\mathrm{Tr}\left(\mathbf{A}\mathbf{X}^{-1}\mathbf{B}\right)\right)}{\partial\mathbf{x}_{i,j}} &= -\mathrm{Tr}(\mathbf{A}\mathbf{X}^{-1}\mathbf{e}_i\mathbf{e}_j^T\mathbf{X}^{-1}\mathbf{B}) \\
&= -\mathrm{Tr}(\mathbf{e}_j^T\mathbf{X}^{-1}\mathbf{B}\mathbf{A}\mathbf{X}^{-1}\mathbf{e}_i) = -\mathbf{e}_j^T\mathbf{X}^{-1}\mathbf{B}\mathbf{A}\mathbf{X}^{-1}\mathbf{e}_i \\
&= -\left(\mathbf{X}^{-1}\mathbf{B}\mathbf{A}\mathbf{X}^{-1}\right)_{j,i} = -(\mathbf{X}^{-1}\mathbf{B}\mathbf{A}\mathbf{X}^{-1})^T_{i,j} \ .
\end{aligned}$$

Q.E.D. (G.15)

$$\frac{\partial \ \mathrm{Tr}\left[(\mathbf{X}^*\mathbf{C}\mathbf{X})^{-1}\mathbf{A}\right]}{\partial \ \mathbf{X}} = -\mathbf{C}\mathbf{X}(\mathbf{X}^*\mathbf{C}\mathbf{X})^{-1}(\mathbf{A}+\mathbf{A}^*)(\mathbf{X}^*\mathbf{C}\mathbf{X})^{-1} \ . \tag{G.16}$$

Now, using chain and product rule

$$\begin{aligned}\frac{\partial \ \mathrm{Tr}\left[(\mathbf{A}+\mathbf{X}^*\mathbf{C}\mathbf{X})^{-1}\mathbf{X}^*\mathbf{B}\mathbf{X}\right]}{\partial \ \mathbf{X}} &= -2\mathbf{C}\mathbf{X}((\mathbf{A}+\mathbf{X}^*\mathbf{C}\mathbf{X})^{-1})\mathbf{X}^*\mathbf{B}\mathbf{X}(\mathbf{A}+\mathbf{X}^*\mathbf{C}\mathbf{X})^{-1} \\ &+ 2(\mathbf{B}\mathbf{X}(\mathbf{A}+\mathbf{X}^*\mathbf{C}\mathbf{X})^{-1}) \ .\end{aligned} \tag{G.17}$$

Lemma G.1.10 (Matrix properties - relation to its eigenvalues)
Given a square (complex or real) matrix $\mathbf{A}^{n\times n}$ with the eigenvalues $\lambda_1, \lambda_2, ..., \lambda_n$, the following is always true

$$\mathrm{Tr}\left(\mathbf{A}\right) = \sum_{i=1}^{n} \lambda_i \ , \tag{G.18}$$

$$\mathrm{Tr}\left(\mathbf{A}^c\right) = \sum_{i=1}^{n} \lambda_i^c \ , \tag{G.19}$$

$$\det\left(\mathbf{A}\right) = \prod_{i=1}^{n} \lambda_i \ . \tag{G.20}$$

Lemma G.1.11 (Trace of Hermitian matrices)
The trace of a Hermitian matrix $\mathbf{A}^*\mathbf{A}$ is the summation of its eigenvalues; the proof (using Lemma G.1.5) is given as follows

$$\mathrm{Tr}\left(\mathbf{A}^*\mathbf{A}\right) = \mathrm{Tr}\left(\mathbf{V}\mathbf{D}\mathbf{V}^*\right) = \mathrm{Tr}\left(\mathbf{V}\mathbf{D}\mathbf{V}^{-1}\right) = \mathrm{Tr}\left(\mathbf{D}\right) \ . \tag{G.21}$$

Lemma G.1.12 (Matrix inversion lemma)
As in [70], suppose $\mathbf{A}$ and $\mathbf{B}$ are square invertible matrices and $\mathbf{X}$ is a general matrix. Therefore,

$$(\mathbf{A}+\mathbf{X}\mathbf{B}\mathbf{X}^*)^{-1} = \mathbf{A}^{-1} - \mathbf{A}^{-1}\mathbf{X}\left[\mathbf{B}^{-1}+\mathbf{X}^*\mathbf{A}^{-1}\mathbf{X}\right] \ . \tag{G.22}$$

Proposition G.1.13 (Matrix Taylor expansion)
If $\mathbf{A}\mathbf{B}$ is a square general matrices and $\mathbf{A}$ and $\mathbf{I}+\mathbf{A}\mathbf{B}$ are invertible, we have

$$\left(\mathbf{I}-\mathbf{A}^{-1}\mathbf{B}\right)^{-1} = \mathbf{I} + \left(\mathbf{A}^{-1}\mathbf{B}\right) + \left(\mathbf{A}^{-1}\mathbf{B}\right)^2 + \left(\mathbf{A}^{-1}\mathbf{B}\right)^3 + \cdots \ . \tag{G.23}$$

Lemma G.1.14 (Matrix inversion with identities – 1)
If $\mathbf{A}$ and $\mathbf{B}$ are square and invertible and $\mathbf{I}+\mathbf{A}\mathbf{B}$ is invertible, we have

$$\left(\mathbf{I}+\mathbf{A}\mathbf{B}^*\right)^{-1}\mathbf{A} = \mathbf{A}\left(\mathbf{I}+\mathbf{B}\mathbf{A}^*\right)^{-1} \ . \tag{G.24}$$

Lemma G.1.15 (Matrix Inversion with identities – 2)
If $\mathbf{A}$ has a rank of 1 and the trace exist and $\mathbf{B}$ is invertible with a non-zero trace, we get

$$\left(\mathbf{A}+\mathbf{B}^*\right)^{-1} = \mathbf{B}^{-1} - \frac{1}{1+\mathrm{Tr}(\mathbf{A})}\mathbf{B}^{-1}A\mathbf{B}^{-1} \ . \tag{G.25}$$

For the special cases when $\mathbf{B} = \mathbf{I}$

$$\left(\mathbf{A}+\mathbf{B}^*\right)^{-1} = \mathbf{I} - \frac{1}{1+\mathrm{Tr}(\mathbf{A})}\mathbf{A} \ . \tag{G.26}$$

Lemma G.1.16 (Matrix inversion with identities – 3)
If $\mathbf{A}$ and $\mathbf{I}+\mathbf{BA}$ are invertible, we get

$$(\mathbf{I}+\mathbf{BA}^*)^{-1} = (\mathbf{I}+\mathbf{BA}^*)^{-1}(\mathbf{I}) \ . \tag{G.27}$$

Without loss of generality, let us assume $\mathbf{I} = \mathbf{I}+\mathbf{BA}-\mathbf{BA}$. Therefore,

$$\begin{aligned}(\mathbf{I}+\mathbf{BA}^*)^{-1} &= (\mathbf{I}+\mathbf{BA}^*)^{-1}(\mathbf{I}+\mathbf{BA}-\mathbf{BA}) \\ &= (\mathbf{I}+\mathbf{BA}^*)^{-1}(\mathbf{I}+\mathbf{BA}) - (\mathbf{I}+\mathbf{BA}^*)^{-1}(\mathbf{BA}) \\ &= \mathbf{I} - (\mathbf{I}+\mathbf{BA}^*)^{-1}(\mathbf{BA}) \ . \end{aligned} \tag{G.28}$$

Proposition G.1.17 (Schur complement)
According to [70], we consider a partitioned $\mathbf{M}$ as

$$\mathbf{M} = \begin{bmatrix} \mathbf{A} & \mathbf{B} \\ \mathbf{B}^* & \mathbf{C} \end{bmatrix} \ . \tag{G.29}$$

If $\mathbf{A}$ is invertible, the Schur complement is defined as

$$\mathbf{S} \preceq \mathbf{C} - \mathbf{B}^*\mathbf{A}^{-1}\mathbf{B} \ . \tag{G.30}$$

Thus, if $\mathbf{A} \succ \mathbf{0}$ and $\mathbf{S} \succeq \mathbf{0}$, then $\mathbf{M} \succeq \mathbf{0}$. In this case, $\mathbf{M} \succeq \mathbf{0}$ is equivalent (via permutations) to

$$\begin{bmatrix} \mathbf{C} & \mathbf{B}^* \\ \mathbf{B} & \mathbf{A} \end{bmatrix} \succeq \mathbf{0} \ . \tag{G.31}$$

Appendix H

List of Mathematical Symbols

$\mathbf{A}$	general (non-diagonal) matrix
$\mathbf{A}^T$	matrix transpose
$\mathbf{A}^*$	matrix conjugate-transpose or Hermitian
$\mathbf{A}^\dagger$	Moore-Penrose generalized inverse (pseudo-inverse)
$\mathbf{A}(:, i)$	i^{th} column of $\mathbf{A}$
$\mathbf{A}(i, :)$	i^{th} row of $\mathbf{A}$
$\text{Tr}(\mathbf{A})$	trace or the diagonal summation of $\mathbf{A}$
$\det(\mathbf{A})$	matrix determinant of $\mathbf{A}$
α^2	channel coefficient square with chi-square distribution
γ_j	noise margin of the j^{th} class
γ_u	noise margin of the u^{th} user
$\mathcal{G}$	CGNR
$\mathcal{I}$	starting index
C	channel capacity
$\mathbb{C}$	complex domain
$\subset$	subset of
b_k^j	k^{th} bit load for the j^{th} class
d_H	Hamming distance
d_0, d_1	inter-symbol distances in hierarchical constellation
$\mathbf{\Delta}$	diagonal channel matrix for covariance feedback
Δ_j	noise-margin separation
∇_x	Nabla operator
$\in$	element of
E_b/N_0	signal-to-noise ratio w.r.t. bit energy
E_s/N_0	signal-to-noise ratio w.r.t. symbol energy
ε	erasure probability
$\mathbf{F}$	precoding matrix
$\mathbf{V}$	beamforming precoding (unitary) matrix
$\mathbf{U}$	post-processing or unitary matrix
$\mathbf{P}$	power loading matrix
$\mathbf{Q}$	covariance matrix
$\mathbf{D}$	diagonal matrix of eigenchannels $\text{diag}[\lambda^{(1)} \ \ldots \ \lambda^{(R)}]$
$\mathbf{H}$	general channel matrix

$\hat{\mathbf{H}}$	Gaussian channel matrix with error
$\mathbf{\Psi}$	overall channel matrix
$\mathbf{H}_w$	white Gaussian channel matrix
$\widetilde{\mathbf{H}}$	uncorrelated Gaussian channel matrix
h_k	k^{th} subcarrier channel coefficient
$\mathbf{U}$	left-hand side singular matrix
$\mathbf{V}$	right-hand side singular matrix
$I(Y;X)$	mutual information between random variables Y and X
N_u	number of users
N_T	number of transmit antennas
N_R	number of receive antennas
N_r^i	number of receive antennas for the i^{th} user
L_p	number of channel paths
$\mathcal{L}$	diversity order $(N_R - N_T - 1)$
$\mathcal{L}_\mu$	Lagrangian function with a Lagrangian multiplier μ
i	general index
l	general index
k	subcarrier index
j	class index
u	user index
λ_2	eigenvalue
λ	singular value
$E(x)$	expectation of x
λ_s	eigenbeam of the s spatial index
Λ	gap approximation value
$\mathcal{M}$	sorted subcarrier indices
$\mathcal{M}_j$	sorted subcarrier indices of the j^{th} class
M	modulation modulation order or 2^b
M_u	number of user u streams
N	number of of subcarriers
$\mathcal{N}$	normal-Gaussian distribution
$\mathcal{N}(m, \sigma^2)$	Gaussian random variable with mean m and variance σ^2
b_k	number of bits of the k^{th} subcarrier
$\mathbf{b_k}$	quantized number of bits of the k^{th} subcarrier
$\mathbf{P}$	normalized symbol gain matrix
$\mathbf{\Psi}$	aggregated channel matrix
P_s	power allocated to the s^{th} eigen-channel
p_k	power allocated to the k^{th} subcarrier
$\mathcal{P}_j^e$	average probability of error for class j
B_T	target sum rate
$\mathbf{B}$	bit-loading matrix
T_j	individual target bit rate for the j^{th} class
T_u	individual target bit rate for the u^{th} user
τ_d	delay spread
τ_j	subcarrier hypothetical threshold for the class j
R	maximum allowed eigenbeams
$\mathbf{R}_e$	covariance matrix of e
n	the rank of the channel matrix $\mathbf{H}$

ρ_s	SINR at the equalizer output for the eigenbeam s
σ_n^2	noise variance
$\sigma_{\mathbf{\Xi}}^2$	channel error variance
$\mathbf{\Xi}$	channel error matrix
$\mathbb{Z}$	ring of integers
$\mathbb{Z}^{1\times N}$	one-dimensional vector of integer of length $1 \times N$
$\mathbb{Z}^{R\times N}$	two-dimensional integer matrix of length $R \times N$
$\mathbb{Z}^{R\times N\times L}$	three-dimensional integer matrix of length $R \times N \times L$
$\mathbb{R}^{R\times N}$	two-dimensional real-field of length $R \times N$
$\mathbb{C}^{R\times N}$	two-dimensional complex-field domain of length $R \times N$
$\frac{\partial F(x)}{\partial x}$	differentiation of $F(x)$ with respect to x
$\int_0^\infty x dx$	integral of x from zero to infinity
$\sum_a^b$	summation over a period
$\succeq$	positive semidefinit
$\succ$	positive definit
$\multimap$	map a vector or a matrix into another vector
$\circ\!\!-$	reverse map of a vector back to its original form
$\|\|\mathbf{x}\|\|$	vector norm, also Frobenius norm
$\|\|\mathbf{A}\|\|_2$	Matrix second norm and also Frobenius norm
$\lfloor x \rfloor$	round to the next smaller integer
$\lfloor x + 1/2 \rfloor$	round to the nearest integer
$\lceil x \rceil$	round to the next higher integer
θ	random phase
$\mathbf{x}$	transmitted vector
$\mathbf{y}$	received vector
$\mathbf{z}$	equalized vector
$\mathbf{X}$	transmitted vector in frequency domain
$\mathbf{Y}$	received vector in frequency domain
$\mathbf{W}$	equalizer matrix
w	error weighting values
E_u	MSE of user u

Appendix I

List of Acronyms

ARQ	automatic repeat request
AoA	angle-of-arrival
AWGN	additive white Gaussian noise
BER	bit-error rate
BC	broadcast channel
BD	block diagonalization
BLAST	Bell labs LAyered Space-Time architecture
BPSK	binary phase shift keying
BS	base station
CGNR	channel gain-to-noise ratio
CSI	channel-state information
CSIT	channel-state information at the transmitter
CSIR	channel-state information at the receiver
CP	cyclic prefix
CD	channel distortion
CDMA	code-division multiple access
CVX	convex programing
DAB	digital audio broadcast
DBC	degraded-broadcast channel
D-BLAST	diagonal BLAST
DMT	discrete multi-tone
DPC	dirty-paper code
DVB	digital video broadcast
FDD	frequency division duplexing
FDMA	frequency-division medium access
FEXT	far-end crosstalk
IC	interference cancellation
IEI	inter-eigen interference
ISI	inter-symbol interference
IUI	inter-user interference
LP	linear programming
MAC	multiple-access channel
MATLAB	high-level programing language

MIMO	multiple-input, multiple-output
MISO	multiple-input, single-output
ML	maximum likelihood
MS	mobile station
MSD	multistage decoding
MU	multiuser
MUI	multiuser interference
NEXT	near-end crosstalk
Octave	high-level programing language
OFDM	orthogonal frequency division multiplexing
OFDMA	orthogonal frequency division multiple access
PAM	pulse amplitude modulation
PSK	phase shift keying
QAM	quadrature amplitude modulation
QPSK	quaternary phase shift keying
Rx	receiver
RD	rate-distortion
SDMA	spatial-division medium access
SDP	semidefinite programming
SER	symbol error-ratio
SeDuMi	interior-point tool
SIC	successive interference cancellation
SIMO	single-input, multiple-output
SISO	single-input, single-output
SINR	signal to interference-plus-noise ratio
SNR	signal-to-noise ratio
TDD	time division duplexing
TDMA	time-division medium access
Tx	transmitter
UEP	unequal error protection
UTP	unshielded twisted pair
EEP	equal error protection
QoS	quality-of-service
V-BLAST	vertical BLAST
YALMIP	yet another LMI parser language programming
ZMCSCG	zero-mean circularly symmetric complex Gaussian
erfc	complementary error-function

Own Publications

[1] K. Hassan and W. Henkel, "Prioritized multiuser transmission using virtual diagonalization and weighted Sum-MSE," in *15th International OFDM-Workshop 2010 (InOWo 10)*, vol. 1, (Hamburg, Germany), pp. 1–5, Septemper 2–3, 2010.

[2] W. Henkel and K. Hassan, "OFDM (DMT) bit and power loading for unequal error protection," in *11th International OFDM-Workshop 2006 (InOWo 06)*, vol. 1, (Hamburg, Germany), pp. 1–5, August 30–31, 2006.

[3] K. Hassan and W. Henkel, "Fast prioritized bit-loading and subcarriers allocation for multicarrier systems," in *IEEE Vehicular Technology Conference 2010 (VTC-10)*, pp. 1–5, May 16–21, 2010.

[4] K. Hassan, G. Sidhu, and W. Henkel, "Multiuser MIMO-OFDMA with different QoS using a prioritized channel adaptive technique," in *Proc. IEEE International Conference on Communications Workshops ICC Workshops 2009*, pp. 1–5, June 14–18, 2009.

[5] W. Henkel, N. von Deetzen, K. Hassan, L. Sassatelli, and D. Declercq, "Some UEP Concepts in Coding and Physical Transport," in *Proc. IEEE Sarnoff Symp*, pp. 1–5, 2007.

[6] K. Hassan and W. Henkel, "Unequal-error protection bit-loading for multicarrier transmission, DE Patent, WO/2008/025510, filed 2007," March 2008.

[7] K. Hassan and W. Henkel, "unequal error protection with eigen beamforming for partial channel information MIMO-OFDM," in *Proc. IEEE Sarnoff Symposium*, pp. 1–5, April 2007.

[8] K. Hassan and W. Henkel, "UEP with adaptive multilevel embedded modulation for MIMO-OFDM systems," in *13th International OFDM-Workshop 2008 (InOWo 08)*, vol. 1, (Hamburg, Germany), pp. 1–5, August 27–28, 2008.

[9] K. Hassan and W. Henkel, "Prioritized multi-layer transmission for MIMO-OFDM multiuser broadcast channel," in *14th International OFDM-Workshop 2009 (InOWo 09)*, vol. 1, (Hamburg, Germany), pp. 1–5, September 2–3, 2009.

[10] W. Henkel, K. Hassan, N. von Deetzen, S. Sandberg, L. Sassatelli, and D. Declercq, "UEP concepts in modulation and coding," *Advances in Multimedia*, vol. 2010, 2010.

[11] K. Hassan and W. Henkel, "UEP MIMO-OFDM with beamforming-combining for imperfect channel information," in *12th International OFDM-Workshop 2007 (InOWo 07)*, vol. 1, (Hamburg, Germany), pp. 1–5, August 29–30, 2007.

[12] K. Hassan and W. Henkel, "UEP exploitation in MIMO-OFDM with beamforming and channel-correlation Feedback," in *Proc. IEEE International Zurich Seminar on Communications*, pp. 124–127, March 12–14, 2008.

[13] K. Hassan and W. Henkel, "Prioritized Adaptive MIMO-OFDM Using Pre-ordered Successive Interference Cancellation," in *ICC - 2011, Submitted to the Wireless Communications Symposium*, vol. 1, pp. 1–5, June 5–9, 2011.

[14] K. Hassan and W. Henkel, "UEP bit-loading for multiuser MIMO-OFDM with weighted sum-MSE and QoS constraint," in *ICC - 2011, Submitted to the Wireless Communications Symposium*, vol. 1, pp. 1–5, June 5–9, 2011.

Bibliography

[15] J. Proakis, *Digital Communications*. McGraw-Hill Science/Engineering/Math, 4th ed., Aug. 2000.

[16] J. Proakis and M. Salehi, *Digital Communications*. McGraw-Hill Science/Engineering/Math, 5th ed., 2007.

[17] Y. Ahmed, F. Jawed, S. Zia, and M. S. Aga, "Real-time implementation of adaptive channel equalization algorithms on TMS320C6x DSP processors," in *Proc. E-Tech 2004*, pp. 101–108, Jul. 31, 2004.

[18] R. Mosier and R. Clabaugh, "Kineplex, multi-carrier HF modem," Jan. 1958.

[19] R. Mosier and R. Clabaugh, "Kineplex, A bandwidth-efficient binary transmission system," Jan. 1958.

[20] S. Weinstein and P. Ebert, "Data transmission by frequency division multiplexing using the discrete Fourier transform," Oct. 1971.

[21] C. Shannon and W. Weaver, *A Mathematical Theory of Communication*. Champaign, IL, USA: University of Illinois Press, 1963.

[22] A. Goldsmith and S.-G. Chua, "Variable-rate variable-power MQAM for fading channels," *IEEE Transactions on Communications*, vol. 45, pp. 1218–1230, Oct 1997.

[23] A. Goldsmith and P. P. Varaiya, "Capacity of fading channels with channel side information," *IEEE Transactions on Information Theory*, vol. 43, pp. 1986–1992, Nov. 1997.

[24] A. Goldsmith, *Wireless Communications*. Cambridge University Press, Aug. 2005.

[25] W. Henkel, "Digital signal processing – Jacobs University lecture notes," Feb. 2010.

[26] T. Cover and J. A. Thomas, *Elements of Information Theory 2nd Edition (Wiley Series in Telecommunications and Signal Processing)*. Wiley-Interscience, 2 ed., Jul. 2006.

[27] M. Costa, "Writing on dirty paper," *Information Theory, IEEE Transactions on*, vol. 29, pp. 439–441, May 1983.

[28] Z.-Q. Luo, T. Davidson, G. Giannakis, and K. M. Wong, "Transceiver optimization for block-based multiple access through ISI channels," *Signal Processing, IEEE Transactions on*, vol. 52, pp. 1037–1052, Apr. 2004.

[29] A. Bourdoux and N. Khaled, "Joint TX-RX optimisation for MIMO-SDMA based on a -space constraint," in *Proc. VTC 2002-Fall Vehicular Technology Conference 2002 IEEE 56th*, vol. 1, pp. 171–174, Sep. 24–28, 2002.

[30] H. Boche, M. Schubert, and E. Jorswieck, "Throughput maximization for the multiuser MIMO broadcast channel," in *Acoustics, Speech, and Signal Processing, 2003. Proceedings. (ICASSP '03). 2003 IEEE International Conference on*, vol. 4, pp. IV–808–11, Apr. 2003.

[31] M. Schubert and H. Boche, "Solution of the multiuser downlink beamforming problem with individual SINR constraints," *Vehicular Technology, IEEE Transactions on*, vol. 53, pp. 18–28, Jan. 2004.

[32] P. Chow, J. Cioffi, and J. Bingham, "DMT-based ADSL: concept, architecture, and performance," in *High speed Access Technology and Services, Including Video-on-Demand (Digest No. 1994/192), IEE Colloquium on*, pp. 3/1–3/6, Oct 1994.

[33] J. Campello, "Practical bit loading for DMT," in *Communications, 1999. ICC '99. 1999 IEEE International Conference on*, vol. 2, pp. 801–805, 1999.

[34] T. Rappaport, *Wireless Communications: Principles and Practice*. Prentice Hall PTR, 2 ed., Jan. 2002.

[35] M. Tzannes, "Test procedure for digital Subscriber line (DSL) transceiver," ITU-T, Draft Recommendation G.996.1, ETSI, Geneva, Switzerland, Oct. 2000.

[36] "Asymmetric digital subscriber line (ADSL) transceiver extended bandwidth ADSL2 (ADSL2plus)," ITU-T, ETSI Recommendation, G.992.5, May 2003.

[37] W. Henkel and T. Kessler, "A wideband impulsive noise survey in the german telephone netwerk - statistical description and modeling," *AEÜ*, vol. 48, pp. 277 – 288, Nov./Dec. 1994.

[38] J. Musson, "Maximum likelihood parameters of pair cables," TD8 981t08a1, ETSI TM6, Madrid, Spain, Jan. 1998.

[39] L. Heylen and J. Musson, "Cable models predict physically impossible behaviour in time domain," plenary no. 16, ETSI TM6, Amsterdam, Nethierland, Nov. 29 - Dec. 3, 1999.

[40] R. Clarke, "A statistical theory of mobile-radio reception," in *Bell Systems Technical Journal*, vol. 47, pp. 957–1000, 1968.

[41] W. Jakes, *Microwave Mobile Communications*. Wiley-IEEE Press, 2nd ed., May 1994.

[42] M. Paetzold, *Mobile Radio Channels*. Wiley-Blackwell, 2nd revised edition ed., Oct. 2010.

[43] J. A. Rice, *Mathematical Statistics and Data Analysis*. Duxbury Press, 3 ed., Apr. 2006.

[44] Z. Shengli and G. Giannakis, "Optimal transmitter eigen-beamforming and space-time block coding based on channel correlations," in *Information Theory, IEEE Transactions on*, vol. 49, pp. 1673–1690, Jul. 2003.

[45] P. Hoeher, "A statistical discrete-time model for the WSSUS multipath channel," *IEEE Transactions on Vehicular Technology*, vol. 41, pp. 461–468, Nov. 1992.

[46] B. Sklar, "Rayleigh fading channels in mobile digital communication systems. I. characterization," *IEEE Communications Magazine*, vol. 35, pp. 136–146, Sep. 1997.

[47] D. Tse and P. Viswanath, *Fundamentals of Wireless Communication*. Cambridge University Press, Jun. 2005.

[48] R. A. Bahai, R. B. Saltzberg, and M. Ergen, *Multi-carrier Digital Communications: Theory And Applications Of OFDM*. Springer, 2nd ed., Oct. 2004.

[49] J. Cioffi, "A multicarrier primer," *ANSI Contribution T1E1, Clearfield, Fla, USA.*, vol. 4, pp. 91–157, Nov. 1991.

[50] R. V. Nee, *OFDM for Wireless Multimedia Communications*. Artech House Universal Personal Communications Publishers, Dec. 1999.

[51] R. Courant and H. Robbins, *What is Mathematics? An Elementary Approach to Ideas and Methods*. Oxford University Press, USA, 2 ed., Jul. 1996.

[52] M. Nisar, "OFDM systems - why cyclic prefix?," 2008.

[53] T. Beth, *Verfahren der schnellen Fourier-Transformation*. Teubner, 1984.

[54] J. Proakis and D. Manolakis, *Digital Signal Processing (4th Edition)*. Prentice Hall, 4 ed., Apr. 2006.

[55] H. Sorensen, C. Burrus, and Zhenyu Li, "FFT and convolution algorithms on DSP microprocessors," vol. 11, pp. 289–292, Apr. 1986.

[56] S. Boyd and L. Vandenberghe, *Convex Optimization*. Cambridge University Press, Mar. 2004.

[57] M. Kuhn, "The Karush-Kuhn-Tucker Theorem." Lecture notes of CDSEM Uni. Mannheim, Nov. 2006.

[58] S. Alamouti, "A simple transmit diversity technique for wireless communications," in *Selected Areas in Communications, IEEE Journal on*, vol. 16, pp. 1451–1458, Oct. 1998.

[59] H. Bölcskei and D. Gesbert and C. B. Papadias and A.-J. van der Veen, ed., *Space-Time Wireless Systems: From Array Processing to MIMO Communications*. Cambridge University Press, Jul. 2006.

[60] C. Chae, M. Katz, C. Suh, and H. Jeong, "Adaptive spatial modulation for MIMO-OFDM," in *Wireless Communications and Networking Conference, 2004. WCNC IEEE*, vol. 1, pp. 87–92, Mar. 2004.

[61] P. Wolniansky, G. Foschini, G. Golden, and R. Valenzuela, "V-BLAST: an architecture for realizing very high data rates over the rich-scattering wireless channel," in *ISSSE*, 1998.

[62] G. Foschini, "Layered space-time architecture for wireless communication in a fading environment when using multiple antennas," *Bell Laboratories Technical Journal*, vol. 1, pp. 41–59, 1996.

[63] E. Biglieri, R. Calderbank, A. Constantinides, A. Goldsmith, A. Paulraj, and H. V. Poor, *MIMO Wireless Communications*. Cambridge University Press, Feb. 2010.

[64] T. Mitsui, M. Otani, K. Sakaguchi, H. Chua, and K. Araki, "Indoor MIMO channel measurements for evaluation of effectiveness of array antenna configurations," in *Vehicular Technology Conference (VTC-fall)*, vol. 1, pp. 84–88, Oct. 2003.

[65] M. Ozcelik, N. Czink, and E. Bonek, "What makes a good MIMO channel model?," in *Vehicular Technology Conference, VTC-Spring*, vol. 1, pp. 156–160, May 30 - Jun. 1, 2005.

[66] W. Weichselberger, M. Herdin, H. Özcelik, and E. Boneck, "A stochastic MIMO channel model with joint correlation of both link ends," in *IEEE transactions on wireless communications* (I. of Electrical and E. Engineers, eds.), vol. 5, pp. 90–100, 2009.

[67] I. E. Telatar, "Capacity of multi-antenna Gaussian channels," *European Transactions on Telecommunications (ETT)*, vol. 10, no. 6, pp. 585–595, 1999.

[68] T. Yoo, E. Yoon, and A. Goldsmith, "MIMO capacity with channel uncertainty: does feedback help?," vol. 1, pp. 96–100, Nov. 30 - Dec. 3, 2004.

[69] Z. quan Luo, S. Member, T. N. Davidson, G. B. Giannakis, and K. M. Wong, "Transceiver optimization for block-based multiple access through ISI channels," *IEEE Trans. Signal Process*, vol. 52, pp. 1037–1052, 2004.

[70] D. Palomar and Y. Jiang, *MIMO Transceiver Design via Majorization Theory (Foundations and Trends(R) in Communications and Information Theory)*. Now Publishers Inc., Jun. 2007.

[71] J. Tomcik, "Part of the QTDD proposal package for 802.20," *EEE 802.20 Working Group on Mobile Broadband Wireless Access*, vol. IEEE C802.20-05/66, pp. 47–48, Nov. 2005.

[72] X. Pengfei, Z. Shengli, and G. Giannakis, "Adaptive MIMO-OFDM based on partial channel state information," in *Signal Processing, IEEE Transactions on*, vol. 52, pp. 202–213, Jan. 2004.

[73] H. Boche and M. Schubert, "Resource allocation for multi-antenna multi-user systems," in *Proc. IEEE International Conference on Communications ICC 2005*, vol. 2, pp. 855–859, May 16–20, 2005.

[74] S. Vishwanath, N. Jindal, and A. Goldsmith, "On the capacity of multiple input multiple output broadcast channels," in *Communications, 2002. ICC 2002. IEEE International Conference on*, vol. 3, pp. 1444–1450, 2002.

[75] N. Jindal, S. Vishwanath, and A. Goldsmith, "On the duality of Gaussian multiple-access and broadcast channels," *Information Theory, IEEE Transactions on*, vol. 50, pp. 768–783, May 2004.

[76] P. Ubaidulla and A. Chockalingam, "Robust THP transceiver designs for multiuser MIMO downlink," in *Wireless Communications and Networking Conference, 2009. WCNC 2009. IEEE*, pp. 1–6, Apr. 2009.

[77] S. Shi, M. Schubert, and H. Boche, "Downlink MMSE transceiver optimization for multiuser MIMO Systems: MMSE Balancing," *Signal Processing, IEEE Transactions on*, vol. 56, pp. 3702–3712, Aug. 2008.

[78] A. Mezghani, M. Joham, R. Hunger, and W. Utschick, "Transceiver designs for multiuser MIMO systems," *Signal Processing, IEEE Transactions on*, vol. 57, pp. 698–713, Feb. 2006.

[79] R. Hunger, M. Joham, and W. Utschick, "On the MSE-Duality of the broadcast channel and the multiple access channel," *Signal Processing, IEEE Transactions on*, vol. 57, pp. 698–713, Feb. 2009.

[80] S. Serbetli and A. Yener, "Transceiver optimization for multiuser MIMO systems," *Signal Processing, IEEE Transactions on*, vol. 52, pp. 214–226, Jan. 2004.

[81] S. Shi, M. Schubert, and H. Boche, "Rate optimization for multiuser MIMO systems with linear processing," *Signal Processing, IEEE Transactions on*, vol. 56, pp. 4020–4030, Aug. 2008.

[82] M. Ding and S. Blostein, "Joint optimization for multiuser MIMO uplink systems with imperfect CSI," in *Proc. 24th Queens Biennial Symposium on Communications*, pp. 191–195, Jun. 2008.

[83] D. Hughes-Hartogs, "Ensemble modem structure for imperfect transmission media," Digital Communication U.S. Patent no. 4833796, filed 1989, published May 1989.

[84] H. Levin, "A complete and optimal data allocation method for practical discrete multitone systems," in *Proc. IEEE Global Telecommunications Conf. GLOBECOM '01*, vol. 1, pp. 369–374, 2001.

[85] H. Ko, K. Lee, S. Oh, and C. Kim, "Fast optimal discrete bit-Loading algorithms for OFDM-based systems," in *Proc. 18th Internatonal Conf. Computer Communications and Networks ICCCN 2009*, pp. 1–6, 2009.

[86] Y. George and O. Amrani, "Bit loading algorithms for OFDM," in *International Symposium on Information Theory, 2004. ISIT 2004. Proceedings*, pp. 391–391, 2004.

[87] R. Fischer and J. Huber, "A new loading algorithm for discrete multitone transmission," in *Proc. 'Communications: The Key to Global Prosperity Global Telecommunications Conf. GLOBECOM '96*, vol. 1, pp. 724–728, 1996.

[88] F. Yu and A. N. J. Willson, "A DMT transceiver loading algorithm for data transmission with unequal priority over band-limited channels," in *Proc. Signals, Systems, and Computers Record of the Thirty-Third Asilomar Conf.*, vol. 1, pp. 685–689, 1999.

[89] W. Yu and J. Cioffi, "On constant power water-filling," in *IEEE ICC*, pp. 1665–1669, 2001.

[90] R. Fischer and J. Huber, "Report on channel coding in German DSL system," tech. rep., Deutsch Telekom, Germany, Nov. 1996.

[91] H. Chernoff, "A note on an inequality involving the normal distribution," *The Annals of Probability*, vol. 9, no. 3, pp. 533–535, 1981.

[92] Analog Devices Inc., "Experiences with the SHARC and Blackfin architecture for embedded systems education," 1999.

[93] M. Cleve., *Numerical Computing with Matlab*. Society for Industrial Mathematics, Jan. 2004.

[94] J. Eaton, *GNU Octave Manual*. Network Theory Limited, 2002.

[95] S. Pfletschinger, *Multicarrier modulation for broadband return channels in cable TV networks*. PhD thesis, Institute of Communications, University of Stuttgart, Germany, Feb. 27, 2003.

[96] R. Graf, *Modern Dictionary of Electronics*. Newnes, 1999.

[97] K. Benson and J. Whitaker, *Television Engineering Handbook: Featuring HDTV Systems*. McGraw-Hill, 1992.

[98] T. Kratochvil, "Hierarchical modulation in DVB-T/H mobile TV transmission," in *MCSS* (S. Plass, A. Dammann, S. Kaiser, and K. Fazel, eds.), vol. 41 of *Lecture Notes in Electrical Engineering*, pp. 333–341, Springer, 2009.

[99] S. Wang, S. Kwon, and S. Lee, "On enhancing hierarchical modulations," Aug. 27, 2007.

[100] P. Vitthaladevuni and M.-S. Alouini, "BER computation of 4/M -QAM hierarchical constellations," *Broadcasting, IEEE Transactions on*, vol. 49, pp. 408 – 408, Dec. 2003.

[101] B. Barmada, M. Ghandi, E. Jones, and M. Ghanbari, "Prioritized transmission of data partitioned H. 264 video with hierarchical QAM," *IEEE Signal Processing Letters*, vol. 12, no. 8, pp. 577–580, 2005.

[102] V. Lau and Y. Kwok, *Channel-Adaptive Technologies and Cross-Layer Designs for Wireless Systems with Multiple Antennas: Theory and Applications*. Wiley-Interscience, 2006.

[103] M. Codreanu, D. Tujkovic, and M. Latva-aho, "Compensation of channel state estimation errors in adaptive MIMO-OFDM systems," in *2004 IEEE 60th Vehicular Technology Conference, 2004. VTC2004-Fall*, pp. 1580–1584, 2004.

[104] N. Higham, "Newton's method for the matrix square root," *Mathematics of Computation*, vol. 46, no. 174, pp. 537–549, 1986.

[105] L. Hanzo and C. Wong, "Upper bound performance of a wide band adaptive modem," *IEEE Transactions on Communications*, vol. 48, no. 3, pp. 367–369, 2000.

[106] Z. Yan, W. Wang, X. wang, and K. Zheng, "Adaptive modulation for SVD-based MIMO systems with outdated CSI," *The Journal of China Universities of Posts and Telecommunications*, vol. 16, no. 4, pp. 78–83, 2009.

[107] P. Li, D. Paul, R. Narasimhan, and J. Cioffi, "On the distribution of SINR for the MMSE MIMO receiver and performance analysis," *IEEE Transactions on Information Theory*, vol. 52, no. 1, pp. 271–299, 2006.

[108] R. Heath, A. Paulraj, and M. Airy, "Multiuser diversity for MIMO wireless systems with linear receivers," in *Asilomar Conf. on Signals Systems and Computers*, vol. 2, pp. 1194–1199, IEEE; 1998, 2001.

[109] R. Gohary, T. Davidson, and Z.-Q. Luo, "An efficient design method for vector broadcast systems with common information," vol. 4, pp. 2010–2014, Dec. 2003.

[110] W. Henkel, G. Taubock, P. Odling, P. Borjesson, N. Petersson, and A. Johansson, "The cyclic prefix of OFDM/DMT - an analysis," in *International Zurich Seminar on Broadband Communications*, pp. 22–22, Citeseer, 2002.

[111] W. Yu, "Multiuser water-filling in the presence of crosstalk," in *Information Theory and Applications Workshop, 2007*, pp. 414–420, 2007.

[112] U. SeDuMi, "1.02, a MATLAB toolbox for optimization over symmetric cones," *Optimization Methods and Software*, pp. 11–12, 1999.

[113] J. Lofberg, "YALMIP: A toolbox for modeling and optimization in MATLAB," in *2004 IEEE International Symposium on Computer Aided Control Systems Design*, pp. 284–289, 2004.

[114] D. Bertsekas and J. Tsitsiklis, *Parallel and Distributed Computation*. Englewood Cliffs, NJ, 1999.

[115] S. Christensen, R. Agarwal, E. Carvalho, and J. Cioffi, "Weighted sum-rate maximization using weighted MMSE for MIMO-BC beamforming design," *IEEE Transactions on Wireless Communications*, vol. 7, no. 12 Part 1, pp. 4792–4799, 2008.

[116] J. Liu, Y. Hou, S. Kompella, and H. Sherali, "Conjugate gradient projection approach for MIMO Gaussian broadcast channels," in *IEEE International Symposium on Information Theory, 2007. ISIT 2007*, pp. 781–785, 2007.

[117] H. Sampath, P. Stoica, and A. Paulraj, "Generalized linear precoder and decoder design for MIMO channels using the weighted MMSE criterion," *IEEE Transactions on Communications*, vol. 49, p. 12, 2001.

[118] E. Jorswieck and H. Boche, "Majorization and matrix-monotone functions in wireless communications," *Foundations and Trends in Communications and Information Theory*, vol. 3, no. 6, pp. 553–701, 2006.

[119] K. B. Petersen and M. S. Pedersen, "The matrix cookbook," Technical University of Denmark, Oct. 2008. online ver. 20081110, http://www2.imm.dtu.dk/pubdb/p.php?3274.